ABSTRACT

YU, SHAOCAI. A Study of Direct and Cloud-Mediated Radiative Forcing of Climate Due to Aerosols.

(Under the direction of Professor V.K. Saxena)

The Intergovernmental Panel on Climate Change (IPCC) has reported that in the southeastern US and eastern China, the general greenhouse warming due to anthropogenic gaseous emissions is dominated by the cooling effect of anthropogenic aerosols. To verify this model prediction in eastern China and southeastern US, we analyzed regional patterns of climate changes at 72 stations in eastern China during 1951-94 (44 years), and at 52 stations in the southeastern US during 1949-94 (46 years) to detect the fingerprint of aerosol radiative forcing. It was found that the mean rates of change of annual mean daily, maximum, minimum temperatures and diurnal temperature range (DTR) in eastern China were 0.8, -0.2, 1.8, and -2.0 C/100 years respectively, while the mean rates of change of annual mean daily, maximum, minimum temperatures and DTR in the southeastern US were -0.2, -0.6, 0.2, and -0.8 C/100 years, respectively. This indicates that the high rate of increase in annual mean minimum temperature in eastern China results in a slightly warming trend of daily temperature, while the high rate of decrease in annual mean maximum temperature and low rate of increase in annual mean minimum temperature lead to the cooling trend of daily temperature in the southeastern US. We found that the warming from the longwave forcing due to both greenhouse gases and aerosols was completely counteracted by the shortwave aerosol forcing in the southeastern US in the past 46 years. A slightly overall warming trend in eastern China is evident; winters have become milder. This finding is explained by hypothesizing that increasing energy usage during the past 44 years has resulted in more coal and biomass burning, thus increasing the emission of absorbing soot and organic aerosols in eastern China. Such emissions, in addition to well-known Asia dust and greenhouse gases, may be responsible for the winter warming trend in eastern China that we have reported here.

The sensitivity of aerosol radiative properties to aerosol composition, size distribution, relative humidity (RH) is examined for the following aerosol systems: inorganic and organic ions (Cl^-, Br^-, NO_3^-, SO_4^{2-}, Na^+, NH_4^+, K^+, Ca^{2+}, Mg^{2+}, $HCOO^-$,

CH_3COO^-, $CH_3CH_2COO^-$, CH_3COCOO^-, $OOCCOO^{2-}$, MSA^{-1}); water-insoluble inorganic and organic compounds (elemental carbon, n-alkanes, SiO_2, Al_2O_3, Fe_2O_3 and other organic compounds). The partial molar refraction method was used to calculate the real part of the refractive index. It was found that the asymmetry factor increased by ~48% with the real part varying from 1.40 to 1.65, and the single scattering albedo decreased by 24% with the imaginary part varying from –0.005 to –0.1. The asymmetry factor increased by 5.4 times with the geometric standard deviation varying from 1.2 to 3.0. The radiation transmission is very sensitive to the change in size distribution; other factors are not as significant.

To determine the aerosol direct radiative forcing (ADRF), the aerosol optical depth (AOD) values at the three operational wavelengths (415, 500 and 673 nm) were determined at a regionally representative site, namely, Mt. Gibbs (35.78^0 N, 82.29^0 W, elevation 2006 m) in Mt. Mitchell State Park, NC, and a site located in an adjacent valley (Black Mountain, 35.66^0 N, 82.38^0 W, elevation 951 m) in the southeastern US. The two sites are separated horizontally by 10 km and vertically by 1 km. It was found that the representative total AOD values at 500 nm at the valley site for highly polluted (HP), marine (M) and continental (C) air masses were 0.68±0.33, 0.29±0.19 and 0.10± 0.04, respectively. A search-graph method was used to retrieve the columnar size distribution (number concentration N, effective radius r_{eff} and geometric standard deviation σ_g) from the optical depth observations at three operational wavelengths. The ground albedo, single scattering albedo and imaginary part of the refractive index were calculated using a mathematically unique procedure involving a Mie code and a radiative transfer code in conjunction with the retrieved aerosol size distribution, AOD, and diffuse-direct irradiance ratio. It was found that N, r_{eff} and σ_g were in the ranges of 10 to $1.7x10^4$ cm^{-3}, 0.09 to 0.68 μm and 1.12 to 2.95, respectively. The asymmetry factor and single scattering albedo were in the ranges of 0.63 to 0.75 and 0.74 to 0.97 respectively. The ground albedo for the forested terrain and imaginary part of refractive index were found to be in the ranges of 0.06 to 0.29 and 0.005 to 0.051 respectively. On the basis of these aerosol radiative properties obtained at the research sites and computations using the Column Radiation Model (CRM) of National Center of Atmospheric Research (NCAR)

Community Climate Model (CCM3), it was found that the average cloud-free 24-hour ADRF values were -13±8, -8±3, -33±16 W m^{-2} for marine, continental, and polluted air masses, respectively. On the assumption that the fractional coverage of clouds is 0.61, it was estimated that the annual mean ADRF was 7±2 W m^{-2} in the southeastern US.

The review with respect to the current knowledge of organic acids shows that aerosol formate and acetate concentrations range from 0.02 to 5.3 nmol/m^3 and from 0.03 to 12.4 nmol/m^3 respectively, and that between 34% to 77% of formate and between 21% to 66% of acetate are present in the fine fraction of aerosols. It was found that although most (98-99%) of these volatile organic acids were present in the gas phase, their concentrations in the aerosol particles were sufficient to make them a good candidate for cloud condensation nuclei (CCN). It is hypothesized that organic acids are at least one of the primary sources of CCN in the atmosphere due to their ubiquitous presence in the troposphere, especially over the continental forested areas.

The results of our measurements at Palmer Station, Antarctica show that the daily average CCN concentrations at 0.3% and 1% supersaturations ranged from 0.3 to 160 cm^{-3} and from 4 to 168 cm^{-3}, respectively, during the period from 17 January to 26 February, 1994. New evidence for substantial and definitive CCN enhancement near and within cloud has been observed at Mt. Mitchell, North Carolina. The results show that the average monthly CCN concentrations were 460±217, 386±286, 429±228 and 238± 134 cm^{-3} for in-cloud, overcast, clear and rainy conditions, respectively. The typical CCN spectra show that there were a lot of small CCN produced and the ion concentrations (especially H^+ and SO_4^{2-}) were very high during the CCN enhancement period. The significantly positive correlation between black carbon (BC) and CCN at 1% supersaturation indicates that a percentage of the BC measured at the site may be in the form of an internal mixture and participated in the formation of CCN.

A STUDY OF DIRECT AND CLOUD-MEDIATED RADIATIVE FORCING OF CLIMATE DUE TO AEROSOLS

by

SHAOCAI YU

A dissertation submitted to the Graduate Faculty of North Carolina State University in partial fulfillment of the requirements for the Degree of Doctor of Philosophy

Marine, Earth and Atmospheric Sciences

Raleigh

1999

Approved By:

Dr. John J. DeLuisi

Dr. Gerald F. Watson

Dr. S. Pal Arya

Dr. Vinod K. Saxena 09/28/99

(Chair of Advisory Committee)

DEDICATION

This research is dedicated to my father and mother, who have provided me with love and support throughout my life. I only wish that my father and mother could be here to share in my achievements, but I know that they are proud of me, a country boy, to be a Doctor of Philosophy in the USA. This research is also dedicated to my wife for her moral support and patience.

BIOGRAPHY

Shaocai Yu was born in Yongan, Fujian, China, on 7 March, 1964, to his parents Zhimei Yu and Guangxin Liao. After graduation from Yongan No. 1 High School in 1981, Shaocai applied to and was accepted for Fall admission to Peking University, Beijing, China. He started studies there in September of 1981. He received his Bachelor of Science degree in Chemistry in 1985 from Peking University. As he was near the top of his class, his graduate entrance exam requirement was waived, and he was subsequently admitted to the Environmental Science Center in the Graduate School of Peking University. He received a Master of Science degree in Atmospheric Chemistry in June of 1988 from Peking University. From July of 1988 to July of 1994, he worked as an environmental engineer in Xiamen Municipal Research Institute and Monitoring Station of Environmental Protection, Xiamen, China. In August 1994, he entered the graduate school at North Carolina State University, and continued his education in Atmospheric Sciences. After completion of his another M.S. degree in Atmospheric Sciences in May 1996, he went on to pursue a Ph.D. degree in Atmospheric Sciences at North Carolina State University.

ACKNOWLEDGMENTS

I would like to express my deep thanks to Professor V. K. Saxena, chairman of my advisory committee, for his expertise, guidance and encouragement throughout this research. Thanks are also due to all of my advisory committee members, Drs. J.J. DeLuisi, S.P. Arya, and G.F. Watson for their contribution to my education. I consider myself fortunate to have conducted my research under their direction. I am also grateful to Dr. G.K. Yue from NASA for providing helpful comments and advice both in scientific discussion and on a personal level.

I am particularly thankful to members of the Cloud-Aerosol Interaction Laboratory (CAIL), both past and present, especially, Surabi Menon, Brian Wenny, John Anderson, Shannon Schafer, Chad Bahrmann, Matt Seybold, Sun Im and Bill Barnard. The help from Brian Wenny, his resourcefulness, patience and kindness have made life and research much easier. The friendship of Mel DeFeo and her family will always be remembered. I would like to thank Dr. I. V. Petropavlovskikh, and Dr. S. Madronich from NCAR for their help in using the UV-Visible Radiative Transfer Model, and Dr. C.S. Zender from NCAR for his help in using the Column Radiation Model (CRM) of NCAR CCM3.

This research was partly supported through the Southeast Regional Center for the National Institute for Global Environmental Change, in Tuscaloosa, Alabama, by the United States Department of Energy under cooperative agreement No. DE-FCO3-90ER61010, and partly by the NASA's Mission to Planet Earth (MTPE) under Contract No. NAS1-18944 from Langley Research Center, Hampton, VA and US EPA's STAR (Science to Achieve Results) grant No. R-825248.

TABLE OF CONTENTS

LIST OF TABLES

LIST OF FIGURES

1. AEROSOL-CLOUD-CLIMATE INTERACTIONS

1.1. Introduction: Statement of the Problem

The effect of aerosol particles on atmospheric solar radiation is not a newly recognized topic. Observations of air molecular interactions with solar radiation, the "blue sky" phenomenon, dates back to ~300 B.C when ancient Chinese philosopher Chuang Tzu (339~295 B.C) described his idea as follows:

"*In the northern darkness there is a fish and his name is Kun. The Kun is so huge that he measures many thousand miles. He changes and becomes a bird whose name is Peng. The back of the Peng also measures many thousand miles across and, when he rises up and flies off, his wings are like clouds all over the sky. When the sea begins to move, this bird journeys to the southern darkness, and the waters are roiled for three thousand miles. He beats the whirlwind and rises ninety thousand miles, setting off on the sixth month gale, wavering heat, bits of dust, living things blown about by the wind—the sky looks very blue. Is that its real color, or is it because it is so far away and has no end*?" (Liou, 1980)

Benjamin Franklin, who theorized that the awful haze or dry fog that hung over Paris in the latter part of 1783 was caused by an eruption in Iceland, is usually credited with first making the association between volcanic aerosols and climate or weather. Aerosol particles can affect climate by two mechanisms: a physical mechanism (through aerosol-cloud-climate interactions) and a chemical mechanism (through the influence of aerosols on greenhouse gases and aerosols themselves by heterogeneous atmospheric chemical reactions). In the physical mechanism, aerosol-cloud-climate interactions involve three interactions as depicted in Figure 1.1, e.g. cloud-climate (radiation) interaction, aerosol-climate (radiation) interaction, and aerosol-cloud interaction. These interactions are obviously nonlinear. Through these three interactions, atmospheric aerosols can influence the Earth's radiation balance both directly and indirectly. The direct aerosol effect refers to the perturbation of the earth's radiative budget due to scattering and absorption of incoming solar (shortwave) radiation and terrestrial outgoing (longwave, IR) radiation by atmospheric aerosols (Andreae, 1995; Kiehl, J.T. and B.P. Briegleb,

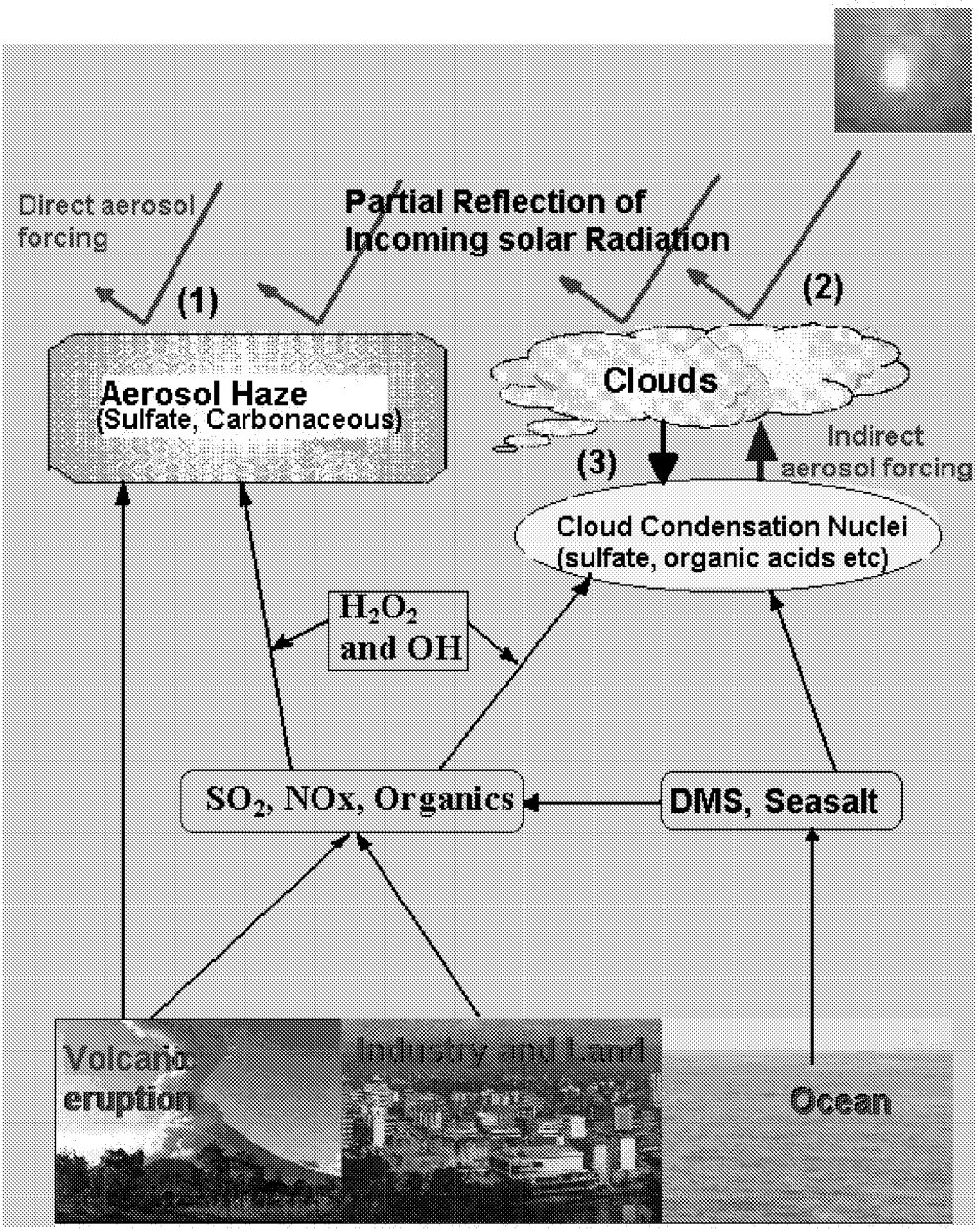

Figure 1.1. Aerosol-Cloud-Climate interaction
(1) Aerosol-Radiation (Climate) interaction
(2) Cloud-Radiation (Climate) interaction
(3) Aerosol-Cloud interaction

1993; Penner et al., 1994; Saxena et al., 1997; Saxena and Yu, 1998). The indirect (also called cloud-mediated) aerosol effect refers to the influence of aerosols on cloud radiative properties and lifetimes of clouds (mainly in the troposphere) through their role as cloud condensation nuclei (CCN) (Charlson et al., 1992; Penner et al., 1994). The indirect aerosol effect is often referred to as the Twomey effect. Twomey (1977) first outlined the potential role of aerosols on cloud droplets and cloud radiative properties. The excellent reviews and discussions of mechanism by which aerosols affect climate have been presented in three books (Hobbs, 1993; Charlson and Heintzenberg, 1995; NRC, 1996).

Current estimates of the global, annually averaged, radiative forcing by anthropogenic aerosols (sulfate, organics, soot, mineral dusts, and biomass smokes) range from about –0.3 to –1.5 W m^{-2}, with an uncertainty factor of about 2 (IPCC, 1995; Charlson et al., 1992; Kiehl and Briegleb, 1993; Penner et al., 1994). It has been suggested that the cooling effect of the aerosols dominates over the warming effects caused by light absorption and that the combined effects of anthropogenic aerosols from the combustion of fossil fuels and biomass may be comparable in magnitude but opposite in sign to the warming effect of the greenhouse gases (2.3±0.35 W m^{-2}) (Charlson et al., 1992; Kiehl and Briegleb, 1993; Penner et al., 1994).

Eastern China, south central Europe and eastern US have been recognized as regions where the effect of anthropogenic aerosols supersedes that of man-made greenhouse gases (GHGs) and manifests itself in terms of cooling of the surface-air temperature (IPCC, 1995; NRC, 1996; Kiehl and Briegleb, 1993). The uncertainty in the magnitude of the estimated direct and indirect cooling effect of aerosols is a major barrier for a reliable prediction of climate change on the scale of a decade and longer (Andreae, 1995; Schwartz and Andreae, 1996). Despite the important influence of aerosols on climate, there are relatively few observational studies that can be used reliably and confidently to support the estimates of the magnitude of radiative forcing (Penner et al., 1994). Saxena et al. (1996) have analyzed the presence of indirect forcing due to sulfate aerosols in the southeastern US. They found that the short-wave albedo of clouds determined from *in situ* measurements increases with a decrease in the cloud water pH, which in turn was

largely affected by the sulfate concentration in the cloud forming air masses and was taken as a surrogate indicator of the concentration of cloud-active particulate matter. These findings indicated that the anthropogenic sulfur emissions are capable of altering the reflectivity of thin, continental clouds in the southeastern US. The model calculation of Boucher and Lohman (1995) further confirmed the existence of an indirect aerosol forcing of more than –4 W m^{-2} in the southeastern US. The quantitative estimate of direct and cloud-mediated radiative aerosol forcing in the southeastern U.S. is not available yet.

For aerosol properties pertinent to the direct aerosol radiative forcing, three parameters, aerosol optical depth (τ), single scatter albedo (ϖ), and asymmetry factor (g), are considered to be the basic parameters needed to describe the direct interaction of aerosol particles with solar radiation (Penner et al., 1994; Charlson et al., 1992). Since the aerosol radiative forcing is determined by the aerosols within the whole atmospheric column instead of the aerosols contained in the surface layer, it will be very useful to obtain the average aerosol radiative properties for the whole atmospheric column through a column-closure experiment. Such a column-closure experiment may be used to relate the transmitted and reflected radiation at a number of wavelengths to the optical properties and total abundance of the aerosols in the column. Several aerosol characterization experiments (ACE) such as ACE-1 in the remote Southern Ocean, Tropospheric Aerosol Radiative Forcing Observation Experiment (TARFOX) off the eastern coast of North America, and ACE-2 in European outflow have been conducted to assess aerosol effects in major regions of the global (Stowe et al., 1995). The upcoming ACE-Asia in the 2000-2004 timeframe aims to accurately quantify the direct and indirect effect of aerosols on the radiative forcing of climate in the Asian-Pacific region.

The response of regional climate to aerosol radiative forcing and greenhouse gases is different. Since the long-lived and uniformly-distributed greenhouse gases essentially act in the infrared spectral range, they would produce an increases of both maximum and minimum temperatures (longwave forcing). In contrast, the enhanced backscattering of incoming solar radiation due to the increase in aerosol loading and low cloud amount would result in a decrease of the maximum daytime temperature (shortwave forcing), and

the enhanced absorption and backscattering of outgoing terrestrial longwave radiation would result in an increase of minimum nighttime temperature (longwave forcing) although the latter mechanism during the daytime does not shut down (Karl et al., 1993). Longwave radiative forcing of both greenhouse gases and aerosols (especially when aerosol particles contain high concentration of absorbing components such as black carbon (BC)) would result in increases of both minimum and maximum temperatures. An important question to answer is: Do the regional temperature change patterns in the southeastern US and eastern China show this fingerprint of aerosol forcing? The eruption of Mt. Pinatubo in the Philippines in June, 1991, which injected massive amounts of dust and gases into the lower stratosphere and upper troposphere, provides a natural test for the effect of aerosol forcing on climate. What are the responses of the regional temperature change patterns in the southeastern US and eastern China to this natural volcanic aerosol? All these critical questions need to be answered for any climate study in the southeastern US and eastern China.

Another important issue with respect to the aerosol indirect radiative forcing regards the origin and nature of cloud condensation nuclei (CCN) in the troposphere. As mentioned above, CCN can strongly modulate cloud microstructure and hence the radiative properties of clouds and affect climate (Charlson et al., 1987; Twomey, 1977). Ghan et al (1990) showed that an increase in CCN number concentration, by as much as a factor of four, would cause an global albedo increase of ~1.7%. The sources and chemical composition of CCN are still under debate. Novakov and Penner (1993) indicated that ~37 % of CCN number concentration measured at the marine site could be accounted for by sulfates and the remaining 63 % by organic aerosols. Measurement of Hegg et al. (1995) showed that most of CCN over the northeastern Atlantic coast of the United States were not sulfates. Saxena et al. (1995) found that organics could enhance water absorption by inorganics at a non-urban location (Grand Canyon). It is in order here to ask: What are the chemical components of organic aerosols that act as CCN and which alter the hygroscopic behavior of atmospheric particles? Presently the answer to this question is not available. Ion Chromatography (IC) analysis shows that the most

frequently observed organic species in the atmosphere are low molecular weight monocarboxylic and dicarboxylic acids, with monocarboxylic acids much more abundant than dicarboxylic acids. Of monocarboxylic acids, formic and acetic acids are the dominant species, which have most frequently been observed in precipitation (Keene and Galloway, 1988; Yu et al., 1988, 1991, 1992, 1998), cloudwater and fogwater (Yu et al., 1991; Weathers et al., 1986), gaseous phase (Dawson et al., 1980; Yu et al., 1990), and in aerosols (Andreae et al., 1988). Since organic acids are ubiquitously present in the troposphere (Keene et al., 1995; Talbot et al., 1995, Yu et al., 1998), it is of interest to analyze the ability of organic acids to act as CCN and their contribution to the formation of CCN in the troposphere.

Another important source of CCN is clouds themselves. Hegg et al. (1990) thought that clouds might be a necessary precursor to the development of significant concentrations of CCN in the marine atmosphere. A number of laboratory and field studies (Twomey and McMaster, 1955; Hegg et al., 1990; Radke and Hobbs, 1991, Hegg and Hobbs, 1992; Saxena, 1996) have reported an enhancement (relative to the one upon which the droplets were formed) in the number of CCN in the vicinity of cloud droplets in the subsaturated environs. Therefore, the process of cloud formation could be a source of CCN, especially under special atmospheric conditions. More evidence with respect to this CCN enhancement phenomenon on the Mt. Mitchell is presented.

1.2. Objectives of this study

The primary objectives of this study are (1) To search for regional fingerprints of aerosol radiative forcing in the southeastern US and eastern China; (2) To quantitatively assess direct radiative forcing due to aerosols on the basis of intensive observations of relevant microphysical and radiative properties of aerosols and computation using Column Radiation Model (CRM) of NCAR Community Climate Model (CCM3) in the southeastern US; and (3) To analyze the sources of organic CCN, present the measurement of CCN concentration at Palmer station, Antarctica, and episodes of

enhanced CCN concentrations near cloud boundaries on Mt. Mitchell in the southeastern US.

The results of this study will provide an improved assessment of the influence of anthropogenic aerosols on the regional climate and will contribute to the upcoming IPCC assessment of the aerosol impact on regional climate. The text of this study is divided in two parts and described in the following chapters:

I) Part I contains the results of searching for the fingerprints of aerosol forcing in eastern China and southeastern US, and the study of direct aerosol forcing in the southeastern US.

1) Chapter 2 presents the search for the regional fingerprint of aerosol radiative forcing in the southeastern US on the basis of analysis of climate data at 52 stations during 1949-1994, and stratospheric volcanic aerosols measured by the Stratospheric Aerosol and Gases Experiment (SAGE II) satellite during 1984-1998.
2) Chapter 3 describes the results of the analysis of climate data at 72 stations of 10 provinces in eastern China during 1951-1994 (44 years) with special focus on the year following the Mt. Pinatubo eruption in June 1991. The analysis is aimed at detecting the signature of a regional aerosol radiative forcing on the regional climate in eastern China.
3) Chapter 4 presents a method to accurately calculate the refractive index of aerosol particles with the known chemical composition, and evaluates the sensitivity of aerosol radiative properties and radiative transmission in the visible range to refractive index, size distribution, and relative humidity under some assumptions with Mie code and radiative transfer model code.
4) Chapter 5 investigates the characteristics of aerosol optical depth (AOD) and diffuse-to-direct solar irradiance ratio (DDR) as a function of air mass type, retrieve columnar aerosol size distribution on the basis of the AOD at the three operational wavelengths (415, 500, and 673 nm), and determines aerosol radiative properties needed to compute direct aerosol forcing using the a mathematically unique procedure involving

a Mie code and a radiative transfer code in conjunction with measurements of AOD, DDR and the retrieved columnar size distribution.

5) Chapter 6 uses NCAR CCM3 CRM to calculate the direct shortwave aerosol forcing in the southeastern US on the basis of field measurement and retrieval of aerosol radiative properties in Chapter 5.

II) Part II contains the results with respect to the source analysis of organic CCN, the measurements of CCN concentrations at Palmer station, Antarctica, and near cloud boundaries on Mt. Mitchell in the southeastern US.

1) Chapter 7 presents the measurement of the real-time CCN activation spectrum at a representative natural Southern Hemisphere remote marine site, Palmer station, Antarctica, during the period of 21 January to 4 February 1994.
2) Chapter 8 reviews the current state of knowledge of water-soluble organic acids (mainly formic, acetic, pyruvic and oxalic acids) in the atmosphere, analyzes the extent to which organic acids actually act as CCN, and identifies the major unknowns in this field.
3) Chapter 9 presents extensive measurement of CCN and BC concentrations and analyzes episodes of enhanced CCN concentrations near cloud boundaries at a regional representative site in the southeastern US, namely, Mt. Mitchell, North Carolina.
4) Chapter 10 discusses the directions for future work in the field of aerosol-cloud-climate interactions.

1.3. Results of this study

1.3.1. Part I: A study of direct aerosol forcing

It was found that the arithmetic average of the annual mean maximum temperature decreased by -0.28 C, while the minimum temperature increased by 0.09 C at 52 stations

in the southeastern US during 1949-1994 (46 years). Obviously, the warming from the longwave forcing due to both greenhouse gases and aerosols was completely counteracted by the shortwave aerosol forcing in the southeastern US in the past 46 years. The study shows that direct and indirect radiative forcing of both natural (such as the Pinatubo volcanic aerosols) and anthropogenic aerosols (such as those transported from the polluted regions of US) may be responsible for the regional cooling trend in the southeastern US in the past 46 years. The dominant decreasing trend of mean maximum temperature and the dominant increasing trend of mean minimum temperature during periods 1992-94 and 1985-87 relative to that during the period 1988-90 are consistent with the distribution of stratospheric volcanic aerosols and predictions from aerosol radiative forcing in the southeastern US.

In eastern China, a decreasing trend in the summer mean maximum temperature at 72 station during the past 44 years and a two-year cooling trend following the Mt. Pinatubo eruption were found. This effect is similar to our finding in the southeastern US. The rates of change of annual mean daily, maximum, minimum temperatures and diurnal temperature range (DTR) in eastern China were 0.8, -0.2, 1.8, and -2.0 C/100 years respectively, while the rates of change of annual mean daily, maximum, minimum temperatures and DTR in the southeastern US were -0.2, -0.6, 0.2, and -0.8 C/100 years respectively. This comparison indicates that the high increasing rate of annual mean minimum temperature in eastern China results in the slightly warming trend of daily temperature, while the high decreasing rate of annual mean maximum temperature and low increasing rate of annual mean minimum temperature lead to the cooling trend of daily temperature in the southeastern US. A slightly overall warming trend in eastern China is evident; winters have become milder. This finding is explained by hypothesizing that increasing energy usage during the past 44 years has resulted in more coal and biomass burning, thus increasing the emission of absorbing soot and organic aerosols in eastern China. Such emissions, in addition to well-known Asia dust, may be responsible for the winter warming trend in eastern China that we have reported here.

In the evaluation of chemical and size effects, the partial molar refraction method and

the volume-average method were used to calculate the real and imaginary parts of the refractive index of real multi-component aerosols respectively. The result shows that the extinction coefficient is sensitive to the changes in RH, and increase by 70% with RH varying from 0% to 80. The asymmetry factor increases by ~48% when real part varies from 1.40 to 1.65. The single scattering albedo decreases by 24% when the imaginary part changes from –0.005 to –0.1. The extinction coefficients, and asymmetry factor were very sensitive to the size distribution. The radiation transmission is also very sensitive to the change in geometric mean radius and geometric standard deviation. Other factors are not as significant.

The aerosol optical depth (AOD) and diffuse-to-direct solar irradiance ratio (DDR) at three operational wavelengths (415, 500, 673 nm) were determined by using Multi-Filter Rotating Shadowband Radiometers (MFRSR) at two sites (a mountaintop site: Mt. Gibbes, 35.78 ^{0}N, 82.29 ^{0}W, 2006 m MSL; a valley site: Black Mountain, 35.66 ^{0}N, 82.38 ^{0}W, 951 m MSL), which are separated horizontally by 10 km and vertically by 1 km. The characteristics AOD and DDR were determined from the field measurements obtained during 1995. It was found that the representative total AOD values at 500 nm at the valley site for highly polluted (HP), marine (M) and continental (C) air masses were 0.68±0.33, 0.29±0.19 and 0.10± 0.04, respectively. The fact that the ratio of the mean 1 km layer optical depth to total mean optical depth at 500 nm from the valley site was 73% indicates that the major portion of the atmospheric aerosol was located in the lowest 1 km surface boundary layer (SBL). There was a significant linear correlation between the DDR and total AOD at both the sites. A simple, fast and operative search-graph method was used to retrieve the columnar size distribution (number concentration N, effective radius r_{eff} and geometric standard deviation σ_g) from the optical depth observations at the three operational wavelengths. The ground albedo, single scattering albedo and imaginary part of the refractive index are calculated using a mathematically unique procedure involving a Mie code and a radiative transfer code in conjunction with the retrieved aerosol size distribution, AOD, and DDR. It was found that N, r_{eff} and σ_g were

in the range of 1.0E1 to 1.7E4 cm^{-3}, 0.09 to 0.68 μm and 1.12 to 2.95 respectively. The asymmetry factor and single scattering albedo were in the ranges of 0.63 to 0.75 and 0.74 to 0.97 respectively. The ground albedo over the forested terrain and the imaginary part of refractive index were found to be in the range of 0.06 to 0.29 and 0.005 to 0.051 respectively.

On the basis of these aerosol radiative properties and CRM calculation, it was found that the cloud-free instantaneous ADRF was –9.2 to 30.2, -14 to –23 and –55 to 185.7 W m^{-2} for continental, marine and polluted air masses respectively, on the basis of measurement in the morning. The average cloud-free 24-hour ADRF was estimated to be -13±8, -8±3, -33±16 W m^{-2} for marine, continental, and polluted air masses respectively. On the assumption that the fractional coverage of clouds is 0.61, the mean ADRF values were -5±3, -3±1 and -13±6 W m^{-2} for marine, continental and polluted air masses respectively, and the annual mean ADRF is 7±2 W m^{-2} in the southeastern US.

In summary, a fingerprint of aerosol radiative forcing has been detected for the climate change in both eastern China and southeastern US. This forcing has been playing an underlying role in reducing the warming rate of the temperature in both regions. Both anthropogenic aerosols, mainly transported from the Northwest, and natural aerosols, such as those injected due to volcanic eruption, result in a high rate of decrease in mean maximum temperature and lead to a slight cooling trend in the southeastern US. The study of direct aerosol forcing for the southeastern US indicates that the regional negative forcing due to aerosols is of greater magnitude than is predicted by models of other investigators, especially for polluted air masses. Our results also confirm the calculation of Hansen et al. (1995), who show that the observed changes of the maximum and minimum temperature can only be explained by the combination of a negative forcing due to aerosols with the known globally-distributed forcing due to greenhouse gases.

1.3.2. Part II: A study of cloud condensation nuclei (CCN)

The review with respect to the current knowledge of organic acids shows that aerosol

formate and acetate concentrations range from 0.02 to 5.3 nmol/m^3 and from 0.03 to 12.4 nmol/m^3 respectively, and that between 34% to 77% of formate and between 21% to 66% of acetate are present in the fine fraction of aerosols. It is found that although most (98-99%) of these volatile organic acids are present in the gas phase, their concentrations in the aerosol particles are sufficient to make themselves a good candidate for CCN. The physical and chemical properties of aerosol organic salts in the atmosphere are in agreement with those of CCN. The results also show that organic acids might make an important contribution to the formation of CCN in some special sources such as vegetation emissions and biomass-burning. It is hypothesized that organic acids are at least one of the primary sources of CCN in the atmosphere due to their ubiquitous presence in the troposphere, especially over the continental forested areas. Thus, organic acids are expected to contribute significantly to the estimates of indirect forcing due to aerosols.

The results of our measurements at Palmer Station of Antarctica shows that the daily average CCN concentrations at 0.3% and 1% supersaturations ranged from 0.3 to 160 cm^{-3} and from 4 to 168 cm^{-3}, respectively, during the period from 17 January to 26 February, 1994. The measurement of water soluble dicarboxylic acids in the Antarctic aerosols showed that oxalic (C_2) or succinic (C_4) acid was the dominant diacid species, followed by azelaic (C_9) and malomic (C_3) acids as indicated by other investigators. It is expected that organic acids in the Antarctic atmospheric aerosols would have some contribution to the formation of CCN in the Antarctic atmosphere.

New evidence for substantial and definitive CCN (cloud condensation nuclei) enhancement near and within cloud has been observed at Mt. Mitchell, North Carolina. The measurements used in this study were obtained during 1996 and 1997. The results show that the average monthly CCN concentrations ranged from 152 to 937 cm^{-3} (average: 460±217 cm^{-3}), 107 to 1006 cm^{-3} (average: 386±286 cm^{-3}), 124 to 548 cm^{-3} (average: 429±228 cm^{-3}) and 66 to 326 cm^{-3} (average: 238±134 cm^{-3}) for in-cloud, overcast, clear and rainy conditions, respectively. The average monthly CCN

concentrations ranged from 261 to 1367 cm^{-3}, 63 to 377 cm^{-3} and 66 to 326 cm^{-3} for polluted, continental and marine air masses, respectively. The typical CCN spectra show that there were a lot of small CCN produced and the ion concentrations (especially H^+ and SO_4^{2-}) were very high during the CCN enhancement period. It also indicates that the meteorological conditions (relative humidity and temperature) were favorable for H_2SO_4 nucleation during the CCN enhancement period on the basis of the classic nucleation theory. The significantly positive correlation between black carbon (BC) and CCN at 1% supersaturation indicates that a percentage of the BC measured at the site may be in the form of an internal mixture and participated in the formation of CCN.

In summary, organic acids or salts have the same activity as inorganic acids or salts, they will have the same impact on CCN activity and can be intrinsically effective CCN. The high sulfate concentration in cloud water and the favorable meteorological conditions for the nucleation on the basis of classic nucleation theory support the hypothesis that the very active photochemical reaction in both inside cloud water droplets and the space surrounding cloud droplets, and the following nucleation burst might be mainly responsible for the CCN enhancement near and within clouds.

1.4. Importance of this study

Direct greenhouse warming has been estimated with a fairly high level of confidence, while confidence level of aerosol cooling is still poorly constrained. An important challenge to the research effort on global or regional climate change, for the purpose of making policy decisions, will be the early detection and quantification of climate changes caused by human activity. One of the greatest uncertainties in climate forcing is that due to tropospheric aerosols (Charlson et al., 1992; IPCC, 1995; Penner et al., 1994). The modeling study of the latest IPCC has been subsequently substantiated by our analysis of the temperature records in eastern China and southeastern US. Our results show that the climate change patterns in both eastern China and southeastern US indicate the fingerprints of the aerosol radiative forcing during the past years. Our regional estimation

of aerosol forcing on the basis of direct observation would help in reducing the uncertainty in the quantification of the effect of aerosol forcing on climate in the southeastern US. In addition, the analyses of the data sets will provide an improvement in our basic understanding of the regional environment. The study also provides a case study of possible effect of aerosol radiative forcing on climate change for two of the three most important aerosol climatological regions (e.g. eastern China, eastern US and Europe). The results of this study will provide an improved assessment of the influence of anthropogenic aerosols on the regional climate in the southeastern US and will contribute to the upcoming IPCC assessment of the aerosol impact on regional climate. Our results here also support the idea that two methods can be used to reduce the effect of greenhouse gases on climate warming, e.g. introducing aerosols into the stratosphere to act as a direct reflector of solar radiation, and introducing aerosols into the troposphere to directly reflect solar radiation or increase the reflectivity of cloud, as suggested by COSEPUP (Committee on Science, Engineers, and Public Policy) (1992). Note that it is necessary to have low absorptive characteristics of the aerosol for the aerosol cooling effect, which can be achieved by reducing the soot content associated with fossil-fuel burning during emissions.

The recent increase in anthropogenic aerosol emissions can partially offset some of the increase in greenhouse radiative forcing due to the elevated concentrations of greenhouse gases. This may slow the rate of projected global warming during the next century. Since major sources of GHGs and aerosols are identical such as fossil fuel combustion, biomass burning etc, any policy decisions to limit the emissions of GHGs could have severe *short-term impact on the regional climate.* Clearly, both the cooling effects of aerosols and the warming caused by greenhouse gases must be taken into account in realistic climate models and implementing prudent industrial policies. This study will help improve understanding of climate system to point where the consequences of these actions to contravene the greenhouse warming may be predicted with reasonable confidence.

1.5. References:

Andreae, M.O., Climatic effects of changing atmospheric aerosol levels, in *World Survey of Climatology*, 16, Future climates of the world, edited by A. Henderson-Sellers, Elsevier, Amsterdam, 1995

Andreae, M.O., Talbot, R.W., Andreae, T.W. and Harriss, R.C., 1988a. Formic and acetic acids over the central Amazon region, Brazil. 1. Dry season. J. Geophys. Res., 93, 1616-1624.

Boucher, O. and U. Lohman, The sulfate-CCN-cloud albedo effect: A sensitivity study with two general circulation model. Tellus, 47B, 281-300, 1995.

Charlson, R.J., Langner, J., Rodhe, H., Leovy, C.B., and S.G. Warren, Perturbation of the northern hemisphere radiative balance by backscattering from anthropogenic sulfate aerosols. Tellus, 43AB, 152-163, 1991.

Charlson R. J., , S.E. Schwartz, J. M. Hales, R. D. Cess, J. A. Coakley, J. E. Hansen, and D. J. Hofmann, Climate forcing by anthropogenic aerosols. *Science*. 225, 423-430,1992.

Charlson, R.J., Lovelock, J.E., Andrea, M.O. and Warren, S.G., 1987. Oceanic phytoplankton, atmospheric sulfur, cloud albedo and climate. Nature. 326: 655-661.

Charlson, R.J., and Heintzenberg, J. (ed.) 1995. Aerosol forcing of climate. John Wiley & Sons.

COSEPUP (Committee on Science, Engineers, and Public Policy), Policy implications of greenhouse warming, mitigation, adaptation, and the science base. Panel on Policy Implications of Greenhouse Warming, National Academy of Sciences, National Academy Press, pp 918, 1992.

Ghan, S.J., K.E. Taylor, and J.E. Penner, Model test of the CCN-cloud albedo climate forcing. *Gephys. Res. Lett.*, 17, 607-610, 1990.

Hegg, D.H., Radke, L.F. and Hobbs, P.V., 1990. Particle production associated with marine cloud. J. Geophys. Res., 95: 917-926.

Hegg, D.H. and Hobbs, P.V., 1992. Cloud concentration nuclei in the marine atmosphere:

A review, In Nucleation and Atmospheric aerosols, edited by N. Fukuta and P. Wagner, 181-191.

Hegg, D.H., Hobbs, P.V., Ferek, R.J. and Waggoner, A.P., Measurements of some aerosol properties relevant to radiative forcing on the East Coast of the United States. *J. Appl. Met.*, 34: 2306-2315, 1995.

Hobbs, P.V. (ed.) 1993. Aerosol-Cloud-Climate Interactions, Academic Press, Inc.

IPCC, Climatic change 1995: Radiative forcing of climate and an evaluation of the IPCC 1992 emission scenarios. J.T. Houghton et al. (Eds). Cambridge University Press, Cambridge, UK, 1995.

Keene, W.C. and Galloway, J.N., 1988. The biogeochemical cycling of formic and acetic acids through the troposphere: An overview of current understanding. Tellus, 40B: 322-334.

Keene, W.C., et al., 1995. Carboxylic acids in clouds at a high-elevation forested site in central Virginia, J. Geophys. Res., 100: 9321-9334.

Kiehl, J.T. and B.P. Briegleb, The relative role of sulfate aerosols and greenhouse gases in climate forcing. Science. 260, 311-314, 1993.

Liou K.-N. 1980. An Introduction to Atmospheric Radiation, Academic Press, New York.

National Research Council (NRC), Aerosol radiative forcing and climate change, National Academy Press, Washington, D.C., 1996.

Novakov, T. and Penner, J.E., 1993. Large contribution of organic aerosols to cloud-condensation-nuclei concentrations. Nature. 365: 823-826.

Penner J.E., R. J. Charlson, J. M. Hales, N. S. Laulainen, R. Leifer, T. Novakov, J. Ogren, L. F. Radke, S. E. Schwartz, and L. Travis, Quantifying and minimizing uncertainty of climate forcing by anthropogenic aerosols. *Bull. Amer. Meteorol. Soc.* 75, 375-400, 1994.

Radke, L.F., and P.V. Hobbs, Humidity and particle fields around some small cumulus clouds. J. Atmos. Sci., 48, 1190-1195, 1991.

Rogge, W.F., Mazurek, M.A., Hildemann, L.M., Cass, G.R. and Simoneit, B.R.T., 1993. Quantification of urban organic aerosols at a molecular level: Identification,

abundance and seasonal variation. Atmos. Environ., 27:1309-1330.

Saxena, V. K. 1996 Bursts of cloud condensation nuclei (CCN) by dissipating clouds at Palmer Station, Antarctica. *Geophys. Res. Lett.*, 23, 69-72, 1996.

Saxena, V.K., and Shaocai. Yu, Searching for a regional fingerprint of aerosol radiative forcing in the southeastern US, *Geophys. Res. Lett., 25,* 2833-2836, 1998.

Saxena V.K., Shaocai. Yu, and J. Anderson, Impact of stratospheric volcanic aerosols on climate: evidence for aerosol shortwave and longwave forcing in the southeastern US. *Atmos. Environ,* 31:4211-4221, 1997

Saxena, V.K., Durkee, P.A., Menon, S., Anderson, J., Burns, K.L and K.E. Nielsen, Physico-chemical measurements to investigate regional cloud-climate feedback mechanisms. Atmos. Environ., 30, 1573-1579, 1996.

Saxena, P., Hildmann, L.M., McMurry, P.H. and Seinfeld, J.H., Organics alter hygroscopic behavior of atmospheric particles. J. Geophys.Res., 100:18755-18770, 1995

Schwartz S.E. and M. O. Andreae, Uncertainty in climate change caused by aerosols. *Science*. 272, 1121-1122, 1996

Stowe, L.L., Hobbs, P.V., and P. Russell, Plans for the implementation of the tropospheric aerosol radiative forcing observational experiment. Paper MB52A-12, p. 308 Abstracts for Week B, XXI Assembly IUGG, Boulder, Colorado., 1995

Twomey, S., and K.N. McMaster, The production of condensation nuclei by crystallizing salt particles. Tellus, 7, 458-461, 1955.

Twomey, S., Atmospheric aerosols, Elsevier, Amsterdam, Oxford and New York, 1977.

Yu, Shaocai., Bi, mutian., and Lin, Xin., Primary investigation about natural sources of organic acids in the atmosphere and rain. Atmos. Environ., 4: 36-40 (in Chinese), 1988.

Yu, Shaocai., Bi, Mutian., and Lin, Xin., An investigation about the determination of formic and acetic acids in the atmosphere. Ch. J. Environ. Sci., 11(3): 43-48, 1990.

Yu, Shaocai., Bi, Mutian., Lin, Xin., Yao, Rongkui., and Tang, Xiaoyan., Organic acids in precipitation from Baiyun Mountain, Guanzhou and in cloudwater from Miaoer

Mountain, Guangxi, Acta Sci. Circumstantiae., 11(1): 25-30, 1991.

Yu, Shaocai., Chen, Xiaojian., and Chen, Zemian., Organic acids in the oceanic acid rain of Xiamen Island. Shanghai Environ. Sci., 11(12): 30-32, 1992.

Yu, Shaocai., Gao, Chentie., Cheng , Zhemian., Cheng, Xiaojian., Cheng, Shuentian., Xiao, Jian. and Ye, Wenxian., An analysis of chemical composition of different rain types in "Minnan Golden Triangle" region in the southeastern coast of China. Atmos. Res., 47-48: 245-269, 1998.

PART I: A STUDY OF AEROSOL DIRECT RADIATIVE FORCING

2. SEARCHING FOR A REGIONAL FINGERPRINT OF AEROSOL RADIATIVE FORCING IN THE SOUTHEASTERN US

V. K. Saxena and Shaocai Yu

North Carolina State University, Raleigh, NC

Geophysical Research Letters, 25, 2833-2836, 1998

2.1. Abstract

Although aerosols have long been considered to exert a cooling influence on the regional climate due to direct and indirect radiative forcing, persuasive evidence of the response to this forcing has been lacking. Here, we analyze the regional patterns of climate change in the southeast US during the period 1949-94 to search for a fingerprint of aerosol radiative forcing. The results show that direct and indirect radiative forcing of both natural (such as Pinatubo volcanic aerosols) and anthropogenic aerosols (such as those transported from the polluted regions of US) may be responsible for the regional cooling trend in the Southeast during the past 46 years. Lack of availability of long term measurements precludes a rigorous cause-and-effect analysis. Circumstantial evidence presented here amply justifies immediate establishment of a network of measurements of aerosol optical depth and cloud reflectivity in the southeastern US.

2.2. Introduction

The southeastern US has been recognized (IPCC, 1995) as a region where the effect of anthropogenic aerosols (NRC, 1996) supersedes that of man-made greenhouse gases (GHGs) and manifests itself in terms of cooling of the surface-air temperature (Boucher and Lohmann, 1995). The uncertainty in the magnitude of the estimated direct and cloud-mediated (also called the indirect effect) cooling effect of aerosols (Andreae, 1995) is a major barrier for a reliable *prediction of climate change on the scale of a decade and longer*. Any policy decisions to limit the emissions of GHGs could have severe *short-term impact on the regional climate* since major sources of GHGs and aerosols are identical such as fossil fuel combustion, biomass burning etc.

Despite the important influence of aerosols on climate there are relatively few observational studies that can be used reliably and confidently to support the estimates of the magnitude of radiative forcing (Schwartz, 1996). The box-model description for direct forcing by Charlson et al. (1991) can be a good first order estimate of the magnitude of forcing for an optically thin atmosphere, if the forcing is linear to aerosol loading. Quantification of the indirect forcing is still under debate due to the large uncertainty in the relationship between aerosol number distribution and anthropogenic pollution. The region most affected by the negative radiative forcing due to sulfates has been predicted by modeling results to be in the *southeastern US* (Boucher and Lohmann, 1995). In this paper, we present the results of our research for a fingerprint of direct and cloud-mediated forcing due to aerosols in the southeastern US based on the changes of climatological variables during 1949-1994.

2.3. Methodology and Database

2.3.1. Database

Monthly, seasonal, and yearly climate data on the duration of growing season (DGS, i.e., the duration between the last spring and first fall freezes), mean maximum, minimum and daily temperatures, total precipitation, and diurnal temperature range (DTR, the difference between maximum and minimum temperature) at 52 stations in the southeastern US used for this study were obtained from the Office of the N.C. State Climatologist. The period covered here was from December 1949 to December 1994 (46 years). The criteria for selecting the stations in a climate zone were based on the following considerations: (1) stations had a good climatic data record; (2) there was a good geographic distribution; (3) only one station was chosen for each climate zone (or division). A map of the southeastern US showing the climate zones and stations used in each climate zone is presented in Fig. 2.1. The time series autoregression model in the Statistical Analysis System (SAS) was used to find whether the changing trend is significant at the 0.05 level.

2.3.2. Methodology

To search the possible fingerprint of aerosol forcing in the Southeast, we compare the change trend of maximum and minimum temperatures instead of daily temperature with the predication from aerosol forcing. Since the long-lived and uniform-distributed GHGs essentially act in the infrared spectral range, GHGs would result in the increases of both maximum and minimum temperatures (longwave forcing). In contrast, the enhanced backscattering of incoming solar radiation due to the increase in aerosol loading and low cloud amount would result in a decrease of the maximum daytime temperature (shortwave forcing), and the enhanced

absorption and backscattering of outgoing terrestrial longwave radiation due to the increase in aerosol loading would result in an increase of minimum nighttime temperature (longwave forcing) although the latter mechanism during the daytime does not shut down (Karl et al., 1993). To study if direct and indirect aerosol forcing exist in the Southeast, field experiments were established to study the aerosol-cloud-climate interaction at a regionally representative site, namely, Mt. Mitchell (35.78 N, 82.29 W, elevation 2006 m), and a site located in an adjacent valley (Black Mountain, 35.66 N, 82.38 W, elevation 951 m) in the Southeast (Saxena et al., 1996).

To study the impact of stratospheric volcanic aerosols on the climate change, the monthly average optical depth of stratospheric volcanic aerosols in a unit column between 15-30 km over the areas between latitude 30 and 40 N and longitude 75 and 90 W in the southeastern US is calculated as follows on the basis of the Stratospheric Aerosol and Gases Experiment (SAGE) II satellite extinction measurement:

$$\tau_\lambda = \int_{z_1}^{z_2} \beta_\lambda (z)\, dz$$

where $\beta\lambda$ is the extinction coefficient of particles at wavelength λ. A detailed description of the SAGE II instrument is given by McCormick (1987).

2.4. Results and Discussion

2.4.1. Regional Patterns of Climate Change in the Southeast

One of the ecological consequences of the greenhouse warming is a change in DGS. The results indicate that DGS became longer at 61.5% stations, and tended to begin earlier at 55.8% stations, and tended to end later at 63.5% stations during the period 1949-94. The increasing trend of DGS at 13% stations was statistically significant. The arithmetic average of DGS at 52 stations became longer by 1.7 days and tended to begin earlier by 0.8 days and end later by 0.9 days during the past 46 years as shown in Fig. 2.2. Is this evidence of a warming

trend in the southeastern US? Verdin (1990) showed that DGS was longer during the cooler 1979-1988 decade compared with the warmer 1931-1940 decade in Scandinavia. He explained that the spring (when the start date of growing season occurs) and fall (when the end date of growing season occurs) might be warmer, while the average temperature conditions might remain unchanged. So, it is difficult to conclude if the climate becomes warmer or cooler only according to the changes in the DGS.

In many climate impact studies, it is generally assumed that the mean surface-air daily temperature will increase due to enhanced greenhouse effect. The annual mean daily temperature indicated the decreasing trend at 51.9% stations and the statistically significant decreasing trend at 13.5% stations (see Table 2.1). The arithmetic average of annual mean daily temperature at 52 stations decreased by -0.09 C during the past 46 years as shown in Fig. 2.2. *This indicates that there was a slight cooling trend instead of a warming trend during the past 46 years.* This is consistent with Dettinger et al. (1995) who showed a cooling trend on the basis of monthly mean surface-air temperature data during the period 1910-87. For the seasonal trend, the seasonal mean daily temperature in winter (Dec-Feb) showed a decreasing trend at 86.5% stations, and significant decreasing trend at 9.6% stations, while the fall (Sept-Nov) and summer (Jun-Aug) mean daily temperatures showed an increasing trend at 80.8% (significant at 13.5% stations) and 57.7% stations (significant at 21.2% stations), respectively. *The winter became much colder, and the summer and fall became much warmer during the period 1949-1994 in the Southeast.* The stations showing decreasing trend of winter mean daily temperatures are depicted in Figure 2.1.

As can be seen from Table 2.1, the annual total precipitation indicated the increasing trend at 82.7% stations, and the statistically significant increasing trend at 9.6% stations. The arithmetic average of annual total precipitation at 52 stations increased by 81 mm during the past 46 years (See Fig. 2.2). A close inspection of Table 2.1 revealed that the warming trend of the fall mean daily temperature was consistent with increasing trend of fall total precipitation. Table 2.1 shows that the annual, winter, and summer mean maximum temperature indicated

decreasing trends at 67%, 90.4%, and 63.5% stations, respectively. The decreasing trend of the annual mean maximum temperature at 15.4% stations was statistically significant. The arithmetic average of the annual mean maximum temperature at 52 stations decreased by -0.28 C during the past 46 years. The annual, spring, summer and fall mean minimum temperature indicated the increasing trend at 59.1%, 51.9%, 69.2% and 82.7% stations, respectively. The arithmetic average of the annual mean minimum temperature increased by 0.09 C during the past 46 years as indicated in Fig. 2.2. The annual, winter, summer and fall mean DTR indicated the decreasing trend at 69.2%, 67.3%, 76.9% and 75.0% stations, respectively (Table 2.1). The arithmetic average of the annual mean DTR decreased by -0.37 C during the past 46 years as shown in Fig. 2.2. The results of this study confirm the results of Karl et al. (1993).

2.4.2. Fingerprints of Aerosol Radiative Forcing

Several factors were suggested as possible mechanisms responsible for the above climatological signals in the Southeast, including regional and large-scale climate forcings. The following findings support our hypothesis that the slight cooling trend in the Southeast mainly results from counteracting the greenhouse warming by the direct and cloud-mediated forcing of aerosols. The preceding analysis about the climate change in the Southeast shows that the arithmetic average of the annual mean maximum temperature at 52 stations decreased by -0.28 C while the minimum temperature increased by 0.09 C during the past 46 years (see Fig. 2.2). Obviously, the warming from the longwave forcing due to both greenhouse gases and aerosols was completely counteracted by the shortwave aerosol forcing because the daily temperature is equal to the average of maximum and minimum temperature. Our results are very different from that of Karl et al. (1993), who found that the average minimum temperature increased 0.84 C while the average maximum temperature increased by 0.28 C on the basis of data covering about 50% of Northern Hemisphere and 10% of Southern Hemisphere for the period 1951-90.

The question here is whether the direct and cloud-mediated forcings due to aerosols exist in the Southeast. Saxena et al. (1996) have shown the presence of indirect or cloud-mediated forcing due to sulfate aerosols in the Southeast. They found that the short-wave albedo of clouds determined from in situ measurements increases with a decrease in the cloud water pH which was largely affected by the sulfate concentration in the cloud forming air masses. These findings indicated that the anthropogenic sulfur emissions are capable of altering the reflectivity of thin, continental clouds in the Southeast. The model calculation of Boucher and Lohman (1995) further confirmed the existence of an indirect aerosol forcing of lower than -4 W m^{-2} in the Southeast.

The study of Husar et al. (1978) has found a general decrease in visibility in the eastern US since 1948. The visibility degradation is probably related to an increase or change in the composition of atmospheric aerosol concentrations. The model calculation of Kiehl and Briegleb (1993) showed that direct negative forcing due to aerosol exceeds the positive forcing by the greenhouse gases and results in negative net forcing in the eastern US. Charlson et al. (1991) used a box model to estimate that anthropogenic sulfate aerosols produced a mean forcing of -2 W m^{-2} in the eastern US. Note that the total mean optical depth used in the calculation of Charlson et al. (1991) was 0.06. A recent study of Yu et al. (1997) reports that the representative total aerosol optical depth at 500 nm at Black Mountain, NC (35.66 N, 82.38 W, elevation 951 m) was 0.68, 0.29 and 0.10 for highly polluted, marine and continental air masses respectively during the period of June 1995 to mid-December 1995. The direct aerosol forcings resulting from highly polluted, marine and continental air masses are -21, -9, and -3 W m^{-2} respectively, when the box model equation (8) of Charlson et al. (1991) was used. This result suggests that the negative forcing due to aerosols is high enough to result in negative net forcing, especially for highly polluted air masses transported from the northwestern US. The results of Ulman and Saxena (1997) confirmed that the air masses from the Northwest were very polluted with abundance in sulfate and the clouds formed in such air masses were more acidic.

Another possible evidence to show the fingerprint of aerosol forcing in the Southeast is from the impact of Pinatubo volcanic aerosols on surface air temperature record. Fig. 2.3 shows the time series of the monthly averaged columnar optical depth and the annual mean optical depth at 0.453 μm for three-year periods 1985-87, 1988-90 and 1992-94. As can be seen, there was a dramatic increase in stratospheric volcanic aerosol optical depth after June of 1991. The annual mean optical depths at 0.453 μm for the three-year periods of 1985-87, 1988-90 and 1992-94 were 0.012, 0.006 and 0.037 respectively. The direct radiative forcing due to stratospheric volcanic aerosols would be -0.36, -0.18 and -1.1 W m^{-2} for 1985-87, 1988-90 and 1992-94 respectively (using the simple parameterization that the forcing in W m^{-2} is -30 times the visible optical depth (Lacis et al. (1992)). It is reasonable for us to use the period 1988-90 as a background profile.

Fig. 2.4 shows a comparison of the arithmetic average annual maximum, minimum temperatures, DTR and precipitation of the periods 1992-1994 and 1985-1987 with those of the period 1988-1990 at 47 stations. As can be seen, average annual maximum temperature of the periods 1992-1994 and 1985-1987 relative to that of the period 1988-1990 had decreased by 0.57 C and 0.09 C, respectively. The mean annual maximum temperature of the periods 1992-94 and 1985-87 relative to that of the period 1988-90 decreased at 97.9% and 55.3% stations, respectively. The three-year annual mean minimum temperature during both periods 1992-94 and 1985-87 increased at 80.9% stations when compared to that during the period 1988-90. The arithmetic averaged annual minimum temperatures of the periods 1992-94 and 1985-87 at 47 stations increased by 0.19 C and 0.32 C, respectively, when compared to that of the period 1988-90. The three-year annual mean DTR during the periods 1992-94 and 1985-87 decreased at 97.9% and 87.2% stations relative to that for the period 1988-90, respectively. The arithmetic averaged annual DTR during the periods 1992-94 and 1985-87 for the 47 stations decreased by 0.77 C and 0.41 C, respectively, when compared to that of the period 1988-90 (see Fig. 2.4). A close inspection of Figs. 2.3 and 2.4 shows that the change patterns of climatological variables (maximum, minimum temperature, and DTR) are

consistent with the prediction from the shortwave and longwave radiative forcing of stratospheric aerosols before and after Pinatubo eruption.

Another possible natural cause for climatic variations is from the complex interactions between the atmosphere and ocean such as the El Nino-Southern Oscillation (ENSO) phenomenon. Portman and Gutzler (1996) showed that the El Nino had some impact on the climatic variations. It should be realized, however, that a direct quantitative link between the changes of the large-scale and local radiative forcing and climatic variations has not been established.

2.5. Concluding Remarks

The field experiment and model calculations indicated that both direct and cloud-mediated forcings of aerosols exist and have been playing an underlying role in counteracting the greenhouse warming in the Southeast. In the absence of long term measurements of aerosol optical depth and cloud reflectivity, our analysis of cause-and-effect relationship can not proceed further. We highly recommend that a network of such measurements be established for a global coverage. Within the continental US, the need for establishing such a network in the southeastern region is rather urgent.

Acknowledgments. This research was supported through the Southeast Regional Center for the National Institute for Global Environmental Change, in Tuscaloosa, Alabama, by the United States Department of Energy under cooperative agreement number DE-FCO3-90ER61010, and by NASA Langley Research Center under contract NAS1-18944. Authors would like to thank Dr. J. M. Davis and Thomas Keever for their help during the climate data preparation, and John Anderson and Mel DeFeo for their help in preparing the manuscript. Dr. D. A. Dickey provided help in statistical analysis. We also thank Drs. Robert Griffin and William Herz for their encouragement.

2.6. References

Andreae, M.O., Climatic effects of changing atmospheric aerosol levels, in *World Survey of Climatology*, **16**, Future climates of the world, edited by A. Henderson-Sellers, Elsevier, Amsterdam, 1995.

Boucher, O., and U. Lohman, The sulfate-CCN-cloud albedo effect: A sensitivity study with two general circulation model, Tellus, 47B, 281-300, 1995.

Charlson, R.J., J. Langner, H. Rodhe, C.B. Leovy, and S.G. Warren, Perturbation of the northern hemisphere radiative balance by backscattering from anthropogenic sulfate aerosols, *Tellus*, 43AB, 152-163, 1991.

Dettinger, M.D., M. Ghill, and C.L. Keppene, Interannual and interdecadal variability in United States surface-air temperatures, 1910-87, *Climatic Change*, 31,35-66, 1995.

Husar, R.B., D.E. Patternson, J.M. Holloway, W.E. Wilson, and T.G. Ellestad, Trends of eastern US haziness since 1948. Fourth Symp. on Turbulence, Diffusion, and Air Pollution. Reno, Amer. Meteor. Soc., 249-256, 1978.

IPCC, Climatic change 1995: *The Science of Climate Change*. J.T. Houghton et al. (Eds). Cambridge University Press, Cambridge, UK, 1994.

Karl, T.R., P.D. Jones, R.W. Knight, G. Kukla, N. Plumme, V. Razuvayev, K.P. Gallo, J. Lindseay, R.J. Charlson, and T.C. Peterson, Asymmetric trend of daily maximum and minimum temperature, *Bull. Amer. Met. Soc.*, 74, 1007-1023,1993.

Kiehl, J.T., and B.P. Briegleb, The relative role of sulfate aerosols and greenhouse gases in climate forcing, *Science*. 260, 311-314, 1993.

Lacis, A., Hansen, J. and M. Sato, Climate forcing by stratospheric aerosols, *Geophys. Res. Lett.*, 19, 1607-1610, 1992.

McCormick, M.P., SAGE II: An overview, *Adv. Space Res.*, 7, 219-226, 1987.

National Research Council (NRC), *Aerosol radiative forcing and climate change*, National Academy Press, Washington, D.C., 1996.

Portman, D.A., and D.S. Guitzler, Explosive volcanic eruptions, the El Nino-southern oscillation, and U.S. climate variability, *J. of Climate.* 9, 17-33, 1996.

Saxena, V.K., P.A. Durkee, S. Menon, J. Anderson, K.L. Burns, and K.E. Nielsen, Physico-chemical measurements to investigate regional cloud-climate feedback mechanisms, *Atmos. Environ.*, 30, 1573-1579, 1996.

Schwartz, S.E., The whitehouse effect- Shortwave radiative forcing of climate by anthropogenic aerosols: An overview, *J. Aerosol. Sci.*, 27, 359-382, 1996.

Ulman, J.C., and V.K. Saxena, Impact of air mass histories on the chemical climate of Mount Mitchell, North Carolina, *J. Geophys. Res.,* 102, 25451-25465, 1997.

Vedin, H., Frequency of rare weather events during periods of extreme climate, *Geogr. Ann.*, 72A, 151-155, 1990.

Yu, Shaocai., V.K. Saxena, B.N. Wenny, J.J. De Luisi, G.K. Yue, and I.V. Petropavlovskikh, A study of the diffuse to direct solar irradiance ratio and aerosol optical depth in the southeastern US, *Proceedings of A&WMA's Visual Air Quality, Aerosols and Global Radiation Balance Conference*, Bartlett, NH, September 9-12, 1997.

V.K. Saxena and Shaocai Yu, Department of Marine, Earth and Atmospheric Sciences, North Carolina State University, Raleigh, NC 27695-8208 (Received October 1, 1997; revised April 21, 1998; accepted June 11, 1998.)

Table 2.1. Percents of stations with decreasing trend (P_1) and significantly decreasing trend (P_2) at the 0.05 level for seasonal mean climatological variables in the southeastern US during the period 1949-94. The parenthetic values represent the increasing trend.

	Annual		Winter(Dec-Feb)		Spring(Mar-May)		Summer(Jun-Aug)		Fall(Sept-Nov)	
Parameters	P_1	P_2	P_1	P_2	P_1	P_2	P_1	P_2	P_1	P_2
Daily temperature	51.9(48.1)	13.5(9.6)	86.5(13.5)	9.6(0)	50.0(50.0)	9.6(1.9)	42.3(57.7)	9.6(21.2)	19.2(80.8)	1.9(13.5)
Maximum temperature	67.0(33.0)	15.4(1.9)	90.4(9.6)	7.7(0)	42.3(57.7)	3.8(1.9)	63.5(36.5)	7.6(7.6)	42.3(57.7)	3.8(11.5)
Minimum temperature	40.9(59.1)	17.3(19.2)	73.1(26.9)	3.8(3.8)	48.1(51.9)	9.6(7.7)	30.8(69.2)	7.8(28.8)	17.3(82.7)	0(17.3)
Temperature range(DTR)	69.2(30.8)	28.9(11.5)	67.3(32.7)	23.0(7.6)	48.1(51.9)	15.3(15.3)	76.9(23.1)	26.9(5.7)	75.0(25.0)	19.2(5.8)
Precipitation	17.3(82.7)	0(9.6)	40.4(59.6)	0(1.9)	36.5(63.5)	0(0)	51.9(48.1)	0(0)	15.4(84.6)	0(5.8)

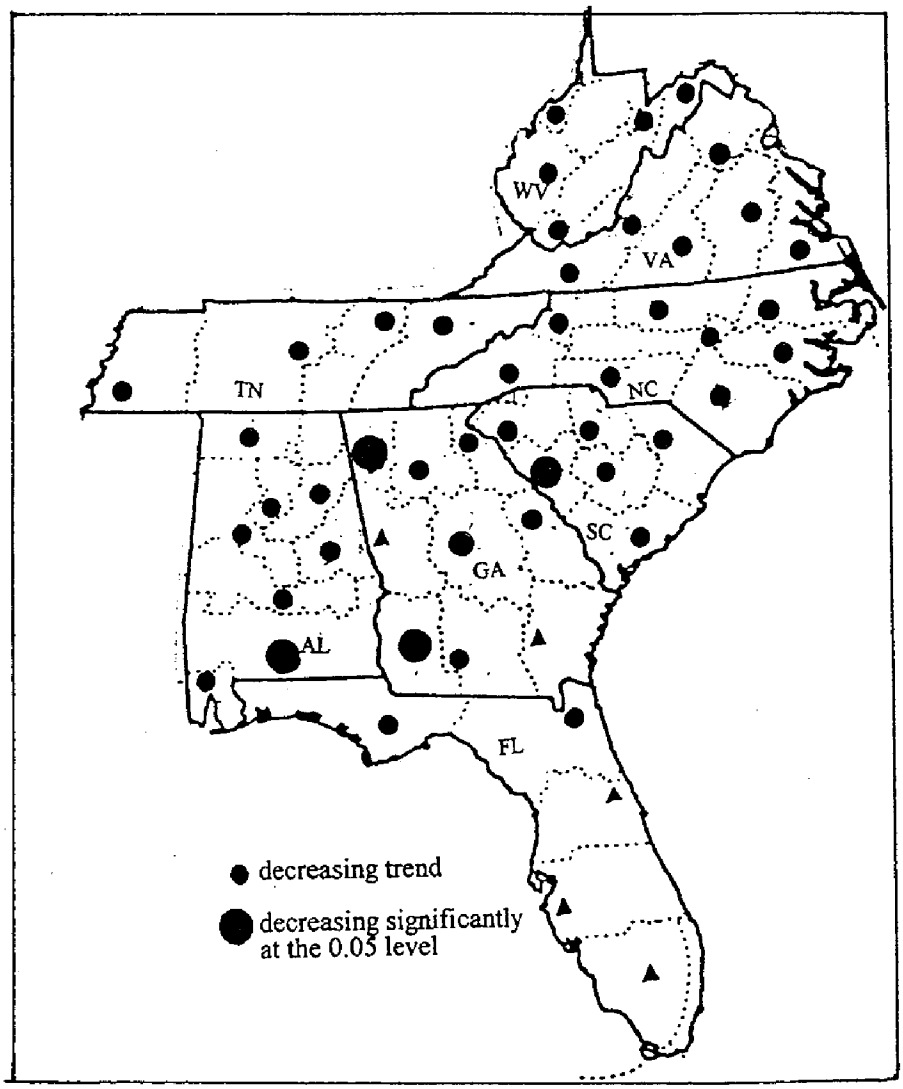

Figure 2.1. Station location (▲) and spatial patterns of winter mean daily temperature in the southeastern US

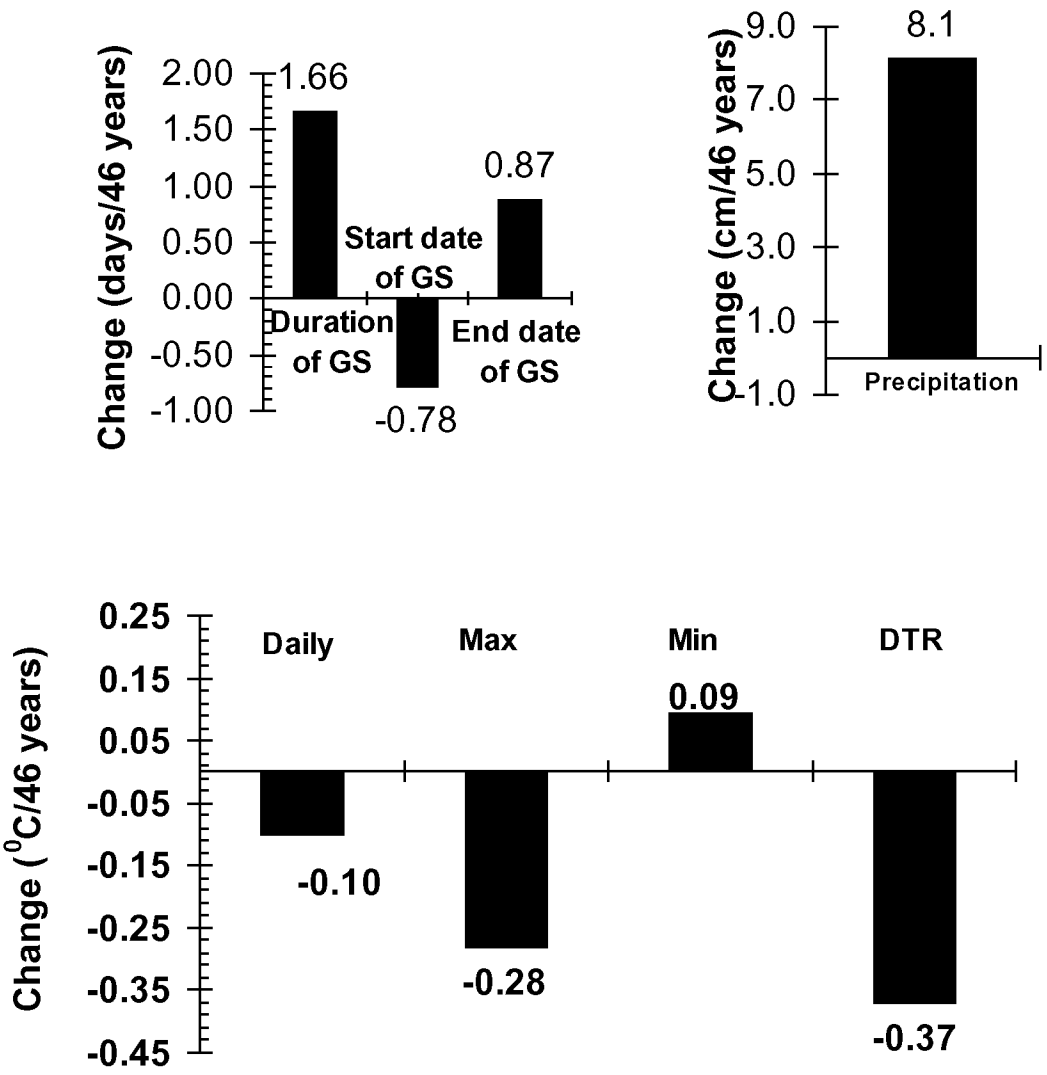

Figure 2.2. The arithmetic average of the annual mean value change for 52 stations in the southeastern US during the period 1949-1994 (46 years)

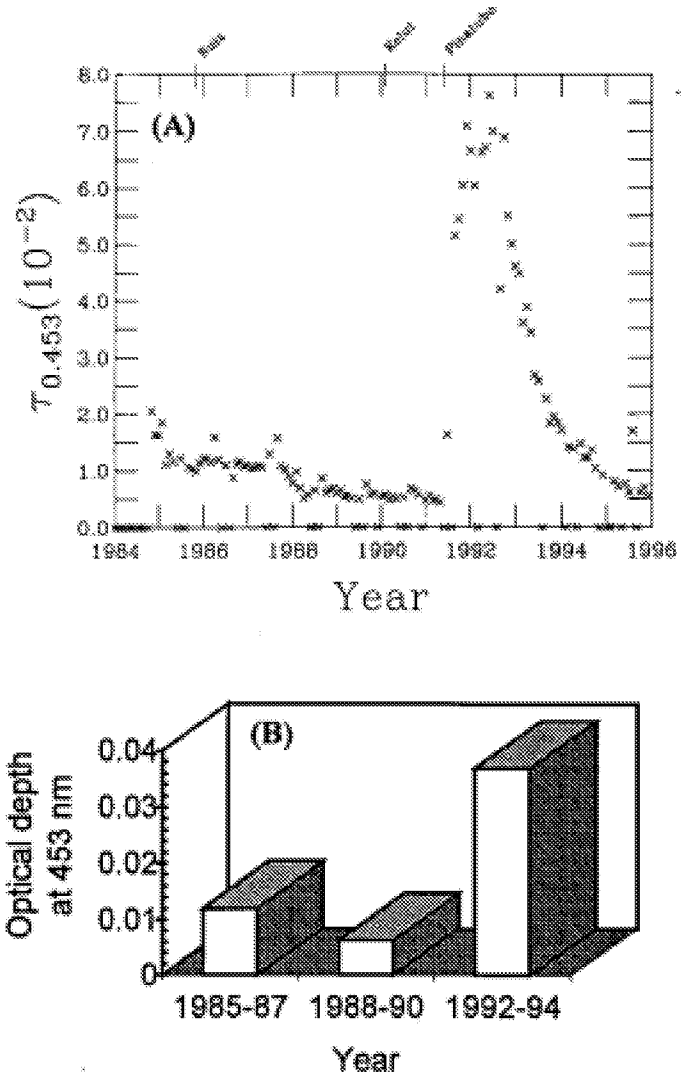

Figure 2.3. (a) Time series of monthly columnar optical depth of volcanic aerosols at 0.453 μm. (b) The three-year mean optical depth of volcanic aerosols at 0.453 μm in the southeastern US

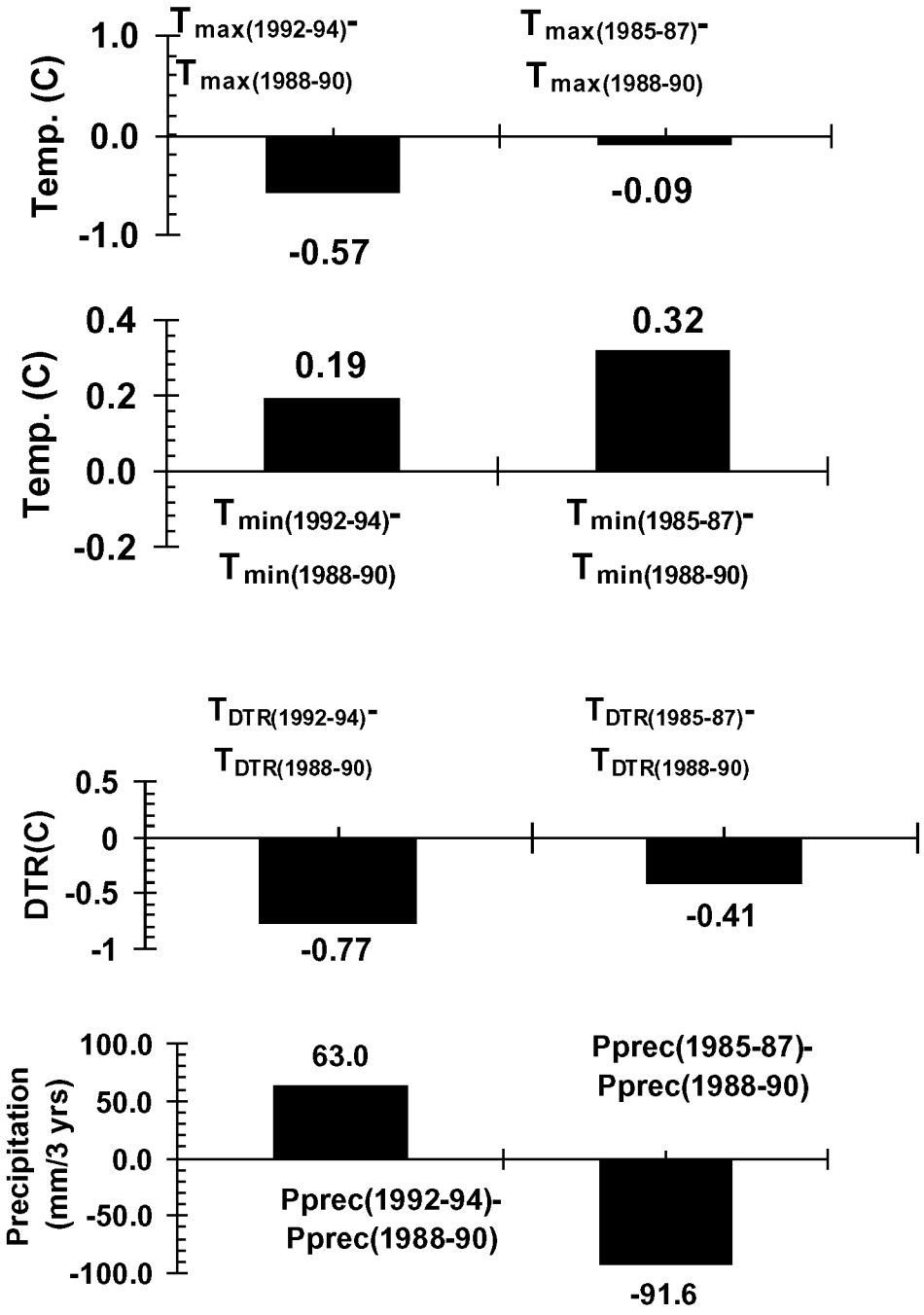

Figure 2.4. Comparison of average annual mean maximum, minimum temperature, temperature range (DTR) and precipitation during the periods 1992-94, 1985-87 with those during the period 1988-90

3. ON DETECTING THE SIGNATURE OF REGIONAL AEROSOL RADIATIVE FORCING IN EASTERN CHINA

Shaocai Yu[1], V. K. Saxena[1], and Zongci Zhao[2]

1. Department of Marine, Earth and Atmospheric Sciences North Carolina State University, Raleigh, NC 27695-8208,USA
2. National Climate Center, State Meteorological Administration, 46 Baishiqiaolu, Beijing 100081, China

Atmospheric Environment, 1999 (in review).

3.1. Abstract

The Intergovernmental Panel on Climate Change (IPCC) has reported that in the southeastern US and eastern China, the greenhouse warming due to anthropogenic gaseous emissions is dominated by the cooling effect of anthropogenic aerosols. In a recent study, we verified this model prediction by analyzing the trend in daily, maximum, minimum temperatures and diurnal temperature range at 52 stations in the southeastern US during 1949-94. In this study, we present an analysis of regional patterns of climate change at 72 stations in eastern China during 1951-94 (44 years) to detect the signal of aerosol radiative forcing. The results support the cooling effect of sulfate aerosols which was evident in the years following the eruption of Mt. Pinatubo. The enhancement in stratospheric aerosol optical depth was obtained by NASA's (National Aeronautics and Spaces Administration) SAGE II (Stratospheric Aerosol and Gas Experiment) satellite measurements. A decreasing trend in the summer mean maximum temperature during the past 44 years and a two-year cooling trend following the Mt. Pinatubo eruption were found. This effect is similar to our finding in the southeastern US. However, a slightly overall warming trend in eastern China is evident; winters have become milder. This finding is explained by hypothesizing that increasing energy usage during the past 44 years has resulted in more fossil fuel consumption and biomass burning thus increasing the emission of absorbing soot and organic aerosols. Such emissions in addition to well-known Asian dust and greenhouse warming may be responsible for the winter warming trend that we have reported here.

Key word index: Eastern China, southeastern US, radiative forcing, aerosols, greenhouse warming, SAGE II.

3.2. Introduction

The eastern China, south central Europe and eastern US have been recognized (IPCC, 1995) as regions where the effect of anthropogenic aerosols supersedes that of man-made greenhouse gases (GHGs) and manifests itself in terms of cooling of the surface-air temperature (Kiehl and Briegled, 1993). Several aerosol characterization experiments (ACE) such as ACE-1 in the remote Southern Ocean, Tropospheric Aerosol Radiative Forcing Observation Experiment (TARFOX) off the eastern coast of North America, and ACE-2 in European outflow have been conducted to assess aerosol effects in major regions of the world (Huebert et al., 1998, Stowe et al., 1995). The upcoming ACE-Asia in the 2000-2004 timeframe aims to accurately quantify the direct and indirect (also called cloud-mediated) effect of aerosols on the radiative forcing of climate in the Asian-Pacific region.

The uncertainty in the magnitude of the estimated direct and cloud-mediated cooling effect of aerosols (Schwartz and Andreae, 1996) is a major barrier for a reliable *prediction of climate change on the scale of a decade and longer*. Any policy decisions to limit the emissions of GHGs could have severe *short-term impact on the regional climate* since major sources of GHGs and aerosols are identical such as fossil fuel combustion, biomass burning etc. Various diurnal, seasonal, and spatial differences in aerosol radiative forcing provide opportunities to develop strategies to detect its signature in the climate record. Since the concentrations of both anthropogenic and natural aerosols in eastern China are among the highest on Earth, the impact of the enhanced aerosol loading on the climate of this region is of considerable interest to IPCC. In this paper, we present the results of our analysis of temperature records at 72 stations in eastern China during 1951-94, with special focus on the

year following the Mt. Pinatubo eruption in June 1991. The analysis is aimed at detecting the signature of aerosol radiative forcing on the regional climate.

3.3. Methodology and Database

3.3.1. Database

Monthly, seasonal, and yearly climate data on the mean maximum, minimum, and daily temperatures, and diurnal temperature range (DTR, the difference between maximum and minimum temperature) at 72 stations in eastern China used for this study were obtained from the National Climate Center of China. The period covered here was from 1951 to 1994 (44 years). Some stations only have climate data after 1955 or 1961. In the latter cases, only their change rates (or slopes with time) were used to calculate the mean rate of change for the region. The ten provinces used in this study are Hebei, Henan, Hubei, Hunan, Shangdong, Jiangsu, Anhui, Jiangxi, Zhejiang and Fujian. Three big cities (Beijing, Tianjin and Shanghai) are also included in the study. The criteria for selecting the stations in each province were based on the following considerations: (1) stations had a good climatic data record; (2) there was a good geographic distribution; (3) only five or six stations were chosen for each province. A map of the eastern China showing the provinces and stations is presented in Fig 1. The time series autoregression model in the Statistical Analysis System (SAS) was used to find whether the changing trend is significant or not at a certain level. The t-test model in SAS was used to test whether two averages were significantly different or not at a certain confidence level.

3.3.2. Methodology

Since the long-lived and uniform-distributed greenhouse gases essentially act in the infrared spectral range, they would produce an increase of both maximum and minimum temperatures

(longwave forcing). In contrast, the enhanced backscattering of incoming solar radiation due to the increase in aerosol loading and low cloud amount would result in a decrease of the maximum daytime temperature (shortwave forcing), and the enhanced absorption and backscattering of outgoing terrestrial longwave radiation would result in an increase of minimum nighttime temperature (longwave forcing) although the latter mechanism during the daytime does not shut down (Karl et al., 1993). Longwave radiative forcing of both greenhouse gases and aerosols (especially when aerosol particles contain high concentration of absorbing components such as black carbon (BC)) would result in an increase of both minimum and maximum temperatures. As indicated by Saxena and Yu (1998), the change in maximum temperature can serve as a more sensitive indicator of climate response to aerosol forcing than surface temperature.

To study the impact of stratospheric volcanic aerosols on the climate change, the monthly average optical depth of stratospheric volcanic aerosols in a unit column between 10-40 km over the areas between latitude 22 N and 38 N and longitude 105 E and 120 E in eastern China is calculated as follows on the basis of the Stratospheric Aerosol and Gases Experiment (SAGE) II satellite extinction measurement:

$$\tau_\lambda = \int_{z1}^{z2} \beta_\lambda(z)dz$$

where β_λ is the extinction coefficient of particles at wavelength λ. A detail description of the SAGE II instrument is given by McCormick (1987). Since the SAGE II satellite was launched in 1984, the optical depth data of stratospheric volcanic aerosols from 1985 to 1994 are used to compare with the changes of the climatological variables during this period.

3.4. RESULTS AND DISCUSSION

3.4.1. Regional Patterns of Climate Change in eastern China

Most analyses of hemispheric and regional temperature series have tended to use time series of monthly mean daily temperature (Hulme et al., 1994). In many climate impact studies, it is generally assumed that the mean surface-air daily temperature will increase due to enhanced greenhouse effect. Table 3.1 shows that the annual mean daily temperature indicates an increasing trend at 77.8% stations (significantly at 33.3% stations at the 0.05 level) in eastern China during 1951-1994. The arithmetic average of annual mean daily temperature at 72 stations increased by 0.35 C during the past 44 years as shown in Table 3.2. *This indicates that there was a slight warming trend in eastern China during the past 44 years.* This is consistent with the analysis of Hulme et al. (1994), who also found a warming trend in eastern China based on the data during 1951-1990. For the seasonal trend, the winter mean daily temperature shows a increasing trend at 98.7% stations (significantly at 40.3% stations at the 0.05 level), while summer mean daily temperatures showed a decreasing trend at 63.8% stations (significantly at 11.1% stations at the 0.05 level). The winter mean daily temperature increased by 1.1 C while summer mean daily temperature decreased by -0.22 C during 1951-94. *The winter became warmer, and the summer became colder in eastern China during the period 1951-1994.* Table 3.1 shows that the annual, winter, and summer mean maximum temperature indicated a decreasing trend at 62.5%, 13.8%, and 80.5% stations, respectively. The arithmetic average of the annual mean maximum temperature at 72 stations decreased by -0.09 C during the past 44 years. Table 3.2 shows that the cooling trend of annual mean maximum temperature was mainly caused by the large cooling trend of summer mean maximum temperature. Figure 3.1a shows the locations of stations with the decreasing trend of summer maximum temperature during 1951-1994. The annual, winter, spring, summer and fall mean minimum temperature indicated the increasing trend at 90.3%, 98.7%, 87.5%, 52.8% and

76.4% stations, respectively. The arithmetic average of the winter mean minimum temperature increased by 1.67 C during the past 44 years. It is apparently that the high warming trend of winter mean minimum temperature result in the warming trend of annual mean daily temperature and minimum temperature in eastern China during the past 44 years.

Table 3.1 shows that the annual, winter, spring, summer and fall mean diurnal temperature ranges (DTRs) in eastern China indicate the decreasing trends at 83.3%, 88.8%, 80.5%, 81.9% and 75.0% stations, respectively. The percents of stations with significantly decreasing trends at the 0.05 level were 61.1%, 51.3%, 48.6%, 59.7 and 38.8% for annual, winter, spring, summer and fall mean DTRs respectively. The arithmetic average of the annual mean DTR decreased by -0.88 C during the past 44 years. The results of this study confirm the results of Karl et al. (1993), who found the strong evidence existed for a widespread decrease in the DTR over the past several decades in many regions of the globe. A close examination of Tables 1 and 2 reveals that the decreasing trend of annual and winter mean DTR mainly result from both decreasing trend of summer maximum temperatures, and increasing trend of winter mean minimum temperatures.

3.4.2. The trends of stratospheric volcanic aerosols in eastern China

Figure 3.2a shows the temporal variation of the monthly averaged stratospheric volcanic aerosol columnar optical depth in eastern China for the period 1985-1998. As can be seen, there was a dramatic increase in stratospheric volcanic aerosol optical depth after June of 1991. This sudden increase was due to the increase of volcanic material from the Pinatubo eruption on June 16, 1991. Figure 3.2 shows that the stratospheric volcanic aerosol optical depth during 1985-1987 was also higher than that during 1988-90. This is due to the impact of the El Chichon eruption on April 4, 1982 and the Nevado del Ruiz eruption on November 13, 1985.

3.4.3. Signature of Aerosol Radiative Forcing in eastern China

The preceding analysis shows that arithmetic average of the annual mean maximum temperature decreased by –0.09 C while the annual mean minimum temperature increased by 0.79 C at 72 stations during the past 44 years (see Table 3.2) in eastern China. Obviously, the warming from the longwave forcing due to both greenhouse gases and aerosols was not counteracted by the shortwave aerosol forcing because the daily temperature is equal to the average of maximum and minimum temperatures. This seems inconsistent with model prediction of IPCC (1995), and Kiehl and Briegled (1993). Our results are similar to that of Karl et al. (1993), who found that the average minimum temperature increased by 0.84 C while the average maximum temperature increased by 0.28 C on the basis of data covering about 50% of Northern Hemisphere and 10% of Southern Hemisphere for the period 1951-90. However, the maximum temperature has a slight decrease instead of an increase in eastern China. The high increasing rate of minimum temperature leads to a slightly warming trend in eastern China. However, the high summer cooling trend in the maximum temperature reduce the increasing rate of the annual mean daily temperature, and is in agreement with the expected aerosol impact.

The major sources of aerosols in China include anthropogenic emissions such as coal and biomass burning and natural sources such as windblown dust, and volcanic aerosols. On the basis of the satellite measurement of advanced very high resolution radiometer (AVHRR) during the period July 1989 to June 1991, Husar et al. (1997) found that the annual, winter, spring, summer and fall mean "radiatively equivalent" aerosol optical thickness τ^{A}_{sat} (EAOT) in the eastern coast of China were 0.25, 0.25, 0.35, 0.23, and 0.18 respectively. The direct aerosol forcing for annual, winter, spring, summer and fall seasons will be 8, 8, 11, 7, and 5 W m^2 respectively, when the box model equation (8) of Charlson et al. (1991) is used. This just suggests that the negative forcing due to aerosols exists in eastern China.

However, why are there increasing trends instead of decreasing trends for both winter maximum and minimum temperatures in eastern China during the past 44 years? Herman et al.

(1997) found that a major source of UV-absorbing aerosol over China occurs in the northeast during January to May that could include dust and smoke from coal burning as indicated by Nimbus 7/TOMS data. The measurement of Hashimoto et al. (1994) during the 2-year period (April 1990-March 1992) indicated that the winter, spring, summer and fall TSP concentrations in Beijing (in the northern China) are 380, 378, 223 and 220 $\mu g\ m^{-3}$ respectively, and are 486, 295, 230 and 289 $\mu g\ m^{-3}$ for Chengdu city (in the southwestern China). Sheng an Mao (1986) found that light absorption coefficients at Beijing were 0.1 and 1-100 km^{-1} for non-heating (summer) and heating (winter) periods respectively. Parungo et al. (1994) indicated that BC concentration at Beijing rural was 1.71 mg C/m^3 during the period July to September. The model calculation of Xu and Carmichael (1999) also indicate that sulfate concentrations are higher in the winter (~20 $\mu g\ m^{-3}$) and lower in the summer (5-10 $\mu g\ m^{-3}$), and seasonal variations are typically strong over eastern China. Penner et al. (1993) estimated that the BC emission in China was 2.68 Tg $year^{-1}$. The adopted BC/S ratio for China used by Penner et al. (1993) is 0.55, much higher than that (0.20) for USA. The BC in the aerosol particles can reduce the negative forcing and in some case counteract the direct aerosol forcing. Haywood and Shine (1995) show that fossil-derived BC can cause a positive global-mean radiative forcing of +0.03 to +0.24 W m^{-2} for the respective BC/sulfate mass ratios of 0.05 and 0.1. Chylek et al. (1995) found that the direct forcing of sulfate was reduced by about 0.034 W m^{-2} for each 1% of BC to sulfate mass ratio in the case of sulfate aerosols containing BC inclusion. Obviously, the high aerosol radiative forcing in winter results in a warming effect probably due to high concentration of BC. However, aerosol radiative forcing in summer results in a cooling effect because of low BC concentration. This is reasonable because in China, the combustion of coal with high sulfur content is the major supply of energy for most factories and heating, and the emissions are released through short chimneys only equipped with dust removers (Yu et al., 1998), and emission of black carbon (BC) appear to be very high in the winter and spring months. Baker et al. (1995) demonstrated that the increase in nighttime minimum temperature in

China was not necessarily the result of changes in cloud cover on the basis of data at 32 stations during 1951-1990.

Economic expansion in the China will unavoidably be accompanied by increases in coal and biomass burning. Figure 3.3 shows the seasonal mean maximum and minimum temperature deviations at 59 stations in eastern China during 1955-1994. Note that there are significant correlation between maximum temperature deviation (ΔT_{max}) and minimum temperature deviation (ΔT_{min}) for all seasons except fall, and that the change pattern of wintertime deviation were similar to those of annual deviation. The highest slope and correlation coefficient in the summer season in Figure 3.3 suggest that the summer maximum temperature has a greater change than the summer minimum temperature. Generally, there was a warming trend from 1956 to 1961, a cooling trend between 1961-1969 and a warming trend between 1969-1978, a cooling trend between 1978 to 1984, and a warming trend after 1984 for both annual maximum and minimum temperatures at the eastern China. During the periods of the Great Leap Forward before 1966 and the Cultural Revolution afterward, many factories were closed and production halted through a reduction of the staff. Industry functions gradually returned to normal between 1972 to 1978, and factory production and economic development rapidly expanded under the new Open Door Policy after 1978. Obviously, the air pollution emission during 1961-1978 will be lower than those during 1978-1994. This is in agreement with estimation of Lefohn et al. (1999), who show that the sulfur emissions in China were 4.5, 4.9, 8.2, 10.9, and 14.2 Tg/year for 1960, 1970, 1980, 1985 and 1990 respectively. The change pattern of summer maximum temperature in Figure 3.3 seems consistent with this change of sulfur emissions in China. The cloud and precipitation in the eastern coast of China are becoming more acidic recently (Yu et al., 1998), especially during the spring season. Obviously, anthropogenic aerosols can change the cloud radiative properties and affect the climate in eastern China although indirect aerosol forcing is still largely unquantified.

Another possible aerosol effect on the climate in eastern China is from the well-known Asia dust and volcanic aerosols. Siliceous materials in soil and desert dust can absorb strongly in the

thermal infrared region (8-14 mm wavelength) and dense dust clouds therefore can lead to a trapping of infrared radiation in the same way as the trace gas green-house effect (Sokolik and Toon, 1996). Natural dust and road dust are other major sources contributing to the aerosol mass loading in China. Arimoto et al. (1996) indicated that the Asian dust fluxes to the North Pacific region show a pronounced seasonally change with the highest fluxes from late winter to late spring, and that the spring season in Beijing was greatly influenced by yellow dust (sand) blown from the vast northern desert. It is believe that eastern Asia dust may also make an important contribution to the winter warming trend in eastern China although the climatic effects of Asian mineral dust are still largely unquantified due to the lack of detailed information on space- and time-varying properties of Asian dust.

The aerosol loading injected by large volcanic eruption such as due to Pinatubo and maximum and minimum temperature change patterns may provide a validation of the signature of aerosol forcing in eastern China. As shown in Figure 3.2, the annual mean optical depths at 0.525 μm for the periods 1985-87, 1988-90, 1990, 1992 and 1992-94 were 0.011, 0.006, 0.005, 0.064 and 0.038 respectively. The direct radiave forcing due to stratospheric volcanic aerosols would be –0.33, -0.18, -0.15, 1.9 and –1.1 W m^{-2} for 1985-87, 1988-90, 1990, 1992 and 1992-94 respectively (using the simple parameterization that the forcing in W m^{-2} is –30 times the visible optical depth (Lacis et al. (1992)). It is reasonable for us to use the period 1988-90 or 1990 as a background profile.

Table 3.3 list the comparison of arithmetic average seasonal daily, maximum, minimum temperature and DTR for the periods 1985-87, 1988-90, 1990, 1992 and 1992-94 at 72 stations in eastern China. As can be seen, the summer mean maximum temperatures of one-year (1992), two-year (1992-1993), three-year (1992-1994) and three-year (1985-1987) decreased by -0.82, -0.37, -0.11, and -0.28 C respectively, when compared to those of 1990, 1989-90, 1988-1990, 1988-1990 respectively. Figure 3.1b shows the locations of stations with the decreasing trend of summer maximum temperature of 1992 relative to that of 1990. However, the winter mean maximum temperature of one-year (1992), two-year (1992-

1993), three-year (1992-1994) and three-year (1985-1987) increased by 1.74, 1.14, 0.92, and 0.34 C respectively, when compared to those of 1990, 1989-90, 1988-1990, 1988-1990 respectively. The winter warming trend is in agreement with Robock and Mao (1995). As pointed by Robock and Mao (1995), this winter warm anomalies are produced by an enhanced polar vortex, which stimulates a wave response in the winter circulation with a pattern of warm advection during the 1992 ENSO warming episode.

Other possible natural cause for climatic variations is from the complex interactions between the atmosphere and ocean such as the El Nino-Southern Oscillation (ENSO) phenomenon. It should be realized, however, that a direct quantitative link between the changes of the large-scale and local radiative forcing and climatic variations has not been established.

3.4.4. Comparison of eastern China and southeastern US

Since the topographical and geographic conditions, the energy consumption, industrialization and population density are very different for the United States and China, it will be of interest to compare the climate change and aerosol radiative forcing signals in eastern China and southeastern US. The aerosol sources in China are unlike those in the North America: much more coal and biomass are burned with small smokestack emission system. This potentially add more absorbing soot and organic aerosol to the atmosphere in this region as analyzed before. In addition, the oxidizing capacity of the atmosphere over eastern China is lower than that in the North America because the lower concentration of NOx over eastern China. Husar et al. (1997) indicate that the annual mean EAOTs was 0.25, and 0.17 for the eastern China, and eastern US respectively during July 1989 to June 1991. Penner et al. (1993) estimated that the BC emission in China was 2.68 Tg $year^{-1}$, much higher than that (0.40 Tg $year^{-1}$) in USA. The adopted BC/S ratio for China used by Penner et al. (1993) is 0.55, much higher than that (0.20) for USA. Obviously, the aerosol pollution in eastern China is higher than eastern US and contains more absorbing components such as BC. Table 3.4 lists the comparison of the daily,

maximum, minimum temperature and DTR in two regions. The analyses of Saxena and Yu (1998) and Saxena et al. (1997) indicate that the rates of change of annual mean daily, maximum, minimum temperatures and DTR in the southeastern US were -0.2, -0.6, 0.2, and -0.8 C/100 years respectively, on the basis of climate data at 52 stations during 1949-94. Table 3.1 shows that the rates of change of annul mean daily, maximum, minimum temperatures and DTR in eastern China were 0.8, -0.2, 1.8, and -2.0 C/100 years respectively, on the basis of climate data at 72 stations during 1951-94. Obviously, the high increasing rate of annul mean minimum temperature in eastern China results in the slightly warming trend of daily temperature, while the high decreasing rate of annual maximum temperature and low increasing rate of annual mean minimum temperature lead to the cooling trend of daily temperature in the southeastern US. The winter mean minimum temperature increased at 98.7% stations in eastern China and but decreased at 73.1% stations for the southeastern US. The change pattern of winter maximum and minimum temperatures are substantially different for the eastern China and southeastern US.

The three-year summer mean maximum temperature during the periods 1992-1994 and 1985-1987 relative to those of the period 1988-90 decreased by -0.11 C and -0.28 C respectively in eastern China, and decreased by -0.46 C and increased by 0.10 C respectively in the southeastern US. The three-year fall mean maximum temperature during 1992-1994 relative to that of the period 1988-90 decreased by -0.21 C and -0.54 C for the eastern China and southeastern US respectively. However, the three-year winter mean maximum temperature during the periods 1992-1994 and 1985-1987 relative to those during the period 1988-90 increased by 0.92 C and 0.34 C for the eastern China respectively, and but decreased by -0.52 C and -0.85 C in the southeastern US respectively. Obviously, the effects of volcanic aerosols in the two regions are a little different although two regions show general cooling effects of Pinatubo volcanic aerosols.

3.5. CONCLUSIONS

Based on the analysis of climate data at 72 stations during 1951-94 (44 years) and stratospheric volcanic aerosols during 1985-1998 in eastern China, it is shown that there is a consistency in the cooling trend in the maximum daily temperature. This signal was undisputedly detected following the eruption of Mt. Pinatubo in June 1991. However, a slight overall warming trend in eastern China exists over the past 44 years. We hypothesze that the high concentrations of absorbing aerosol components such as soot and siliceous material from well-known Asian dust in the winter time might be one of the reasons leading to a rising rate of winter mean maximum and minimum temperatures. The latter is responsible for leading the general warming trend in eastern China. The comparison of aerosol forcing in eastern China and southeastern US indicates that both regions show a decreasing trend in the mean maximum temperature over the past years and the cooling effect of Pinatubo volcanic aerosols. Obviously, the continuity in the long-term monitoring of aerosol properties such as composition, size distribution and vertical distribution and climatological variables such as maximum and minimum temperatures in different seasons is crucial in understanding the effect of aerosols on climate change in eastern China.

Acknowledgments. This research was supported by the NASA's Mission to Planet Earth (MTPE) under Contract No. NAS1-18944 from Langley Research Center, Hampton, VA and US EPA's STAR (Science to Achieve Results) grant No. R-825248. Authors would like to thank Dr. Lamont Poole, and Prof. Patrick McCormick for their encouragement. Li Ji and Zhang Dekuan provide data assistance.

3.6. References

Arimoto R., Duce R.A., Savoie D.L., Prospero J.M., Talbot R., Cullen J.D., Tomza U., Lewis N.F., and Ray B.J. (1996) Relationship among aerosol constituents from Asia and North Pacific during PEM-West A. *Journal of Geophysics Research*. **101**, 2011-2023.

Baker C.B., Quayle R.G., and Wang W. (1995) The influence of night time cloud cover on the observed minimum temperature in China. *Atmospheric Research*. **37**, 27-35.

Charlson, R.J., Langner, J., Rodhe, H., Leovy, C.B., and Warren S.G. (1991) Perturbation of the northern hemisphere radiative balance by backscattering from anthropogenic sulfate aerosols. *Tellus*, **43AB**, 152-163.

Chyleck P., Videen G., Ngo D., Pinnick R.G., and Klett J.D. (1995) Effect of black carbon on the optical properties and climate forcing of sulfate aerosols. *Journal of Geophysics Research*. **100**, 16325-16332.

Hashimoto Y., Sekine Y., Kim H.K., Chen Z.L., and Yang Z.M. (1994) Atmospheric fingerprints of East Asia, 1986-1991: An urgent record of aerosol analysis by the JACK network. *Atmospheric Environment*. **8**, 1437-1445.

Haywood J.M., and Shine K.P. (1995) The effect of anthropogenic sulfate and soot aerosol on the clear sky planetary radiation budget. *Geophysics Research Letters*. **22**, 603-606.

Herman J.R., Bhartia P.K., Torres O., Hsu C, Seftor C., and Celarier E. (1997) Global distribution of UV-absorbing aerosols from Nimbus 7/TOMS data. *Journal of Geophysics Research*. **102**, 16911-16922.

Huebert B.J., Zhuang L., Howell S., Noone K., and Noone B. (1996) Sulfate, nitrate, methanesulfonate, chloride, ammonium, and sodium measurements from ship, island, and aircraft during the Atlantic Stratocumulus Transition Experiment/Marine Aerosol Gas Exchange. *Journal of Geophysics Research*. **101**, 4413-4423.

Hulme M., Zhao Z.C., and Jiang T. (1994) Recent and future climate change in east Asia. *International Journal of Climatology*. **14**, 637-658.

Husar R.B., Prospero J.M., and Stowe L.L. (1997) Characterization of tropospheric aerosols over the oceans with the NOAA advanced very hgih resolution radiometer optical thickness operational product. *Journal of Geophysics Research.* **102**, 16889-16909.

IPCC, (1995) Climatic change 1995: Radiative forcing of climate and an evaluation of the IPCC 1992 emission scenarios. J.T. Houghton et al. (Eds). Cambridge University Press, Cambridge. UK

Karl T.R., Jones P.D., Knight R.W., Kukla G., Plumme N., Razuvayev V., Gallo K. P., Lindseay J., Charlson R. J., and T. C. Peterson. (1993) Asymmetric trends of daily maximum and minimum temperature. *Bulletin of American Meteorological Society.* **74**, 1007-1023.

Kiehl J. T. and Briegleb B. P. (1993) The relative role of sulfate aerosols and greenhouse gases in climate forcing. *Science.* **260**, 311-314

Lacis, A., Hansen, J. and M. Sato M. (1992) Climate forcing by stratospheric aerosols. *Geophysical Research Letter.*, **19**, 1607-1610.

Lefohn A.S., Husar J.D., and Husar R.B. (1999) Estimating historical anthropogenic global sulfur emission patterns for the period 1985-1990. *Atmospheric Research.* **33**, 3435-3444.

McCormick M. P. (1987). SAGE II: An overview, *Advance Space Research.* **7**, 219-226.

Penner J.E., Eddleman H., and Novakov T. (1993) Towards the development of a global inventory for black carbon emissions. *Atmospheric Environment.* **27**, 1277-1295.

Parungo F., Nagamoto C., Zhou M.Y., Hansen A.D.A., and Harris J. (1994) Aeolian transport of aerosol black carbon from China to the ocean. *Atmospheric Environment.* **28**, 3251-3260.

Robock A. and Mao J. (1995) The volcanic signal in surface temperature observation *Journal of Climatology.* **8**, 1086-1103.

Saxena V.K., and Yu Shaocai (1998) Searching for a regional fingerprint of aerosol forcing in the southeastern US. *Geophysics Research Letters.* **25**, 2833-2836.

Saxena V.K., Yu Shaocai, and J. Anderson J. (1997) Impact of stratospheric volcanic aerosols on climate: Evidence of aerosol radiative forcing in the southeastern US. *Atmospheric Environment*. **31**, 4211-4221.

Schwarts S.E., and Andreae M.O. (1996) Uncertainty in climate change caused by aerosols. *Science*. **272**, 1121-1122.

Sheng J., and Mao J. (1986) The measurement of the absorption coefficient of the atmospheric aerosols. *Acta Meterological Sinica*. **44**, 321-327.

Sokolik I.N., and Toon O.B. (1996) Direct radiative forcing by anthropogenic airborne mineral aerosols, *Nature*, **381**, 681-683.

Stowe L.L., Hobbs P.V., and Russell P, Plans for the implementation of the tropospheric aerosol radiative forcing observational experiment. Paper MB52A-12, p. 308 Abstracts for Week B, XXI Assembly IUGG, Boulder, Colorado., 1995

Xu Y., and Carmichael G.R. (1999) An assessment of sulfur deposition pathways in Asia. *Atmospheric Environment.* **33**, 3473-3486.

Yu, Shaocai, Chen, Zemian., Cai, Xiaopin., and Chen Shuentian, 1998. An analysis of chemical composition of different rain types in "Minnan Golden Triangle" region in the southeastern coast of China. *Atmospheric Research.* **47-48**: 245-269.

Table 3.1. Percent of stations with decreasing trend (P_1), and significantly decreasing trend (P_2) at the 0.05 level for seasonal and annual mean variables during the period 1951-1994 in the eastern China. The parenthetic values denote percentage of stations with increasing trend.

	Annual		Winter (Dec.-Feb.)		Spring (March-May)		Summer (Jun-Aug.)		Fall (Sept.-Nov.)	
Variable	P1	P2	P1	P2	P1	P2	P1	P2	P1	P2
DT	22.2(77.8)	1.3(33.3)	1.3(98.7)	0(40.3)	30.5(69.5)	0(22.2)	63.8(36.2)	11.1(8.3)	37.5(62.5)	5.5(9.7)
MaT	62.5(37.5)	9.7(6.9)	13.8(86.2)	0(9.7)	61.1(38.9)	9.7(2.8)	80.5(19.5)	23.6(4.2)	69.4(30.6)	8.3(1.4)
MiT	9.7(90.3)	1.3(54.2)	1.3(98.7)	0(73.6)	12.5(87.5)	2.7(40.3)	47.2(52.8)	4.1(22.2)	23.6(76.4)	1.3(26.4)
DTR	83.3(16.7)	61.1(2.8)	88.8(11.2)	51.3(0)	80.5(19.5)	48.6(4.2)	81.9(18.1)	59.7(2.8)	75.0(25.0)	38.8(6.9)

*DT: Daily temperature, MaT: Maximum temperature, MiT: Minimum temperature, DTR: Temperature range.

Table 3.2. The arithmetic average of change rates for climatological variables at 72 stations in the eastern China during the period 1951-1994

	Annual		Winter (Dec.-Feb.)		Spring (March-May)	
Rate	(^{0}C/yr)	(^{0}C/44yr)	(^{0}C/yr)	(^{0}C/44yr)	(^{0}C/yr)	(^{0}C/44yr)
DT	0.008±0.012	0.35±0.51	0.025±0.014	1.1±0.63	0.007±0.016	0.31±0.68
MaT	-0.002±0.012	-0.088±0.51	0.012±0.013	0.52±0.59	-0.003±0.017	-0.13±0.77
MiT	0.018±0.017	0.79±0.76	0.038±0.021	1.67±0.94	0.017±0.021	0.75±0.93
DTR	-0.020±0.018	-0.88±0.81	-0.026±0.021	-1.14±0.93	-0.021±0.023	-0.92±1.0

	Summer (June-Aug.)		Fall (Sept.-Nov.)	
Rate	(^{0}C/yr)	(^{0}C/44yr)	(^{0}C/yr)	(^{0}C/44yr)
DT	-0.005±0.014	-0.22±0.63	0.003±0.013	0.13±0.58
MaT	-0.013±0.018	-0.57±0.80	-0.004±0.013	-0.18±0.57
MiT	0.004±0.015	0.17±0.64	0.011±0.021	0.48±0.91
DTR	-0.017±0.016	-0.75±0.71	-0.015±0.022	-0.66±0.98

*DT: Daily temperature, MaT: Maximum temperature, MiT: Minimum temperature, DTR: Temperature range.

Table 3.3. Percent (P) of stations with negative or positive (in parenthesis) differences among the comparisons of different climatological variables, and the arithmetic average of differences (^{0}C, Diff) and their standard deviations among the climatological variables for the different period at 72 stations in the eastern China. The T_{9293} and T_{8990} represent the two-year averages of periods 1992-1993 and 1989-1990 respectively. The T_{929394}, T_{888990} and T_{859697} represent the three-year averages of the periods 1992-1994, 1988-1990 and 1985-1987 respectively. Differences significant at the 0.05 level are in bold face.

	Annual		Winter (Dec.-Feb)		Spring (March-May)		Summer (June-Aug.)		Fall (Sept.-Nov.)	
	P(%)	Diff (^{0}C)	P(%)	Diff (^{0}C)	P(%)	Diff (^{0}C)	P(%)	Diff (^{0}C)	P(%)	Diff (^{0}C)
T_{max92}-T_{max90}	62.5 (37.5)	-0.09±0.40	13.8(86.2)	**1.74±1.19**	70.8(29.2)	-0.28±0.58	83.3(16.7)	-0.82±0.75	76.3(23.7)	**-1.01±1.03**
T_{min92}-T_{min90}	100(0)	-0.71±0.29	26.3(73.7)	0.09±0.62	55.5(44.5)	-0.13±0.53	95.8(4.2)	**-1.02±0.56**	100(0)	**-1.79±0.56**
$T_{daily92}$-$T_{daily90}$	94.4(5.6)	-0.40±0.29	19.4(80.6)	0.91±0.81	65.2(34.8)	-0.20±0.46	97.2(2.8)	**-0.92±0.59**	100(0)	**-1.40±0.64**
T_{DTR92}-T_{DTR90}	5.5(94.5)	**0.62±0.38**	4.1(95.9)	**1.64±0.98**	56.9(43.1)	-0.15±0.62	37.5(62.5)	0.20±0.59	13.8(86.2)	**0.77±1.05**
$T_{max9293}$-$T_{max8990}$	38.8(61.2)	0.05±0.26	6.9(93.1)	**1.14±0.80**	66.6(33.7)	-0.13±0.31	73.6(26.4)	-0.37±0.48	66.6(334)	-0.41±0.71
$T_{min9293}$-$T_{min8990}$	93.0(7.0)	-0.42±0.29	63.8(36.2)	-0.25±0.58	61.1(38.9)	-0.09±0.52	88.8(11.2)	-0.43±0.38	94.4(5.6)	**-0.93±0.51**
$T_{daily9293}$-$T_{daily8990}$	81.9(18.1)	-0.18±0.23	27.7(72.3)	0.44±0.59	59.7(40.3)	-0.11±0.34	86.1(13.9)	-0.40±0.35	94.4(5.6)	-0.67±0.47
$T_{DTR9293}$-$T_{DTR8990}$	44.4(55.6)	**0.48±0.31**	48.6(51.4)	**1.40±0.74**	47.2(52.8)	-0.05±0.50	51.3(48.7)	0.06±0.51	45.8(54.2)	**0.51±0.81**
$T_{max929394}$-$T_{max888990}$	6.9(93.1)	0.27±0.18	4.1(95.9)	**0.92±0.54**	2.7(97.3)	**0.49±0.24**	62.5(37.5)	-0.11±0.53	54.1(45.9)	-0.21±0.73
$T_{Tmin929394}$-$T_{min888990}$	37.5(62.5)	0.04±0.26	37.5(62.5)	0.16±0.45	8.3(91.7)	0.44±0.46	65.2(34.8)	-0.06±0.33	72.2(27.8)	-0.37±0.48
$T_{daily929394}$-$T_{daily888990}$	12.5(87.5)	0.15±0.31	6.9(93.1)	0.54±0.62	4.1(95.9)	**0.46±0.47**	63.8(36.2)	-0.09±0.36	65.2(34.8)	-0.29±0.54
$T_{DTR929394}$-$T_{DTR888990}$	12.5(87.5)	0.23±0.25	5.5(94.5)	**0.76±0.63**	40.2(59.8)	0.05±0.44	51.3(48.7)	-0.06±0.47	36.1(63.9)	0.16±0.67
$T_{max858687}$-$T_{max888990}$	55.5(44.5)	-0.11±0.35	34.7(65.3)	0.34±0.77	43.0(57.0)	0.07±0.54	83.3(16.7)	-0.28±0.47	79.1(20.9)	**-0.61±0.65**
$T_{min858687}$-$T_{min888990}$	93.0(7.0)	-0.37±0.26	90.2(9.8)	-0.79±0.47	66.6(33.4)	-0.16±0.44	91.6(8.4)	-0.30±0.22	68.0(32.0)	-0.22±0.48
$T_{daily858687}$-$T_{daily888990}$	77.7(22.3)	-0.24±0.28	66.6(33.4)	-0.22±0.58	50.0(50.0)	-0.05±0.46	87.5(12.5)	-0.29±0.31	70.8(29.2)	-0.41±0.54
$T_{DTR858687}$-$T_{DTR888990}$	12.5(87.5)	0.25±0.24	1.3(98.7)	**1.14±0.53**	19.4(80.6)	0.24±0.31	54.1(45.9)	0.02±0.40	86.1(13.9)	**-0.38±0.36**

Table 3.4. Comparison of the climatological variables for the southeastern US (Saxena et al., 1997; Saxena and Yu, 1998) and eastern China. $P(T_{daily})$, $P(T_{max})$, $P(T_{min})$, $P(T_{DTR})$ represents the percent of stations with negative or positive (in parenthesis) trend of mean daily, maximum, minimum temperature, and DTR for the eastern China (period 1951-1994) and southeastern US (period 1949-1994) respectively. T_{929394}, T_{888990} and T_{859697} represent the three-year averages of the periods 1992-1994, 1988-1990 and 1985-1987 respectively.

	Annual		Winter (Dec.-Feb.)		Spring (March-May)		Summer (June-Aug.)		Fall (Sept.-Nov.)	
Parameters	China	USA	China	USA	China	USA	China	USA	China	USA
$P(T_{daily})$ (%)	22.2(77.8)	51.9(48.1)	1.3(98.7)	86.5(13.5)	30.5(69.5)	50.0(50.0)	63.8(36.2)	42.3(57.7)	37.5(62.5)	19.2(80.8)
$P(T_{max})$ (%)	62.5(37.5)	67.0(33.0)	13.8(86.2)	90.4(9.6)	61.1(38.9)	42.3(57.7)	80.5(19.5)	63.5(36.5)	69.4(30.6)	42.3(57.7)
$P(T_{min})$ (%)	9.7(90.3)	40.9(59.1)	1.3(98.7)	73.1(26.9)	12.5(87.5)	48.1(51.9)	47.2(52.8)	30.8(69.2)	23.6(76.4)	17.3(82.7)
$P(T_{DTR})$ (%)	83.3(16.7)	69.2(30.8)	88.8(11.2)	67.3(32.7)	80.5(19.5)	48.1(51.9)	81.9(18.1)	76.9(23.1)	75.0(25.0)	75.0(25.0)
$P(T_{max929394}-T_{max888990})$(%)	6.9(93.1)	97.9(2.1)	4.1(95.9)	91.5(8.5)	2.7(97.3)	93.6(6.4)	62.5(37.5)	93.6(6.4)	54.1(45.9)	89.4(10.6)
$P(T_{max858687}-T_{max888990})$(%)	55.5(44.5)	55.3(44.7)	34.7(65.3)	97.8(2.2)	43.0(57.0)	21.3(78.7)	83.3(16.7)	34.0(66.0)	79.1(20.9)	14.9(85.1)
$P(T_{min929394}-T_{min888990})$(%)	37.5(62.5)	19.1(80.9)	37.5(62.5)	8.5(91.5)	8.3(91.7)	85.1(14.9)	65.2(34.8)	19.1(80.9)	72.2(27.8)	12.8(87.2)
$P(T_{min858687}-T_{min888990})$(%)	93.0(7.0)	19.1(80.9)	90.2(9.8)	85.1(14.9)	66.6(33.4)	27.8(70.2)	91.6(8.4)	19.1(80.9)	68.0(32.0)	0(100.0)
$P(T_{daily929394}-T_{daily888990})$(%)	12.5(87.5)	70.2(27.3)	6.9(93.1)	44.7(55.3)	4.1(95.9)	91.5(8.5)	63.8(36.2)	66.0(34.0)	65.2(34.8)	55.3(44.7)
$P(T_{daily858687}-T_{daily888990})$(%)	77.7(22.3)	40.4(59.6)	66.6(33.4)	93.6(6.4)	50.0(50.0)	19.1(80.9)	87.5(12.5)	27.7(72.3)	70.8(29.2)	2.1(97.9)
$P(T_{DTR929394}-T_{DTR888990})$(%)	12.5(87.5)	97.9(2.1)	5.5(94.5)	97.9(2.1)	40.2(59.8)	74.5(23.4)	51.3(48.7)	93.6(6.4)	36.1(63.9)	89.4(10.6)
$P(T_{TDTR858687}-T_{DTR888990})$(%)	12.5(87.5)	87.2(12.8)	1.3(98.7)	78.7(21.3)	19.4(80.6)	21.3(78.7)	54.1(45.9)	63.8(36.2)	86.1(13.9)	97.9(2.1)
$T_{max929394}-T_{max888990}$ (C)	0.27±0.18	-0.57±0.37	0.92±0.54	-0.52±0.45	0.49±0.24	-0.68±0.51	-0.11±0.53	-0.46±0.45	-0.21±0.73	-0.54±0.46
$T_{max858687}-T_{max888990}$ (C)	-0.11±0.35	-0.09±0.31	0.34±0.77	-0.85±0.48	0.07±0.54	0.57±0.67	-0.28±0.47	0.10±0.37	-0.61±0.65	0.29±0.39
$T_{min929394}-T_{min888990}$ (C)	0.04±0.26	0.19±0.43	0.16±0.45	0.41±0.49	0.44±0.46	-0.40±0.51	-0.06±0.33	0.22±0.36	-0.37±0.48	0.40±0.55
$T_{min858687}-T_{min888990}$ (C)	-0.37±0.26	0.32±0.56	-0.79±0.47	-0.37±0.68	-0.16±0.44	0.32±0.74	-0.30±0.22	0.28±0.41	-0.22±0.48	1.30±0.59
$T_{daily929394}-T_{daily888990}$ (C)	0.15±0.31	-0.20±0.32	0.54±0.62	-0.06±0.39	0.46±0.47	-0.52±0.44	-0.09±0.36	-0.11±0.33	-0.29±0.54	-0.09±0.34
$T_{daily858687}-T_{daily888990}$ (C)	-0.24±0.28	0.07±0.45	-0.22±0.58	-0.65±0.44	-0.05±0.46	0.46±0.65	-0.29±0.31	0.19±0.29	-0.41±0.54	0.80±0.39
$T_{DTR929394}-T_{DTR888990}$ (C)	0.23±0.25	-0.76±0.48	0.76±0.63	-0.93±0.48	0.05±0.44	-0.27±0.50	-0.06±0.47	-0.68±0.54	0.16±0.67	-0.95±0.74
$T_{TDTR858687}-T_{DTR888990}$ (C)	0.25±0.24	-0.41±0.56	1.14±0.53	-0.47±0.68	0.24±0.31	0.24±0.74	0.02±0.40	-0.18±0.41	-0.38±0.36	-1.01±0.59

Figure 3.1A. The station locations (●) and spatial patterns of the summer mean maximum temperature during the period 1951-1994 in eastern China.

Figure 3.1B. The station locations (●) and spatial pattern of the summer mean maximum temperature of 1992 relative to that of 1990 in eastern China

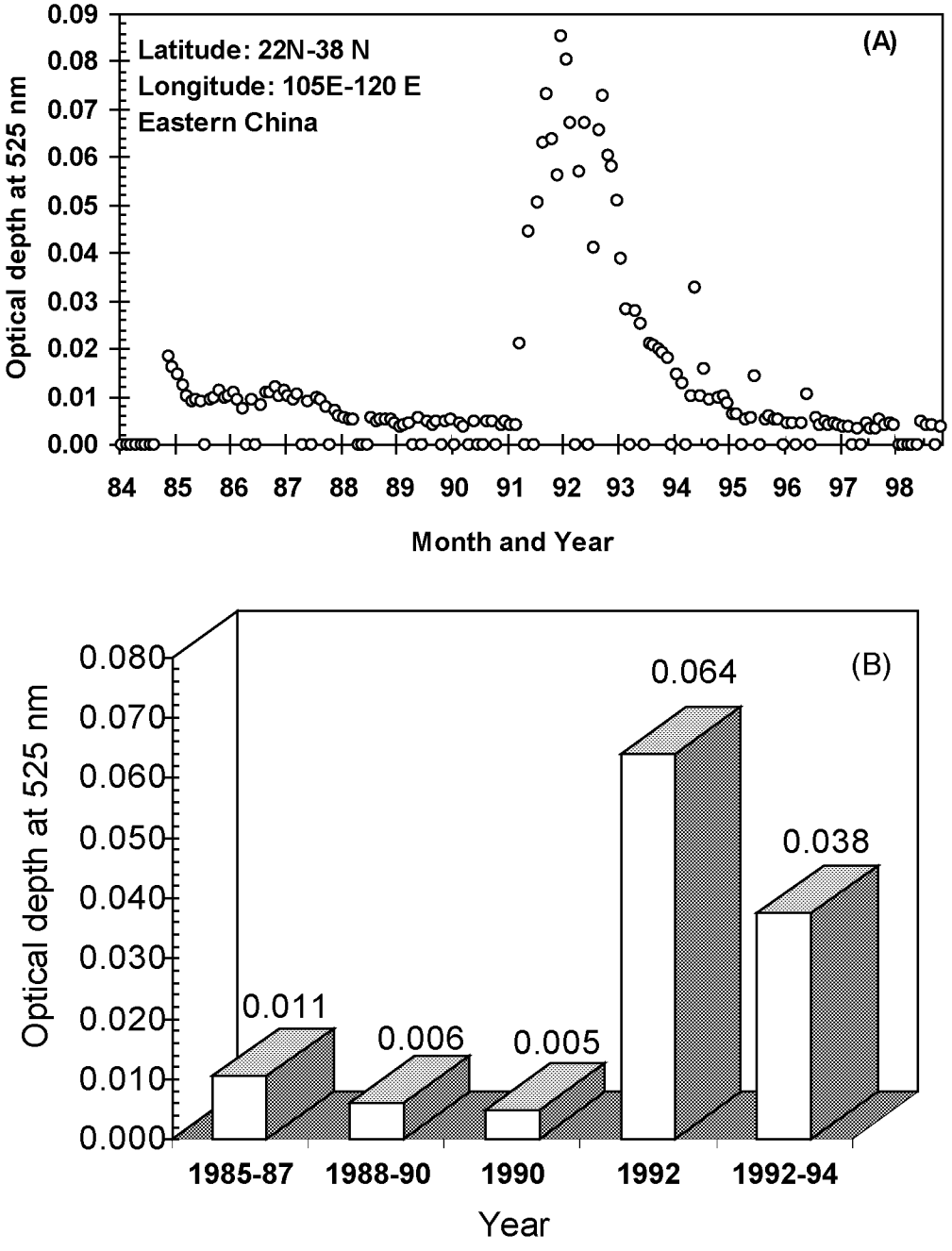

Figure 3.2. The time series of monthly mean columnar optical depth (A) and one-year, two-year, and three-year mean optical depth (B) at 525 nm in eastern China during the period 1985-1998

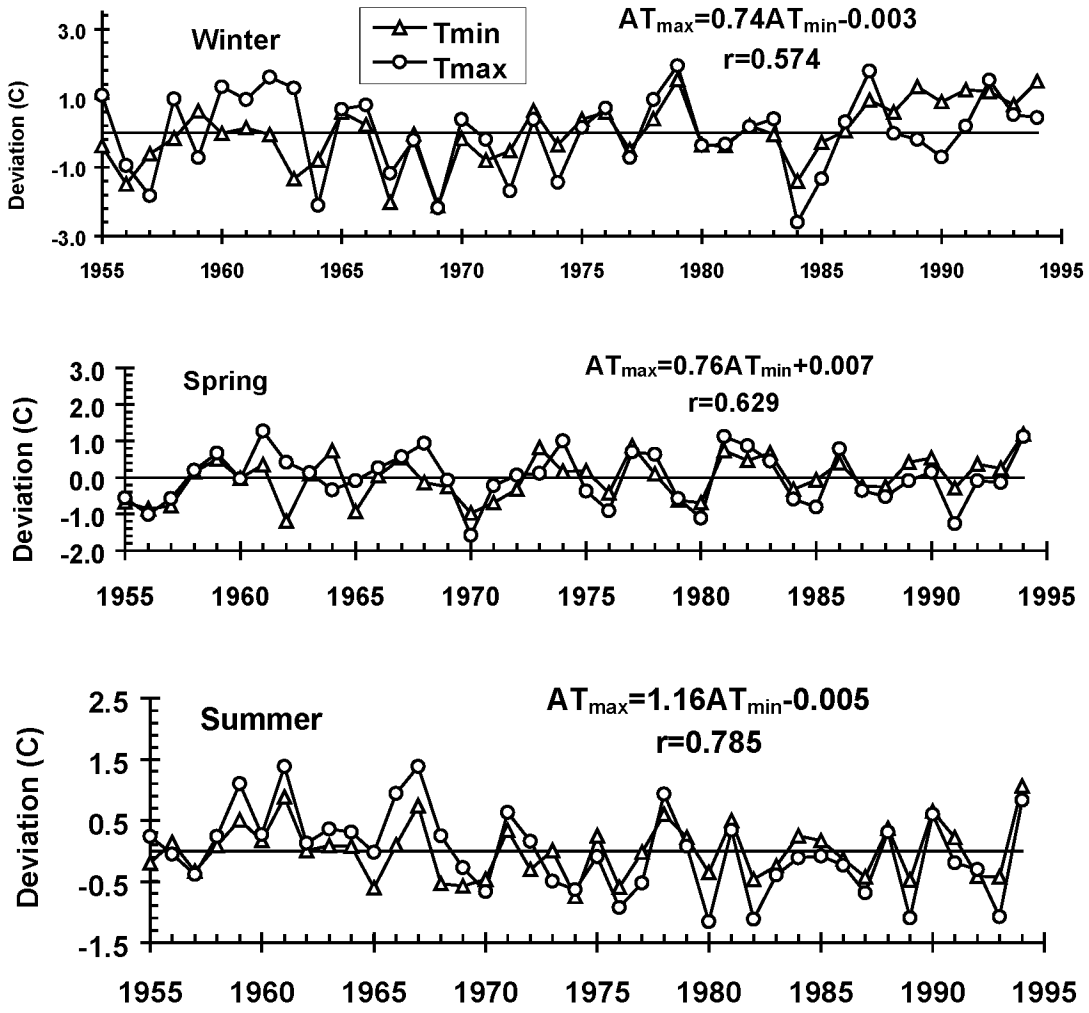

Figure 3.3. Seasonal mean maximum temperature deviation (AT_{max}) and minimum temperature deviation (AT_{min}) at 59 stations in eastern China during the period 1955 to 1994. r is correlation coefficient between AT_{max} and AT_{min}

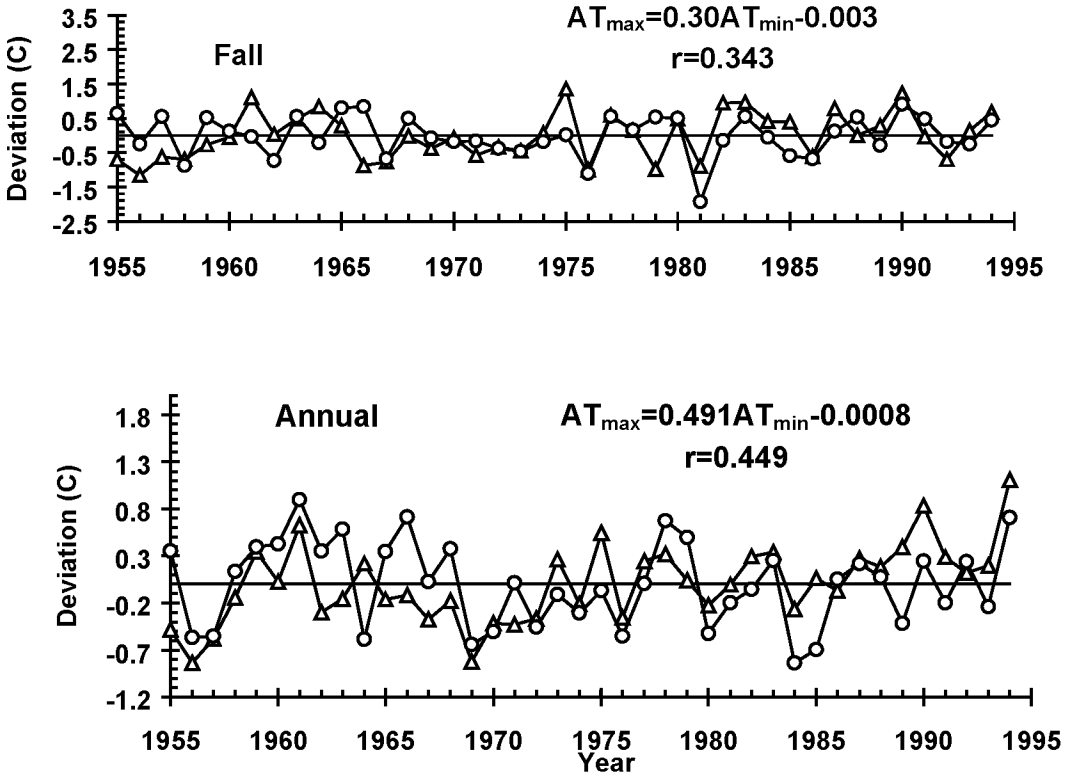

Figure 3.3. (Continued)

4. AN EVALUATION OF CHEMICAL AND SIZE EFFECTS ON RADIATIVE PROPERTIES OF MULTI-COMPONENT AEROSOLS

Shaocai Yu, V. K. Saxena and B.N. Wenny

Department of Marine, Earth and Atmospheric Sciences

North Carolina State University

Raleigh, NC 27695-8208, USA

In preparation for Submission to Atmospheric Research, 1999.

4.1. Abstract

The sensitivity of aerosol radiative properties (scattering coefficient, extinction coefficient, single scatter albedo and asymmetry factor) and radiation transmission to aerosol composition, size distribution, relative humidity (RH) is examined in this paper. Mie calculation and tropospheric visible radiation model are used. The following aerosol systems are considered: inorganic and organic ions (Cl^-, Br^-, NO_3^-, SO_4^{2-}, Na^+, NH_4^+, K^+, Ca^{2+}, Mg^{2+}, $HCOO^-$, CH_3COO^-, $CH_3CH_2COO^-$, CH_3COCOO^-, $OOCCOO^{2-}$, MSA^{-1}); water-insoluble inorganic and organic compounds (elemental carbon, n-alkanes, SiO_2, Al_2O_3, Fe_2O_3 and other organic compounds). The partial molar refraction method and the volume-average method were used to calculate the real and imaginary parts of refractive index of real aerosols respectively. The sensitivity test shows that the extinction coefficient increased by 70% with RH varying from 0% to 80. Both extinction coefficient and asymmetry factor increase by ~48% with real part varying from 1.40 to 1.65. The scattering coefficient and single scattering albedo decrease by 18% and 24% respectively, with the imaginary part varying from –0.005 to –0.1. The scattering and extinction coefficients increased by 118 times and 123 times with the geometric mean radius varying from 0.05 to 0.3 μm respectively. The scattering and extinction coefficients, and asymmetry factor increased by 389 times, 334 time and 5.4 times with the geometric standard deviation varying from 1.2 to 3.0 respectively. The radiation transmission is very sensitive to the change in geometric mean radius and geometric standard deviation; other factors are not as significant.

4.2. Introduction

Atmospheric aerosols may influence the Earth's radiation balance directly by backscattering and absorption of solar radiation, and indirectly by increasing cloud condensation nucleus (CCN) concentrations, which in turn increase cloud droplet concentrations and thus backscattering of solar radiation (Twomey, 1977; Charlson et al., 1992; Penner et al., 1994; Kiehl and Briegleb, 1993; Pilinis et al., 1995; Saxena et al., 1997). IPCC (1995) summarized that global mean forcing resulting from anthropogenic sulfate was in the range of -0.25 to -0.9 W m^{-2}, with substantial uncertainty, and biomass burning aerosol forcing was between -0.05 and -0.6 W m^{-2}. Evaluation of aerosol direct radiative forcing is complicated by the fact that aerosols are highly nonuniformly distributed over the Earth and comprise a variety of chemical species, and their abundance varies with particle size, location and time. As mentioned by Penner et al. (1994), one of central scientific questions related to the direct radiative influence of aerosols is how the aerosol composition and size distribution affect the optical depth and radiative properties of aerosols, including dependence on relative humidity. Up to today the sensitivity of direct aerosol forcing to chemical composition, size distribution and relative humidity on a global scale has been tested with a "refrence box model" (Charlson et al., 1992; Pilinis et al., 1995) and a GCM model (Kiehl and Briegleb, 1993; Boucher and Anderson, 1995). All these model works on direct aerosol forcing only focused on anthropogenic sulfate aerosols.

The objective of this paper is (1) to accurately calculate the refractive index of aerosol particles with the known chemical composition; (2) to theoretically evaluate the sensitivity of aerosol radiative properties and radiation transmission in the visible range to refractive index, size distribution and relative humidity under some assumptions with Mie code and radiative

transfer code. Since the aerosol particle refractive index is determined by its chemical composition, the dependence of radiative properties of aerosol particles on the refractive index can indicate the effects of chemical composition. Since most of the light scattering and extinction are caused by particles in the accumulation mode range, and these particles are neither removed effectively by impaction nor by diffusion, the accumulation mode particles (0.1-1.0 μm, diameter) are the most important in terms of aerosol radiative forcing. In this study the sensitivity of aerosol radiative properties to size distribution is tested on the basis of the calculation of the particle radiative properties for the accumulation mode only.

4.3. Model formulation

4.3.1. Atmospheric aerosol composition and size distribution

Atmospheric aerosol particles are composed of complex mixtures of natural and anthropogenic chemical species that include (1) water-soluble inorganic and organic compounds such as sulfate, nitrate, formate and acetate, (2) water-insoluble inorganic and organic compounds such as elemental carbon, Al_2O_3 and n-alkanes, and (3) water itself. When ambient aerosol chemical composition measurements are performed, typically soluble individual anion and cation concentrations are measured by IC (Andreae et al., 1988), element such as Al and Pb by partial-induced X ray emission (PIXE) (Ouimete and Flagan, 1982). The insoluble high molecular weight organic compounds in aerosols are measured by gas-chromatography-mass-spectrometer (GS/MS) method (Rogge et al., 1993). The IC and PIXE methods provide no information on the concentrations of specific salts or classes of inorganic and organic salts. GC/MS method can quantify the concentrations of individual organic compounds in the atmospheric particles. However, typically only about 10% of the total organic mass can be identified by GC/MS method (Rogge et al., 1993). In general the water-soluble materials within atmospheric aerosol particles are expected to be a mixture of different chemicals and the water-

soluble parts of aerosol particles are regarded to be a mixture of electrolytes together with any other water-soluble material. There is possible interaction between those ions that the chemical components do not have in common, especially at high relative humidity (Hanel, 1976). For example, in a mixture of KNO_3 and NaCl, there is a possible interaction between K^+ and Na^+. Thus it is reasonable to consider water-soluble parts of aerosol particles as a mixed solute, and the aerosol particles at dry state composed of a mixed solute and insoluble substances. Since the composition of the aerosol particles depends upon the sources and subsequent transformation while airborne, it is possible to separate aerosols into urban, rural continental and marine aerosols in a first approximation (Pueschel, 1995). Table 4.1 lists the estimates of chemical components for three atmospheric aerosol types. In Table 4.1, the concentrations of inorganic compounds (Cl^-, Br^-, NO_3^-, SO_4^{2-}, Na^+, NH_4^+, K^+, Ca^{2+}, Mg^{2+}, SiO_2, Al_2O_3, Fe_2O_3), total concentrations of organics and total mass concentrations of aerosol particles for three aerosol types were taken from the estimates of Pueschel (1995). For organics, over 80 individual organic compounds found in the aerosol particles were identified and quantified (Roggie et al., 1993; Saxena et al., 1995). In this study, the concentrations of soluble organic compounds ($HCOO^-$, CH_3COO^-, $CH_3CH_2COO^-$, CH_3COCOO^-, $OOCCOO^{2-}$, MSA) were taken from the estimates of Yu (1999). Chylek et al. (1996) showed that the average black carbon atmospheric concentration in continental air masses was 0.23 ± 0.04 $\mu g/m^3$ compared with 0.03 ± 0.01 $\mu g/m^3$ for maritime air in the measurements over the southern Nova Scotia. Shah et al. (1982) indicated that the average black carbon for 26 cities in USA was 3.8 $\mu g/m^3$. In this study, the black carbon concentration used for urban, continental and marine aerosols are 3.8, 0.23 and 0.06 $\mu g/m^3$, respectively. The other organic compound concentrations in Table 4.1 were taken from the estimates of Roggie et al. (1993). In Table 4.2 are listed the physical-chemical and optical properties of various pure salts in the atmospheric particles.

For the aerosol model computation, the lognormal distribution function has been found suitable to characterize the size distribution of atmospheric aerosols (Pueschel, 1995). The accumulation mode particles (0.1-1.0 μm, diameter) are the most important in terms of aerosol

radiative forcing. In Table 4.4 is listed the typical size distributions for three types of aerosol for the accumulation mode at dry state obtained by the experiments of other researches. As can be seen, the total number concentration, the geometric mean diameter (D_g), and the geometric standard deviation (σ_g) for the accumulation mode are in the ranges of 18.6 to 3000 cm^{-3}, 0.076 to 0.75 μm, and 1.35 to 2.0, respectively.

4.3.2. The parameterization of the influence of relative humidity

Table 4.2 lists the RH (RHD) at which the deliquescence will occur for some pure salts. The effects of continuously increasing RH on the growth of a pure salt aerosol particle can be calculated from equilibrium thermodynamics (Hanel, 1976, Tang et al., 1981). However, it is very difficulty to predict this so-called 'hysteresis effects' of water uptake for actual multi-component aerosol particles because this not only depends on the history of relative humidity but also varies from one sample to the other (Hanel, 1976). Here, the particle hysteresis effects should not be considered in detail. Instead, the density, refractive index and radius of aerosol particles are regarded as a unique function of relative humidity where the "hysteresis effects" are partially taken into account for three aerosol types using the experimental data of Hanel (1976). The equations for density, refractive index and radius are as follows (Hanel, 1976):

$$\rho = \rho_w + (\rho_0 - \rho_w)(1 + \frac{\rho_0}{\rho_w}\bar{\mu}\frac{RH}{1-RH})^{-1} \qquad (4.1)$$

$$m_r = m_{r\,w} + (m_{r0} - m_{rw})(1 + \frac{\rho_0}{\rho_w}\bar{\mu}\frac{RH}{1-RH})^{-1} \qquad (4.2)$$

$$m_i = m_{i\,w} + (m_{i0} - m_{i\,w})(1 + \frac{\rho_0}{\rho_w}\bar{\mu}\frac{RH}{1-RH})^{-1} \qquad (4.3)$$

$$r = r_0(1 + \frac{\rho_0}{\rho_w}\bar{\mu}\frac{RH}{1-RH})^{\frac{1}{3}} \qquad (4.4)$$

where the subscript "w" denotes pure water and "0" the dry substance, m_r and m_i are the real and imaginary parts of refractive index. $\bar{\mu}$ is mean linear mass increase coefficient. Figure 4.1 shows the $\bar{\mu}$ as a function of relative humidity for three aerosol types, which are obtained from the experimental results in Table IV of Hanel (1976). As can be seen, the dependence of mean linear mass increase coefficient on RH for difference types of aerosols is rather complicated as indicated by the crossing of three curves. The effect of RH on radiative properties of aerosol particles must ultimately act through changes in the particle size and refractive index. In Figure 4.2 are the changes of densities, refractive indices and radius for three type aerosol as a function of RH. As can be seen, the RH effect is important at RH> 80% for density and refractive index, but the radius is insensitive to the change in RH until RH>90%.

4.4. Results and Discussion

4.4.1. Refractive index calculation

One of central question for prediction of radiative properties of aerosol particles is to accurately calculate their refractive index. As shown in Table 4.1, the available information on the particle compositions is the ion concentrations of soluble components and compound concentrations of insoluble components. It has been shown that the partial molar refraction approach is applicable to calculate refractive index for ionic solid-aqueous electrolyte mixture (Moelwyn-Hughes, 1961; Stelson, 1990). The partial molar refraction R is defined as (Weast, 1988):

$$R = \left(\frac{n^2 - 1}{n^2 + 2}\right)\left(\frac{M}{\rho}\right) \qquad (4.5)$$

where n=refractive index, M=molecular weight and ρ is density (g cm^{-3}). The unit of R will be $cm^3 mol^{-1}$. If the molar refractions of components are known, the mean refractive index of a medium can be calculated as follows:

$$n = \left(\frac{1 + 2\frac{R}{V}}{1 - \frac{R}{V}} \right)^{\frac{1}{2}} \qquad (4.6)$$

for an aerosol particle:

$$\frac{R}{V} = \frac{\Sigma(\frac{Ri}{Mi})[Si]}{[AV]} \qquad (4.7)$$

where Ri is the partial molar refraction of component i in $cm^3\ mol^{-1}$, Mi is the molecular weight of component i in $g\ mol^{-1}$, [Si] is the concentrations of component i in $\mu g\ m^{-3}$, and [AV] is the aerosol volume in $\mu m^3\ cm^{-3}$. The aerosol volume can be either measured or predicted by:

$$[AV] = \Sigma \frac{S_i}{\rho_i} \qquad (4.8)$$

where ρ_i is the density of component i in $g\ cm^{-3}$. Table 4.3 lists the partial molar refractions for ions. Table 4.2 contains the refractive index and density for possible salts existing in atmospheric aerosol particles. As can be seen, the ranges of refractive index and density for most compounds in aerosol particles are from 1.332 to 2.654 and from 0.783 to 11.344 $g\ cm^{-3}$ respectively. Volz (1972) reported on densities of water-soluble materials from different rainfalls and locations ranging between 1.76 and 1.96 $g\ cm^{-3}$. In this study the average value (1.86 $g\ cm^{-3}$) is used as the mean density for water-soluble parts in aerosol particles. The density (1.40 $g\ cm^{-3}$) and refractive index (1.55) for other organic compounds in Table 4.2 were taken from the estimates of Sloane (1984). Additionally, the mean aerosol density, ρ, can be calculated from: $\rho = \frac{\Sigma[S_i]}{\Sigma\frac{[S_i]}{\rho_i}}$. In this study, the above partial molar refraction approach is extended to calculate the refractive index of any atmospheric particles with the known chemical compositions. Table 4.3 lists the partial molar refraction for other aerosol components including insoluble inorganic and organic compounds, which were calculated on the basis of Weast

(1988)'s method. In this study, an internal mixture is assumed for the atmospheric aerosol chemical species. Tang (1996) showed that both internal and external mixtures exhibited similar light-scattering properties. Pilinis et al. (1995) concluded that the sensitivity of aerosol radiative forcing to aerosol mixing state (internal or external) is small if strongly absorbing components are not present. Table 4.1 lists refractive index and mean density for three typical aerosol types calculated by the partial molar refractive approach. As can be seen, the mean density for three aerosol types at dry state range from 1.803 to 1.890 g/m^3. The real parts of refractive index for urban, continental and marine aerosols are 1.575, 1.557 and 1.479, respectively.

As reviewed by Horvath (1993), only elemental carbon (the main constituent of soot) in atmospheric aerosol particles is highly absorbed. Hematite (a-Fe_2O_3) is the only other substance having a light absorption comparable to elemental carbon in the near u. v. (Bohren and Huffman, 1983), but absorption rapidly decreases in the visible. There are some discrepancies about the value of the complex refractive index of elemental carbon because of the difficulty of its experimental determination. The values given in the literature range from 1.2 to 2.0 for the real part and from -0.1 to -1.0 for the complex part (Horvath, 1993). In this study, the refractive index used for elemental carbon is 2.0-0.66i. Since the imaginary parts for all ions in Table 4.1 are zero and the densities of each ion in Table1 are not known, it is not easy to calculate the partial mole refractions of the ions for imaginary parts using the definition equation (4.5). In this study, the imaginary part of muti-component aerosols was calculated using the volume average of the imaginary parts of refractive index of the individual species present as follows (Sloane, 1984):

$$\overline{m_i} = [\sum_{i=1}^{N} m_i \frac{[s_i]}{\rho_i}][\sum_{i=1}^{N} \frac{[s_i]}{\rho_i}]^{-1}$$

where m_i is the imaginary part of refractive index of component i. With the estimates of black carbon concentration for three types of aerosols in Table 4.1, it was found that the complex refractive indices for urban, continental and marine aerosols were $1.575 - 0.027i$, $1.557 - 0.016i$, $1.479 - 0.0027i$ respectively. Hanel (1976) found that the real part of

refractive index for urban aerosols at city of Mainz, Germany, is 1.57 ± 0.04 by actual measurement. Grams et al. (1972) determined that the complex refractive index for urban aerosols at city of Boulder, CO, was 1.55-0.044i on the basis of light scattering measurements. Our results are very close to these from the actual measurements. These complex refractive indices for three types of aerosols will be used in the following model calculation.

4.4.2. The sensitivity to relative humidity

A Mie theory computer code developed by Dave (1968) was used to compute aerosol radiative properties. All aerosol particles are assumed to be spherical in shape in calculation. In Table 4.4 are shown the values of the particle light scattering and extinction coefficient calculated with the above assumption at 30%, 80% and 99% relative humidity for different particle size distributions of several aerosol types at wavelength (580 nm). The wavelength, 580 nm, is chosen as recommended by Horvath (1993) to give the maximum perception of an object under the daylight conditions. As can be seen, the growth factors from 30% to 80% RH range from 1.57 to 1.92 (average 1.77 ± 0.12) and from 1.55 to 1.90 (average 1.71 ± 0.11) for scattering and extinction coefficients, respectively. This is in agreement with the criterion value of the hydroscopic growth factor (1.7 ± 0.3) (which is defined as the ratio of the light scattering coefficient by an aerosols at 80% RH to that at 30%) derived from the direct nephelometer measurement (Charlson et al., 1984). This value has been utilized to date as a first estimate in climate change modeling studies (Charlson et al., 1992). It is interesting to note that Hegg et al. (1993) got substantially larger values of the hygroscopic growth (see Table 4.1 of Hegg et al. (1993)) for the same size distribution as those in Table 4.4. Hegg et al. (1993) ascribed it to be influenced by the position of the initial dry aerosol size distribution relative to the effective light-scattering droplet size range. What makes our calculation results different from those of Hegg et al. (1993) is from the different values of the refractive index and mean linear mass increase coefficient used for the aerosol particles. The consistence of our results in Table 4.4 with the

hygroscopic growth factor ranges (1.5 to 1.8) from the direct measurement of Charlson et al. (1984) indicated that our calculation for the effect of relative humidity on scattering coefficient was reasonable. At high RH such as 99%, the growth factors are much high and variable as shown in Tables 4.

Table 4.4 shows that the growth factors from 30% to 80% RH and to 99% range from 1.06 to 1.18 (average 1.12 ± 0.04) and from 1.10 to 1.53 (average 1.32 ± 0.13) for asymmetry factor, respectively. The growth factors from 30% to 80% RH and to 99% RH range from 1.01 to 1.06 (average 1.03 ± 0.02) and from 1.02 to 1.14 (average 1.08 ± 0.04) for the single scattering albedo, respectively. The single scattering albedo is not sensitive to RH. At the high RH such as 99%, the single scatter albedo is close to 1.0. The single scattering albedo and asymmetry factor are insensitive to the change in RH. This is in agreement with those of Pilinis et al. (1995). Both scattering and extinction coefficients are more sensitive to the change in RH than the single scatter albedo and asymmetry factor.

4.4.3. The sensitivity to refractive index

In the following sensitivity test study, the parameters used for three types of aerosols are assumed as follows: (1) urban aerosols of Meszaros (1978), N=560 cm^{-3}, D_g=0.100 μm, σ_g =2.0, m=1.590-0.027*i*, RH=80%; (2) continental aerosols of Hoppel et al. (1984), N=3000 cm^{-3}, D_g=0.080 μm, σ_g =2.0, m=1.564-0.016*i*, RH=80%; (3) marine aerosols of Gathman (1983), N=67 cm^{-3}, D_g=0.266 μm, σ_g =1.622, m=1.479-0.003*i*, RH=80%. Note that the values of radius, refractive index in the above assumptions are for dry state. RH is set to be 80% in the Mie calculation.

Table 4.5 listed the the ranges and averaged values of the change factors for the effects of real and imaginary part of refractive index on the aerosol radiative properties. As can be seen, the scattering and extinction coefficients increase by about 48% and asymmetry factor decrease by 6% with real part increasing from 1.4 to 1.65. But the single scattering albedo is insensitive

to the change in real part. Figures 3a and 3b show extinction coefficients, and single scatter albedo as a function of real part of refractive index for three types of aerosols at 580 nm.

Table 4.5 shows that the scattering coefficient and single scattering albedo decrease by 18% and 24% with imaginary part varying from –0.005 to 0.10, respectively. The extinction coefficient and asymmetry factor are insensitive to the change in imaginary part. As expected, the extinction coefficient and asymmetry factor increase slightly as imaginary part increases.

4.4.4. The sensitivity to size distribution

As shown in Table 4.5, scattering and extinction coefficients are very sensitive to the change in geometric mean radius. The scattering and extinction coefficients increase by 118 times and 123 times respectively, however, the asymmetry factor only increases by 17% and the single scattering albedo decreases by 0.8%, with the geometric mean radius varying from 0.05 to 0.3 μm. Figures 4a and 4b show the sensitivity test for the case of marine at different wavelengths.

Table 4.5 list the ranges and averaged values of the change factors of radiative properties for three types of aerosols with geometric standard deviation (σ_g) varying from 1.2 to 3.0. As can be seen, the scattering and extinction coefficients and asymmetry factor are very sensitive to the change in geometric standard deviation. The scattering and extinction coefficients increase by 389.3 times and 334 times respectively with geometric standard deviation varying from 1.2 to 3.0. This change of (σ_g) results in the increase of asymmetry factor by 5.4 times and the increase of single scattering albedo by 10%. Figures 4c and 4d show the sensitivity of asymmetry factor and single scattering albedo to change in σ_g for the case of urban aerosols at different wavelength.

Figures 5a and 5b show how the shape of size distribution changes for geometric mean radius varying from 0.1 to 0.4 μm at N_o=560 cm^{-3} and σ_g=2.0 and for geometric standard deviation varying from 1.2 to 3.0 at N_o=560 cm^{-3} and r_g=0.15 μm, respectively. Since the light scattering efficiency of an individual particle is dependent on the particle size, with peak

efficiencies occurring between ~0.2 and 0.7 μm in particle radius for a light wavelength of 580 nm, aerosol particles can have large scattering and extinction coefficients if their size distribution move into this efficient light scattering size range. Figure 4.5 indicates that both cases can result in the more particles in the efficient light scattering size range (0.2 to 0.7 μm, radius). It is not surprised to find that the scattering and extinction coefficients are very sensitive to the changes in geometric mean radius and geometric standard deviation.

4.4.5. The sensitivity of wavelength dependence of radiative properties.

It is interesting to note that the wavelength dependence of aerosol radiative properties is very sensitive to geometric mean radius, and rather complicated. When the geometric mean radius is small, single scattering albedo and asymmetry factor decrease with the increase of wavelength, but after geometric mean radius is larger than a value, the single scattering albedo and asymmetry factor increase with the increase of wavelength. At the latter case, the Angstrom law will not be applicable. The values of geometric mean radius at the crossing point are different for asymmetry factor and single scattering albedo as shown in Figures 4a and 4b, and are also determined by the geometric standard deviation as analyzed below. Since the light scattering efficiency of an individual particle is a nonlinear function of particle size and depends on the particle size and light wavelength tested, and the refractive index is wavelength dependent, the wavelength dependence of aerosol radiative properties will strongly rely on the size distribution and refractive index. For the wavelength dependence of refractive index, available data (Kent et al., 1983) were closely matched by setting $n(\lambda)=n(\lambda=0.598\ \mu m)-0.03(\lambda-0.598)$, where λ is the wavelength in μm. As can be seen, the wavelength dependence of refractive index is small. As shown in Figure 4.4, the wavelength dependence of asymmetry factor and single scattering albedo strongly relies on the geometric mean radius and geometric standard deviation. But the wavelength dependence of scattering and extinction coefficients on the geometric mean radius and geometric standard deviation is small. At the small geometric

mean radius and small geometric standard deviation, the asymmetry factor and single scattering albedo increase with the decrease of wavelength, however, at the large geometric mean radius and geometric standard deviation the asymmetry factor and single scattering albedo will increase with the increase of wavelength, especially for single scattering albedo, as shown in Figure 4.4.

4.4.6. Radiation transmission

Since human-induced aerosols are likely to greatly influence the future regional climate change instead of the global climate change, it is of interest to test the sensitivity of the aerosol-induced radiation transmission changes at a local or regional scale to aerosol composition, size distribution and RH. In this study, the radiation transmission was calculated for the assumed 2 kilometer aerosol layer by Madronich's Tropospheric Ultraviolet-Visible Radiation Transfer Model (TUVRTM) (Madronich, 1993). The optical depth $\tau = \int_{z1}^{z2} \sigma_e(z)dz$ was calculated by assuming that the extinction coefficient is constant within the aerosol layer. The sensitivity of aerosol-induced radiation transmission changes at 580 nm is tested under the following constant conditions: date=7/01/1995, O_3=278 DU, ground albedo=0.15, air pressure=940 mb, Latitude=35.63, longitude=82.33, UT=17.90, zenith angle=13.31, the aerosol layer=2km. Three aerosol radiative properties (optical depth, asymmetry factor and single scattering albedo) are needed in TUVRTM model to calculate the aerosol-induced radiation transmission change. In this section, the sensitivity of the aerosol-induced radiation transmission change to RH, refractive index and size distribution is tested on the basis of the previous calculation results about the aerosol radiative properties for three types of aerosols.

Tables 6 lists the radiation transmissions at 580 nm for different aerosol types at 30%, 80% and 99% relative humidity. Figure 4.6 shows the sensitivity of radiation transmission to RH, refraction index, number concentration and size distribution for three types of aerosols. Table 7 lists the change factors for radiation transmission for three types of aerosol. Note that the

radiation transmission at 580 nm is 0.911 without the aerosol layer under the assumed atmospheric conditions. It is interesting to note that the radiation transmission is not sensitive to the changes in the above parameters if total number concentration is small such as that in the case of maritime aerosols of Gathman (1983) (total number concentration is only 67 cm^{-3} as indicated in Table 7). As can be seen, the radiation transmission only decreases by 0.4% and 0.5% with the RH varying from 0% to 95% and the real part varying from 1.40 to 1.65, respectively. The radiation transmission is sensitive to the change in imaginary part and number concentration with the decrease of visible radiation transmission by 2.7% and 4.2% when the imaginary part varies from –0.005 to –0.1 and number concentration from 50 to 4000 cm^{-3}, respectively. The radiation transmission is very sensitive to the changes in geometric mean radius and geometric standard deviation. The radiation transmission decreases by 76% when geometric mean radius varies from 0.05 to 0.3 μm and decreases by 12% when geometric standard deviation varies from 1.2 to 3.0. This is in agreement with the strong dependence of scattering and extinction coefficients on geometric mean radius and geometric standard deviation. It should be emphasized that the radiation transmission also strongly depends on the zenith angle, latitude and longitude, ozone concentration.

4.5. Conclusions

In this paper, the partial molar refraction method was used to accurately calculate the real part of refractive index of aerosol particles with actual measured chemical compositions including soluble inorganic and organic ions and insoluble inorganic and organic substances. It was found that the complex refractive indices for urban, continental and marine aerosols were 1.575-0.027i, 1.557-0.016i and 1.479-0.003i, respectively. The scattering and extinction coefficients are sensitive to the changes in RH, while Both single scattering albedo and asymmetry factor are not sensitive to the change in RH. The extinction coefficient and asymmetry factor are sensitive to the change in real part. While the scattering coefficient and

single scattering albedo sensitive to the imaginary part changes. The aerosol radiative properties are very sensitive to the change in size distribution of both geometric mean radius and geometric standard deviation. The radiation transmission decreases by 76% and 12% for geometric mean radius varying from 0.05 to 0.3 μm and geometric standard deviation varying from 1.2 to 3.0 respectively. Other sensitivities are not as significant. The comparison between the theoretical calculation and actual measurement is necessary in the future work.

Acknowledgments. This research was supported by the NASA's Mission to Planet Earth (MTPE) under Contract No. NAS1-18944 from Langley Research Center, Hampton, VA and US EPA's STAR (Science to Achieve Results) grant No. R-825248.

4.6. References

Angstrom , A., On the atmospheric transmission of sun radiation and on dust I the air. Geogr. Ann., 11, 156-166, 1929.

Andreae, M. O., R. W. Talbot, T. W. Andreae and R. C. Harriss, Formic and acetic acids over the central Amazon region, Brazil. 1. Dry season. *J. Geophys. Res.* **93**, 1616-1624, 1988.

Boucher O., and T. L. Anderson, General circulation model assessment of the sensitivity of direct climate forcing by anthropogenic sulfate aerosols to aerosol size and chemistry. *J. geophys. Res.* **100**, 26117-26134, 1995

Charlson R. J., , S.E. Schwartz, J. M. Hales, R. D. Cess, J. A. Coakley, J. E. Hansen, and D. J. Hofmann, Climate forcing by anthropogenic aerosols. *Science.* **225**, 423-430,1992.

Charlson R. J., D. S. Covert, and T. V. Larson, Observations of the effect of humidity on light scattering by aerosols, in *Hygroscopic Aerosols,* edited by Ruhnke T. H. and Deepak A. pp 35-44, A. Deepak, Hampton, VA, 1984.

Chylek P., and J. Wong, Effect of absorbing aerosols on global radiation budget. *Geophys. Res. Lett.,* 22, 929-931.

Dave J. V., Subroutines for computing the parameters of electomagnetic radiation scattered by a sphere. IBM J. Res. Dev., 13, 302-312, 1969.

Gathman S. C., Optical properties of the maritime aerosols as predicted by the Navy aerosol model. Opt. Engineer, 22, 56-62, 1983.

Hanel G., The real part of the mean complex refractive index and the mean density of samples of atmospheric aerosol particles. Tellus, **20**, 371-379, 1968.

Hanel G., The properties of atmospheric aerosol particles as functions of relative humidity at thermodynamic equilibrium with the surrounding air. *Adv. Geophys.*, **19**, 73-188, 1976.

Haywood, J. M., and K. P. Shine, The effect of anthropogenic sufate and soot aerosol on the clear sky planetary radiation budget. Geophys. Res. Lett., 22, 603-606, 1995

Hegg D., T. Larson ,and P. F. Yuen, A theoretical study of the effect of relative humidity on light scattering by tropospheric aerosols. . *J. geophys. Res.* **98**, 18435-18439, 1993.

Hoppel W. A., R. Larson and M. A. Vietti. Aerosol size distributions at a site on the east coast of the United States. *Atmos. Environ.* **18**, 1613-1621, 1984.

Hoppel W. A., J. W. fitzgerald, G. M. Frick, and R. Larson, Aerosol size distributions and optical properties found I the marine boundary layer over the Atlantic ocean. *J. geophys. Res.* **95**, 3659-3686, 1990.

Horvath H., Atmospheric light absorption-a review. *Atmos. Environ.* **27**, 293-317, 1993.

IPCC, Climatic change 1995: Radiative forcing of climate and an evaluation of the IPCC 1992 emission scenarios. J.T. Houghton et al. (Eds). Cambridge University Press, Cambridge, UK, 1995.

Leaitch W. R. and G. A. Isaac, Tropospheric aerosol size distributions from 1982 to 1988 over eastern North America. *Atmos. Environ.* **25**, 601-619, 1991.

Malm W. C., J. F. Sisler, D. Huffman, R. A. Eldred, and T. A. Cahill, Spatial and seasonal trends in particle concentration and optical extinction in the United States. *J. geophys. Res.* **99**, 1347-1370, 1994.

Meszaros A., On the concentration and size distribution of atmospheric sulfate particles under rural conditions. *Atmos. Environ.* **12**, 2425-2428, 1978.

Moelwyn-Hughes E. A., Physical chemistry, 2nd rev. ed.; Pergamon Press, New York, 1961.

Pilinis C., S. N. Pandis, and J. H. Seifeld, Sensitivity of direct climate forcing by atmospheric aerosols to aerosol size and composition. *J. geophys. Res.* **100**, 18739-18754, 1995.

Penner J.E., R. J. Charlson, J. M. Hales, N. S. Laulainen, R. Leifer, T. Novakov, J. Ogren, L. F. Radke, S. E. Schwartz, and L. Travis, Quantifying and minimizing uncertainty of climate forcing by anthropogenic aerosols. *Bull. Amer. Meteorol. Soc.* **75**, 375-400, 1994.

Pueschel R. F., Atmospheric aerosols. In *Composition, Chemistry and Climate of the Atmsophere.* Ed. Singh H. B.,Van Nostrand Reinhold. pp120-175, 1995.

Rogge, W. F., M. A. Mazurek, L. M. Hildemann, G. R. Cass, and B. R. T. Simoneit, Quantification of urban organic aerosols at a molecular level: Identification, abundance and seasonal variation. *Atmos. Environ.*, **27**, 1309-1330, 1993.

Saxena V.K., and Yu Shaocai (1998) Searching for a regional fingerprint of aerosol forcing in the southeastern US. *Geophysics Research Letters*. **25**, 2833-2836.

Saxena V.K., Yu Shaocai, and J. Anderson J. (1997) Impact of stratospheric volcanic aerosols on climate: Evidence of aerosol radiative forcing in the southeastern US. *Atmospheric Environment*. **31**, 4211-4221.

Sloane C. S., Optical properties of aerosols of mixed composition. *Atmos. Environ.*, **18**, 871-878, 1984.

Stelson A. W., Urban aerosol refractive index prediction by partial molar refraction approach. *Environ. Sci. Technol.*, **24**, 1676-1679, 1990.

Tang I. N., W.T. Wong, and H.R. Munkelwiz., The relative importance of atmospheric sulfates and nitrates in visibility reduction. *Atmos. Environ.*, **15**, 2463-2471, 1981.

Tang I.N. Chemical and size effects of hydroscopic aerosols on light scattering coefficients. *J. geophys. Res*. **101**, 19245-19250, 1996.

Twomey, S., Atmospheric aerosols, Elsevier, Amsterdam, Oxford and New York, 1977.

Volz F., Infrared absorption by atmsopheric aerosol substances. *J. geophys. Res*. **77**, 1017-1031, 1972.

Weast R. C., CRC Handbook of Chemical and Physics, Cleveland, OH, 1988.

Whitby K. T., The physical characteristics of sulfur aerosols. *Atmos. Environ.*, **12**, 135-159, 1978.

Yu Shaocai, The role of organic acids (formic, acetic, pyruvic and oxalic) in formation of cloud condensation nuclei (CCN). *Atmos. Res*., 1999 (in review)

Table 4.1. The aerosol chemical composition for the different environments and their calculated refractive index (real part) (see text for explanation)

Species	Urban aerosols ($\mu g/m^3$)	Continental ($\mu g/m^3$)	Marine ($\mu g/m^3$)
Soluble component			
OH^-	0	0	0
F^-	0	0	0
Br^-	0.1	0.02	0.02
Cl^-	3.2	0.11	4.6
NO_3^-	3	0.9	0.05
SO_4^{2-}	14	2.8	2.6
Na^+	1.2	0.05	2.9
NH_4^+	4.8	1.2	0.16
K^+	0.4	0.06	0.1
Ca^{2+}	1.6	0.17	0.2
Mg^{2+}	0.6	0.09	0.4
$HCOO^-$	0.108	0.045	0.025
CH_3COO^-	0.118	0.018	0.01
$CH_3CH_2COO^-$	0	0	0
$CH_3(CO)COO^-$(pyruvic)	0	0	0
$(OOCCOO)^{2-}$)(oxalic)	0.158	0.015	0.015
$CH_3S(O)_2OH$ (MSA)	0.008	0.008	0.008
Insoluble component			
C(element carbon)	3.8	0.23	0.06
SiO_2	5.9	0.7	0
Al_2O_3	3.6	0.24	0
Fe_2O_3	5.3	0.22	0.07
$CH_3(CH_2)_{14}COOH$(n-Hexadecanoic acid)	0.118	0.014	0.014
$CH_3(CH_2)_{16}COOH$(n-Octadecanoic acid)	0.057	0.002	0.002
$HOOCCH_2COOH$(Malonic acid)	0.028	<0.00001	<0.00001
$HOOC(CH_2)_2COOH$(Succinic acid)	0.055	<0.00001	<0.00001
$HOOC(CH_2)_3COOH$(Glutaric acid)	0.028	<0.00002	<0.00002
$C_6H_4(COOH)_2$(1,2-Benzenedicarxylic acid)	0.06	<0.00002	<0.00002
other organic compounds	26	0.9	0.8
Total organic mass ($\mu g/m^3$)	30.6	1.17	0.9
Total inorganic mass ($\mu g/m^3$)	43.5	6.4	11.2
Total mass ($\mu g/m^3$)	74.24	7.79	12.03
Mean density ($\mu g/m^3$)	1.820	1.890	1.825
Refractive index for aerosol particle	1.590	1.564	1.479

Table 4.2. The physical-chemical and optical properties of different salts in atmospheric aerosol particles. RHD is the R.H of deliquescence, and ref. index is refractive index

Salts	refr. index	density (g/cm^3)	RHD (%)	Salts	refr. index	density (g/cm^3)	RHD (%)
NH_4CH_3COO		1.174		$Mg(CH_3COO)_2(H_2O)_4$	1.491	1.454	
NH_4Br	1.712	2.429		$MgBr_2$		3.724	
NH_4HCO_3	1.423	1.580		$MgCO_3$	1.717	2.958	
NH_4Cl	1.642	1.527	80	$MgCO_3(H_2O)_5$	1.456	1.730	
NH_4F		1.009		$MgCl_2$	1.675	2.320	
NH_4NO3		1.725	62	$MgCl_2(H_2O)_6$	1.495	1.569	
$(NH_4)_2SO_4$	1.521	1.769	80	$Mg(NO_3)_2(H_2O)_6$		1.636	
NH_4HSO_4	1.473	1.780	40	$MgSO_4$	1.560	2.660	
$Ca(CH_3COO)_2$	1.550			$MgSO_4(H_2O)_7$	1.433	1.680	
Ca(Br)		3.353		$MgSO_4(H_2O)$	1.523	2.445	
$CaCO_3$	1.658	2.710		KBr	1.559	2.750	84
$CaCO_3(H_2O)_6$	1.460	1.771		K_2CO_3	1.531	2.428	43
$CaCl_2$	1.520	2.150	32	$K_2CO_3(H_2O)_2$	1.380	2.043	43
$CaCl_2(H_2O)_6$	1.417	1.710		$KHCO_3$	1.482	2.170	
$Ca(HCOO)_2$	1.510	2.015		KCl	1.490	1.984	88
$Ca(NO_3)_2(H_2O)_4$	1.465	1.896		KF	1.363	2.480	
$CaSO_4$	1.505	2.610		$KF(H_2O)_2$	1.352	2.454	
$CaSO_4(H_2O)_2$	1.521	2.320		K_2SO_4	1.494	2.662	
$NaCH_3COO$	1.464	1.528	78	$KHSO_4$	1.480	2.322	86
NaBr	1.641	3.203	58	Pb	2.010	11.344	
Na_2CO_3	1.535	2.532	90	c	2.000	2.250	
$Na_2CO_3(H_2O)_{10}$	1.405	1.440		O_3	1.223		
$NaHCO_3$	1.500	2.159		SiC	2.654	3.217	
NaCl	1.544	2.165	75.3	SiO_2	1.487	2.320	
NaF	1.336	2.558		$H_2SO_4(H_2O)_2$	1.405		
NaNO3	1.587	2.261	74.5	$PbCl_2$	2.199	5.850	
Na_2SO_4	1.484	2.680	84	Fe_2O_3	3.220	5.240	
$Na_2SO_4(H_2O)_{10}$	1.394	2.680	84	Al_2O_3	1.768	3.965	
$NaHSO_4(H_2O)$	1.460	2.476	52	PbO	2.51	8.000	
CH_3CHO	1.332	0.783		H_2O	1.333	1.000	
CH3(CH2)14COOH	1.433	0.8527		$CH_3(CH_2)_{14}COOH$	1.434	0.853	
CH3(CH2)16COOH	1.422	0.9408		formic acid	1.371	1.220	
HOOCCH2COOH		1.619		acetic acid	1.372	1.049	
HOOC(CH2)2COOH	1.45	1.572		pyruvic acid	1.428	1.227	
HOOC(CH2)3COOH	1.419	1.424		oxalic acid		1.900	
C6H4(COOH)2	1.431	1.462					
Other organics	1.55	1.4					

Table 4.3. The partial molar refraction of aerosol chemical components. MH (1961) is Moelwyn-Hughes (1961)

	Species	Partial molar refraction (Ri, cm^{-3})	Ri/Mi	Reference
	Soluble component			
1	H^+	0.00	0.000	MH (1961)
2	OH^-	4.43	0.261	MH (1961)
3	F^-	2.17	0.114	MH (1961)
4	Br^-	11.84	0.148	Stelson (1990)
5	Cl^-	8.39	0.237	Stelson (1990)
6	NO_3^-	10.19	0.164	MH (1961)
7	SO_4^{2-}	13.45	0.140	Stelson (1990)
8	Na^+	0.93	0.040	Stelson (1990)
9	NH_4^+	4.89	0.271	Stelson (1990)
10	K^+	3.03	0.078	Stelson (1990)
11	Ca^{2+}	1.93	0.048	Stelson (1990)
12	Mg^{2+}	0.03	0.001	Stelson (1990)
13	$HCOO^-$	7.27	0.161	This study
14	CH_3COO^-	12.94	0.219	This study
15	$CH_3CH_2COO^-$	17.59	0.241	This study
16	$CH_3(CO)COO^-$(pyruvic)	17.65	0.203	This study
17	$(OOCCOO)^{2-}$)(oxalic)	14.53	0.165	This study
18	$CH_3S(O)_2OH$ (MSA)	16.82	0.175	This study
19	H_2O	3.71	0.206	Stelson (1990)
	Insoluble component			
20	C(element carbon)	2.11	0.176	This work
21	SiO_2	7.43	0.124	Stelson (1990)
22	Al_2O_3	10.62	0.104	Stelson (1990)
23	Fe_2O_3	22.21	0.139	Stelson (1990)
24	PbO	18.40	0.082	Stelson (1990)
25	Pb	9.24	0.045	Stelson (1990)
26	$CH_3(CH_2)_{14}COOH$(n-Hexadecanoic acid)	78.00	0.305	This work
27	$CH_3(CH_2)_{16}COOH$(n-Octadecanoic acid)	87.29	0.307	This work
28	$HOOCCH_2COOH$(Malonic acid)	17.24	0.166	This work
29	$HOOC(CH_2)_2COOH$(Succinic acid)	24.20	0.205	This work
30	$HOOC(CH_2)_3COOH$(Glutaric acid)	28.47	0.216	This work
31	$C_6H_4(COOH)_2$	39.99	0.241	This work
32	other organic compounds	50.00	0.240	This work

Table 4.4. Scattering and extinction coefficients, asymmetry factor and single scattering albedo and their growth factor for selected aerosol types. Scattering coefficient (σ_{sp}, km^{-1}), extinction coefficient (σ_{ep}, km^{-1}), asymmetry factor (g) and single scattering albedo (ω)

Sepctrum Source	Aerosol types	Accumulation mode $n(cm^{-3})$	$D_g(\mu m)$	σ_g	$\sigma_{sp2}(RH=80)/\sigma_{sp1}(RH=30)$	$\sigma_{sp3}(RH=99)/\sigma_{sp1}(RH=30)$
Meszaros (1978)	Urban	560	0.100	2.00	1.89	20.76
Whitby(1978)	Continental	2300	0.076	2.00	1.72	14.99
Hoppel et al(1984)	Continental	3000	0.080	2.00	1.71	14.47
Leaitch and Isaac (1991)	Continental	1000	0.240	1.35	1.74	16.76
Jenning et al. (1991)	Continental-marine	950	0.200	1.35	1.82	21.52
Gathman (1983)	Maritime	67	0.266	1.62	1.92	16.41
Jaenicke and Schutz (1982)	Polar aerosol	18.6	0.75	2.00	1.57	5.53
Average		1127	0.24	1.76	1.77	15.78
Sepctrum Source	Aerosol types	$n(cm^{-3})$	$D_g(\mu m)$	σ_g	$\sigma_{ep2}(RH=80)/\sigma_{ep1}(RH=30)$	$\sigma_{ep3}(RH=99)/\sigma_{ep1}(RH=99)$
Meszaros (1978)	Urban	560	0.100	2.00	1.78	18.22
Whitby(1978)	Continental	2300	0.076	2.00	1.66	13.80
Hoppel et al(1984)	Continental	3000	0.080	2.00	1.65	13.34
Leaitch and Isaac (1991)	Continental	1000	0.240	1.35	1.68	15.57
Jenning et al. (1991)	Continental-marine	950	0.200	1.35	1.75	19.75
Gathman (1983)	Maritime	67	0.266	1.62	1.90	16.08
Jaenicke and Schutz (1982)	Polar aerosol	18.6	0.75	2.00	1.55	5.37
Average		1127	0.24	1.76	1.71	14.59
Sepctrum Source	Aerosol types	$n(cm^{-3})$	$D_g(\mu m)$	σ_g	$g_2(RH=80)/g_1(RH=30)$	$g_3(RH=99)/g_1(RH=30)$
Meszaros (1978)	Urban	560	0.100	2.00	1.12	1.26
Whitby(1978)	Continental	2300	0.076	2.00	1.11	1.29
Hoppel et al(1984)	Continental	3000	0.080	2.00	1.11	1.28
Leaitch and Isaac (1991)	Continental	1000	0.240	1.35	1.14	1.39
Jenning et al. (1991)	Continental-marine	950	0.200	1.35	1.18	1.53
Gathman (1983)	Maritime	67	0.266	1.62	1.12	1.35
Jaenicke and Schutz (1982)	Polar aerosol	18.6	0.75	2.00	1.06	1.10
Average		1127	0.24	1.76	1.12	1.32
Sepctrum Source	Aerosol types	$n(cm^{-3})$	$D_g(\mu m)$	σ_g	ω_2/ω_1	ω_3/ω_1
Meszaros (1978)	Urban	560	0.100	2.00	1.06	1.14
Whitby(1978)	Continental	2300	0.076	2.00	1.04	1.09
Hoppel et al(1984)	Continental	3000	0.080	2.00	1.04	1.09
Leaitch and Isaac (1991)	Continental	1000	0.240	1.35	1.03	1.08
Jenning et al. (1991)	Continental-marine mix	950	0.200	1.35	1.04	1.09
Gathman (1983)	Maritime	67	0.266	1.62	1.01	1.02
Jaenicke and Schutz (1982)	Polar aerosol	18.6	0.75	2.00	1.01	1.03
Average		1127	0.24	1.76	1.03	1.08

Table 4.5. The change factors for radiative properties of aerosols as a function of real part, imaginary part, geometric mean radius (r_g) and geometric standard deviation (σ_g). The values in parenthesis are the average change factors.

	Real part from 1.40 to 1.65	Imaginary part from -0.005 to -0.10	R_g from 0.05 to 0.3 μm	σ_g from 1.2 to 3.0
	Change factor	Change factor	Change factor	Change factor
Scattering coefficient	1.34-1.65 (1.49)	0.80-0.84 (0.82)	51.5-248.5 (118.8)	153-753 (389.3)
extinction coefficient	1.32-1.65 (1.47)	1.01-1.15 (1.07)	59.2-249.3 (123.7)	155-607 (334.5)
Asymmetry factor	0.92-0.95 (0.94)	1.03-1.01 (1.02)	1.09-1.32 (1.17)	3.1-8.3 (5.4)
Single scattering albedo	1.00-1.01 (1.01)	0.79-0.73 (0.76)	0.87-1.00 (0.92)	0.99-1.24 (1.10)

Table 4.6. The radiation transmission at 580 nm calculated by radiative transfer model for different aerosol types by assuming that aerosol layer is 2 km, date is 7/1/1995, O_3=278 DU, latitude=35.63, longitude=-82.33, UT=17.90, zenth angle=13.31

		Accumulation mode			Transmission at 580 nm				
Sepctrum Source	Aerosol types	n(cm^{-3})	D_g(μm)	σ_g	T_1 (RH=30)	T_2 (RH=80)	T_3 (RH=99)	T_2/T_1	T_3/T_1
Meszaros (1978)	Urban	560	0.100	2.00	9.08E-01	9.08E-01	9.06E-01	1.00	1.00
Whitby(1978)	Continental	2300	0.076	2.00	9.06E-01	9.06E-01	8.90E-01	1.00	0.98
Hoppel et al(1984)	Continental	3000	0.080	2.00	9.04E-01	8.95E-01	8.40E-01	0.99	0.93
Leaitch and Isaac (1991)	Continental	1000	0.240	1.35	8.97E-01	8.95E-01	8.44E-01	1.00	0.94
Jenning et al. (1991)	Continental-marine mix	950	0.200	1.35	9.04E-01	9.03E-01	0.876	1.00	0.97
Gathman (1983)	Maritime	67	0.266	1.62	9.11E-01	9.11E-01	9.11E-01	1.00	1.00
Jaenicke and Schutz (1982)	Polar aerosol	18.6	0.75	2.00	9.10E-01	9.11E-01	9.11E-01	1.00	1.00
Background	Without aerosol layer	0	0	0.00	9.11E-01	9.11E-01	9.11E-01		

Table 4.7. The change factors for radiation transmission at 580 nm as a function of relative humidity and radiative properties for three types of aerosols. * The average is only for urban and continental aerosols.

Parameter	Urban aerosols Change factor	Continental aerosols Change factor	Marine aerosols Change factor	average* Change factor
Relative humidity from 0 to 95%	0.999	0.993	1.000	0.996
Real part from 1.40 to 1.65	0.998	0.992	1.000	0.995
Imaginary part from -0.005 to -0.10	0.979	0.967	0.998	0.973
Number concentration from 50 to 4000 cm^{-3}	0.940	0.977	0.977	0.958
R_g from 0.05 to 0.3 μm	0.467	0.022	0.990	0.244
σ_g from 1.2 to 3.0	0.934	0.831	0.997	0.883

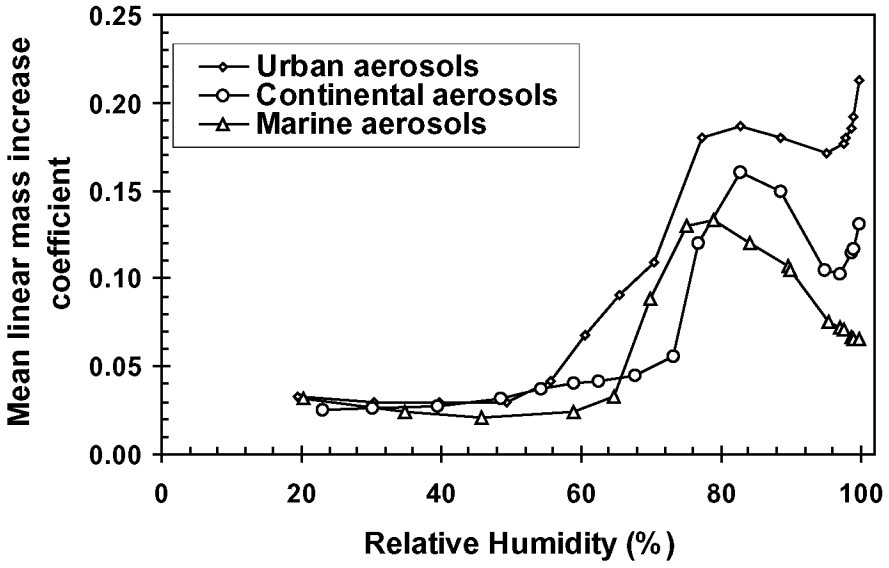

Figure 4.1. Mean linear mass increase coefficient (μ) as a function of relative humidity for three types of aerosols (Maritime aerosols over the Atlantic, 13-16 April, 1969; Urban aerosols at Mainz, January, 1970; Continental aerosols on top of the Hohenpeissenberg, 1000m MSL, summer, 1970) (Hanel, 1976)

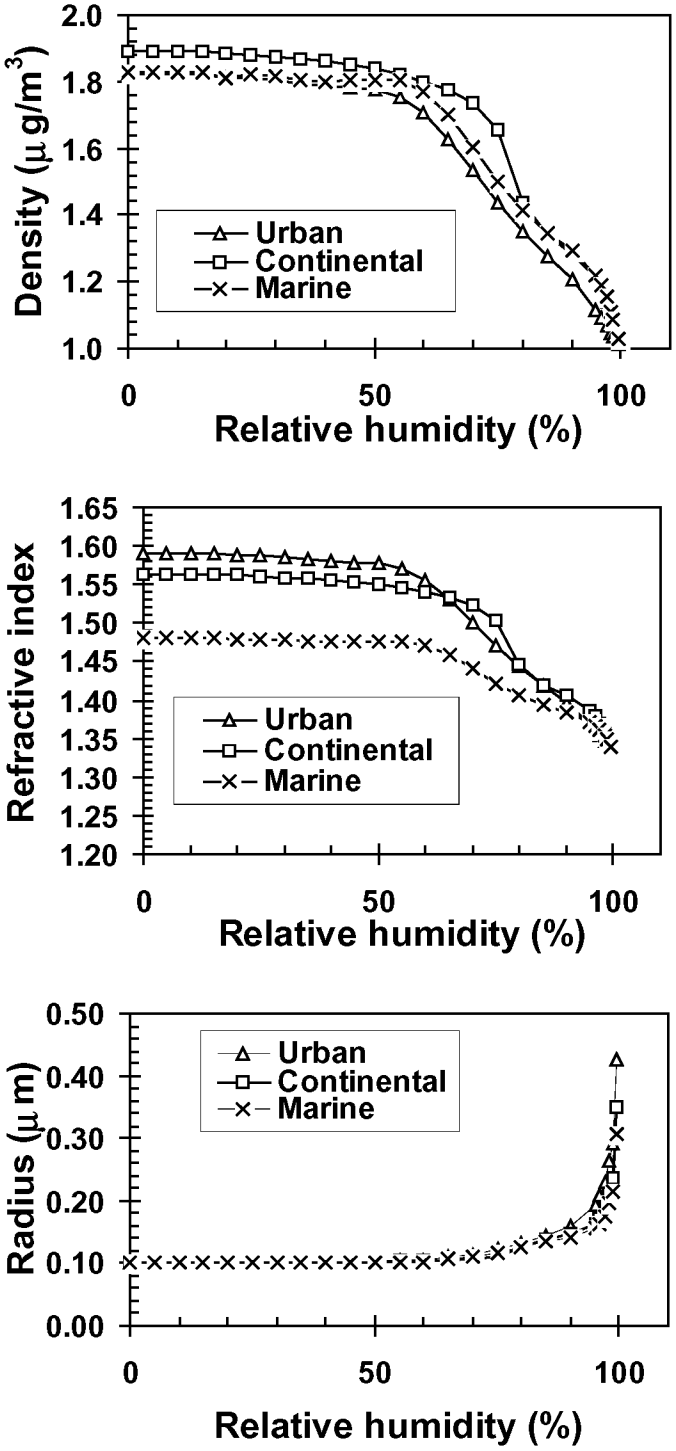

Figure 4.2. Density, refractive index and radius as a function of RH for three types of aerosols

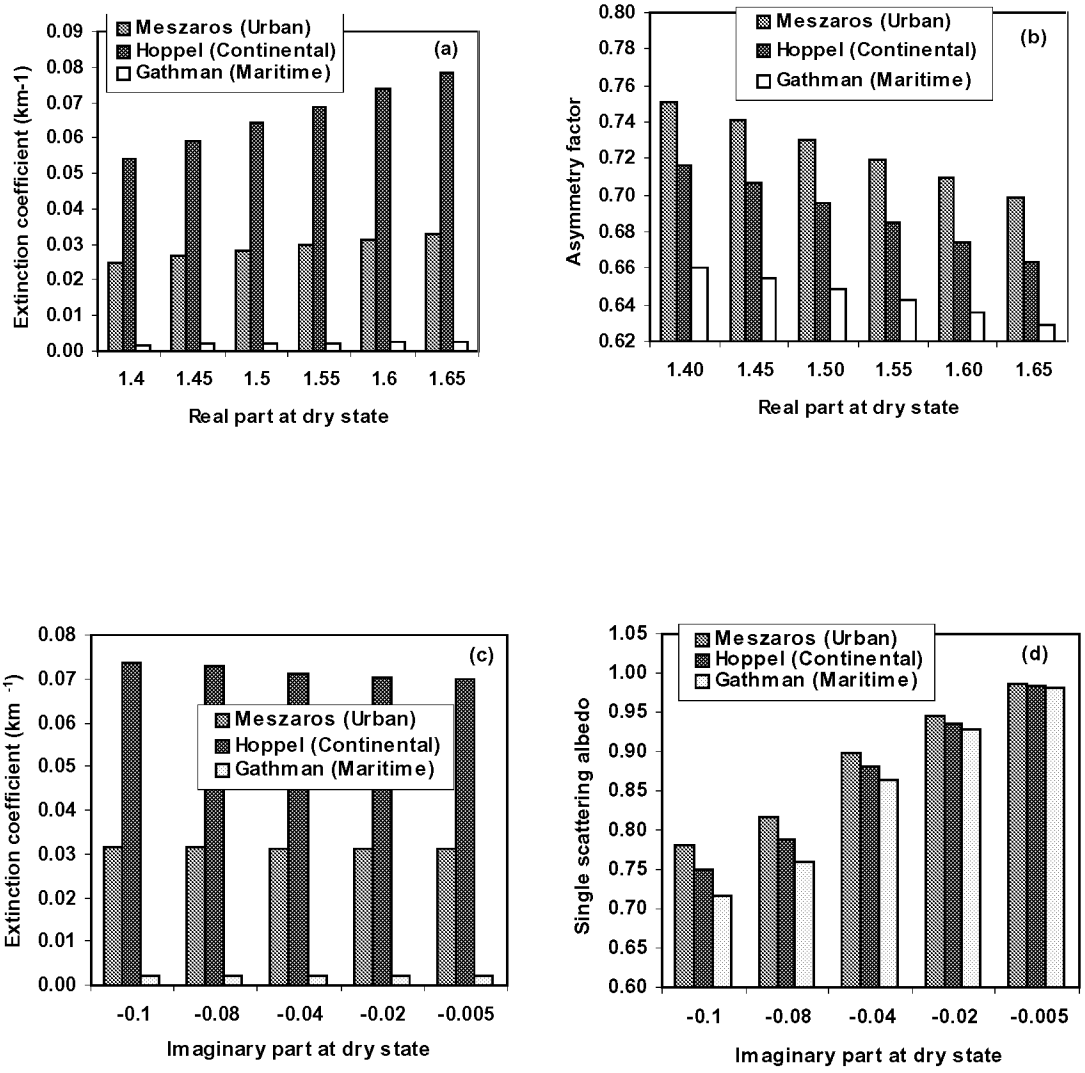

Figure 4.3. The radiative properties at 580 nm as a function of real part and imaginary part of refractive index for three types of aerosols.

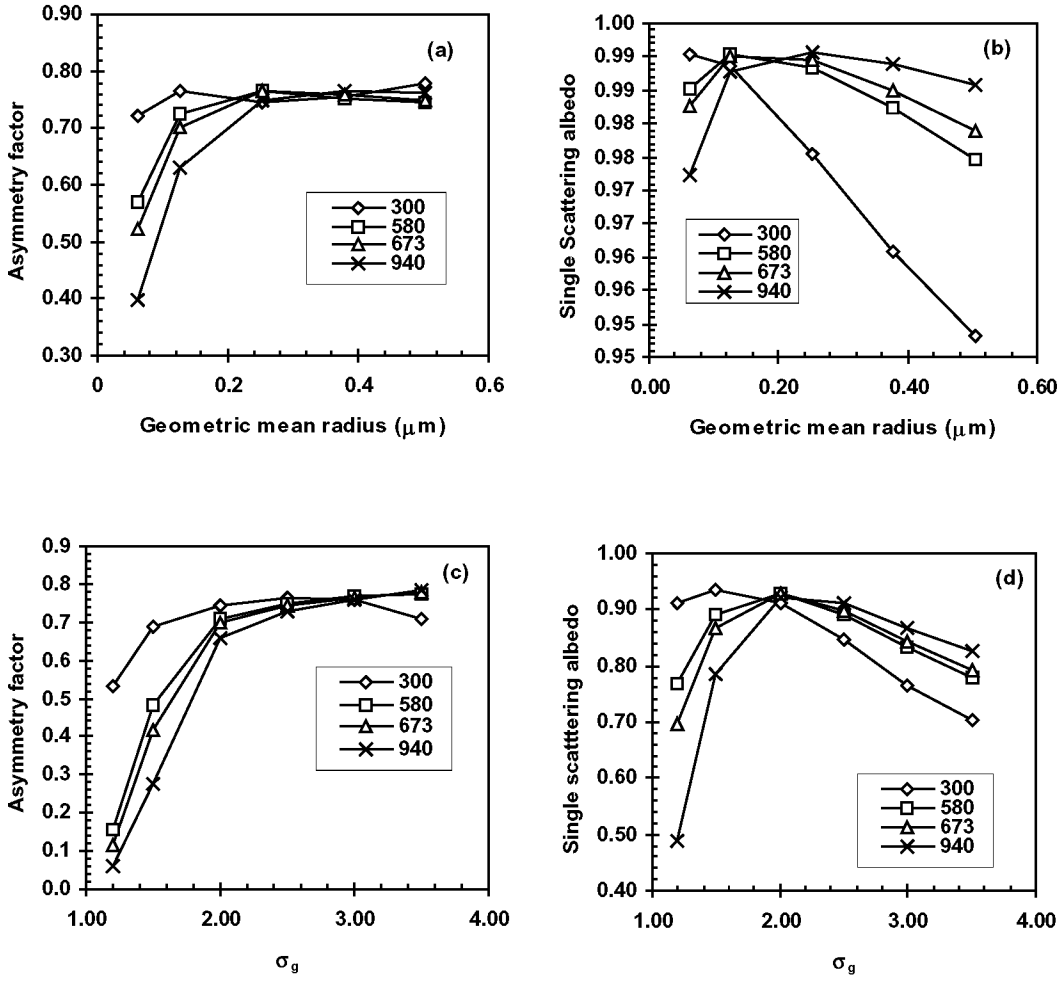

Figure 4.4. The radiative properties at 580 nm as a function of geometric mean radius (for Gathma's maritime aerosols (a, b), and geometric standard deviation (for Meszaros' urban aerosols (c, d)).

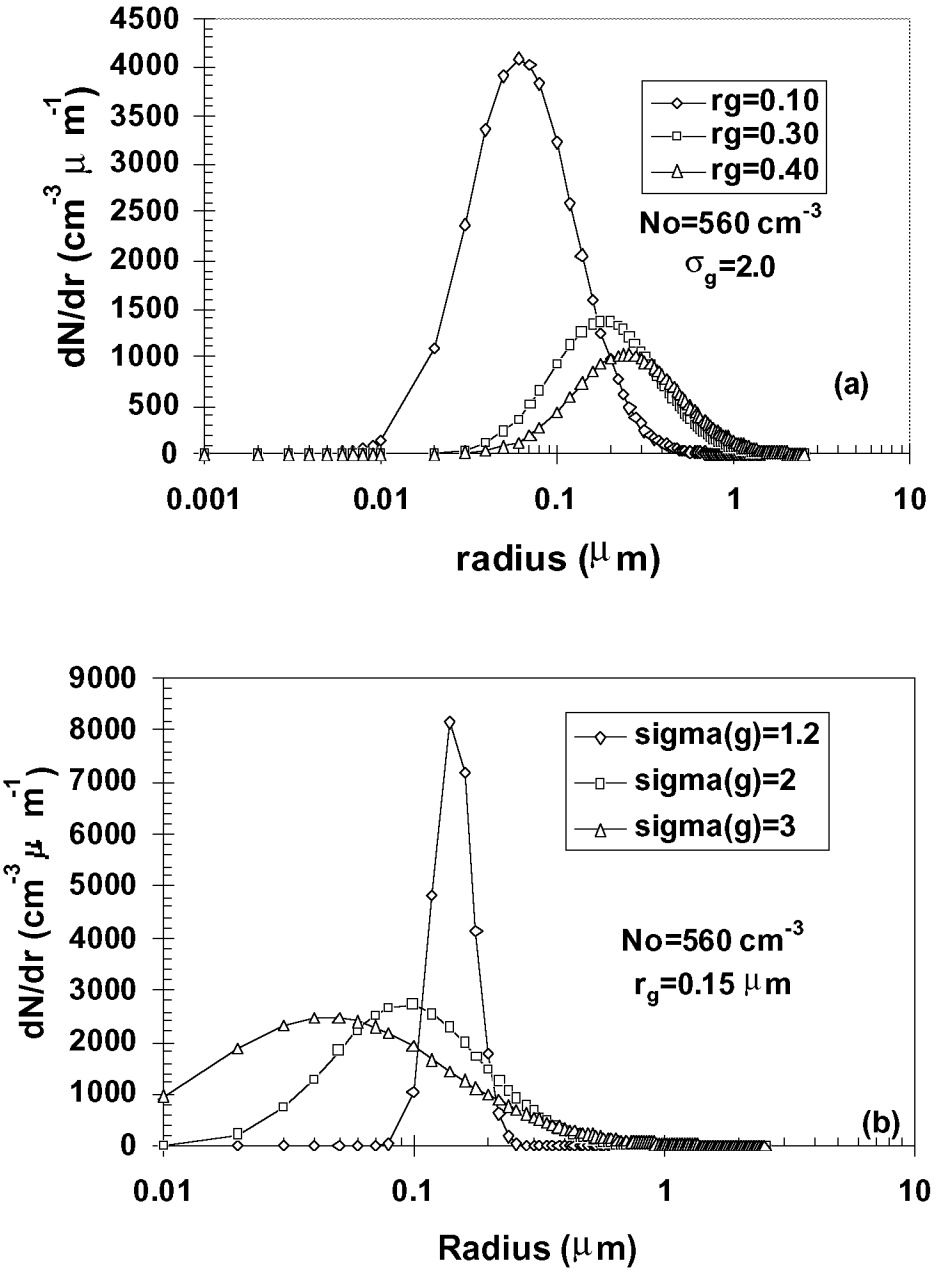

Figure 4.5. The size distribution of aerosol number concentration as a function of geometric mean radius (a) and standard deviation (b)

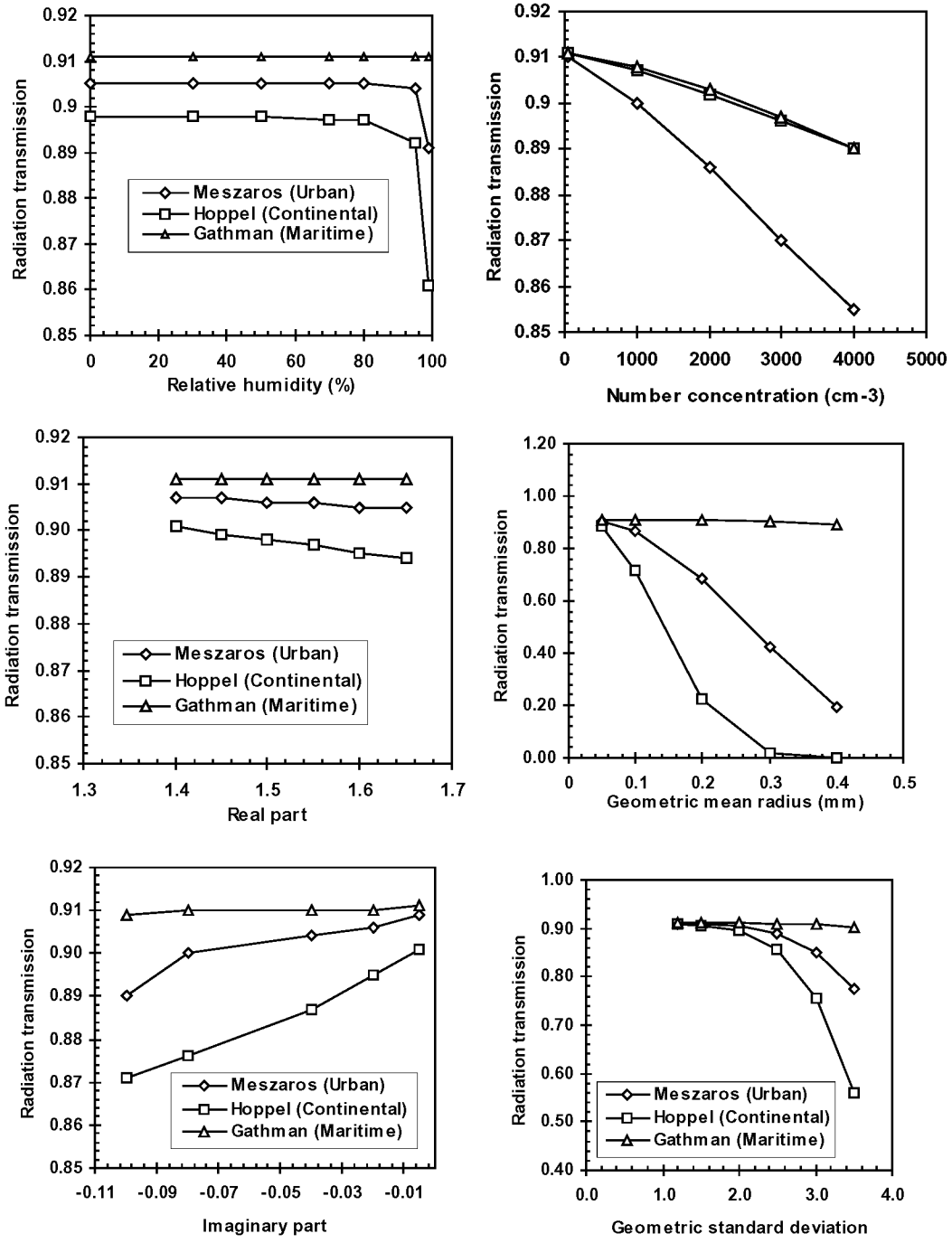

Figure 4.6. The radiation transmission at 580 nm across a 2-km aerosol layer as a function of RH, real and imaginary parts, number concentration and size distribution for three types of aerosols.

5. A STUDY OF THE AEROSOL RADIATIVE PROPERTIES NEEDED TO COMPUTE DIRECT AEROSOL FORCING IN THE SOUTHEASTERN US

Shaocai Yu[1], V. K. Saxena[1*], B. N. Wenny[1], J. J. DeLuisi[2], G. K. Yue[3] and I. V. Petropavlovskikh[4]

1. Department of Marine, Earth and Atmospheric Sciences, North Carolina State University, Raleigh, NC 27695-8208
2. Surface Radiation Research Branch, NOAA, Boulder, Colorado
3. Atmospheric Sciences Division, NASA Langley Research Center, Hampton, Virginia
4. CIRES, University of Colorado, Boulder, Colorado

Submitted to Journal of Geophysical Research (in revision)

5.1. Abstract

In order to assess the direct radiative forcing due to aerosols in southeastern U.S. where a mild cooling is underway, an accurate set of data describing the aerosol radiative properties are needed. We report here aerosol optical depth (AOD) and diffuse-to-direct solar irradiance ratio (DDR) at three operational wavelengths (415, 500, 673 nm) determined by using Multi-Filter Rotating Shadowband Radiometers (MFRSR) at two sites (a mountaintop site: Mt. Gibbes, 35.78 ^{0}N, 82.29 ^{0}W, 2006 m MSL; a valley site: Black Mountain, 35.66 ^{0}N, 82.38 ^{0}W, 951 m MSL), which are separated horizontally by 10 km and vertically by 1 km. The characteristics AOD and DDR were determined from the field measurements obtained during 1995. It was found that the representative total AOD values at 500 nm at the valley site for highly polluted (HP), marine (M) and continental (C) air masses were 0.68±0.33, 0.29±0.19 and 0.10± 0.04, respectively. The fact that the ratio of the mean 1 km layer optical depth to total mean optical depth at 500 nm from the valley site was 73% indicates that the major portion of the atmospheric aerosol was located in the lowest 1 km surface boundary layer (SBL). There was a significant linear correlation between the DDR and total AOD at both the sites. A simple, fast and operative search-graph method was used to retrieve the columnar size distribution (number concentration N, effective radius r_{eff} and geometric standard deviation σ_g) from the optical depth observations at the three operational wavelengths. The ground albedo, single scattering albedo and imaginary part of the refractive index are calculated using a mathematically unique procedure involving a Mie code and a radiative transfer code in conjunction with the retrieved aerosol size distribution, AOD, and DDR. It was found that N, r_{eff} and σ_g were in the range of 1.0E1 to 1.7E4 cm^{-3}, 0.09 to 0.68 μm and 1.12 to 2.95 respectively. The asymmetry factor and single scattering albedo were in the ranges of 0.63 to 0.75 and 0.74 to 0.97 respectively. The ground albedo over the forested terrain and the imaginary part of refractive index were found to be in the range of 0.06 to 0.29 and 0.005 to 0.051 respectively.

5.2. Introduction

It has been recognized for several decades that atmospheric aerosols can affect the radiative balance of the Earth both directly and indirectly. The direct aerosol effect refers to backscattering and absorption of incoming solar (shortwave) radiation and outgoing (longwave, IR) radiation by the aerosol particles [*Penner et al.,* 1994; *Kiehl and Briegleb*, 1993; Schwartz and Andreae, 1996; *IPCC,* 1995]. The backscattering of incoming solar radiation by aerosols will lead to a cooling effect, whereas the absorption of incoming solar radiation and trapping of the outgoing longwave radiation have a warming effect.

With a three-dimensional diagnostic climate model, *Kiehl and Briegleb* [1993] estimated a global mean anthropogenic sulfate forcing of -0.3 W m^{-2}, and a Northern Hemispheric forcing of -0.4 W m^{-2}. They found that in eastern US and eastern China, negative forcing even exceeds the positive forcing due to greenhouse gases (GHGs) and results in net negative forcing. This is consistent with the analysis of *Saxena et al.* [1997] and *Saxena and Yu* [1998], who showed that the arithmetic average of mean daily temperature at 52 stations in the southeastern US decreased by 0.09 C during 1949-94. The conclusion of *IPCC* [1995] is that global mean forcing resulting from anthropogenic sulfate may range from -0.25 to -0.9 W m^{-2}, with substantial uncertainty; and biomass burning aerosol forcing may range from -0.05 to -0.6 W m^{-2}. Aerosols may counteract the greenhouse warming on regional and temporal scales more effectively due to large differences in the residence times of GHGs (decades to centuries) and tropospheric aerosols (few days to a week) as mentioned by *Schwartz and Andreae* [1996].

The objectives of this study are to: (1) investigate the characteristics of aerosol optical depth (AOD) and diffuse-to-direct solar irradiance ratio (DDR) as a function of air mass type at a regionally representative site in western North Carolina, namely, Mt. Mitchell, and a site located in an adjacent valley in the southeastern US; (2) retrieve columnar aerosol size distribution on the basis of the AOD at the three operational wavelengths (415, 500 and 673 nm); (3) determine single scattering albedo, asymmetry factor, the ground albedo and the imaginary part of the refractive index.

5.3. Instrumentation and Database

A detailed description of the instrumentation, methodology, data quality assurance and quality control of the data has been given by *Wenny et al.* [1998]. The research sites include a mountain top station located on the peak of Mt. Gibbes (35.78 ^{0}N, 82.29 ^{0}W, 2006 m MSL) in Mt. Mitchell State Park, and a valley station located adjacent to the Burnett Reservoir near the town of Black Mountain, North Carolina (35.66 ^{0}N, 82.38 ^{0}W, 951 m MSL) [for details see *Wenny et al.,* 1998]. The two sites are separated horizontally by 10 km and vertically by 1 km. All instrumentation was fully operational at both sites from June 1995 through mid-December 1995. Of the instruments used in this study, Yankee Multi-Filter Rotating Shadowband Radiometer (MFRSR) provides simultaneous determination of global, diffuse and direct components of solar irradiance at six wavelengths (415, 500, 615, 673, 870, and 940 nm). The TSI Differential Mobility Particle Sizer (DMPS) measures particle size distributions

(0.016-0.6 μm). Lognormal parameters for the distribution were determined using the fitting software DISTFIT^{TM} provided with the instrument.

The AODs at the three operational wavelengths are determined on the basis of the direct components of solar irradiance determined by the MFRSR [*Wenny et al.,* 1998]. An extraterrestrial constant (V_0), unique to each instrument and for each wavelength, was determined by application of the Bouguer-Langley method. The Bouguer-Langley method consists of measuring the direct irradiance (or in our case the voltage output signal for each instrument, V) at various solar zenith angles; plotting ln (V) versus air mass (m) and extrapolating to m = 0 gives the extraterrestrial value, V_0. The Langley method assumes that atmospheric attenuation is constant throughout the measurement period (ranging from m=2 to m=6), which is generally true for a clear, stable atmosphere [*Harrison and Michalsky*, 1994]. The resulting V_0 was calculated as an average of the morning and afternoon Langley V_0 values. Working estimates of V_0 for the three wavelength channels of each instrument were determined by the average of multiple retrieval of V_0 over the measurement period. The standard deviation of the valley MFRSR V_0 values varied by 3.6, 4.2, and 3.5 % for the three operational wavelengths [*Wenny et al.*, 1998]. The propagating these uncertainties through the AOD calculation yields an estimated uncertainty in the AOD of the order of 0.036, 0.042 and 0.034 for the three operational wavelengths.

The value of τ_λ was calculated for each wavelength for the same zenith angle range using an application of Beer's law

$$\tau_\lambda = -\ln\left(\frac{V_\lambda}{V_{o\lambda}}\right) * \cos(\theta)$$

where τ_λ is the optical depth, V_λ is the instrument output, $V_{0\lambda}$ is the extraterrestrial constant adjusted for earth-sun distance on the day of interest, and θ is the zenith angle. Since the total AOD is the sum of Rayleigh and aerosol components, Rayleigh scattering by air molecules was removed from the measurements, as it is a significant non-aerosol contributor to τ_λ. The following equation [*Wenny* et al., 1998] was used to closely estimate the Rayleigh scattering ($\sigma_{Rayleigh}$) for each channel:

$$\sigma_{Rayleigh} = 0.0087 * \lambda^{-4.05} * \left(\frac{P_s}{1.013 \times 10^5}\right)$$

where λ is wavelength in micrometers and P_s is the atmospheric pressure at the site expressed in Pascals. The absorption optical depth of atmospheric gases, O_3, NO_2, and SO_2 were estimated through calculations using a measured (O_3) and assumed (NO_2, SO_2) column amounts. All three gases were found to have an extremely small contribution to τ_λ at the three operational wavelengths and were thus considered negligible.

5.4. Results and Discussion

5.4.1. Characteristics of Aerosol Optical Depth (AOD)

The mean total AOD and standard deviation as measured from the valley and mountain sites and mean layer AOD between the two sites as a function of air mass type at the three operational wavelengths for cloud-free days are listed in Table 5.1. The air masses are classified [*Ulman and Saxena*, 1997] as highly polluted (HP), continental (C), and marine (M) based on the SO_2 and NOx emission inventory of the U.S. Environmental Protection Agency. Table 5.1 shows that the highly polluted (HP) air masses exhibit the largest average AOD, compared to marine (M) and continental (C) air masses. The mean total AOD values at 500 nm at the valley site were 0.10±0.04, 0.29±0.19 and 0.68±0.33 for C, M and HP air masses, respectively. There are two reasons that the mean AOD of marine air masses is higher than that of continental air masses at the research site. First, the marine classification for the sampling site does not imply pure marine air, but rather a modified marine air caused by additional influence from continental sources between the ocean and the site (the shortest distance between the site and the ocean is about 290 km). Second, the AOD is typically very low during winter months [*Peterson et al.*, 1981]. In this study period, the majority of the marine air mass cases occurred during September and early October and the majority of continental air mass cases occurred during late October and November. Bahrmann and Saxena (1998) found that the percentages of air masses influencing our research site were 43.2, 22.4 and 34.4% for

continental, marine and polluted air masses respectively, on the basis of back trajectory analysis of air masses from June 1996 to October 1996, and from March 1997 to June 1997. If these percentages were used, the mean annual AOD at 500 nm would be 0.25±0.12. This is in reasonable agreement with the mean annual aerosol optical thickness of 0.336 at 500 nm (0.147 turbidity) over central North Carolina as indicated by Peterson et al. (1981) on the basis of observation from July 1969 to July 1975.

It is of interest to note that the AODs for the 1-km intervening layer are higher than the mean total AODs from the mountain site. Overall, the ratios of mean 1-km layer AOD to total mean AOD from the valley site for HP air mass were 73%, 73% and 79% for 415, 500 and 673 nm respectively. This indicates that the major portion of atmospheric aerosols, which make an important contribution to the AOD, is located in the lowest 1-km boundary layer of the troposphere at the research site. This is in reasonable agreement with that of *Hegg et al.* [1997], who found that AOD for the lowest 4 km of the troposphere constituted over 90% of the total column AOD off the mid-Atlantic coast of US.

The spatial variation of AOD is due to variations in the size distribution, concentration and chemical composition of the aerosol particles in the column. Therefore, the changes in atmospheric conditions such as relative humidity, wind speed and air mass history, which can affect the aerosol properties, will lead to changes in AOD. Figure 5.1 shows the total AOD at 500 nm at the valley site as a function of surface level relative humidity and wind speed during the period from July to September 1995. There is no significant correlation between AOD and

these meteorological parameters at the valley site. *Smirnov and Shifrin* [1989] also reported a lack of correlation between AOD and relative humidity above the ocean. The effect of relative humidity on the AOD relies on the original dry aerosol characteristics, and must ultimately manifest itself through changes in the particle size and refractive index. The 'hysteresis effects'' of water uptake for actual multi-component aerosol particles depend upon the history of relative humidity [*Hänel, 1976*]. The effect of relative humidity on the AOD is apparently non-linear. Figure 5.1b shows that the AOD was very small at high wind speed.

5.4.2. Characteristics of Diffuse-to-Direct Solar Irradiance Ratio (DDR)

The directly transmitted solar radiation is defined as that part of the solar radiation reaching the earth's surface which has not been affected by scattering or absorption within the atmosphere. The diffusely transmitted radiation, on the other hand, originates from radiation that is scattered from the direct solar beam. The relative amounts that are scattered to the surface and to space are controlled by the molecular and particle-scattering phase functions, the solar zenith angle, and the total scattering optical depth [*Herman, et al.*, 1975]. For large AODs >0.1, multiple scattering becomes appreciable and complicates the scattering process.

Since the diffuse and direct components contain the manifestation of the atmospheric effects, it offers a means for determining aerosol optical properties by studying the characteristics of the DDR. The advantage of the DDR measurement is that the need for absolute calibration is

eliminated. The wavelength dependence of DDR for six days at a fixed solar zenith angle of 55^0 is presented in Figure 5.2a. The DDRs monotonically decrease with wavelength and exhibit slight negative curvature because the magnitude of the scattering increases with decreasing wavelength and the extinction increases with decreasing wavelength. This is consistent with the observation and theoretical computations presented by *King* [1979] and *King and Herman* [1979].

Since the AOD was determined mainly by air mass types as analyzed before, it is of interest to study the effect of air masses on the DDR. Table 5.1 shows that the average DDR values at the valley site for HP, M and C air masses at 500 nm were 1.02±0.35, 0.38±0.31 and 0.15± 0.08 respectively. Since the AOD is a very important atmospheric variable that determines the magnitude of the DDR, it is of interest to calculate the correlation coefficients between the AOD and the DDR. The regression equations between the DDR and the total aerosol optical depth (τ) for all air mass types at the mountain and the valley sites for the three operational wavelengths are as follows (n is number of samples and R^2 is square of correlation coefficient):

At the valley site:

$DDR_{415}=2.537x\tau_{415}-0.056$ n=213, $R^2=0.801$

$DDR_{500}= 1.754x\tau_{500}-0.068$ n=213, $R^2=0.926$

$DDR_{673}=1.554x\tau_{673}-0.084$ n=213, $R^2=0.944$

At the mountain site:

$DDR_{415}=1.781x\tau_{415}-0.117$ n=228 $R^2=0.975$

$DDR_{500}=1.436x\tau_{500}-0.040$ n=228 $R^2=0.959$

$DDR_{673}=1.320x\tau_{673}-0.002$ n=228 $R^2=0.787$

For the layer optical depth ($\Delta\tau$) and the difference of the DDR between the mountain and the valley sites (Δ DDR), the regression equations are as follows:

$\Delta DDR_{415}=2.766x\Delta\tau_{415}-0.140$ n=211, $R^2=0.685$

$\Delta DDR_{500}=1.837x\Delta\tau_{500}-0.094$ n=211, $R^2=0.858$

$\Delta DDR_{673}=1.605x\Delta\tau_{673}+0.077$ n=211, $R^2=0.916$

As can be seen, there was a significant linear correlation between the DDR and the AOD at both the sites. The difference of the DDR between the mountain and the valley sites was also significantly linearly correlated with the difference in layer AOD between the two sites. This is in agreement with the results of the theoretical calculations of *King and Herman* [1979], that indicated a linear correlation between the DDR and AOD at certain values of zenith angle and ground albedo. This result also shows that the DDR is much more sensitive to the change in AOD than a change in the zenith angle.

5.4.3. Retrieval of Aerosol Columnar Size Distribution and Radiative Properties from Optical Depth at the Three Operational Wavelengths

The aerosol optical depth $\tau\lambda$ at wavelength λ can be defined for spherical particles by Mie theory:

$$\tau_\lambda = \int_0^\infty Q(m_r, r, \lambda)\pi r^2 n_c(r)dr \qquad (5.1)$$

where Q is the extinction efficiency factor for spherical particles and m_r is the refractive index. The $n_c(r)$ is aerosol columnar number concentration between particle radius r and r+dr, i.e., the number of particles per unit area per unit radius interval in a vertical column through the atmosphere. The above equation may be written [*Twomey,* 1977] in the following form:

$$\tau_\lambda = \int_0^\infty K(m_r, r, \lambda)n_c(r)dr \qquad (5.2)$$

The kernel function is $K(m_r,r,\lambda)=Q(m,r,\lambda)\pi r^2$. The techniques used for the inversion of spectral data and to determine the aerosol size distribution can be grouped into two categories: the shape-constrained method and the shape-constrained-free method as summarized by *Wang et al.* [1996]. In this study, it is assumed that the size distribution of tropospheric aerosols can be expressed by the following lognormal formula with only one peak:

$$n_c(r) = \frac{N_c}{\sqrt{2\pi} r \ln \sigma_g} \exp\left(-\frac{\ln^2 \frac{r}{r_g}}{2\ln^2 \sigma_g}\right) \qquad (5.3)$$

where N_c is the total columnar number concentration (cm^{-2}), r_g is the geometric mean radius, and σ_g is the geometric standard deviation. The optical effective radius, r_{eff}, was defined as follows [*Hansen and Travis*, 1974]:

$$r_{eff} = \frac{\int_0^\infty r^3 n_c(r)dr}{\int_0^\infty r^2 n_c(r)dr} \qquad (5.4)$$

for a lognormal size distribution, r_{eff} is given by:

$$r_{eff} = r_g \exp(2.5 \ln^2 \sigma_g) \tag{5.5}$$

By substituting equation (5.3) into (5.1), it is apparent that for a given aerosol composition, τ_λ / N_c is a function of r_g (or r_{eff}) and σ_g. To eliminate the unknown N_c, aerosol optical depth ratios R_1 and R_2 are defined as follows:

$$R_1 = \frac{\tau_{673}}{\tau_{500}} = \frac{\int_{r_1}^{r_2} n_C(r) Q(\lambda=0.673, m_r, r) \pi r^2 dr}{\int_{r_1}^{r_2} n_C(r) Q(\lambda=0.500, m_r, r) \pi r^2 dr} = f_1(\sigma_g, r_g) = f_3(\sigma_g, r_{eff}) \tag{5.6}$$

$$R_2 = \frac{\tau_{415}}{\tau_{500}} = \frac{\int_{r_1}^{r_2} n_C(r) Q(\lambda=0.415, m_r, r) \pi r^2 dr}{\int_{r_1}^{r_2} n_C(r) Q(\lambda=0.500, m_r, r) \pi r^2 dr} = f_2(\sigma_g, r_g) = f_4(\sigma_g, r_{eff}) \tag{5.7}$$

If τ_{673}, τ_{500}, and τ_{415} are obtained by measurement, R_1 and R_2 can be calculated by the above equations. Then σ_g, r_g and r_{eff} can be retrieved by solving equations (5.6) and (5.7) simultaneously. The standard numerical methods, such as the Newton-Raphson and the Levenberg-Marquardt methods can be used to retrieve r_g and σ_g from equations (5.6) and (5.7) [*Yue et al.,* 1989]. In this study, a search-graph method (SGM) was developed to solve simultaneously for r_g, r_{eff} and σ_g. The basic idea of this SGM is similar to that of the table-lookup method of *Yue et al.* [1986]. However, the solution in the SGM was obtained by the intersection of the two curves with the procedure as outlined below.

The kernel functions ($Q(m,r,\lambda)\pi r^2$) at the three operational wavelengths are calculated for each radius from 0.01 to 10 μm by a Mie code (step-width is 0.01 μm). According to

equations (5.3), (5.6) and (5.7), values of R_1 and R_2 can be calculated for values of r_g ranging from 0.01 to 10 μm and values of σ_g ranging from 1.05 to 4.0 on the basis of kernel function. Then the calculated R_1 and R_2 were compared with the measured R_1 and R_2. All possible r_g and σ_g, which can give the same calculated R_1 and R_2 as the measured R_1 and R_2, are saved. In this study, it is assumed that when the relative error between the calculated R_1 (or R_2) and measured R_1 (or R_2) is less than 0.5%, the two are identical. By this SGM, one data set of r_g and σ_g can be obtained from measured R_1 and another data set of r_g and σ_g from measured R_2. If these solutions for each ratio are plotted on the same graph, the mathematically unique solution satisfying both ratios is found by the intersection of the two curves. The corresponding r_{eff} can be calculated by equation (5.5). To find the mathematically unique solution, all root mean square errors ($RMSE_1$) can be calculated as follows:

$$RMSE_1 = \left(\frac{1}{2}\left(\left(\frac{R_{1ca} - R_{1me}}{R_{1me}}\right)^2 + \left(\frac{R_{2c} - R_{2me}}{R_{2me}}\right)^2\right)\right)^{\frac{1}{2}} \tag{5.8}$$

where *ca* and *me* represent calculated and measured values of optical depth ratio respectively. One set of r_g (or r_{eff}) and σ_g, which make the above root mean square error a minimum, can be found. If this root mean square error minimum is less than 0.01, r_g and σ_g are regarded as a solution. Figure 5.3 shows the example of solutions for the cases on 9 September and 17 November 1995. It is of interesting to note that r_{eff} and σ_g are more independent (or more orthogonal) than r_g and σ_g as indicated in Figure 5.3. This is in agreement with Tanre et al. [1996]. Since r_{eff} is less dependent on the derived standard deviation of the distribution [*Hansen*

and Travis, 1974], r_{eff} instead of r_g is presented in the following part of this study. Figure 5.3 shows that r_{eff} and σ_g of 9 September 1995 (R_1=0.44, R_2=0.76) were 0.14 μm and 1.76 respectively, and r_{eff} and σ_g of 17 November 1995 (R_1=0.62, R_2=0.87) were 0.23 μm and 1.68 respectively.

After the values of r_{eff} and σ_g have been determined, the total columnar aerosol number concentration was easily obtained by the following process: According to equations (5.1), (5.3) and (5.5), all possible AOD at the three operational wavelengths can be calculated for values of N_c ranging from $1x5.5x10^5$ to $20000x5.5x10^5$ cm^{-2} (or more) (it is assumed that the height of atmospheric column is 5.5 $x10^5$ cm) and then calculate the relative error between measured AOD and calculated AOD for each wavelength and their root mean square error as follows:

$$RMSE_2 = \left(\frac{1}{3}\left(\left(\frac{\tau_{415ca} - \tau_{415me}}{\tau_{415me}}\right)^2 + \left(\frac{\tau_{500ca} - \tau_{500me}}{\tau_{500me}}\right)^2 + \left(\frac{\tau_{673ca} - \tau_{673me}}{\tau_{673me}}\right)^2\right)\right)^{\frac{1}{2}} \qquad (5.9)$$

where ca and me represent the calculated and measured values of AOD at each wavelength respectively. The result is N_c, which can make the root mean square error ($RMSE_2$) a minimum. Since N_c is the number concentration which can give the best explanation of the observed total AOD, N_c is called effective columnar number concentration in the paper.

A sensitivity study was performed to test the accuracy of the SGM and the effects of anticipated sources of calibration errors on the retrieved aerosol size distribution. It is assumed that the refractive index, m_r is 1.50-0.01*i* [*Herman et al.*, 1975]. The effect of experimental error on the accuracy of the SGM was simulated by seven uncertainty cases in which Gaussian distributed random errors with standard deviations of 0, 5, 10, 20, 30, 40 and 50% were

added to the values of AOD at the three operational wavelengths. For each uncertainty case, 100 sets of R1 and R2 were generated with 100 random numbers from Gaussian distribution. Then the SGM was used to find the solutions of 100 sets of R_1 and R_2. The average value and root-mean-square deviation of r_{eff} and σ_g for each case are calculated for those cases which have solutions. Table 5.2 lists the sensitivity test results of the SGM using two idealized lognormal aerosol size distributions.

Table 5.2 shows that there is no error in the result of the SGM if there is no uncertainty in the measurement of AOD. If the uncertainties were less than ±30% in the values of AOD, r_{eff} and σ_g can be recovered roughly to within 10%. The solution number for the total 100 data sets decreases with the increases of uncertainties and the relative errors in retrieved r_{eff} and σ_g also increase with the increases of uncertainties as indicated in Table 5.2. Only one solution can be obtained for ±40% uncertainties and no solution can be retrieved in the presence of ±50% AOD errors. Obviously, the chance to have a solution by SGM decreases with the increases of uncertainties in measurement. It is of interest to note that the integrated aerosol properties such as single scattering albedo (ϖ) and asymmetry factor (g) can be recovered to within 5% when the uncertainties were less than ±30% in the values of AOD. The error in the number concentrations inferred by the SGM is very large when the measurement error is larger than 40% as indicated in Table 5.2. In Case B, there are similar results to those of Case A. The aerosol radiative properties (single scattering albedo and asymmetry factor) at the three operational wavelengths were calculated by a Mie theory code developed by *Dave* [1968]

using the mean values of retrieved r_{eff} and σ_g. It is apparent that the SGM is capable of recovering the integrated aerosol radiative properties accurately regardless of the large error of r_{eff} and σ_g. There is always a possibility that those two curves from R_1 and R_2 do not intersect and then the solution cannot be found by the SGM. This may be due to the following reasons: (1) the aerosol size distribution can not be represented by a lognormal function; (2) there are large errors in the measurements of R_1 and R_2.

Although post-Pinatubo stratospheric aerosol size distributions were typical bimodal, a unimodal lognormal form was assumed when retrieving size distributions from the extinction spectra in many studies [*Yue et al.*, 1986, 1994; *Russell et al.*, 1996]. *Russell et al.* [1996] thought that typical measurements of post-Pinatubo extinction spectra do not have enough information to constrain retrievals of the six parameters of a bimodal lognormal distribution. *Russell et al.* [1996] found that there was a near-perfect match between the extinction spectra of the actual bimodal and the retrieved unimodal size distribution due to the fact that particles in the first mode (nucleation mode), which have radii <0.1 μm, contribute essentially nothing to the extinction spectrum.

Figures 5.4a, b, and c show the comparison of the representative original tri-modal, bimodal and unimodal size distributions, which were obtained by DMPS measurement at the research site, with those unimodal lognormal distribution retrieved by the SGM on the basis of extinction coefficients at the three operational wavelength. Note that the retrieved unimodal distributions completely reproduce the curves of the three original size distributions between 0.1

and 1.0 μm but fail to account for the particles in the other size ranges. This is due to the fact that the particles in the nucleation mode, which have radii<0.1 μm, contribute essentially nothing to the spectra of aerosol integrated radiative properties in the visible range. It was found that the relative errors between the inferred and practical radiative integrated properties (g and ϖ)were less than 8%. Note that the single scattering albedo and asymmetry factor derived by the SGM represent weighted average values over the entire column while those obtained by in situ measurement represent the values only at the valley site.

Table 5.3 lists the retrieved values of N, r_{eff} and σ_g, and radiative properties (asymmetry factor) on the basis of the AOD at the three operational wavelengths sing the SGM and Mie code. Table 5.3 shows that the total columnar number concentrations for 9 September (8:05 AM) and 17 November (11:45 AM) were 1.8×10^9 and 7.9×10^7 /cm^2 respectively. Note that in Table 5.3, N is total average number concentration ($N=N_c/(5.5 \times10^5$ cm)). As can be seen, N, r_{eff} and σ_g are in the range of 1.0E1 to 1.7E4 cm^{-3}, 0.09 to 0.68 μm and 1.12 to 2.95, respectively. The asymmetry factors at 500 nm are in the range of 0.61 to 0.75. No specific trend based upon air mass is discernable. *Lacis and Mishchenko* [1995] presented a slight difference in asymmetry factor for aerosols of differing chemical composition. They showed that the asymmetry factor of soot and large desert aerosols was about 0.9, but for sulfate, marine and smaller dust aerosols the asymmetry factor ranges from 0.65 to 0.8. For the UV wavelength region, *Wenny et al.* [1998] found that the asymmetry factor determined for the site ranged from 0.63 to 0.76. The values of asymmetry factor reported here are close to those

for sulfate, marine and smaller dust aerosols. Table 5.3 shows that most of the relative errors of the inferred AOD were less than 1% (also see Figure 5.2b). This also indicates that the SGM is capable of recovering the integrated aerosol radiative properties.

5.4.4. Determination of single scattering albedo and ground albedo

Since the imaginary part of the refractive index is just the absorption term in the total extinction, the term absorption is used to refer to the imaginary part of refractive index in this paper. It has been demonstrated that the ratio of the hemispheric diffuse-to-directly transmitted solar radiation versus solar zenith angle at the earth's surface can be used as an indirect means of inferring both the ground albedo and single scattering albedo of the atmospheric aerosols, given a knowledge of the aerosol size distribution and AOD [*Herman et al.,* 1975; *King and Herman*, 1979; *King*, 1979]. The calculation of *King and Herman* [1979] showed that several radiative transfer parameters such as the real part of the particle refractive index, total ozone content, and vertical distribution of the atmospheric aerosol particles had very little effect on the DDR at the ground. *King and Herman* [1979] developed a statistical technique with a nonlinear least-squares procedure to infer the optimum values of the ground albedo and the effective absorption of atmospheric aerosols.

In this study, a technique similar to that of *Herman et al.* [1975] is used to solve simultaneously for ground albedo and absorption using a mathematically convergent unique

procedure involving the SGM, a Mie code and a radiative transfer code in conjunction with the retrieved aerosol size distribution, AOD, and DDR. First, the size distribution (r_{eff} and σ_g) was derived by the SGM on the basis of AOD at the three operational wavelengths and the asymmetry factor was calculated by the Mie code under the assumption that the refractive index is 1.50-0.01*i*. Fortunately, neither the SGM nor the asymmetry factor is very sensitive to the refractive index [*King and Herman*, 1979; *King*, 1979]. For example, in the case of 11:45 am November 17 1995 in Table 5.3 (τ_{415}=0.16, τ_{500}=0.14 and τ_{673}=0.10), the SGM method shows that r_{eff}, σ_g and g_{500} are 0.24 μm, 1.68 and 0.71 respectively for m_r=1.50-0.01*i*, and are 0.21 μm, 1.48 and 0.78 respectively for m_r=1.50-0.08*i*. As can be seen, even though imaginary part increases by 8 times, the asymmetry factor only increases by 10%. The single scattering albedo (ϖ) is defined as the ratio of scattering to total extinction coefficient. On the basis of the consideration that ϖ is very sensitive to the absorption [*Herman et al.*, 1975; *Yu et al.,* 1997] and absorption affects the radiation transmission mainly through its effect on ϖ, ground albedo and ϖ were varied in the radiative transfer model in order to obtain a matched DDR. If the DDR is available for at least two zenith angles, then a mathematically unique solution can be found for single scattering albedo and ground albedo. Each DDR allows an infinite set of solutions for ground albedo and single scattering albedo. If the allowed solutions for each ratio are plotted on the same graph, a unique solution satisfying both ratios can be found by the intersection of the two curves.

After the single scattering albedo was derived, the Mie code was then iterated, varying the absorption until the single scattering albedo matched the value resulting from the radiative transfer model. In this study, a Tropospheric Ultraviolet-Visible Radiation Model (TUVRM), utilizing a two-stream radiative transfer scheme, developed by *Madronich* [1993] was used. The following constant conditions at the research sites are set in the TUVRM model: O_3=300 DU, air pressure=940 mb, latitude=35.63, longitude=-82.33, wavelength=500 nm. Since only the total AOD is available, the vertical AODs per km in 1 km intervals from 0.951 km (elevation of valley site) to 50 km at 500 nm were normalized by the aerosol data of *Elterman*'s profile [*Elterman*, 1968]. It was assumed that the single scattering albedo and asymmetry factor are constant within the whole column. Since the ratio of scattering to absorption may vary with altitude within the whole column, the single scattering albedo and asymmetry factor obtained in this study are considered to be "optically effective", meaning that the resulting values yield the best agreement between measurement and radiative transfer theory. There are a total of five cases which allowed a solution by the two-variable solution technique of *Herman et al.* [1975] on the basis of data in Table 5.3. It was found that the values of ground albedo (single scattering albedo) of 9/29, 10/1, 10/2, 9/3 and 9/4 were 0.29 (0.88), 0.12 (0.82), 0.18 (0.98), 0.29 (0.94) and 0.08 (0.84) respectively. Figure 5.5 gives an example of the two-variable solution technique for the case on 9/4/1995. The average ground albedo is 0.19±0.10 at the research site.

Note that the two-variable solution technique can not have solutions for the cases whose AODs at 500 nm were less than 0.1 or larger than 0.30. As mentioned by *King* [1979], one of the limitations of the DDR method for inferring the ground albedo and absorption of atmospheric aerosols is the sensitivity of the DDR to particles ≤ 0.10 μm in radius. The effect of small particles is insignificant in the determination of the ground albedo [*King,* 1979]. The successful implementation of the two-variable solution technique requires stable atmospheric conditions during a measurement period, with the exception that the AOD can change. According to the study of *Herman et al.* [1975], the two-variable solution technique can not have a solution unless the measurement uncertainties of the DDRs are less than 5% in their special case (τ_d=0.10). All these limitation results in the small number of the cases with solutions. More experimental case studies in the future are obviously needed in order to obtain more solutions. Considering the above situation, the average ground albedo (0.19) was used at the research sites, and then the absorption was recalculated for all cases using the above method. Table 5.4 lists the results of absorption for all the cases that can have a solution under the assumption that the ground albedo was 0.19. As can been seen, ϖ was in the range of 0.63 to 0.96 and the absorption was in the range of 0.005 to 0.051. Reported values of ϖ in scientific literature show ϖ to be 1.0 for sulfate and pure marine aerosols and range from 0.5 to 0.7 for desert dust and soot aerosols [*Lacis and Mishchenko*, 1995]. *Wenny* et al. [1998] reported that ϖ at 312 nm varied from 0.75 to 0.93. The values of ϖ from this study are compatible with these values given by other authors. It is to be emphasized that the effect of the

assumption of ground albedo (0.19) on single scattering albedo is apparent. For example, solution can be found for the case of day 321 (911/17/1995) if the ground albedo is assumed to be 0.19 as shown in Table 5.4.

DeLuisi et al. [1976] found the ground albedo values ranging between 0.20 and 0.35 for Quartzite, Arizona. By modeling the scattering properties of the atmospheric aerosols, *Otterman and Fraser* [1976] inferred value for the ground albedo as 0.264 in the wavelength range of 0.5 to 0.6 μm. *King* [1979] reported that the ground albedo was 0.279±0.100 and the absorption was 0.0306±0.0082 in the mid-visible region in Tucson, Arizona, by the DDR method. It is to be emphasized that the ground albedo derived from the DDR method is the "optically effective" reflectivity compatible with the assumptions made. *Kuriyan et al.* [1979] found that the absorption was in the range of 0.02 to 0.05 during the days having dry continental air masses in the Los Angeles area. Grams et al. [1974] deduced the values of absorption in the range of 0.001 to 0.021 (average 0.005) by employing a laser polar nephelometer to measure the phase function of aerosols in a small volume of the free atmosphere. *DeLuisi et al.* [1976] reported values of absorption on the order of 0.013±0.028 for Quartzite, Arizona. *Wenny et al.* [1998] found that the absorption was in the range of 0.009 to 0.055 on the basis of the UV-B transmission and Mie code calculation. The values of ground albedo and absorption obtained by this study are in close agreement with the results obtained elsewhere.

5.5. Concluding Remarks

The results obtained are as follows:

1) The representative AOD values at 500 nm at the valley site for highly polluted (HP), marine (M) and continental (C) air masses were 0.68, 0.29 and 0.10 respectively. It is found that the major portion of the atmospheric aerosol is located in the lowest 1-km boundary layer of the troposphere at the research site.

2) The representative DDR values at 500 nm during the study period at the valley site for HP, M and C air masses were 1.02, 0.38 and 0.15, respectively. There was a significant linear correlation between the DDR and the total AOD at both the mountain and the valley sites (R^2>0.8).

3) The retrieved parameters, N, r_{eff} and σ_g are in the range of 1.0E1 to 1.7E4 cm^{-3}, 0.09 to 0.68 μm and 1.12 to 2.95 respectively, and the asymmetry factors are in the range of 0.61 to 0.75.

4) The single scattering albedo was found to be in the range of 0.74 to 0.99. The ground albedo and imaginary part of refractive index were found to be in the range of 0.06 to0.29 (average is 0.19±0.10) and 0.005 to 0.051 respectively.

The above parameters are needed to model the direct effect of aerosols on climate and to reduce the uncertainty in the estimate of this effect [see *Schwartz and Andreae*, 1996], especially in the southeastern US where a cooling trend has been observed [*IPCC,* 1995; *Saxena et al.,* 1997; *Saxena and Yu*, 1998].

Acknowledgments. This research was supported by the NASA's Mission to Planet Earth (MTPE) under Contract No. NAS1-18944 from Langley Research Center, Hampton, VA (50% supported), and by the U.S. Environmental Protection Agency under the grant assistance No. R825248 (50%). Authors would like to thank Dr. S. Madronich for his help in the transfer model calculation. We also thank Dr. Lamont Poole, Prof. Patrick McCormick and Mr. William Stelz for their encouragement. The authors are also grateful to three anonymous reviewers for providing insightful comments that led to substantial strengthening of the contents of this paper.

5.6. References

Dave, J.V., Subroutines for computing the parameters of electromagnetic radiation scattered by a sphere. *IBM J. Res. Dev., 13*, 302-312, 1969.

DeLuisi, J.J., P.M. Furukawa, D.A. Gillette, B.G. Schuster, R.J. Charlson, W.M. Porch, R.W. Fegley, B.M. Herman, R.A. Rabinoff, J.T. Twitty, and J.A. Weinman, Results of a comprehensive atmospheric aerosol-radiation experiment in the southwestern United States. Part II: radiation flux measurements and theoretical interpretation. *J. Appl. Meteor., 15,* 455-463, 1976.

Elterman, L., *UV, visible, and IR attenuation for altitudes to 50 km,* Rep. AFCRL-68-0153, Environ. Res. Pap. No. 285, Air Force Cambridge Research Laboratories, pp. 49, 1968.

Grams, G.W., I.H. Blifford, D.A. Gillette, and P.B. Russell, Complex index of refraction of airborne soil particles. *J. Appl. Meteor.*, *13*, 459-471, 1974.

Hänel, G., The properties of atmospheric aerosol particles as functions of relative humidity at thermodynamic equilibrium with the surrounding air. *Adv. Geophys.*, *19*, 73-188, 1976.

Hansen, J., and L. Travis, Light scattering in planetary atmospheres, *Space Sci. Rev., 16*, 527-610, 1974

Harrison, L., and J. Michalsky, Objective algorithms for the retrieval of optical depths from ground based measurements. *Appl Opt.*, *33*, 5118-5125, 1994.

Hegg, D.A., J. Livingston, P.V. Hobbs, T. Novakov, and P. Russell, Chemical apportionment of aerosol column optical depth off the mid-Atlantic coast of the United States. *J. geophys. Res.,* 102, 25293-25303, 1997

Herman, B.M., S.R. Browning, and J.J. DeLuisi, Determination of the effective imaginary term of the complex refractive index of atmospheric dust by remote sensing: the diffuse-to-direct radiation method. *J. Atmos. Sci.*, *32*, 918-925, 1975.

IPCC, *Climatic change 1995: Radiative forcing of climate and an evaluation of the IPCC 1992 emission scenarios*. J.T. Houghton et al. (Eds), Cambridge University Press, Cambridge, UK, 1995.

Kiehl, J.T., and B.P. Briegleb, The relative role of sulfate aerosols and greenhouse gases in climate forcing. *Science*, *260*, 311-314, 1993.

King, M.D., Determination of the ground albedo and the index of absorption of the atmospheric particulates by remote sensing. Part II: application *J. Atmos. Sci.*, *36*, 1072-1083, 1979.

King, M.D., D.M. Byrne, B.M. Herman, and J.A. Reagan, Aerosol size distributions obtained by inversion of spectral optical depth measurements. *J. Atmos. Sci., 35*, 2153-2166, 1978.

Kuriyan, J.G., S.K. Mitra, and D.M. Laudau, Effective optical characteristics of atmospheric aerosol particles in the L.A. basin. *Tellus,31*, 99-110, 1979.

Madronich, S., The atmosphere and UV-B radiation at ground level, In *Environmental UV Photobiology*, Edited by A.R. Young, Plenum Press, 1993.

Penner, J.E., R.J. Charlson, J.M. Hales, N.S. Laulainen, R. Leifer, T. Novakov, J. Ogren, L.F. Radke, S.E. Schwartz, and L. Travis, Quantifying and minimizing uncertainty of climate forcing by anthropogenic aerosols, *Bull. Amer. Meteorol. Soc.*, *75*, 375-400, 1994.

Peterson, J.T., E.C. Flowers, G.J. Berri, C.L. Reynolds, and J.H. Rudesill, Atmospheric turbidity over central North Carolina, *J. Appl. Meteor.* 20, 229-241, 1981.

Russell, P.B., J.M. Livingston, R.F. Pueschel, J.J. Bauman, J.B. Pollack, S.L. Brooks, P. Hamill, L.W. Thomason, L.L. Stowe, T. Deshler, E.G. Dutton, and R.W. Bergstrom, Global to microscale evolution of the Pinatubo volcanic aerosol derived from diverse measurements and analyses, *J. geophys. Res., 101*, 18745-18763, 1996.

Saxena, V.K., and Shaocai. Yu, Searching for a regional fingerprint of aerosol radiative forcing in the southeastern US, *Geophys. Res. Lett., 25,* 2833-2836, 1998.

Saxena, V.K., Shaocai. Yu, and J. Anderson, Impact of stratospheric volcanic aerosols on climate: evidence for aerosol shortwave and longwave forcing in the Southeastern US. *Atmos. Environ., 31*, 4211-4221, 1997.

Smirnov, A.Y., and K.S. Shifrin, Relationship of optical thickness to humidity of air above the ocean, *Izv. Acad. Sci. USSR Atmos. Oceanic Phys., Enhl. Transl., 25*, 374-379, 1989.

Smirnov, A.Y., N.T. O'Neil, A. Royer, and A. Tarussov, Aerosol optical depth over Canada and the link with synoptic air mass types, *J. Geophys. Res., 101*, 19299-19318, 1996.

Schwartz, S.E., and M.O. Andreae, Uncertainty in climate change caused by aerosols. *Science, 272*, 1121-1122, 1996.

Tanre, D., M. Herman, and Y.J. Kaufman, Information on aerosol size distribution contained in solar reflected spectral radiances, *J. geophys. Res.,* 101, 19043-19060, 1996

Twomey, S., Atmospheric aerosols, Elsevier, Amsterdam, Oxford and New York, 1977.

Ulman, J.C., and V.K. Saxena, Impact of air mass histories on the chemical climate of Mount Mitchell, North Carolina, *J. Geophys. Res., 102*, 25451-25465, 1997.

Wang, P.-H., G.S. Kent, M.P. McCormick, L.W. Thomason, and G.K. Yue, Retrieval analysis of aerosol size distribution using simulated extinction measurements at SAGE III wavelengths, *Appl. Opt.,35*, 433-440, 1996.

Wenny, B.N., J.S. Schafer, J.J. DeLuisi, V.K. Saxena, W.F. Barnard, I.V. Petropavlovskikh, and A.J. Vergamini, A study of regional aerosol radiative properties and effects on ultraviolet-B radiation, *J. Geophys. Res.,* 103, 17,083-17,097, 1998.

Yu, Shaocai., V.K. Saxena, and B.N. Wenny, "A theoretical evaluation of chemical and size effects on radiative properties of multicomponent aerosols". In *Proceedings of AGU 1997 Spring Meeting*, May 26-29, Baltimore, MD, pp.70, 1997.

Yue, G.K., M.P. McCormick, and W.P. Chu, Retrieval of composition and size distribution of stratospheric aerosols with the SAGE II satellite experiment. *J. Atmos. and Oceanic Tech., 3*, 371-380, 1986.

Yue, G.K., M.P. McCormick, W.P. Chu, P.-H. Wang, and E. Chiou, The simultaneous retrieval of aerosol properties from wavelength dependence of extinction measured by the SAGE II experiment. *Advances in Remote Sensing Retrieval Methods*, edited by Deepak, A., H. E. Fleming, and J. S. Theon, A. Deepak Publishing, pp 253-268, 1989.

Table 5.1. Mean total optical depth, diffuse to direct ratio and their standard deviation at 415, 500 and 673 nm as measured at the valley and mountain sites. The data for the intervening layer were obtained from the difference between the two sites. The sites were influenced by highly polluted (HP), continental (C) and marine (M) air masses. V, M, and L denote the valley, mountain and the intervening layer respectively.

	τ_v at the valley site			τ_m at the mountain site			τ_l for the intervening layer			Ratio (τ_l /τ_v)		
Air mass	415	500	673	415	500	673	415	500	673	415	500	673
HP	0.78±0.41	0.68±0.33	0.51±0.22	0.22±0.14	0.19±0.12	0.12±0.07	0.56±0.28	0.50±0.25	0.40±0.20	0.73±0.12	0.73±0.15	0.79±0.17
M	0.36±0.25	0.29±0.19	0.19±0.12	0.13±0.12	0.10±0.09	0.06±0.05	0.23±0.13	0.20±0.11	0.14±0.09	0.69±0.14	0.71±0.15	0.73±0.14
C	0.11±0.07	0.10±0.04	0.07±0.02	0.04±0.02	0.03±0.01	0.03±0.01	0.07±0.04	0.07±0.03	0.04±0.02	0.62±0.12	0.68±0.09	0.51±0.25
	Diffuse to direct ratio (DDR_v)			Diffuse to direct ratio (DDR_m)			Ratio (DDR_v/DDR_m)					
	415	500	673	415	500	673	415	500	673			
HP	1.63±0.87	1.02±0.35	0.76±0.30	0.43±0.27	0.25±0.20	0.13±0.12	0.75±0.11	0.76±0.17	0.74±0.28			
M	0.74±0.58	0.38±0.31	0.17±0.13	0.35±0.20	0.19±0.13	0.08±0.07	0.44±0.13	0.45±0.14	0.45±0.23			
C	0.32±0.16	0.15±0.08	0.06±0.03	0.22±0.07	0.10±0.05	0.04±0.03	0.29±0.11	0.29±0.11	0.37±0.16			

Table 5.2. Sensitivity test of the search-graph method (SGM) using two idealized lognormal aerosol size distribution with added error. r_{eff}, σ_g and N are the effective radius, geometric standard deviation and number density respectively. Solution No. is the number of solutions by SGM for total 100 data sets. The relative error is defined as the ratio of the difference between the inferred and practical values to the practical value. The single scattering albedo (ϖ) and asymmetry factor (g) are calculated by the mean values of r_{eff} and σ_g.

			Search-graph-method (SGM)			Original data		By SGM		relative error		relative error		
No.	Error(%)	Solution No.	r_{eff}(μm)	σ_g	N(cm^{-3})	ω_{500}	g_{500}	ω_{500}	g_{500}	ω_{500}	g_{500}	r_{eff}	σ_g	N(cm^{-3})
Case A (r_{eff}=0.151 μm, σ_g=1.50, N=700 cm^{-3})														
1	0	100	0.151	1.500	700	0.948	0.650	0.948	0.650	0.000	0.000	0.000	0.000	0.000
2	5	23	0.152±0.020	1.477±0.165	902±671	0.948	0.650	0.949	0.656	0.001	0.009	0.007	-0.015	0.289
3	10	8	0.146±0.017	1.417±0.190	899±631	0.948	0.650	0.947	0.638	-0.001	-0.018	-0.033	-0.055	0.284
4	20	4	0.142±0.010	1.420±0.200	905±355	0.948	0.650	0.947	0.632	-0.001	-0.028	-0.060	-0.053	0.293
5	30	3	0.142±0.007	1.386±0.293	870±252	0.948	0.650	0.946	0.619	-0.002	-0.048	-0.060	-0.076	0.243
6	40	1	1.429	2.000	2343	0.948	0.650	0.941	0.658	-0.007	0.012	8.464	0.333	2.347
7	50			No solution										
Case B (r_{eff}=0.162 μm, σ_g=1.70, N=700 cm^{-3})														
8	0	100	0.162	1.700	700	0.946	0.668	0.946	0.668	0.000	0.000	0.000	0.000	0.000
9	5	21	0.161±0.021	1.688±0.207	1034±889	0.946	0.668	0.947	0.674	0.001	0.009	-0.006	-0.007	0.477
10	10	7	0.157±0.016	1.571±0.171	707±340	0.946	0.668	0.948	0.664	0.002	-0.006	-0.031	-0.076	0.010
11	20	3	0.145±0.019	1.693±0.232	1072±123	0.946	0.668	0.945	0.653	-0.001	-0.022	-0.105	-0.004	0.531
12	30	3	0.152±0.019	1.600±0.434	871±443	0.946	0.668	0.947	0.661	0.001	-0.010	-0.062	-0.059	0.244
13	40	1	0.131	1.32	809	0.946	0.668	0.943	0.593	-0.003	-0.112	-0.191	-0.224	0.156
14	50			No solution										

Table 5.3. The measured optical depth (τ), N, r_{eff} (effective radius) and σ_g inferred by the search-graph method and asymmetry factor (g) at the valley site. The relative error is defined as the ratio of the difference between the inferred and measured optical depth to the measured optical depth. The height of atmospheric column is assumed to be 5.5 km when total number concentration N is calculated.

day	Time(EST)	Air mass	Tau measured			Search-graph-method			Relative error of inferred Tau			g_{500}
			415	500	673	N (cm^{-3})	σ_g	r_{eff} (μm)	415	500	673	
189(7/8)	7:10	C	0.32	0.27	0.18	2.2E+02	1.49	0.22	-0.010	0.003	0.031	0.70
189(7/8)	8:00	C	0.33	0.28	0.18	1.7E+02	1.35	0.22	0.011	0.012	0.011	0.72
189(7/8)	8:26	C	0.30	0.25	0.16	8.4E+01	1.12	0.23	-0.020	-0.023	-0.023	0.74
191(7/10)	7:12	C	0.39	0.32	0.20	6.8E+02	1.62	0.17	0.002	0.003	0.004	0.68
191(7/10)	8:02	C	0.33	0.27	0.17	3.3E+02	1.50	0.19	0.005	0.005	0.005	0.69
246(9/3)	8:09	C	0.21	0.16	0.10	1.9E+03	1.98	0.14	0.006	0.004	0.022	0.66
246(9/3)	8:59	C	0.21	0.16	0.10	5.4E+02	1.68	0.16	-0.004	0.000	-0.003	0.67
246(9/3)	9:53	C	0.23	0.18	0.11	6.7E+02	1.72	0.16	-0.003	-0.008	-0.004	0.67
247(9/4)	8:09	C	0.18	0.13	0.08	2.3E+03	2.00	0.12	-0.008	0.001	0.002	0.64
247(9/4)	9:01	C	0.17	0.14	0.08	1.6E+03	1.94	0.13	-0.006	-0.003	0.001	0.65
247(9/4)	9:28	C	0.19	0.15	0.09	6.2E+02	1.74	0.16	-0.007	-0.005	0.004	0.66
256(9/13)	9:10	C	0.47	0.40	0.27	4.4E+02	1.57	0.21	-0.003	-0.003	-0.004	0.70
256(9/13)	9:52	C	0.45	0.38	0.25	3.8E+02	1.55	0.21	0.002	-0.001	-0.001	0.70
290(10/17)	10:00	C	0.08	0.07	0.07	7.2E+01	2.25	0.42	0.011	0.011	0.011	0.71
290(10/17)	10:40	C	0.08	0.08	0.08	3.2E+01	1.77	0.38	0.032	0.031	0.031	0.72
295(10/22)	10:30	C	0.08	0.08	0.06	2.4E+01	1.48	0.30	0.015	0.016	0.015	0.72
298(10/25)	11:09	C	0.08	0.08	0.07	1.9E+01	1.47	0.33	-0.028	-0.026	-0.034	0.73
320(11/16)	9:06	C	0.08	0.07	0.06	3.0E+02	2.70	0.37	-0.012	-0.017	-0.017	0.70
320(11/16)	11:38	C	0.07	0.07	0.06	9.6E+00	1.15	0.34	-0.002	-0.014	-0.019	0.75
321(11/17)	10:27	C	0.14	0.12	0.09	3.2E+02	1.96	0.21	0.009	0.011	-0.001	0.69
321(11/17)	10:58	C	0.15	0.13	0.09	1.5E+02	1.71	0.23	0.005	0.001	-0.005	0.70
321(11/17)	11:45	C	0.16	0.14	0.10	1.4E+02	1.68	0.24	-0.003	0.001	0.002	0.71
325(11/21)	9:52	C	0.08	0.08	0.06	9.2E+01	1.94	0.28	0.012	0.012	0.012	0.70

Table 5.3 (continued)

day	Time(EST)	Air mass	Tau measured			Search-graph-method			Relative error of infered Tau			g_{500}
			415	500	673	N (cm^{-3})	σ_g	reff (μm)	415	500	673	
248(9/5)	7:58	M	0.34	0.25	0.14	1.7E+04	2.12	0.09	-0.006	-0.001	0.001	0.61
248(9/5)	10:58	M	0.30	0.23	0.14	1.1E+03	1.74	0.15	0.004	0.006	0.008	0.65
252(9/9)	8:05	M	0.64	0.48	0.28	3.3E+03	1.76	0.14	-0.001	0.001	0.005	0.64
252(9/9)	9:19	M	0.81	0.62	0.36	3.0E+03	1.71	0.15	-0.006	-0.004	0.001	0.65
272(9/29)	8:32	M	0.25	0.19	0.12	6.0E+03	2.13	0.11	0.013	0.041	0.019	0.63
272(9/29)	8:59	M	0.24	0.18	0.11	4.1E+03	2.11	0.12	-0.027	0.000	-0.009	0.69
274(10/1)	8:21	M	0.12	0.10	0.07	5.8E+02	2.26	0.21	-0.007	-0.007	-0.002	0.67
274(10/1)	9:01	M	0.11	0.09	0.07	5.3E+02	2.37	0.24	0.009	0.011	0.015	0.68
274(10/1)	9:15	M	0.11	0.10	0.08	2.0E+02	2.01	0.25	-0.001	-0.001	-0.002	0.68
275(10/2)	8:36	M	0.19	0.16	0.11	1.1E+03	2.12	0.18	0.012	0.015	0.018	0.67
275(10/2)	9:32	M	0.20	0.16	0.11	1.5E+03	2.20	0.18	-0.005	-0.009	-0.004	0.67
275(10/2)	10:06	M	0.21	0.18	0.12	6.7E+02	1.97	0.19	-0.005	-0.007	-0.002	0.67
183(7/2)	7:08	P	0.46	0.40	0.27	2.7E+02	1.44	0.22	0.005	0.005	0.005	0.71
183(7/2)	8:22	P	0.57	0.50	0.33	3.6E+02	1.38	0.23	0.031	0.007	-0.020	0.72
227(8/15)	8:07	P	0.83	0.68	0.43	8.4E+02	1.52	0.20	0.005	0.000	-0.003	0.69
227(8/15)	9:50	P	0.87	0.71	0.45	5.9E+02	1.44	0.21	-0.005	-0.002	-0.001	0.70
229(8/17)	8:23	P	1.10	0.94	0.62	6.5E+02	1.43	0.22	0.005	-0.007	-0.024	0.70
229(8/17)	9:12	P	1.06	0.90	0.59	5.6E+02	1.40	0.23	0.009	0.011	0.005	0.71
229(8/17)	10:31	P	0.99	0.84	0.54	4.8E+02	1.37	0.23	0.000	0.000	-0.002	0.71
235(8/23)	9:04	P	0.78	0.65	0.43	6.6E+02	1.51	0.20	-0.003	-0.002	-0.002	0.70
235(8/23)	9:18	P	0.76	0.64	0.41	5.8E+02	1.48	0.21	0.003	0.002	0.002	0.79
288(10/15)	11:00	P	0.53	0.55	0.68	4.0E+01	1.28	0.62	0.001	-0.004	-0.003	0.67
289(10/16)	8:24	P	0.35	0.36	0.42	2.4E+01	1.36	0.68	0.008	0.008	0.008	0.70
289(10/16)	9:40	P	0.51	0.52	0.64	3.6E+01	1.30	0.64	-0.015	-0.012	-0.013	0.68

Table 5.4. The single scattering albedo (ϖ), asymmetry factor (g) and imaginary part of refractive index at the valley site on the basis of the assumption that the ground albedo is 0.19.

day	Time(EST)	Air mass	Zenith angle	Tau at valley site			Diffuse-direct ratio			g_{500}	ω_{500}	Refractive index
				415	500	673	415	500	673			
321(11/17)	10:27	C	60	0.14	0.12	0.09	0.30	0.14	0.06	0.69	0.74	1.50-0.051*i*
321(11/17)	10:58	C	57.5	0.15	0.13	0.09	0.30	0.14	0.06	0.70	0.74	1.50-0.051*i*
321(11/17)	11:45	C	55	0.16	0.14	0.10	0.30	0.15	0.06	0.71	0.76	1.50-0.049*i*
246(9/3)	8:09	C	65	0.21	0.16	0.10	0.42	0.19	0.07	0.66	0.97	1.50-0.010*i*
246(9/3)	8:59	C	55	0.21	0.16	0.10	0.38	0.19	0.08	0.67	0.94	1.50-0.015*i*
246(9/3)	9:53	C	45	0.23	0.18	0.11	0.40	0.21	0.10	0.67	0.99	1.50-0.005*i*
247(9/4)	8:09	C	65	0.18	0.13	0.08	0.38	0.16	0.06	0.64	0.86	1.50-0.020*i*
247(9/4)	9:01	C	55	0.17	0.14	0.08	0.34	0.16	0.06	0.65	0.82	1.50-0.031*i*
247(9/4)	9:28	C	50	0.19	0.15	0.09	0.34	0.16	0.06	0.66	0.82	1.50-0.031*i*
274(10/1)	8:21	M	67.5	0.12	0.10	0.07	0.33	0.14	0.06	0.67	0.86	1.50-0.020*i*
274(10/1)	9:01	M	60	0.11	0.09	0.07	0.28	0.13	0.05	0.68	0.76	1.50-0.049*i*
274(10/1)	9:15	M	57.5	0.11	0.10	0.08	0.28	0.13	0.05	0.68	0.76	1.50-0.049*i*
275(10/2)	9:32	M	55	0.20	0.16	0.11	0.37	0.19	0.08	0.67	0.98	1.50-0.006*i*
275(10/2)	10:06	M	50	0.21	0.18	0.12	0.37	0.20	0.09	0.67	0.97	1.50-0.010*i*
272(9/29)	8:32	M	65	0.25	0.19	0.12	0.47	0.20	0.07	0.63	0.90	1.50-0.017*i*
272(9/29)	8:59	M	60	0.24	0.18	0.11	0.43	0.20	0.07	0.69	0.97	1.50-0.010*i*

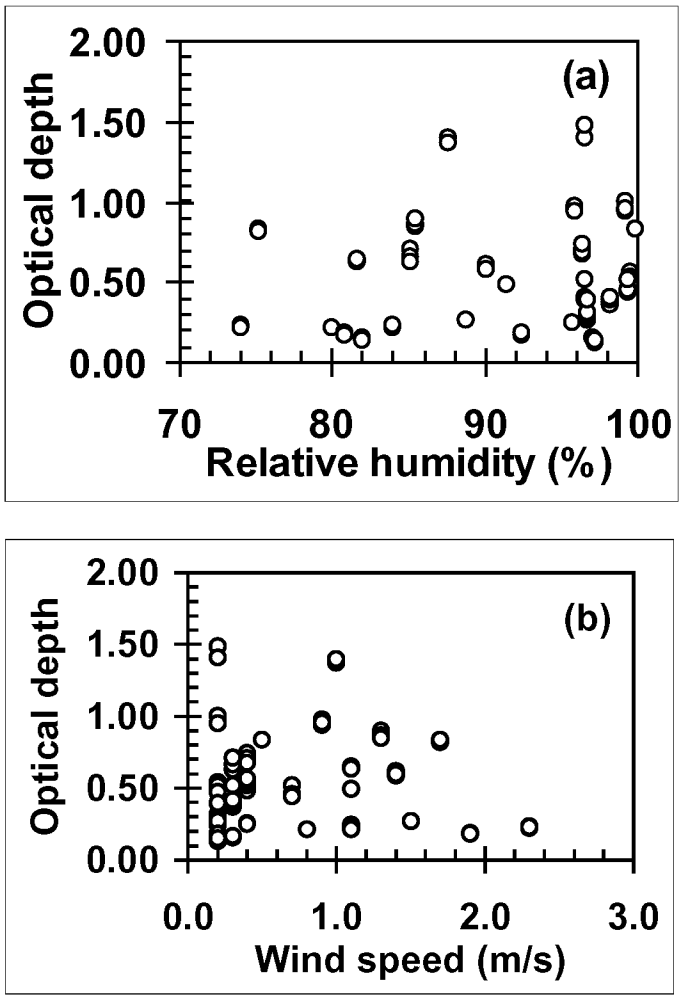

Figure 5.1. Total optical depth at the valley site at 500 nm as a function (a) relative humidity and (b) wind speed

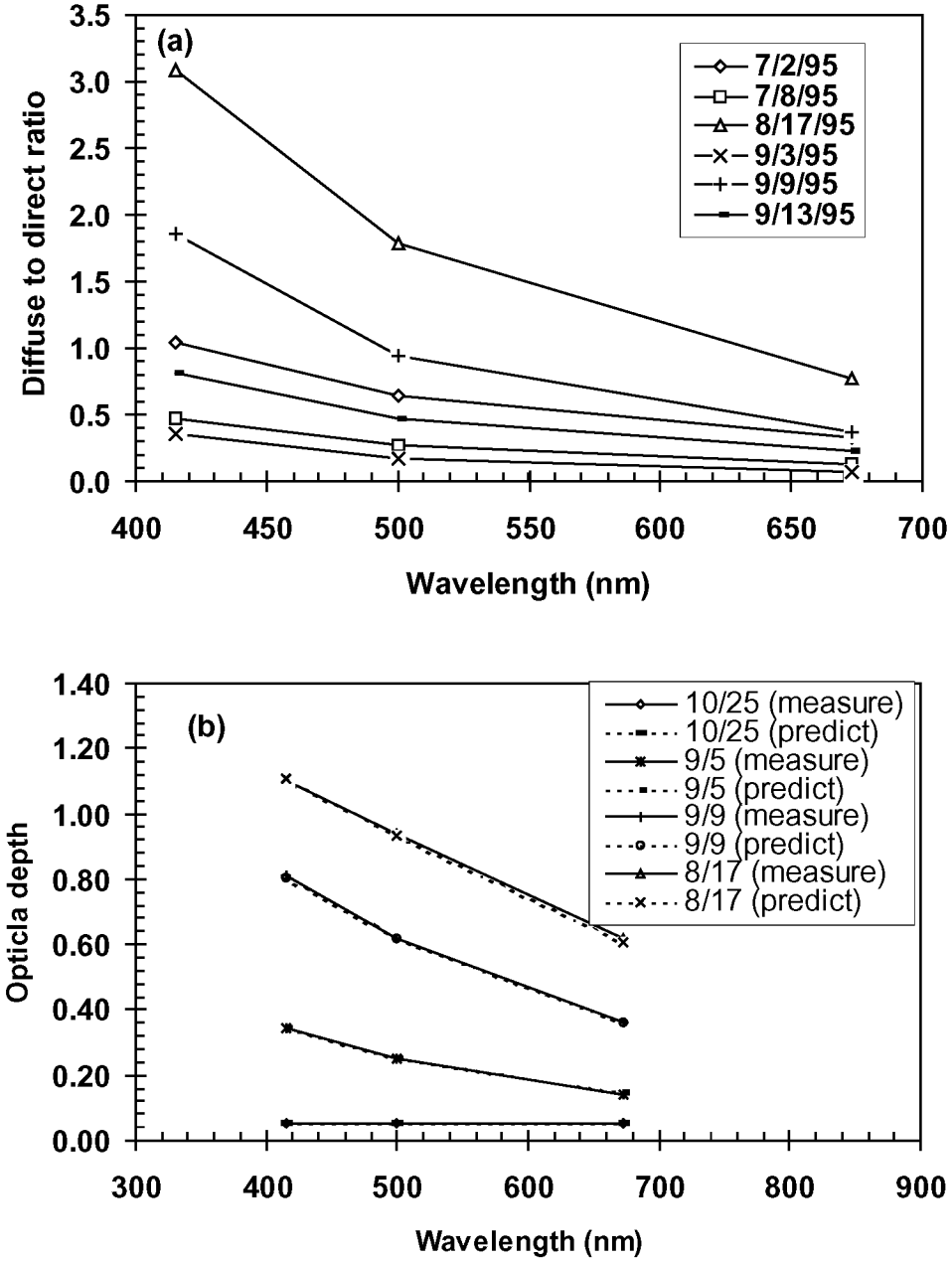

Figure 5.2.(a) The wavelength dependence of diffuse-to-direct ratio for several days, (b) comparison of the wavelength dependence of the inferred by search-graph method and practical total optical depth at the valley site

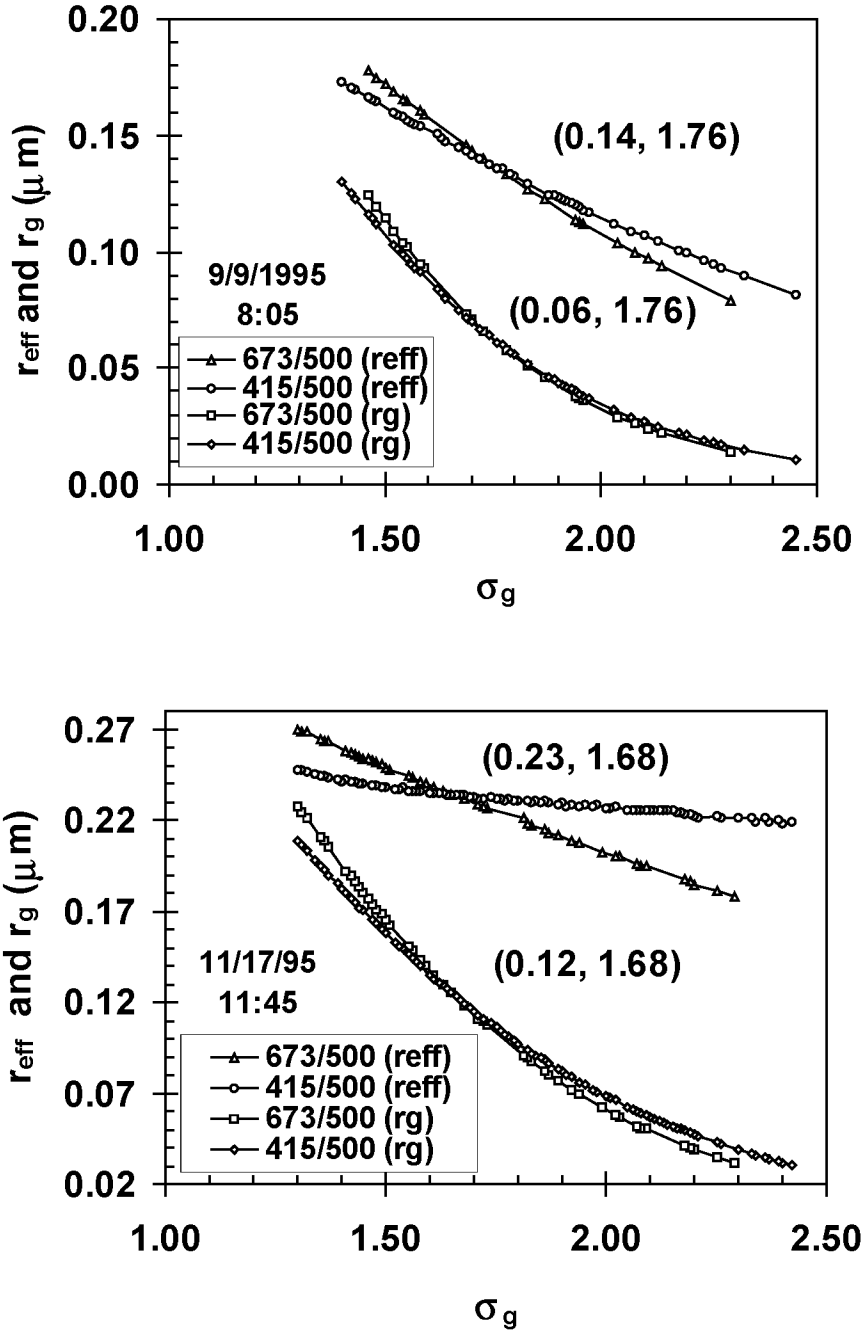

Figure 5.3. r_g, r_{eff} vs σ_g demonstrating the search-graph method of simultaneous solution for r_g, r_{eff} and σ_g on 9 September and 17 November 1995. The intersection point of the lines is the solution

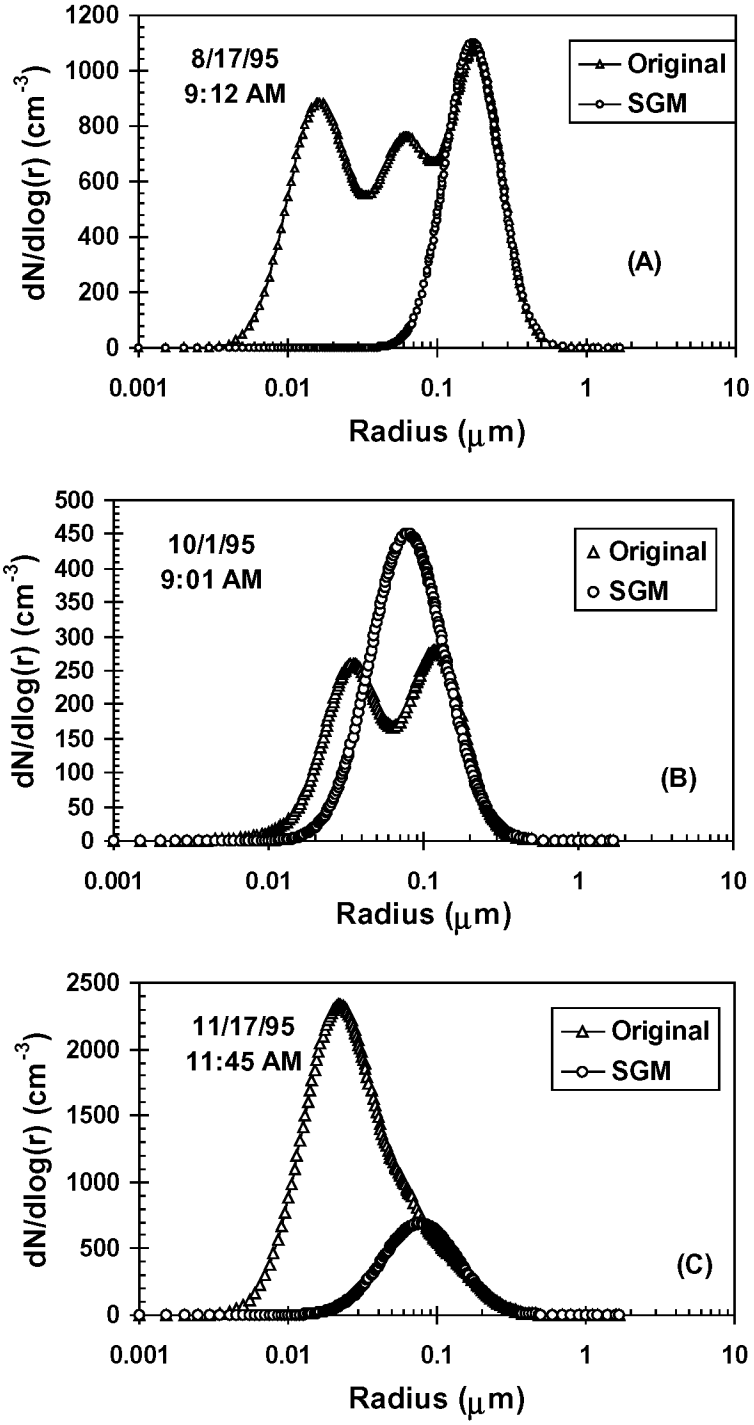

5.4. Comparison between original tri-modal size distribution and that retrieved from its extinction coefficient at the three operational wavelengths by search-graph method (SGM) (a) on 17 August 1995, (b) on 1 October 1995, (c) on 11 November 1995

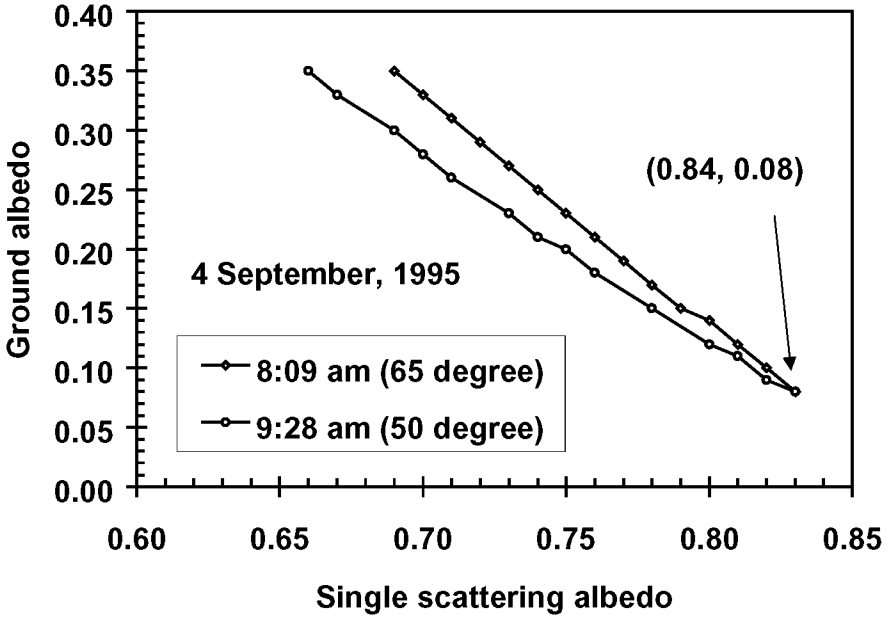

Figure 5.5. Single scattering albedo vs ground albedo demonstrating the method of simultaneous solution for ground albedo and single scattering albedo

6. AEROSOL DIRECT RADIATIVE FORCING IN THE SOUTHEASTERN US: ESTIMATES FROM THE MEASUREMENT AND MODEL RESULTS

Shaocai Yu[1], Charles S. Zender[2] and V. K. Saxena[1]

[1] Department of Marine, Earth and Atmospheric Sciences
North Carolina State University, Box 8208, Raleigh, NC 27695-8208, U.S.A

[2] National Center for Atmospheric Research, Boulder, Colorado 80307-3000

In preparation for submission to Geophysical Research Letters, 1999

6.1. Abstract

In an effort to reduce uncertainties in the quantification of aerosol radiative forcing, a field column-closure experiment was conducted to measure aerosol radiative properties and effects at a representative site, e.g. Mt. Mitchell, and an adjacent valley site in the southeastern US. The experimental period was from June 1995 to mid-December 1995. It was found that the representative total AOD values at 500 nm at the valley site for highly polluted (HP), marine (M) and continental (C) air masses were 0.68±0.33, 0.29± 0.19 and 0.10± 0.04, respectively, during the study period. The regional values of aerosol direct radiative forcing (ADRF) are derived using the measured aerosol radiative properties as inputs to a Community Climate Model (CCM3) Column Radiation Model (CRM). It was found that the cloud-free instantaneous ADRF was –9.2 to 30.2, -14 to –23 and –55 to 185.7 W m^{-2} for continental, marine and polluted air masses respectively. The average cloud-free 24-hour ADRF was estimated to be -13±8, -8±3, -33±16 W m^{-2} for marine, continental, and polluted air masses respectively. On the assumption that the fractional coverage of clouds is 0.61, the annual mean ADRF is 7±2 W m^{-2}, and the mean ADRF values were -5±3, -3±1 and -13±6 W m^{-2} for marine, continental and polluted air masses respectively.

6.2. Introduction

The eastern China, south central Europe and eastern US have been recognized (IPCC, 1995) as regions where the effect of anthropogenic aerosols supersedes that of man-made greenhouse gases (GHGs) and manifests itself in terms of cooling of the surface-air temperature (Kiehl and Briegled, 1993). *Saxena et al.* (1997) and *Saxena and Yu* (1998) have verified this model prediction in the southeastern US by finding that the arithmetic average of mean daily temperature at 52 stations in the southeastern US decreased by -0.09 C during 1949-94 (46-year period). The direct aerosol effect refers to backscattering and absorption of radiation by the aerosol particles themselves (*Charlson et al.*, 1991; *Penner et al.*, 1994; *Kiehl and Briegleb*, 1993; *IPCC*, 1995; *Saxena and Yu*, 1998).

Charlson et al. (1991) used a box model to estimate that natural sulfate aerosols produced a global mean forcing of -0.42 W m^{-2}, and that anthropogenic sulfate adds -0.11 W m^{-2} in the Southern Hemisphere and -1.07 W m^{-2} in the Northern Hemisphere, with considerable variation depending on specific assumptions made with respect to aerosol properties. The conclusion of *IPCC* (1995) is that global mean forcing resulting from anthropogenic sulfate may range from -0.25 to -0.9 W m^{-2}, with substantial uncertainty; and biomass burning aerosol forcing may range from -0.05 to -0.6 W m^{-2}. The uncertainty in the magnitude of the estimated direct and cloud-mediated (also called the indirect effect) cooling effect of aerosols (Schwartz and Andreae, 1996) is a major barrier for a reliable *prediction of climate change on the scale of a decade and longer*. Any policy decisions to limit the emissions of GHGs could have severe *short-term impact on the regional climate* since major sources of GHGs and aerosols are identical such as fossil fuel combustion, biomass burning etc. Since the aerosol direct radiative forcing (ADRF) is determined by the aerosols within the atmospheric column instead of the

aerosols contained in the surface layer, it is very useful to obtain the average aerosol radiative properties for the atmospheric column, for example, through a column-closure experiment.

The objectives of this study are to estimate the ADRF in the southeastern US with Column Radiation Model (CRM) of the National Center for Atmospheric Research (NCAR) Community Climate Model (CCM3) (Kiehl and Briegleb, 1993; Kiehl et al., 1998; Briegleb, 1992) on the basis of a field column-closure experiment, and compare our result with the results from other investigators. Since one of the field sites (Mt. Mitchell) is at a remote and elevated location which is frequently influenced by air masses arriving from marine, continental and polluted sectors and is often embedded into the free troposphere, the data sets are considered to be regionally representative of the southeastern US.

6.3. Aerosol radiative properties in the southeastern US

A detailed description of the instrumentation, methodology, data quality assurance and quality control of the data has been given by *Wenny et al.* (1998) and Yu et al. (1999). The research sites include a mountain top station located on the peak of Mt. Gibbes (35.78 ^{0}N, 82.29 ^{0}W, 2006 m MSL) in Mt. Mitchell State Park, and a valley station located adjacent to the Burnett Reservoir near the town of Black Mountain, North Carolina (35.66 ^{0}N, 82.38 ^{0}W, 951 m MSL) [for details see *Bahrmann and Saxena,* 1998]. The two sites are separated horizontally by ten kilometers and vertically by one kilometer. The aerosol optical depths (AODs) at the three operational wavelengths (415, 500 and 673 nm) are determined on the basis of the direct components of solar irradiance measured by the Multi-Filter Rotating Shadowband Radiometer (MFRSR) (*Wenny et al.*, 1998; Yu et al., 1999). Table 6.1 lists the mean total AOD and standard deviation as measured from the valley and mountain sites and mean layer AOD between the two sites

as a function of air mass type at the three operational wavelengths for cloud-free days during the experimental period. The air masses are classified (*Bahrmann and Saxena*, 1998) as highly polluted (HP), continental (C), and marine (M) based on the SO_2 and NOx emission inventory of the U.S. Environmental Protection Agency. It is clear from Table 6.1 that the highly polluted (HP) air masses exhibit the largest average AOD, compared to marine (M) and continental (C) air masses at the three operational wavelengths. As can be seen, the mean total AOD at 500 nm at the valley site was 0.10± 0.04, 0.29±0.12 and 0.68±0.33 for C, M and HP air masses, respectively. Overall, the ratios of mean 1-kilometer layer AOD to total mean AOD from the valley site for HP air mass were 73%, 73% and 79% for 415, 500 and 673 nm respectively. This indicates that the major portion of atmospheric aerosols, which make an important contribution to the AOD, is located in the lowest 1-kilometer boundary layer of the troposphere on the basis of our site results. This is in reasonable agreement with that of *Hegg et al.* (1997), who found that AOD for the lowest 4 km of the troposphere constituted over 90% of the total column AOD off the mid-Atlantic coast of US.

Table 6.2 lists the experimental results of AOD, and retrieved columnar lognormal size distribution (number concentration (N), geometric mean radius (r_g) and geometric standard deviation (σ_g)) by the search-graph method, aerosol radiative properties (imaginary part, asymmetry factor and singe scattering albedo) and ground albedo using a mathematically unique procedure involving a Mie code and a radiative transfer code in conjunction with the retrieved aerosol size distribution, AOD, and diffuse-direct ratio (*Yu et al.*, 1999). A detailed description of the search-graph method and the mathematically unique procedure has been given by Yu et al. (1999). Table 6.2 shows that N, r_g and σ_g are in the range of 1.0E1 to 1.7E4 cm^{-3}, 0.02 to 0.54 μm and 1.12 to 2.95, respectively. The asymmetry factors at 500 nm are in the range of 0.64 to 0.77. ϖ was in the range of 0.72 to 0.97 and the imaginary part of refractive index was in the range of 0.005 to 0.051. Reported values of ϖ in scientific literature show ϖ to be 1.0 for sulfate and pure marine

aerosols and range from 0.5 to 0.7 for desert dust and soot aerosols (*Lacis and Mishchenko*, 1995). *Wenny* et al. (1998) reported that ϖ at 312 nm varied from 0.75 to 0.93. The values of ϖ from this study are compatible with these values given by other authors. *Lacis and Mishchenko* (1995) showed that the asymmetry factor of soot and large desert aerosols was about 0.9, but for sulfate, marine and smaller dust aerosols the asymmetry factor ranges from 0.65 to 0.8. For the UV wavelength region, *Wenny et al.* (1998) found that the asymmetry factor determined for the site ranged from 0.63 to 0.76. The values of asymmetry factor reported here are close to those for sulfate, marine and smaller dust aerosols. Ground albedo is 0.19 on the basis of our result. Since the size distribution was inferred from the total AOD, the aerosol radiative properties derived by this method represents a weighted average over the entire column, which affects the transfer of radiation.

6.4. Calculation of aerosol direct radiative forcing (ADRF)

The NCAR CCM3 CRM (Kiehl and Briegleb, 1993; Kiehl et al., 1998; Briegleb, 1992) is used to estimate the ADRF in the southeastern US. The CCM3 CRM uses a δ-Eddington approximation with 19 spectral intervals (7 for O_3, 2 for the visible, 7 for H_2O, and 3 for CO_2) spanning the solar spectrum from 0.2 to 5.0 μm. A detailed description of all the physical and numerical methods used in CCM3 CRM is given in Kiehl et al. (1998) and Briegleb (1992). The atmospheric initial conditions of Kiehl and Briegleb (1993) were used in the CRM. The mass extinction coefficient, single scattering albedo and asymmetry factor at 19 spectral interval wavelengths calculated by the Mie code (Dave, 1969) with the retrieved columnar size distribution, and ground albedo (0.19) were input into the CRM. The density of aerosol particles was assumed to be 1.86 g cm^{-3} when the mass extinction coefficient was calculated. The direct aerosol radiative forcing

is obtained as the different in shortwave net radiative flux at the surface level when the CRM is run once with and without any aerosol mass loading.

Table 6.2 lists the instantaneous ADRF for each cloud-free time during the experiment. The zenith angle, air mass types, AOD at the three wavelengths, size distribution, retrieved aerosol radiative properties and refractive index are also listed in Table 6.2. As mentioned by Yu et al. (1999), the mathematically unique procedure can only have solutions for the cases whose AODs at 500 nm were between 0.1 to 0.3. The averages of imaginary part of refractive index for September, October and November are -0.017±0.009, -0.027±0.021, -0.050±0.001 on the basis of available results in Table 6.2. The values of -0.017, -0.027 and -0.050 will be used for the cases, whose imaginary parts are not available, between July and September, in October and in November respectively, as indicated in Table 6.2. Figure 6.1 shows the diurnal variation of instantaneous ADRF for continental, marine and polluted air masses, calculated on the basis of measurement at 321 (11/17/1995, 10:27), 272 (9/29/1995, 8:59) and 227 (8/15/1995, 9:50) (see Table 6.2). As can be seen, the times of maximum ADRF are in early-to-mid morning and mid-to-late afternoon, rather than at the midday peak of incident sunlight except November case. This result is in agreement with that of Russell et al. (1997). The low ADRF at the mid-day is due to the low of hemispheric upscatter fractions (Russell et al., 1997). So the instantaneous ADRFs in Table 6.2 should be considered as maximums for the day. Table 6.2 shows that the instantaneous ADRF ranges from -9.2 to 30.2, -16.7 to -24.3, and –55.3 to -156.5 W m^{-2} for continental, marine, and polluted air masses respectively. A sensitivity test was performed by calculating the ADRF difference between the case with our aerosol radiative properties and that with the sulfate optical properties of *Kiehl and Briegleb* (1993), but the AOD is the same. It is found that the instantaneous ADRF is 27.2 W m^{-2} on the basis of measurement of aerosol radiative properties on 10:58 11/17/1995, while the ADRF is -10.0 W m^{-2} on the basis of sulfate aerosol radiative properties of *Kiehl and Briegleb* (1993). Obviously, the ADRF from this study is much

higher. This is reasonable because the aerosol of this study is total aerosol and the imaginary part of refractive index is also considered.

To estimate the 24-hour average ADRF for different air mass types, the typical aerosol radiative properties for different air masses are needed. In this study, the typical aerosol radiative properties (mass extinction coefficient, single scattering albedo, asymmetry factor) of 321 (11/17/1995, 10:27 ET, continental air mass), 272 (9/29/1995, 8:59, marine air mass) and 227 (8/15/1995, 9:50, polluted air mass) were used for the continental, marine and polluted air masses respectively in CRM calculation. These three cases were selected because their AODs were close to the mean AODs of corresponding air masses and most of continental, marine, and polluted air masses occurred during winter, fall and summer season respectively. The mean optical depths at Table 6.1 for three air mass types are used. It was found that cloud-free, 24-hour averages ADRF are -8±3, -13±8, and -33±8 W m^{-2} for continental, marine, and polluted air masses respectively, as listed in Table 6.3. To assess the annual average ADRF in the southeastern US, the relative contributions of three air masses is needed. Bahrmann and Saxena (1998) found that the percentages of air masses influencing our research site were 43.2, 22.4 and 34.4% for continental, marine and polluted air masses respectively, on the basis of back trajectory analysis of air masses from June 1996 to October 1996, and from March 1997 to June 1997. If these percentages were used, the annual cloud-free, 24-hour mean ADRF was estimated to be -17±6 W m^{-2}. The mean annual AOD at 500 nm would be 0.25±0.12. This is in reasonable agreement with the mean annual aerosol optical thickness of 0.336 at 500 nm (0.147 turbidity) over central North Carolina as indicated by Peterson et al. (1981) on the basis of observation from July 1969 to July 1975. If the mean fraction of the area with clear sky condition in the southeastern US is assumed to be 0.39, which is the globally average clear sky condition (Charlson et al., 1991), the mean ADRFs will be -3±1, -5±3, 13±6 W m^{-2} for continental, marine and polluted air masses, respectively. The annual mean ADRF is -7±2 W m^{-2}.

Table 6.3 lists the comparison of our estimate of ADRF with those of other investigators for the southeastern US or eastern US. As can be seen, the estimates of ADRF in the eastern US (or southeastern US) have a large variation because of different assumptions in each model and relative uncertainty of aerosol radiative properties. Our estimated ADRF is a little higher than those of Bergstrom and Russell (1999), Kiehl and Rodhe (1995) and Haywood and Ramaswamy (1998). Bergstrom and Russell (1999) show that cloud-free, 24-hour average ADRF is -9 W m^{-2} near the eastern US coast in summer on the basis of AVHRR/NOAA AOD measurement reported by Husar et al. (1997). Both Kiehl and Rodhe (1995) and Haywood and Ramaswamy (1998) indicated that the ADRF of anthropogenic sulfate was -5 W m^{-2}. Since our calculations are for total aerosols (anthropogenic + natural) and for whole aerosol components (sulfate+organic), our ADRF should provide an upper bound on the anthropogenic aerosol effects.

6.5. Conclusion

Using a CCM3 CRM model, estimates were made of the instantaneous and cloud-free 24-hour average ADRF for continental, marine and polluted air masses in the southeastern US on the basis of measurement of aerosol radiative properties from the aerosol vertical column closure experiment. The results show that the annual regional 24-hour cloud-free mean ADRF is –17±6 W m^{-2}. Considering the effect of cloud fraction, the annual regional mean ADRF is –7±2 W m^{-2}. The comparison indicates that our estimates of ADRF in the southeastern US is a little higher than that (-5 W m^{-2}) of recent calculations of Kiehl and Rodhe (1995) and Haywood and Ramaswamy (1998) because the total aerosol (anthropogenic + nature) instead of anthropogenic and whole aerosol (sulfate + organics) instead of sulfate were considered in this study.

Acknowledgments This research was supported by the NASA's Mission to Planet Earth (MTPE) under Contract No. NAS1-18944 from Langley Research Center, Hampton, VA. Authors would like to thank Dr. Lamont Poole, and Prof. Patrick McCormick for their encouragement.

6.6. References

Bahrmann, C.P., and V.K. Saxean, The influence of air mass history on black carbon concentrations in the southeastern US. *Journal of Geophysical Research*, 103, 23153-23161, 1998

Briegleb, B.P., Delta-{Eddington} Approximation for Solar Radiation in the NCAR Community Climate Model, *J. Geophys. Res.*,97, 7603-7612, 1992.

Bergstrom, R.W., and P.B. Russell., Estimation of aersol direct radiative effects over the mid-latitude North Atlantic from satellite and in situ measurements. *Geophys. Res. Lett.*, 26, 1731-1734, 1999.

Boucher O., and T. L. Anderson, General circulation model assessment of the sensitivity of direct climate forcing by anthropogenic sulfate aerosols to aerosol size and chemistry. *J. geophys. Res.* 100, 26117-26134, 1995

Charlson, R.J., Langner, J., Rodhe, H., Leovy, C.B., and S.G. Warren, Perturbation of the northern hemisphere radiative balance by backscattering from anthropogenic sulfate aerosols. Tellus, 43AB, 152-163, 1991.

Dave, J.V., Subroutines for computing the parameters of electromagnetic radiation scattered by a sphere. *IBM J. Res. Dev., 13*, 302-312, 1969.

Haywood, J.M., and K.P. Shine, The effect of anthropogenic sulfate and soot aerosol on the clear sky planetary radiation budget. Geophysics Research Letters, 22, 603-606, 1995.

Haywood, J.M., and V. Ramaswamy, Global sensitivity studies of the direct radiative forcing due to anthropogenic sulfate and black carbon aerosol. *J. Geophys. Res.*, 103, 6043-6058, 1998

Hegg, D.A., J. Livingston, P.V. Hobbs, T. Novakov, and P. Russell, Chemical apportionment of aerosol column optical depth off the mid-Atlantic coast of the United States. *J. geophys. Res.,* 102, 25293-25303, 1997

IPCC, Climatic change 1995: The Science of Climate Change. J.T. Houghton et al. (Eds). Cambridge University Press, Cambridge, UK, 1994.

Kiehl, J.T. and B.P. Briegleb, The relative role of sulfate aerosols and greenhouse gases in climate forcing. *Science.* 260, 311-314, 1993

Kiel, J. T., J. J. Hack, G. B. Bonan, B. A. Boville, D. L. Williamson and P. J. Rasch, The National Center for Atmospheric Research Community Climate Model: CCM3, *J. of Climate*, 11, 1131-1149, 1998.

Kiehl, J.T., and H. Rodhe, 1995. Modeling geographical and seasonal forcing due to aerosols, *in Aerosol Forcing of Climate,* edited by R.J. Charlson and J. Heintzenberg, John Wiley & Sons, Chichester, U.K., 1995.

Lacis, A., and M.I. Mishchenko, Climate forcing, cloud sensitivity, and climate response: a radiative modeling perspective on atmospheric aerosols, *in Aerosol Forcing of Climate,* edited by R.J. Charlson and J. Heintzenberg, John Wiley & Sons, Chichester, U.K., 1995.

Langner, J., and H. Rodhe, 1991. A global three-dimentional sulfur cycle. *J. Atmos. Chem.*, 13, 225-263.

Penner, J.E., R.J. Charlson, J.M. Hales, N.S. Laulainen, R. Leifer, T. Novakov, J. Ogren, L.F. Radke, S.E. Schwartz, and L. Travis, Quantifying and minimizing uncertainty of climate forcing by anthropogenic aerosols, *Bull. Amer. Meteorol. Soc.*, *75*, 375-400, 1994.

Peterson, J.T., Flowers, E.C., Berri, G.J., Reynolds, C.L., and J.H. Rudesill, Atmospheric

turbidity over central North Carolina, *J. Appl. Meteor.* 20, 229-241, 1981

Russell, P.B., S.A. Kinne, and R.W. Bergstrom, Aerosol climate effects: local radiative forcing and column closure experiments. *J. Geophys. Res.*, 102, 9397-9407, 1997.

Saxena, V.K., Shaocai. Yu, and J. Anderson, Impact of stratospheric volcanic aerosols on climate: evidence for aerosol shortwave and longwave forcing in the Southeastern US, *Atmos. Environ., 31*, 4211-4221, 1997.

Saxena, V.K., and Shaocai. Yu, Searching for a regional fingerprint of aerosol radiative forcing in the southeastern US, *Geophys. Res. Lett., 25,* 2833-2836, 1998.

Schwartz, S.E., and M.O. Andreae, Uncertainty in climate change caused by aerosols. *Science, 272*, 1121-1122, 1996.

Schult, I., J. Feichter, and W.F. Cooke, Effect of black carbon and sulfate aerosols on the global radaition budget, *J. Geophys. Res.*, 102, 30107-30117, 1997.

Taylor, K., and J.E. Penner, Response of the climate system to atmospheric aerosols and greenhouse gases, *Nature*, 369, 734-737, 1994.

Wenny, B.N., J.S. Schafer, J.J. DeLuisi, V.K. Saxena, W.F. Barnard, I.V. Petropavlovskikh, and A.J. Vergamini, A study of regional aerosol radiative properties and effects on ultraviolet-B radiation, *J. Geophys. Res.,* 103, 17,083-17,097, 1998.

Yu, Shaocai., Saxena, V.K., Wenny, B.N., DeLuisi, J.J., Yue, G. K. and I.V. Petropavlovskikh, A study of the aerosol radiative properties needed to compute direct aerosol forcing in the southeastern US, *J. Geophys. Res.*, 1999 (in review).

Table 6.1. Mean total optical depth, and their standard deviation at 415, 500 and 673 nm as measured at the valley and mountain sites. The data for the intervening layer were obtained from the difference between the two sites. The sites were influenced by highly polluted (HP), continental (C) and marine (M) air masses. V, M, and L denote the valley, mountain and the intervening layer respectively.

	τ_v at the valley site			τ_m at the mountain site			τ_l for the intervening layer			Ratio (τ_l /τ_v)		
Air mass	V415	V500	V673	M415	M500	M673	L415	L500	L673	415	500	673
HP	0.78±0.41	0.68±0.33	0.51±0.22	0.22±0.14	0.19±0.12	0.12±0.07	0.56±0.28	0.50±0.25	0.40±0.20	0.73±0.12	0.73±0.15	0.79±0.17
M	0.36±0.25	0.29±0.19	0.19±0.12	0.13±0.12	0.10±0.09	0.06±0.05	0.23±0.13	0.20±0.11	0.14±0.09	0.69±0.14	0.71±0.15	0.73±0.14
C	0.11±0.07	0.10±0.04	0.07±0.02	0.04±0.02	0.03±0.01	0.03±0.01	0.07±0.04	0.07±0.03	0.04±0.02	0.62±0.12	0.68±0.09	0.51±0.25

Table 6.2. The measured optical depth (τ) (at 415, 500, 673 nm), columnar size distribution inferred by the search-graph-method, single scattering albedo (ω), asymmetry factor, refractive index, zenith angle, air mass types and instantaneous aerosol direct radiative forcing (ADRF) calculated by CRM model. * The refractive index was obtained by the averaging available results (see the text for explanation).

				τ measured			Search-graph-method						
Day (1995)	Time(EST)	Zenith angle	Air mass	415	500	673	Ng (cm^{-3})	rg (μm)	σ_g	g_{500}	ω_{500}	Refractive index	ADRF (W m-2)
189(7/8)	8:00	59.2	C	0.33	0.28	0.18	1.7E+02	0.17	1.35	0.74	0.91	1.50-0.017*i**	-30.2
189(7/8)	8:26	53.9	C	0.30	0.25	0.16	8.4E+01	0.23	1.12	0.76	0.92	1.50-0.017*i**	-26.8
191(7/10)	8:02	58.9	C	0.33	0.27	0.17	3.3E+02	0.13	1.50	0.73	0.91	1.50-0.017*i**	-29.7
246(9/3)	8:59	55.4	C	0.21	0.16	0.10	5.4E+02	0.08	1.68	0.67	0.92	1.50-0.015*i*	-17.5
246(9/3)	9:53	45.3	C	0.23	0.18	0.11	6.7E+02	0.08	1.72	0.70	0.97	1.50-0.005*i*	-14.3
247(9/4)	8:09	65.5	C	0.18	0.13	0.08	2.3E+03	0.04	2.00	0.64	0.86	1.50-0.020*i*	-16.6
247(9/4)	9:01	55.2	C	0.17	0.14	0.08	1.6E+03	0.04	1.94	0.65	0.82	1.50-0.031*i*	-17.2
247(9/4)	9:28	50.2	C	0.19	0.15	0.09	6.2E+02	0.07	1.74	0.66	0.82	1.50-0.031*i*	-21.7
256(9/13)	9:10	55.7	C	0.47	0.40	0.27	4.4E+02	0.12	1.57	0.72	0.91	1.50-0.017*i**	-45.1
256(9/13)	9:52	48.2	C	0.45	0.38	0.25	3.8E+02	0.13	1.55	0.71	0.83	1.50-0.017*i**	-43.1
290(10/17)	10:00	56.9	C	0.08	0.07	0.07	7.2E+01	0.08	2.25	0.72	0.81	1.50-0.027*i**	-15.2
290(10/17)	10:40	51.7	C	0.08	0.08	0.08	3.2E+01	0.17	1.77	0.73	0.84	1.50-0.027*i**	-17.2
295(10/22)	9:50	59.8	C	0.07	0.07	0.06	5.2E+01	0.13	1.80	0.71	0.83	1.50-0.027*i**	-13.4
295(10/22)	10:30	54.4	C	0.08	0.08	0.06	2.4E+01	0.21	1.48	0.73	0.85	1.50-0.027*i**	-15.3
296(10/23)	12:42	47.3	C	0.07	0.07	0.06	2.4E+01	0.19	1.61	0.72	0.82	1.50-0.027*i**	-14.0
296(10/23)	13:54	51.1	C	0.07	0.07	0.06	4.4E+01	0.10	2.13	0.73	0.75	1.50-0.027*i**	-15.5
298(10/25)	8:36	72.7	C	0.06	0.05	0.05	5.0E+01	0.05	2.95	0.76	0.85	1.50-0.027*i**	-12.5
298(10/25)	11:09	51.3	C	0.08	0.08	0.07	1.9E+01	0.23	1.47	0.73	0.78	1.50-0.027*i**	-16.3
308(11/4)	8:48	72.9	C	0.04	0.04	0.04	1.2E+01	0.22	1.47	0.75	0.72	1.50-0.050*i**	-9.2
320(11/16)	9:06	72.5	C	0.08	0.07	0.06	3.0E+02	0.03	2.70	0.73	0.8	1.50-0.050*i**	-16.3
320(11/16)	11:38	55.6	C	0.07	0.07	0.06	9.6E+00	0.32	1.15	0.77	0.74	1.50-0.050*i**	-20.4

Table 6.2. (Continued)

Day (1995)	Time(EST)	Zenith angle	Air mass	τ measured			Search-graph-method			g_{500}	ω_{500}	Refractive index	ADRF (W m-2)
				415	500	673	Ng (cm^{-3})	rg (μm)	σ_g				
321(11/17)	10:27	61.8	C	0.14	0.12	0.09	3.2E+02	0.07	1.96	0.69	0.74	1.50-0.051*i*	-25.5
321(11/17)	10:58	58.6	C	0.15	0.13	0.09	1.5E+02	0.11	1.71	0.70	0.74	1.50-0.051*i*	-27.1
321(11/17)	11:45	55.5	C	0.16	0.14	0.10	1.4E+02	0.12	1.68	0.71	0.76	1.50-0.049*i*	-29.1
325(11/21)	9:52	66.8	C	0.08	0.08	0.06	9.2E+01	0.09	1.94	0.71	0.76	1.50-0.050*i**	-17.9
326(11/22)	10:16	64.0	C	0.06	0.06	0.05	1.6E+01	0.23	1.45	0.74	0.78	1.50-0.050*i**	-15.5
326(11/22)	10:42	61.2	C	0.07	0.07	0.06	1.6E+01	0.22	1.48	0.75	0.78	1.50-0.050*i**	-17.7
329(11/25)	9:18	72.3	C	0.08	0.08	0.06	5.6E+01	0.12	1.85	0.73	0.76	1.50-0.050*i**	-17.7
248(9/5)	10:58	35.5	M	0.30	0.23	0.14	1.1E+03	0.07	1.74	0.61	0.9	1.50-0.017*i**	-24.3
272(9/29)	8:32	66.9	M	0.25	0.19	0.12	6.0E+03	0.03	2.13	0.63	0.90	1.50-0.017*i*	-23.1
272(9/29)	8:59	61.9	M	0.24	0.18	0.11	4.1E+03	0.03	2.11	0.69	0.97	1.50-0.010*i*	-19.2
274(10/1)	8:21	69.6	M	0.12	0.10	0.07	5.8E+02	0.04	2.26	0.67	0.86	1.50-0.020*i*	-14.6
274(10/1)	9:01	62.1	M	0.11	0.09	0.07	5.3E+02	0.04	2.37	0.68	0.76	1.50-0.049*i*	-20.2
274(10/1)	9:15	59.6	M	0.11	0.10	0.08	2.0E+02	0.07	2.01	0.68	0.76	1.50-0.049*i*	-21.4
275(10/2)	9:32	56.9	M	0.20	0.16	0.11	1.5E+03	0.04	2.20	0.67	0.98	1.50-0.006*i*	-16.7
275(10/2)	10:06	51.5	M	0.21	0.18	0.12	6.7E+02	0.06	1.97	0.67	0.97	1.50-0.010*i*	-19.6
183(7/2)	8:22	54.8	HP	0.57	0.50	0.33	3.6E+02	0.18	1.38	0.72	0.91	1.50-0.017*i**	-55.3
227(8/15)	8:07	62.1	HP	0.83	0.68	0.43	8.4E+02	0.13	1.52	0.69	0.9	1.50-0.017*i**	-69.1
227(8/15)	9:50	41.6	HP	0.87	0.71	0.45	5.9E+02	0.15	1.44	0.70	0.91	1.50-0.017*i**	-73.0
229(8/17)	9:12	49.3	HP	1.06	0.90	0.59	5.6E+02	0.17	1.40	0.71	0.91	1.50-0.017*i**	-93.9
229(8/17)	10:31	34.6	HP	0.99	0.84	0.54	4.8E+02	0.18	1.37	0.71	0.92	1.50-0.017*i**	-87.4
235(8/23)	9:18	49.3	HP	0.76	0.64	0.41	5.8E+02	0.14	1.48	0.69	0.91	1.50-0.017*i**	-67.6
252(9/9)	9:19	53.0	HP	0.81	0.62	0.36	3.0E+03	0.07	1.71	0.64	0.9	1.50-0.017*i**	-64.8
288(10/15)	11:00	48.8	HP	0.53	0.55	0.68	4.0E+01	0.53	1.28	0.65	0.82	1.50-0.027*i**	-156.5
289(10/16)	8:24	72.7	HP	0.35	0.36	0.42	2.4E+01	0.54	1.36	0.65	0.84	1.50-0.027*i**	-83.4
289(10/16)	9:40	59.7	HP	0.51	0.52	0.64	3.6E+01	0.54	1.30	0.64	0.84	1.50-0.027*i**	-142.3

Table 6.3. Comparison of aerosol direct radiative forcing (ADRF) in the southeastern US and eastern US. * "no cloud" means cloud-free 24-hour average, "with cloud" means that the fractional coverage of clouds is assumed to be 0.61.

Aerosols	Method	Regional ADRF (W m-2)	regions	Author
Total aerosol(marine)	Measurement and CCM3 CRM	-5±3 (with cloud)*	southeastern US	This work
Total aerosol (continental)	Measurement and CCM3 CRM	-3±1 (with cloud)*	southeastern US	This work
Total aerosol(polluted)	Measurement and CCM3 CRM	-13±6 (with cloud)*	southeastern US	This work
Total aerosol (average)	Measurement and CCM3 CRM	-7±2 (with cloud)*	southeastern US	This work
Total aerosol(marine)	Measurement and CCM3 CRM	-13±8 (no cloud)*	southeastern US	This work
Total aerosol (continental)	Measurement and CCM3 CRM	-8±3 (no cloud)*	southeastern US	This work
Total aerosol(polluted)	Measurement and CCM3 CRM	-33±16 (no cloud)*	southeastern US	This work
Total aerosol (average)	Measurement and CCM3 CRM	-17±6 (no cloud)*	southeastern US	This work
Total aerosol (marine)	Box model	-9	southeastern US	Saxena and Yu (1998)
Total aerosol (continental)	Box model	-3	southeastern US	Saxena and Yu (1998)
Total aerosol (polluted)	Box model	-21	southeastern US	Saxena and Yu (1998)
Sulfate	GCM model	~-2	southeastern US	Boucher and Anderson (1995)
Anthropogenic sulfate	Box model	-2	eastern US	Charlson et al. (1991)
Anthropogenic sulfate	3-D chemical and CCM3 CRM	-3	eastern US	Kiehl and Briegleb (1993)
Sulfate	AGCM model	~-0.5-~-1.5	eastern US	IPCC (1995)
Anthropogenic sulfate		-3	eastern US	Taylor and Penner (1994)
Total aerosol	radiative transfer model	-5.1~-1.5	mid-latitude North Atlantic	Bergstrom and Russell (1999)
Total aerosol	radiative transfer model	-9	eastern US	Russell (1997)
Total aerosol	radiative transfer model	-8 ~ -50 (no cloud)*	eastern US	Bergstrom and Russell (1999)
Anthropogenic sulfate	slow oxidation rate case	-2	eastern US	Langner and Rodhe (1991)
Anthropogenic sulfate	chemical model	-5	eastern US	Kiehl and Rodhe (1995)
Antropogenic aerosol	internal mixture	-1.5	eastern US	Haywood and Shine (1995)
Sulfate+BC	1-D radiative transfer model	-2 to -3	eastern US	Schult et al. [1997]
Sulfate	GCM model	-5	eastern US	Haywood and Ramaswamy [1998]
Sulfate+BC	GCM model	-3	eastern US	Haywood and Ramaswamy [1998]

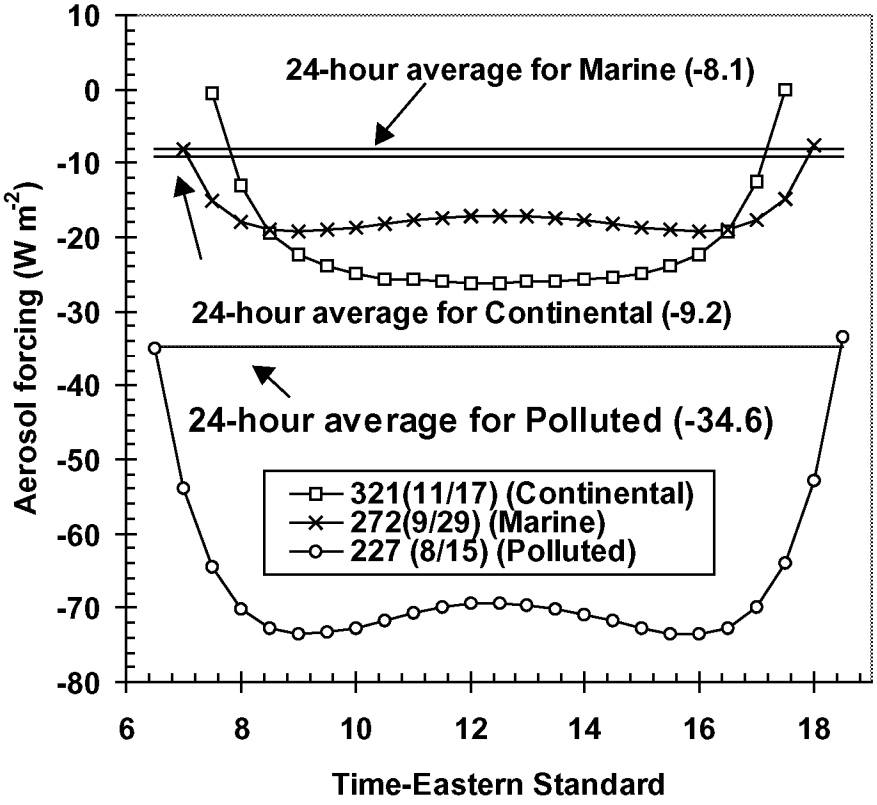

Figure 6.1. Instantaneous aerosol direct radiative forcing (ADRF) as a function of eastern standard local time and cloud-free 24-hour mean ADRF for three cases on basis of the aerosol measurements on 11/17/1995 10:27, 9/29/1995 8:59, and 8/15/1995 9:50. Calculations assume that the aerosol radiative properties measured are constant for whole day.

PART II: A STUDY OF CLOUD CONDENSATION NUCLEI (CCN)

7. ON THE MEASUREMENTS OF CLOUD CONDENSATION NUCLEI AT PALMER STATION, ANTARCTICA

T.P. DeFelice[1], V.K.Saxena[2] and Shaocai Yu[2]

Atmospheric Environment, 31, 4039-4044, 1997.

1. Department of Geosciences, Atmospheric Sciences Group
   University of Wisconsin at Milwaukee, Milwaukee, WI 53211
2. Department of Marine, Earth and Atmospheric Sciences
   North Carolina State University, Raleigh, NC 27695-8208

7.1. Introduction

Cloud condensation nuclei (CCN) spectral measurements are among the recent priorities for the study of aerosol/ climate interactions (e.g. WMO/WMP No.19. August 1992; Hobbs and Huebert, 1996). For example, the potential link between CCN formation, the oxidation of dimethylsulfide (DMS), and particle nucleation in the marine atmosphere represents an important component in the DMS-cloud-climate hypothesis (Charlson et al.. 1987; Shaw, 1983). However, there are large uncertainties existing with respect to such a link due to poor understanding of the intricate mechanisms that control the relationship among the DMS sea-to air flux, atmospheric DMS chemistry and CCN formation in the marine atmosphere (Bates et al., 1989).

Palmer station, Antarctica offers a unique and unusual opportunity to investigate the CCN-DMS relationship due to the known and limited sources of aerosol in the vicinity of Palmer Station, Antarctica (Robinson et al., 1984; Hogan et al., 1990). However, CCN spectral measurements are especially rare in the Antarctic region. Consequently, we present and discuss the predominant characteristics associated with a first dataset of daily daylight period (i.e.≈13-15h long) averaged CCN spectral measurements at a remote region of the globe, namely Palmer Station, Antarctica. Palmer Station is located on the Antarctic Peninsula and sits on a glacial moraine between the piedmont glacier and the Bellings-Hausen Sea in the midst of natural Antarctic sources (Hogan, 1975; Shaw.1979), which could include sea-to air emission of marine organic nuclei. The predominant local pollution source is a diesel power plant approximately 100 m WNW of the sampling platform. Other natural pollution sources during January and February are minor and include: a total of 6 tourist ships, the Polar Duke, occasional outdoor paint work and the use of on/off load vehicles. Daily daylight period averages are chosen since (i) the day is dominated by daylight during our sampling period, (ii) the CCN measurement frequency is a maximum during the daylight period, (iii) DeFelice (1996) has related temporal CCN concentrations to smaller-scale phenomena (i.e. mesoscale and shorter) at the same

remote region, and (iv) they are sufficient for most climate modelling efforts. The Palmer data represent a natural Southern Hemisphere remote marine arctic climate, especially after all significant local pollution sources are filtered out.

7.2. Background

First-time measurement of CCN spectra were made at Palmer Station, Antarctica (64^0 46'S, $64^0$05' W) during January 1994 (Saxena.1996) and February 1994 (DeFelice, 1996), using the CCN-spectrometer (e.g. DeFelice and Saxena, 1994) during the daily observing periods (≈0730- 2200 h local time) of 11 January-26 February 1994. The CCN spectra may be described by

$$N=Cs^k \qquad (7.1)$$

where N is the number of CCN activated at a given supersaturation s. C and k are constants of the distribution. A small k parameter (i.e. k <1.0) indicates that the observed cloud droplet spectra is determined by the CCN population. A value of k > 1 indicates that the observed cloud droplet spectra is determined by the inherent cloud dynamics. A large k value may also mean that sampling takes place in the vicinity of a non-steady-state phenomenon (i.e. in the vicinity of evaporating rain droplet, or a frontal boundary), or there is a source of small CCN. Small CCN require high supersaturation, consequently, an increase in small CCN pushes the high supersaturation end of the distribution upward relative to the lower end , resulting in higher k values. Spectra may have multiple k values if sampling within polluted air masses, inhomogeneously mixed air masses, or non-steady-state phenomena, and in this case it means that the k values were varying in time. More that one value of k parameter for the same air sample might also suggest that the measurements do not conform to equation (7.1) form although the measurements may be fitted to this form in small supersaturation intervals. It may be recalled that Twomey (1997) used equation (7.1) for mathematical convenience, and it

may not be a valid representation of the CCN activity spectrum during periods of non-steady-state phenomena.

The instantaneous temporal CCN concentration at 0.3 and 1.0% supersaturation ranged between 79 and 158 cm^{-3} and between 110 and ≈2300 cm^{-3} respectively, during the period of 11 January-7 February. The instantaneous CCN concentrations at 0.3 and ~1.1% supersaturation ranged between 0 and 200 cm^{-3} and between < 1 and 692 cm^{-3} respectively, during the period of 13-26 February. The lower CCN concentrations measured during the 13-26 February period occurred under foggy, precipitating and non-foggy period following widespread precipitation. CCN concentrations may be greater than 200 cm^{-3} at Palmer, if sampling takes place in the vicinity of virga, high wind speed, dissipating clouds under certain conditions, local pollution and dimethylsulfide phytoplankton bloom episodes. The instantaneous k values were generally below 1 during the period of 11 January-7 February, and they were generally between ~0 and ~3 during 13-26 February. Many of the spectra during the latter period had multiple k values (DeFelice, 1996). The wind speeds were most frequently between ~3 and ~23 m s^{-1} during the daily period represented in this study. Saxena (1996) observed CCN concentrations beyond those which could be traditionally accounted for when the cloudbase descended to surface and dissipated on 17, 19, 20 January and February 1994 under typical meteorological conditions for his sampling period. The aforementioned non-traditional amounts of CCN were termed CCN bursts by Saxena (1996). However, DeFelice (1996) provides an example of a cloudbase passage on 16 February without an equivalent increase in CCN, and discusses some of the possible reasons behind these observations.

Drizzle, rain and/or snow fell during ~50% of the days on the average between 11 January and 4 February 1994, and ~85% of the days on the average during 13-25 February 1994. The occurrence of the precipitation was most frequently between 2200 and 0700 h local time during 13-25 February. The 21 January daily period had light precipitation falling during its last ~4 h. Sampling associated with winds < 3 m s^{-1}, and obvious contamination from local anthropogenic pollution sources and the

aforementioned CCN bursts (Saxena, 1996) are not included below. Samples associated with wind speeds <3 m s^{-1} were excluded because of the increased likelihood of including local unnatural pollution. The result of the latter is a dataset (Table 7.1) that is representative of the natural environment of Palmer Station, Antarctica between 21 January and 4 February, arbitrarily termed the January period, and between 13 and 25 February, arbitrarily termed the February period. Saxena (1996) and DeFelice (1996) provide some additional details of their CCN spectral measurements.

7.3. Results

The 21 January -4 February 1994 period, or the January period, is characterized by: (i) relatively constant temporal CCN concentrations (Table 7.1); (ii) relatively constant equivalent potential temperatures. Theta E (Fig. 7.la). (iii) partly cloudy skies with respect to wind direction during the daytime (Fig. 7.lb), and (iv) winds predominantly from the east-southeast through the southwest (i.e. ~100 and ~240 true). The equivalent potential temperature is a good tracer of air masses since it is conserved during both dry and moist adiabatic processes.

The 13-25 February 1994 period or the February period, is characterized by: (i) relatively variable temporal CCN concentrations (Table 7.1); (ii) relatively variable Theta E (Fig. 7.la); (iii) variable cloudy to overcast skies with respect to wind direction during the daytime (Fig. 7.lb) and (iv) winds predominantly from the northeast, southwest and the northwest (i. e ~30 and 60, ~210 and 240, and ~315 and 345 true) with none between southeast and southwest.

7.4. Discussion and Summary

The data suggest that this site was generally under the influence of an air mass from the Antarctic Plateau during the January period based on the relatively constant wind directions, equivalent potential temperatures (Theta E: Fig. 7.la), CCN (Fig. 7.la) and the

CCN spectra (Table 7.1). According to Hogan et al. (1990) relatively cold air temperatures and nearly constant aerosol concentrations in the boundary layer are characteristic of air from the Antarctic Plateau. The mean surface air temperature was slightly cooler during January than during the February period (Fig. 7.1 b). In contrast, the site was under the influence of a transitionary weather period during the February period since the aerosol concentrations were highly variable and associated with different air-mass origins as indicated by k (Table 7.1) and Theta E (Fig. 7.la). Highly variable CCN concentrations would be measured as the result of sampling both sides of the meandering boundary, between warmer, aerosol-enhanced maritime polar air and colder, constant aerosol-laden air from the Antarctic Plateau, and are typically found February in this region (Hogan et al., 1990). Note to ignore the other possible sources of CCN variability as suggested in the background section.

For instance, it has been shown that ~80-90% of the aerosol mass in the Antarctic troposphere deposited to the ice sheet is composed of fine particle (< 1 μm diameter) non-sea -salt (NSS) sulfate (Shaw, 1988), and that atmospheric conversion processes involving the marine biogenic sulfur gas DMS are a major source of Antarctic NSS sulfate aerosols (Delmas, 1982). The CCN at Palmer Station generally have significant amounts of NSS sulfate. However, the recent study of Kawamura et al. (1996) indicates that there are water-soluble dicarboxylic acids in Antarctic aerosols. They found that oxalic (C_2) or succinic (C_4) was the dominant diacid species, followed by azelaic (C_9) and malomic (C_3) acids. The concentrations of oxalic , succinic and pyruvic acids in the summer Antarctic aerosols were 10.29, 61.53 and 0.78 ng m^{-3}, respectively (Kawamura et al.. 1996). They concluded that organic aerosols over the coast of Antarctica result from the sea-to-air emission of marine organics and subsequent photochemical transformation. Since the organic acids in aerosol particles may also be one of the primary sources of CCN in the atmosphere, the organic acids in Antarctic aerosols can also make a contribution to the formation of CCN in the Antarctic atmosphere.

In summary, a first time daily daylight averaged CCN spectral database covering January and February 1994 at Palmer Station, Antarctica is presented in response to the

recent research need for the area of aerosol/climate research. It is suggested that significantly different temporal characteristics in the daily daylight period averages of CCN concentrations could be attributed to differences in the naturally inherent meteorological conditions, once the data have been quality assured.

Acknowledgements. This work was supported by the UWM graduate school, and the Division of Polar Programs, National Science Foundation under OPP-9218538.

7.5. References

Bates, T. S., Clarke, A. D., Kaustin, V. N., Johnson, J. E. and Charlson, R. J. (1989). Oceanic dimethylsulfide and marine aerosols: difficulties associated with assessing their covariance. Global Biogeochemical Cycles 3, 299-304.

Charlson, R. J., Lovelock, J. E., Andrea, M. O. and Warren. S. G. (1987) Oceanic phytoplankton, atmospheric sulfur, cloud albedo and climate. Nature 326, 655-661.

DeFelice, T. P. (1996) Variations in cloud condensation nuclei at Palmer Station Antarctica during February 1994. Atmospheric Research 41, 229-248.

DeFelice, T. P. and Saxena, V. K. (1994) On the variation of cloud condensation nuclei in association with cloud systems at a mountain-top location. Atmospheric Research 31, 13-39.

Delmas, R. J. (1982) Antarctic sulfate budget. Nature 299, 677-678.

Hobbs, P. V. and Huebert, B. J., eds (1996) Atmospheric Aerosols. A new focus of the International Global Atmospheric Chemistry (IGAC) Project, 40 pp, +6 pp appendix. [Available from the International Global Atmospheric Chemistry (IGAC) project office, Building 24-409, MIT, Cambridge, Massachusetts, 02139-4307, U.S.A.]

Hogan, A. W. (1975) Antarctic aerosols. Journal of Applied Meteorology 14, 550-559.

Hogan, A. W., Egan, W. G., Samson, J. A., Barnard. S. C., Riley, D. M. and Murphy, B. B. (1990) Seasonal variation of some constituents of Antarctic tropospheric air. Geophysical Research Letters 17, 2365-2368.

Kawamura. K., Semere. R., Imai. Y., Fujii, Y. and Hayashi. M. (1996) Water soluble dicarboxylic acids and related compounds in Antarctic aerosols. Journal of Geophysical Research 101, 18721-18728.

Robinson, E., Bamesberger, W. L., Menzia. F A., Waylett. A. S. and Waylett, S. F. (1984) Atmospheric trace gases measurements at Palmer Station, Antarctica. Journal of Atmospheric Chemistry 2, 65-81.

Saxena, V. K. (1996) Bursts of cloud condensation nuclei (CCN) by dissipating clouds at Palmer Station, Antarctica . Geophysical Research Letters 23, 69-72.

Shaw, G. E. (1979) Considerations on the origin and properties of the Antarctic aerosols. Review of Geophysics 17, 1983-1988.

Shaw. G. E. (1983) Antarctic aerosols: A review. Review of Geophysics 26. 89-112.

Towmey, S. (1977) Atmospheric Aerosols. 302 pp. Elsevier, New York.

Twomey, S. and Wojciechowski, T. A. (1969) Observations of the geographical variation of cloud nuclei. Journal of Atmospheric Science 26, 684-688.

World Meteorological Organization, WMO, WMP (1992) Proceedings of the WMO workshop on cloud microphysics and applications to global change, 10-14 August 1992, 406 pp. Toronto, Canada. (World Meteorological Organization Programme on physics and chemistry of clouds and weather modification research. WMP report #19. WMO, 41 Giuseppe-Motta, Case postale No.2300,CH-1211 Geneve 2.)

Table 7.1. Daily average CCN spectral parameters during 2 Januaryuary-26 Februaryruary 1994 at Palmer Station, Antarctica

Date (1994)	Julian day	CCN(1%) (cm^{-3})	CCN(0.3%) (cm^{-3})	K
21-January	21	151	116	0.22
22-January	22	151	123	0.27
23-January	23	149	141	0.18
24-January	24	148	107	0.28
25-January	25	175	106	0.42
26-January	26	135	119	0.39
27-January	27	138	105	0.32
28-January	28	148	117	0.32
29-January	29	149	124	0.22
30-January	30	146	146	0
31-January	31	152	145	0.15
1-February	32	139	126	0.18
2-February	33	171	131	0.21
3-February	34	150	120	0.19
4-February	35	142	106	0.25
5-February	36	161	146	0.22
6-February	37	142	106	0.24
7-February	38	160	160	0
Average-January period		125	151	0.2
12-February	43	63	35	0.49
13-February	44	33	5	1.5
14-February	45	33	9	1.1
15-February	46	8	2	1.2
16-February	47	4	0.3	2.1
17-February	48	10	1	1.9
18-February	49	7	0.5	2.2
19-February	50	35	9	1.1
20-February	51	6	1	1.3
21-February	52	6	3	0.64
22-February	53	4	3	0.22
23-February	54	5	4	0.18
24-February	55	13	11	0.16
25-February	56	27	17	0.38
26 February	57	61	52	0.14
Average-February period		21	10	1.0

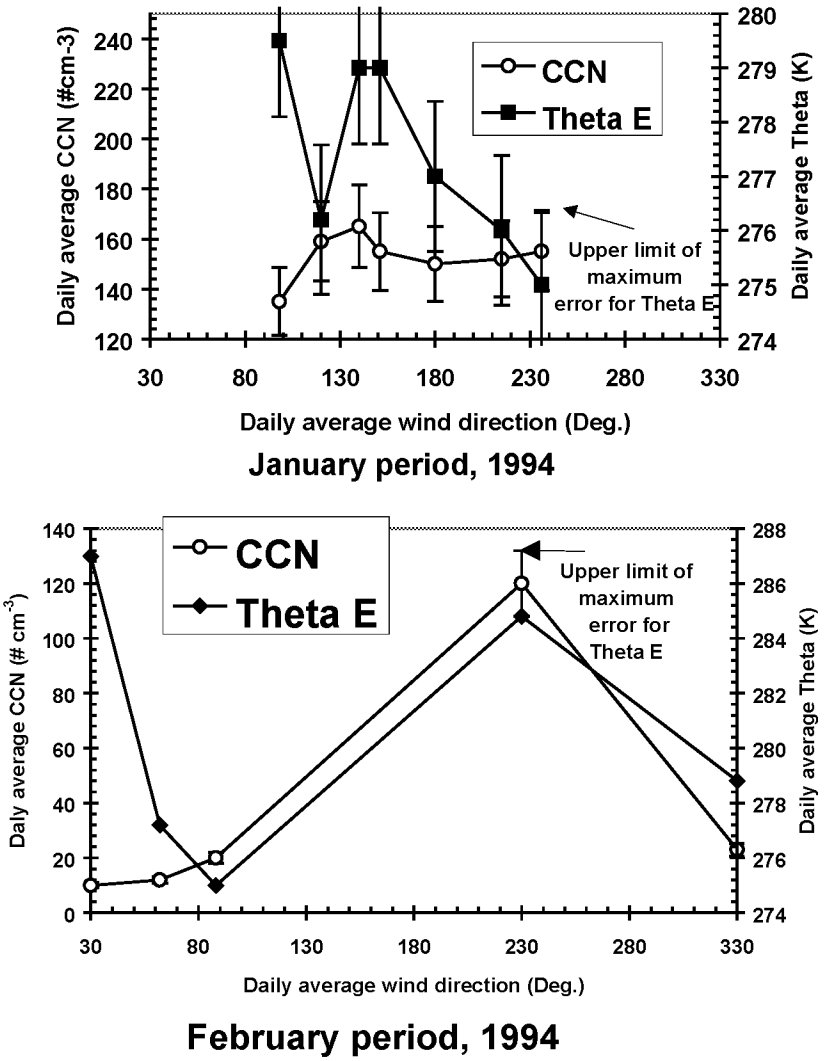

Figure 7.1.(a) The daily average CCN concentration at 1% supersaturation and equivalent potential temperature (Theta-E) as well as (b) cloud cover (tenths) and air temperature vs wind direction during 21 January-25 February 1994. The daily averages represent the time between ≈ 07:30 (± 00:30) and ≈ 22:00 (±00:30) LDT. The mean WD is ≈ 210 and ≈ 175^0 during the January and February periods, respectively.

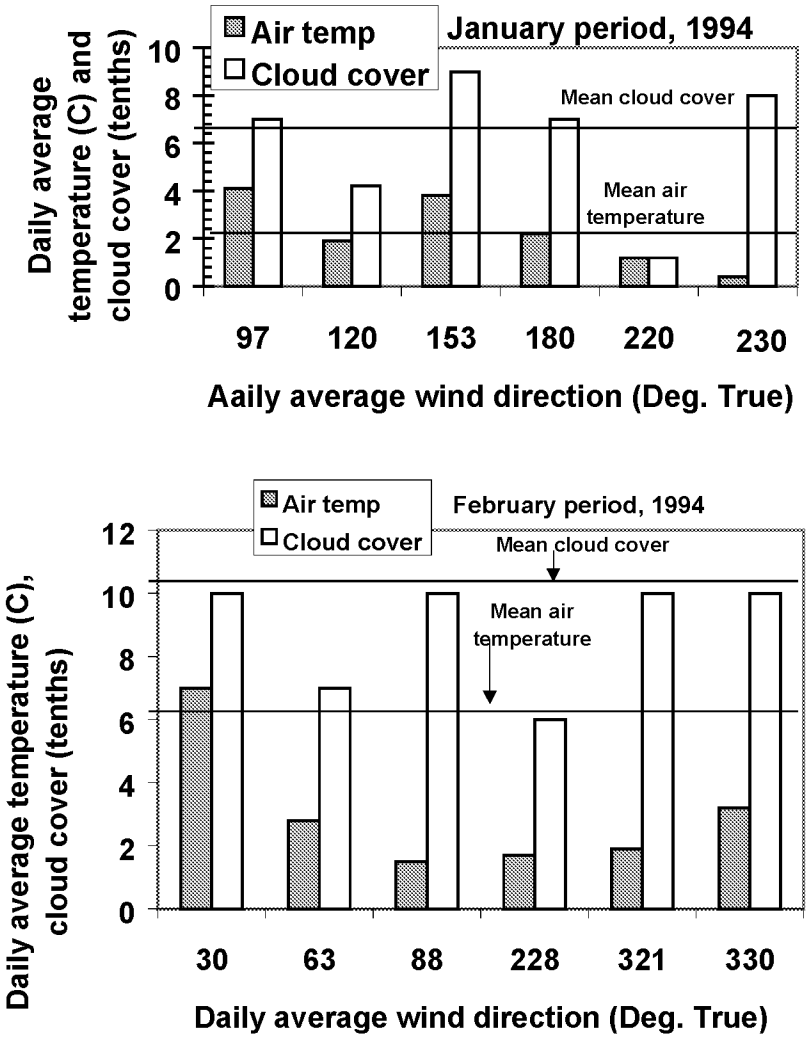

Figure 7.1b. (Continued)

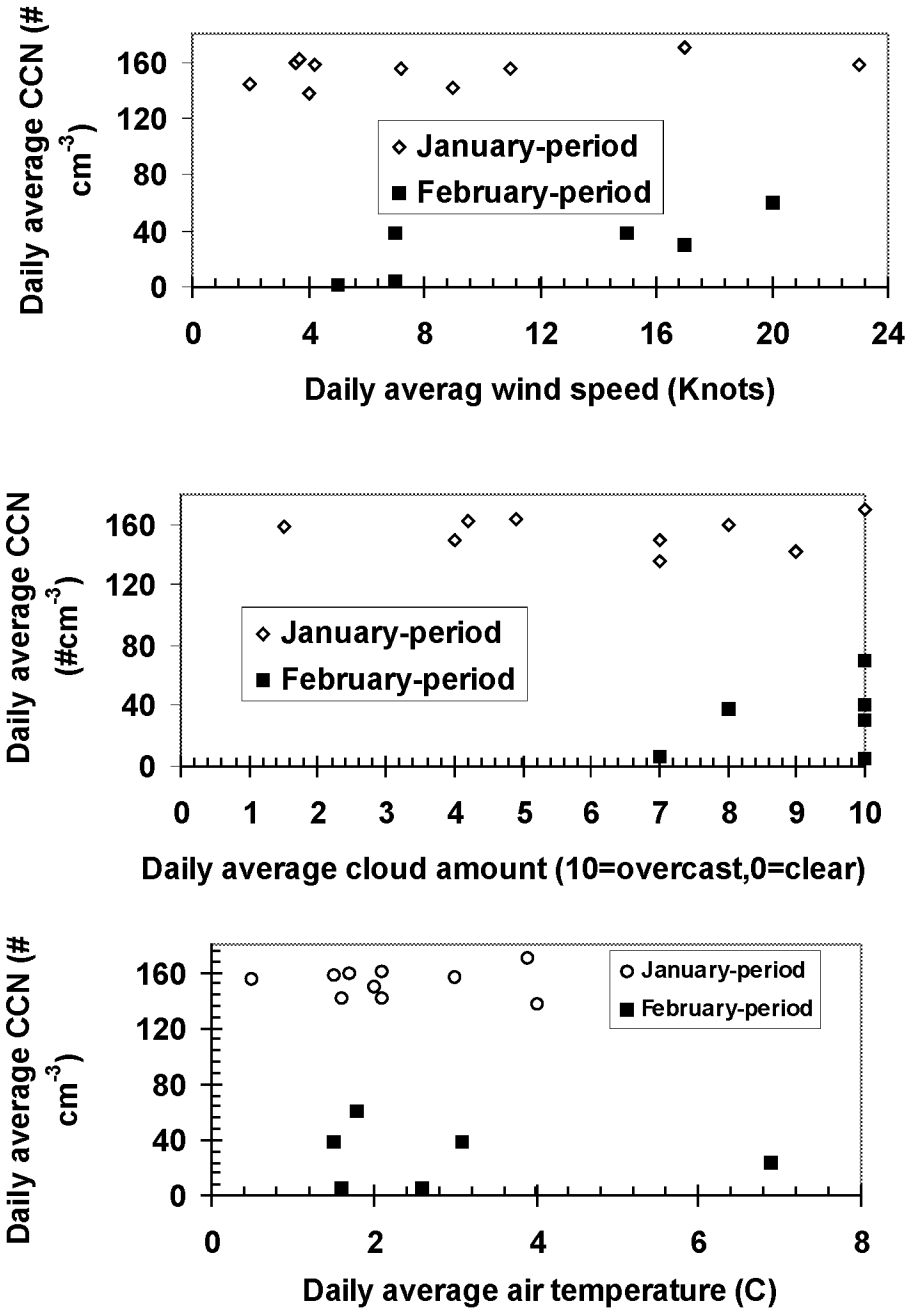

Figure 7.2. The relationships between the concurrent daily average CCN concentration at 1% supersaturation and air temperature, cloud amount and wind speed during the January and February periods.

8. ROLE OF ORGANIC ACIDS (FORMIC, ACETIC, PYRUVIC AND OXALIC) IN THE FORMATION OF CLOUD CONDENSATION NUCLEI (CCN)

Shaocai Yu

Department of Marine, Earth and Atmospheric Sciences
North Carolina State University
Raleigh, NC 27695-8208, USA

Submitted to Atmospheric Research, June 1999

8.1. Abstract

Although it is believed that organic aerosols play a key role in cloud nucleation and make an important contribution to cloud condensation nuclei (CCN) population, their specific species remain poorly characterized. This paper reviews the current knowledge of organic acids (mainly formic, acetic, pyruvic and oxalic acids. without specification, organic acids in this paper refer to these four organic acids in the gas and aerosol phases), analyzes the extent to which organic acids act as CCN, and compares the physical and chemical properties of organic acids with those of CCN. The results show that aerosol formate and acetate concentrations range from 0.02 to 5.3 nmol/m^3 and from 0.03 to 12.4 nmol/m^3 respectively, and that between 34 to 77% of formate and between 21 to 66% of acetate are present in the fine fraction of aerosols. It was found that although most (98-99%) of these volatile organic acids are present in the gas phase, their concentrations in the aerosol particles are sufficient to make themselves a good candidate for CCN. The results also show that organic acids may make an important contribution to the formation of CCN in some special sources such as vegetation emissions and biomass-burning. Organic acids are expected to contribute significantly to the estimates of indirect (cloud-mediated) forcing due to aerosols.

8.2. Introduction

Aerosol nucleation properties, i.e. the propensity of particles to form water droplets at atmospheric supersaturation levels, are determined by the particle size, chemical composition, and surface characteristics (Andreae et al., 1995; Mason, 1971; Twomey, 1977). The nucleation properties of water-soluble inorganic aerosols, such as sulfate and chloride, are well documented. However, until recently, the nucleation properties of organic aerosols have not received much attention. This is partly because chemical composition of particulate organic matter itself is poorly understood. In the continental United States, White (1990) reported that organic compounds typically accounted for 20-50% of total fine particle mass concentration. Cadle and Groblicki (1982) found that on average about 40% of total organic mass was water soluble for samples collected at Denver, Colorado. Among the organic compounds, identified in urban environments using gas chromatography/mass spectroscopy (GC/MS), are low-molecular weight aliphatic dicarboxylic acids, and high-molecular weight alkanes (Rogge et al., 1993). However, typically only about 10% of total organic mass was identified, and approximately 50% of organic mass either did not extract in organic solvents or did not elute in the GC column used, and the remaining 40% could not be resolved into specific molecular entities by GC/MS (Rogge et al., 1993). On the other hand, IC (Ion Chromatography) analysis shows that the most frequently observed organic species in the atmosphere are low molecular weight monocarboxylic and dicarboxylic acids, with monocarboxylic acids much more abundant than dicarboxylic acids. Of monocarboxylic acids, formic and acetic acids are the dominant species, which have most frequently been observed in precipitation (Keene and Galloway, 1988; Yu et al., 1991a, b, 1992, 1998), cloudwater and fogwater (Yu et al., 1991a, b; Weathers et al., 1986), gaseous phase (Dawson et al., 1980; Yu et al., 1990), and in aerosols (Andreae et al., 1988a,b).

The origin and nature of cloud condensation nuclei (CCN) recently have become one of the central issues in climate change because CCN strongly modulate cloud microstructure and hence the radiative properties of clouds (Charlson et al., 1987).

Observation of Desalmand et al. (1982) showed that vegetation could produce CCN. Novakov and Penner (1993) indicated that ~37 % of CCN number concentration measured at the marine site could be accounted for by sulfates and remaining 63 % by organic aerosols. Measurement of Hegg et al. (1995) also showed that most of CCN over the northeastern Atlantic coast of the United States were not sulfates. Saxena et al. (1995) found that organics could enhance water absorption by inorganics at the nonurburn location (Grand Canyon). It is in order here to ask: what are the chemical components of CCN produced by vegetation and the chemical components of organic aerosols that act as CCN and alter hygroscopic behavior of atmospheric particles? Presently this question can not be answered.

The purposes of this study are to review the current state of knowledge of water-soluble organic acids in the atmosphere, analyze the extent to which organic acids actually act as CCN, and identify the major unknowns in this field. We will focus principally on formic and acetic acids for two reasons. First, formic and acetic acids are found to be ubiquitous trace gases in the troposphere (Keene et al., 1995), and their concentrations are usually more than one order of magnitude higher than others (such as propionic, butyric, pyruvic, lactic acids) (Andreae et al., 1987; Keene and Galloway, 1988; Yu et al., 1991). Second, there are a lot of available experimental results regarding the occurrence, sources and sinks of formic and acetic acids in the gas, aerosol and liquid phases (precipitation, cloud and fog). The role of pyruvic and oxalic acids in the formation of organic CCN is analyzed as well.

8.3. Current state of water-soluble organic acids in the troposphere

The role of organic acids as chemical constituents in the troposphere has become an issue of growing interest in the past two decades. Excellent reviews and discussions of occurrence, sources and sinks of organic acids in the troposphere have been presented by Chebbi and Carlier (1996). Organic acids can be directly emitted by vegetation (Talbot et al., 1990; Keene and Galloway, 1988; Yu et al., 1988). Natural biomass-burning (Talbot

et al., 1988; Andreae et al., 1988b), atmospheric oxidation of biogenic isoprene (Jacob and Wofsy, 1988), olefins and hydrocarbons (Madronich and Calvert, 1990) are thought to be the secondary sources of organic acids in the atmosphere. Formic acid can be produced by oxidation of HCHO (Chameides and Davis, 1983) which is one of the oxidation products of DMS in the marine atmosphere.

Saxena and Hildemann (1996) constructed a list of candidate water-soluble organic compounds in atmospheric particles on the basis of the compilation of Graedel et al. (1986). Among organic compounds that are completely miscible with water are monocarboxylic acids and alcohols (complete miscibility up to C_4 or C_5); diols and triols (complete miscibility up to C_7); and keto-carboxylic acids (complete miscibility up to C_4) (Saxena and Hildemann, 1996). On the basis of theoretical analysis of air-water equilibrium, they concluded that C_1-C_6 monocarboxylic acids, alcohols, carbonyls and ethers were too volatile to be distributed in the fine particles, and would be completely partitioned into the gas phase. This result seems consistent with that of the model calculation of Meng et al. (1995). However, as pointed out by Saxena and Hildemann (1996), there are some discrepancies between their theoretical assessments and observations. They thought that this might be due to modification of air-water distribution of these compounds as a result of aqueous phase reactions and/or the presence of an organic film. Dicarboxylic acids, ketoacids and dicarbonyls, which were thought to be present in the aerosol phase (Saxena and Hildemann, 1996), constituted only a small fraction of the total particulate water-soluble organic compounds in the atmosphere. For example, Rogge et al. (1993) indicated that water-soluble dicarboxylic acids accounted for approximately 2 to 4% of total particulate organic mass.

Table 8.1 summarizes the published aerosol and gaseous carboxylic acids in different parts of the world. Organic acids have been measured over a wide range of environments, e.g., marine and continental air, free atmosphere and surface layer, urban as well as remote atmospheres. There is a general consensus that formic and acetic acids constitute the most abundant carboxylic acids in the troposphere (Keene et al., 1995). The concentrations of formic and acetic acids in the gas phase ranged from 0.8 to 531

nmol /m^3 and 1.2 to 653 nmol/m^3, respectively. Unlike the gas phase data, relatively few measurements of aerosol-phase carboxylic acids have been reported. Table 8.1 shows that the concentrations of formate and acetate in the aerosols were typically in 0.02-5.3 nmol/m^3 ($1.36x10^{-15}$-$3.60x10^{-13}$ g/cm^3, assuming sodium salts) and 0.03-12.4 nmol/m^3 ($2.46x10^{-15}$-$1.02x10^{-12}$ g/cm^3, assuming sodium salts) ranges, respectively. Table 8.1 also shows that between 34% to 77% (average 58%) of formate and between 21 to 66% (average 45%) of acetate were present in the fine fraction. On the basis of simultaneously available measurements of data on aerosol and gas phase shown in Table 8.1, only about 2% of total formic acid and about 1% of total acetic acid are present in the aerosol phase. It indicates that the phase-partitioning is as much a function of the aerosol substrate as it is of the gas equilibrium vapor pressure.

The results about pyruvic acid ($CH_3(C=O)COOH$), oxalic acid (HOOCCOOH), MSA ($CH_3S(O_2)OH$) and propanoic acids (CH_3CH_2COOH) in the gaseous and aerosol phases are listed in Table 8.1. The pyruvate and oxalate concentrations in the aerosols were in the ranges of 0.03-0.6 nmol/m^3 ($3.3x10^{-15}$-$6.6x10^{-14}$ g/cm^3, assuming sodium salts) and 0.17-1.8 nmol/m^3 ($2.28x10^{-14}$-$2.41x10^{-13}$ g/cm^3, assuming sodium salts), respectively. Smog chamber experiments showed that pyruvic acid was formed by photooxidation of o-cresol (Grosjean, 1984). Jacob and Wofsy (1988) reported that photochemical oxidation of isoprene, which was emitted directly in large quantities from trees and other plants (Lamb et al., 1985), was likely to be the predominant source of pyruvic acid in the atmosphere. Of dicarboxylic acids, oxalic acid (C_2) was found to be the most abundant diacid species in the gaseous and aerosol phases, followed by malonic acid (C_3) or succinic acid (C_4) (Sempere and Kawamura, 1994). Pyruvic and oxalic acids are mostly associated with aerosol particles due to their low vapor pressures. It is of interest to note that levels of organic acids are lower in the remote marine atmosphere than in the continental atmosphere or highly polluted urban areas. Organic acids are significantly enriched in the aerosol and gas phases derived from biomass burning plume.

8.4. The extent to which organic acids act as CCN

8.4.1. Aerosol organic salts as CCN

Theoretical consideration on water vapor condensation (Dufour and Defay, 1963) shows that there is a well-determined relationship between physical and chemical properties of the particles and their activities in the condensation processes. Larger and more hygroscopic particles have lower critical supersaturations than smaller and less water-soluble ones.

Table 8.2 lists the comparison of chemical-physical properties of common organic and inorganic salts. It is of interest to note that formate and acetate salts are more soluble than sulfate salts for the same cation, and may have more affinity for water than sulfate salts. The oxalate salts are less soluble than sulfate salts. The relationship between saturation ratio and particle size for droplets containing dissolved materials is given by the traditional Köhler theory (Twomey, 1977). Table 3 lists the calculation results of the critical radii (r_c) and supersaturations (S_c) for droplets containing different dissolved organic salts. Figure 8.1a shows the results of calculation for different masses of sodium formate. The similar pictures as Figure 8.1a can be drawn for all organic salts in Table 8.2. Table 8.3 shows that the critical supersaturations are in the range of 0.04% to 0.71% for formate and acetate salt mass range of 10^{-14} to 10^{-17} g, corresponding to the critical radius range of 0.11 μm to 1.91 μm. For pyruvate and oxalate salt mass range of 10^{-14} to 10^{-17} g, the critical supersaturations are in the range of 0.05% to 0.82%, corresponding to the critical radius range of 0.09 to 1.66 μm. Figure 8.1b shows the comparison of relationships between saturation ratio and droplet size for droplets containing different organic and inorganic salts with the same nuclear mass (10^{-16} g). Note that the differences among these curves are very small.

If an ambient supersaturation S_a is applied, only those organic nuclei with $S_c<S_a$

will surpass the equilibrium size r_c and thus become activated cloud droplets. To assess the contribution of organic salts to CCN concentration, we assume that the aerosol components are external mixtures and that one CCN particle contains only 10^{-16} g aerosol organic salts (assuming sodium salts). Although one might expect that some organic nuclei could contain more or less than 10^{-16} g mass, for the sake of comparison, this assumption was made. The critical supersaturations for droplets containing different organic salts with the mass of 10^{-16} g can be found in Table 8.3. We can calculate the concentrations of CCN in the atmosphere by using the aerosol organic data in Table 8.1. The calculation results are summarized in Table 8.4. Table 8.5 lists the results of CCN observations at 0.1% and 0.5% supersaturations carried out under the different conditions. A close inspection of Tables 3, 4, and 5 indicates that CCN sources from aerosol organic salts are comparable to the CCN concentrations observed in the different environments.

Unfortunately, most studies in Table 8.4 didn't have the simultaneously observed CCN concentrations at the locations selected. The exceptions are the studies of Liu et al. (1996) and Li and Winchester (1989). In the experiments made at Chebogue point, Nova Scatia, Liu et al. (1996) simultaneously measured major inorganic ions and organic ions (formate, acetate, oxalate, pyruvate, MSA, propionate, glyoxalate, glycoaldehyde and formaldehyde) in the aerosol particles and CCN concentrations at 0.06% and 0.4% supersaturations. They found that three most abundant species of the measured organics in their experiments were oxalate, MSA and acetate, but formate and other organics were low. Liu et al. (1996) reported that particulate CH_3COO^- and oxalate concentrations were <0.3-3.3 nmol/m^3 (<0.02-0.19 μg/m^3) and <0.3-4.6 nmol/m^3 (<0.03-0.36 μg/m^3) respectively. As can be seen from Table 8.3, the critical supersaturations for $4x10^{-16}$g CH_3COONa ($4.88x10^{-9}$ nmol) and $(COO)_2Na_2$ ($2.99x10^{-9}$nmol) were 0.22% and 0.23% respectively. Here, if we assume that one CCN particle contains only $4x10^{-16}$g aerosol organic salt, the CCN concentrations would be in the range of <62 to 676 cm^{-3} from acetate salts and in the range of <100 to 1538 cm^{-3} from oxalate salts. Total CCN concentration from organic salts would be <162-2214 cm^{-3}. The actual observed CCN concentration at 0.4% supersaturation was in the range of 267 to 2619 cm^{-3} (Liu et al.,

1996). Figure 8.2 shows the correlation coefficients between CCN concentrations at 0.4% and 0.06% supersaturations and oxalate, MSA, acetate in the aerosol particles (data obtained from Table 8.2 of Liu et al. (1996)). As can be seen, there are strong linear correlations between CCN concentrations at 0.4% and 0.06% supersaturations and oxalate concentration. Liu et al. (1996) found that total organics (formate, acetate, oxalate, pyruvate, MSA, propionate, glyoxalate, glycoaldehyde and formaldehyde) strongly correlated with CCN concentration at 0.4% but not at 0.06% supersaturation. This might be due to the fact that soluble organics were present in the smaller particles and that the large fraction of CCN at 0.4% was associated with smaller particles which contributed a small fraction of mass (Liu et al., 1996). Very high (i.e., 10^4 cm^{-3}) condensation nuclei (CN) concentrations have been reported from time to time in the Arctic. Schnell et al. (1988) reported that CN concentration at North of Barrow in the AGASP-II field experiment was as high as $1x10^4$ cm^{-3}. This values is close to the estimation of organic CCN ($1.4x10^4$ cm^{-3}) in Table 8.4 on the basis of organic salt data of Li and Winchester (1989), who measured organic salts at the same AGASP-II field experiment period.

In the early experiment of marine fog, Fukuta and Saxena (1975) reported finding an organic, ester-like material in the marine CCN that formed clouds in their chamber during a ship cruise over the Atlantic. In their infrared spectrum of CCN samples, there was an absorption peak appearing around the frequency of ~1600 cm^{-1}. They thought it was indicative of an organic ester-like material that was water soluble. Formate and acetate have been frequently observed in cloudwater and fog water (Weathers et al., 1986; Yu et al., 1991a), and have infrared absorption bands around the frequencies of ~1580 cm^{-1} and ~1413 cm^{-1} respectively (Marley et al., 1993). So it is reasonable to infer that formate was the organic material of CCN that Fukuta and Saxena (1975) reported in their experiment. Organic esters are often less soluble. It is currently assumed that organic esters are non-CCN related contaminants (Williams et al., 1994). This result directly indicates that formate is a component of CCN.

It is of interest to note the recent study of Matsumota et al. (1997) about contribution

of particulate sulfates and organic carbon to CCN in the marine atmosphere. They found that not only sulfates but also water soluble organic salts (formate, acetate, oxalate and MSA) were dominant in fine aerosols. There was a significant correlation between total water soluble organic salt (formate, acetate, oxalate and MSA) concentrations and CCN concentrations at 1% and 0.5% supersaturations (Matsumota et al., 1997). Their results also showed that the soluble organic salts (formate, acetate, oxalate and MSA) were relatively more predominant than nss-sulfate and made a significant contribution to CCN number concentration under the lower sulfate conditions. Cruz and Pandis (1997) reported that pure glutaric acid and adipic acid aerosols did act as CCN and their behaviors were analogous to those of inorganic salts, as observed in the shape of the activation curves. They also reported that no CCN activity was observed for water-insoluble dyoctylphthalate (DOP) for dry particle diameters as large as 0.15 μm at the supersaturation as high as 1.2%. Since glutaric and adipic acids can be formed from the oxidation of unsaturated cyclic olefins as suggested by smog chamber experiments (Grosjean, 1977), the results of Cruz and Pandis (1997) confirm some sources of CCN from the photochemical oxidation of organic compounds.

8.4.2. Organic acids in the gas phase to form particles

As shown in Table 8.1, most volatile organic acids are present in the gas phase in the atmosphere, and on average about 56±14% of organic salts are present in the size fraction below 1.0 μm diameter. It has been found that aerosol particles in the size range from 0.01 to 1.0 μm diameter grow principally by gas-to-particle conversion, the process by which vapor molecules diffuse to the surface of a particle and subsequently get incorporated into the particle (Seinfeld and Bassett, 1982). This suggests that organic salts are at least partly of secondary origin. Organic acids like formic and acetic acids have strong solubility and surface activity, and can be incorporated into the aerosol particles by adsorption to the particle surfaces (Andreae et al., 1988a). Both alkaline

mineral particles and organic materials must be expected to have a relatively high affinity for volatile organic acids, especially if their surfaces are wetted by water films. Organic acids are not expected to be driven out of the aerosol phase by strong involatile acids such as sulfuric acid, which is present in aerosols in polluted areas (Andreae et al., 1988a). This pointview was supported by the results of Andreae et al. (1987) that indicated no significant difference in the gas/aerosol partitioning of organic acids between the Amazon areas and polluted regions.

An critical problem here is whether alkaline mineral particles such as Na_2CO_3 or organic materials such as elemental carbon (EC) are necessary for organic acid vapors to form organic particles. To answer this, first, we try to find if alkaline mineral particles or organic materials are available in the atmosphere. It is found that carbonaceous aerosol particles are ubiquitous in the atmosphere (Cadle and Groblicki, 1982). A large number of carbon size-distribution measurements performed at several rural and urban locations in the US revealed that about 80% of EC and about 70% of OC were present in particles with diameter < 2-2.5 μm, and that average diameters for the fine fraction were 0.28 and 0.32 μm for EC and OC respectively (Wolff et al., 1982). Due to their ubiquitous presence, small dimensions, large specific surface and adsorbing properties, EC particles provide sites where organic acids are adsorbed. It is apparent that organic acids in the gas phase can form organic particles with the aid of alkaline mineral particles or organic materials because these materials are ubiquitous in the atmosphere.

It is important to study whether organic acid vapors can form new droplets or particles by interaction between two vapor species without the aid of a foreign nucleus or surface, e. g. by homogeneous nucleation mechanism under special atmospheric conditions. The conditions favorable for homogeneous-bimolecular nucleation from H_2SO_4 and H_2O vapors are extremely small total surface area of the ambient aerosols, high concentrations of H_2SO_4 and H_2O vapors, and low temperature (Kiang et al., 1973; Hegg et al., 1990). The laboratory experiments regarding the homogeneous nucleation of formic, acetic and propanoic acids were reported by Russell and Heist (1978) and Heist et al. (1976). Russell and Heist (1978) found that the critical supersaturation of unary system for the

homogeneous nucleation of formic acid was in the range of 4 to 6 for temperatures ranging from -13 C to 32 C. Heist et al (1976) reported that the critical supersaturation of unary system for the homogeneous nucleation of acetic acid was in the range of 2.5 to 5.2 for temperatures ranging from -13 C to 67 C. In the binary nucleation and condensation experiment of the water-acetic acid system, Studzinski et al. (1986) observed the onset of nucleation/condensation for this water-acetic acid system over a range of activities for acetic acid of 0 to 7 and for water of 0 to 6 for a condensation temperature range of –3 C to 17 C. The nucleation rate of $1x10^{16}$ drops/cm^3s was measured for the acetic acid-water system (Studzinski et al., 1986). Their results showed that the presence of the relatively stable association clusters of organic acid vapor tended to stabilize the vapor with regard to the homogeneous nucleation.

Although classic nucleation theory gives the best explanation of organic acid nucleation experiments performed under controlled laboratory conditions (Heist et al., 1976; Studzinski et al., 1986), it may be much different for atmospheric conditions. It is clear that homogeneous nucleation/condensation of organic acid vapors can occur under some special atmospheric conditions. In the experiments on late winter Arctic aerosols, Li and Winchester (1989) found evidence that high aerosol formate and acetate concentrations were due to condensation of organic acid vapors and the cocondensation of organic acid vapors with NH_3 at the low Arctic temperature. They concluded that even at ppt levels for these gases, the equilibrium could produce organic salt particles. Although Li and Winchester (1989) did not mention the homogeneous nucleation of formic and acetic acids, it does not rule out the possibility that this process occurred in the late winter Arctic atmosphere because organic acid concentrations were high and the temperature was very low (-25 C).

By using "Köhler surface" on the basis of two Kelvin equations in the Köhler theory, Kulmala et al (1993) studied the effect of acid vapor (HNO_3) on CCN activity. They found that the presence of acid vapor depressed the effective vapor pressure of water over the growing solution droplets. As a result, a higher fraction of aerosol particles can serve as CCN than in an acid-free atmosphere. Laaksonen et al. (1998) has

modified the traditional Köhler theory by adding a term to Raoult effect to include the effect of soluble gases and slightly soluble aerosol substances. However, there are some technical limitations in this modification. Recently, Kerminen et al. (1997) have studied the role of NH_3, H_2SO_4, HNO_3 and HCl in the condensational growth of freshly nucleated particles in the lower troposphere. Kerminen et al. (1997) found that the growth of these freshly nucleated particles was dictated initially by the flux of sulfuric acid into the particles and whether or not the HNO_3/HCl-driven condensation occurred depended on the partial pressure product of NH_3 and HNO_3/HCl, ambient temperature and relative humidity. They suggested that the condensable volatile vapors had preferentially condensed on the pre-existing particles instead of causing particle formation. This seems consistent with the field experimental results of Marti et al. (1997), who studied the relative contributions of SO_2 and organic precursors to the formation of ultrafine particles at a remote continental site (Idabo Hill, Colorado). Marti et al. (1997) foun d that, in general, sulfates probably dominated the observed new ultrafine particle formation, while organic compounds formed in the gas phase reactions appeared to be predominantly involved with particle growth by condensation upon the pre-existing aerosols. Even if organic acid vapors are incorporated into the particles by condensation upon the pre-existing particles or by causing new particle formation, organic acids will affect the activity of aerosol particles.

8.4.3. Other sources of CCN in the atmosphere

Any atmospheric process and compound that participate in the formation of soluble compounds will affect the sources of CCN in the atmosphere. The soil particles and dust that enter the atmosphere probably serve as CCN, but they do not appear to be a dominant source (Pruppacher and Klett, 1978). The sea-salt particles cannot be the main CCN (Hobbs, 1971; Pruppacher and Klett, 1978). There is no doubt that sulfates such as $(NH_4)_2SO_4$ can serve as active CCN. DMS emitted by marine phytoplankton can be oxidized in the atmosphere to produce sulfates (Fitzgerald, 1991) and is proposed to be

the major source of CCN over the oceans, but there are also many significant gaps in DMS-CCN-Climate hypothesis (Charlson et al., 1987).

Other low molecular organic acids such as C_4-C_6 dicarboxylic acids and C_3-C_{10} carboxylic acids, aromatic polycarboxylic acids and diterpenoid acids have been determined in the atmosphere (Talbot et al., 1990; Rogge et al., 1993). Smog chamber experiments have shown that a number of dicarboxylic acids are formed from the oxidation of unsaturated cyclic olefins (Grosjean, 1977). These acids include succinic, glutaric and adipic acids. The model calculation of Shulman et al. (1996) indicated that dicarboxylic acids (C2-C6), phthalic acid and cis-pionic acid can affect cloud droplet growth by two mechnisms: by gradual dissolution in the growing droplet which affects the shape of Köhler growth curve, and by lowing of surface tension which decreases the critical supersaturation. However, the concentrations of these organic acids in the atmosphere are often too low to be effective CCN and their solubility will decrease with the increase of their molecular weights. If the concentrations of these organic acids are high in the atmosphere such as in the urban polluted air, they can also affect the formation of CCN in the atmosphere. Organic compounds, such as terpenes, alpha- and beta pinene that can be emitted by vegetation and are precursors of organic acids in the atmosphere, are not soluble and have no affinity for water. It can be expected that they could not act as CCN by themselves and could not enhance nucleation.

8.5. Some specific sources of CCN in the atmosphere and their possible explanations from organic acids

8.5.1. Natural emissions of CCN

According to the analysis of the averaged weekly CCN concentrations, Desalmond et al. (1982) reported that vegetation could produce CCN, and smaller CCN originating from vegetation were released every day into the atmosphere after sunrise in the Ivory Coast of West Africa. In the DEAFE 88 experiment in the African equatorial rainforest,

Helas et al. (1992) showed that concentrations of organic acids at the surface had a distinct diurnal behavior and rose after sunrise. They thought that this diurnal variation was due to the release of organic acids from vegetation. The experiments of Talbot et al. (1990) and Yu et al. (1988) showed that vegetation could directly emit organic acids. Lacaux et al. (1992) indicated that 22% of total anion concentration was organic acids in precipitation from the coastal forest of equatorial Congo in the DEAFE 88 experiment. To some extent, it is reasonable to infer that CCN originating from vegetation might be primarily composed of organic acids in the coastal forest of West Africa.

In the another experiment of Desalmand et al. (1985), they found evidence that continental savanna soil could produce CCN at Lamto savanna in West Africa, a rural site located far away from industrial sources. Sanhueza and Andreae (1991) observed that tropical savanna soil could directly emit organic acids and that savanna soil was a significant source of organic acids to the tropical savanna atmosphere. The diurnal behavior of CCN in the tropical savanna atmosphere (Desalmand et al., 1985) is close to that of organic acids (Sanhueza and Andreae, 1991). Note that inorganic condensable vapors such as H_2SO_4 could also be produced by the atmospheric photochemical oxidation of precursors such as H_2S and CS_2 (Penkett, 1994), which can be emitted directly by vegetation. So, the diurnal behavior of CCN could be due to the production of either organic or inorganic condensable vapors from the photochemical reactions in the atmosphere.

8.5.2. Biomass burning

Biomass burning can produce formic and acetic acids (Talbot et al., 1988). In the ABLE 2A experiment, Andreae et al. (1988b) found that organic ions were significantly enriched in aerosols derived from biomass burning and that organic anions contributed 9-25% of the anion sums in the plume aerosols. The aerosol formate, acetate, and pyruvate concentrations in the biomass-burning plume over the Amazonia were 2.8 ± 1.4, 2.0 ± 0.6, and 0.4 ± 0.1 nmol/m^3 respectively as shown in Table 8.1.

Unfortunately, Andreae et al. (1988b) did not measure organic acids in the gas phase in the biomass-burning plume. In the DECAFE 88 experiment, Helas et al (1992) showed that the average gaseous formic and acetic acids in the plume consisting of the aged air masses from the biomass burning were 151 and 110 nmol/m^3 respectively. Considering the results of the ABLE 2A and DECAFE 88 experiments, it appears that major part of organic acids in the biomass-burning plume still existed in the gas phase although aerosol organic salts were very high in the biomass-burning plume. It should be emphasized that the absolute concentrations of organic acids in the biomass-burning plumes of DECAFE 88 and ABLE 2A might be very different because these two experiments were conducted at different place and time. Under the assumption that one CCN particle contains only 10^{-16} g organic salts, the concentration of CCN in biomass-burning plume would be in the 11.0 X 10^4 to 30.0 X 10^4 /cm^3 range. Andreae et al. (1992) showed that the concentrations of CN in plume consisting of aged air masses from biomass burning in the DECAFE 88 experiment was in the 1500 to 3200 /cm^3 range. It seems that the source from organic acids can explain these unusually high CN levels in the biomass-burning plume. Many investigations also observed a significant local increase in the concentration of CCN as a result of the burning of sugar cane leaves in Hawaii and Australia (Warner and Twomey, 1968) and a similar CCN increase as a result of forest fires (Hobbs and Radke, 1969) . Hudson et al. (1991) found similar results from forest fires in that most of the particles were classified as CCN. Novakov and Corrigan (1996) indicated that the water-soluble carbonaceous fraction of smoke particles produced by smoldering combustion of eucalyptus and redwood biomass fuels was principally associated with the most volatile organic components. Novakov and Corrigan (1996) concluded that the water-soluble organic species in the smoke particles from smoldering biomass combustion were responsible for their intrinsic CCN activity.

8.5.3. Polar atmosphere

In the AGASP-II field experiment made in the Alaska sector (Barrow) of the Arctic Basin from 16 March to 6 May 1986, Schnell et al. (1988) reported the unexplained high concentration (10^4 cm^{-3}) of CN. Their results also showed that the majority of CN were acid and probably formed by coagulation of smaller acidic nuclei. Measurements made over the Arctic Ocean in June by Saxena and Rathore (1984) showed CCN concentrations on the order of 1000 cm^{-3} at 1% supersaturation. They thought the high levels of CCN (and CN) were likely due to long-range transport of pollutants into the Arctic Basin. Shaw (1989) tried to explain this result with production of CN by homogeneous nucleation of H_2SO_4, but there was still an open question about his explanation.

During the same AGASP-II field experimental period, Li and Winchester (1989) reported very high concentrations of organic acids in the Arctic aerosols. The formate, acetate, propionate and pyruvate altogether contributed 20% to the mean mass concentration in the fine fraction and 21% in the coarse fraction. These proportions were comparable to those of nss-SO_4^{2-}, 14% and 26%, respectively (Li and Winchester, 1989). Their aerosol formate and acetate concentrations were the highest ever reported. Note that organic anions contributed more to the mass concentration of the fine particles than nss-SO_4^{2-}. Their analysis showed that organic acids most probably originated at lower latitude and were transported to the Arctic. They thought that organic acid vapors from lower latitudes might partition and form particles by their condensation and cocondensation with NH_3 at the low Arctic temperature, causing most organic acid vapors to be present in the aerosol particles. The small organic acids might coagulate together to form the larger organic acid particles during their transport poleward in the winter season. As analyzed before, the concentration of CCN from organic acids is close to the high concentration (10^4 cm^{-3}) of CN reported in the AGASP-II field experiments. The concurrent measurements of sulfate mass and CCN concentration by Hegg et al. (1995a)

also showed that most of CCN activating at supersaturation present in the Arctic stratus clouds (i.e., less than approximately 1%) were commonly not sulfates, and likely to be organics. This indirectly suggeststhat organic acids might be the major components of CCN in the Arctic in that period although Hegg et al. (1995a) did not mention the specific species of organics.

In the Arctic Boundary Layer Experiment (ABLE 3A) in July-August 1988, Talbot et al. (1992) reported that the North American Arctic and sub-Arctic summer troposphere was an acidic environment with HCOOH and CH_3COOH, and that organic acids were principal components of precipitation over sub-Arctic tundra in the summertime. They also observed the highest gas concentrations of organic acids over the sub-Arctic tundra and boreal forest during the study period. The fact that the principal components of sub-Arctic precipitation were organic acids also implies that organic acids could make a significant contribution to the formation of CCN in the Arctic atmosphere.

In contrast to the Arctic, the Antarctic region has the lowest aerosol concentration compared with any other maritime region on the Earth (Hogan, 1975). Saxena and Ruggiero (1990) reported that the average CCN concentrations on November 3, 1980 were in the range of 9 to 53 cm^{-3}. The recent measurement of DeFelice et al. (1997) at Palmer Station of Antarctica shows that the daily average CCN concentrations at 0.3% and 1% supersaturations ranged from 0.3 to 160 cm^{-3} and from 4 to 168 cm^{-3}, respectively, during the period of 17 January to 26 February, 1994. Little data have been reported on organic acids in the Antarctic atmosphere. The measurement of water soluble dicarboxylic acids in the Antarctic aerosols (Kawamura et al., 1996) showed that oxalic (C_2) or succinic (C_4) acid was the dominant diacid species, followed by azelaic (C_9) and malomic (C_3) acids. The concentrations of oxalic, succinic and pyruvic acids in the summer Antarctic aerosols were 10.29, 61.53 and 0.78 ng/m^3, respectively (Kawamura et al., 1996). They thought that organic aerosols over the coast of Antarctica were due to the sea-to-air emission of marine organic matter and subsequent photochemical transformation. The sources of organic acids in the Arctic and Antarctica aerosols are different. This is consistent with the result of Legrand and De Angelis (1995), who

showed that the concentrations of organic acids in Antarctic ice cores were much lower than those observed during the same time period in Greenland and that organic acids in the Antarctic might mainly be due to marine sources. The high concentration of oxalate in the Antarctic aerosols is also consistent with those in the marine aerosols determined by Matsumota et al. (1997) and Liu et al. (1996). It can be expected that the concentrations of organic acids in the Antarctic atmosphere would be lower than that in Arctic atmosphere, and that the contribution of organic acids to the formation of CCN would be also small in the Antarctic atmosphere.

8.6. Conclusions

In so far organic acids or salts have the same activity as inorganic acids or salts, they will have the same impact on CCN activity and can be intrinsically effective CCN. However, direct experiments to prove this are not yet available. Organic acids in the gas phase can partition into aerosol particles with the aid of foreign nuclei such as alkaline mineral particles and elemental carbon, and by condensation and cocondensation with NH_3. The surprisingly high concentrations of CCN in the forested areas, savannah soil air, biomass-burning plume and the Arctic atmosphere at least partly were due to the sources of organic acids. It is hypothesized that these organic acids are at least one of the primary sources of CCN in the atmosphere, especially over the continental forested areas, due to their ubiquitous presence in the troposphere. The contributions of other high molecular organic acids are small due to their relatively low concentrations. Since the overall CCN-sulfate mass relationship could be quite variable (Hegg, 1994; Hegg et al., 1995a,b), the CCN-organic acid mass relationship would also be quite variable. Novakov et al. (1997) report that organic aerosol mass concentrations measured at Cape San Jun, a coastal site located on the extreme northeastern tip of Puerto Rico, significantly exceed sulfate concentration and that organic aerosol matter is water soluble and dominated by naturally occurring compounds such as fatty and carboxylic acids. If these natural organic species significantly contribute to the oceanic CN and CCN number concentrations, as

suggested by their results, they can make a significant contribution to the indirect forcing from anthropogenic sulfate aerosols in the marine environment. Listed below are a few of the areas in which future research is needed to advance our understanding.

(1) There is a need for accurate laboratory and field experiments to prove that pure organic acids and their salts can be intrinsically CCN active in atmospheric conditions. These organic acids studied must have atmospheric importance. Photochemical reaction experiments in a smoke chamber are needed to study the role of photochemical reactions of natural organic compounds such as terpene in the formation of CCN in the atmosphere.

(2) Homogeneous and heterogeneous nucleation/condensation model study is needed for multiple gas systems such as an $HCOOH$-CH_3COOH-NH_3-H_2SO_4-HNO_3-HCl-H_2O system. The prediction of particle nucleation rate and the role of each gas in the growth of freshly nucleated particles in the troposphere or in special atmospheric conditions such as under the Arctic conditions is essential if one is to quantify the relative contribution of each specie to CCN concentration. This relative contribution is critical in the estimates of indirect aerosol forcing.

(3) The important role of organic acids in the formation of CCN from special sources in the atmosphere needs to be better confirmed. If organic acids can make a major contribution to the formation of CCN in biomass-burning plume, organic acids can significantly affect the indirect forcing by biomass-burning aerosols.

(4) Determination of relative contributions of sulfates, organic acids and other non-sulfate aerosols to the formation of CCN at the representative locations such as the marine and remote continental sites is needed. At a minimum, the relations between the mass of each specie and number size distribution, especially in CCN size range (diameter<0.1 μm), must be established.

Acknowledgments. This study was supported through the Southeast Regional Center of the National Institute for Global Environmental Change by the U.S. Department of Energy under cooperative agreement No. DE-FC03-90ER61010. The authors (Shaocai

Yu) wishes to thank the friendly help from S. Menon, J. S. Schafer and B. N. Wenny of NCSU. We are also indebted to Dr. Austin W. Hogan for his insightful discussion and encouragement.

8.7. References

Alofs, D.J., and Lin, T.H., 1981. Atmospheric measurements of CCN in the supersaturation range 0.013-0.681. J. Atmos. Sci., 38, 2772-2778.

Andreae, M.O., Talbot, R.W. and Li, S.-M., 1987. Atmospheric measurements of pyruvic and formic acids. J. Geophys. Res., 92, 6635-6641.

Andreae, M.O., Talbot, R.W., Andreae, T.W. and Harriss, R.C., 1988a. Formic and acetic acids over the central Amazon region, Brazil. 1. Dry season. J. Geophys. Res., 93, 1616-1624.

Andreae, M.O. et al., 1988b. Biomass-emissions and associated haze layer over Amazonia. J. Geophys. Res., 93, 1509-1527.

Andreae, M.O., Chapuis, A., Cros, B., Fontan, J., Helas, G., Justice, C., Kaufman, Y.J., Minga, A. and Nganga, D., 1992. Ozone and aitken nuclei over Equatorial Africa: airborne observations during DECAFE 88. J. Geophys. Res., 97, 6137-6148.

Andreae, M.O., Cofer, W.R., Crutzen, P.J., Hobbs, P.V., Hollander, J.M., Kuhlbusch, T., Novakov, T. and Penner, J.E., 1995. Climate impacts of carbonaceous and other non-sulfate aerosols: a proposed study. Lawrence Berkeley Laboratory Document - PUB-5411.

Arlander, D.W., Crann, D.R., Farmer, J.C., Menzia, F.A. and Westberg, H.H., 1990. Gaseous oxygenated hydrocarbons in the remote marine troposphere. J. Geophys. Res., 95, 16391-16403.

Cadle, S.H. and Groblicki, P.J., 1982. An evaluation of methods for the determination of organic and elemental carbon in particulate samples, in Particulate Carbon-

Atmospheric Life Cycle, edited by G. T. Wolff and R. L. Klimisch, pp. 89-109, Plenum, New York.

Chameides, W.L. and Davis, D.D., 1983. Aqueous-phase sources of formic acids in clouds. Nature, 304, 427-429.

Charlson, R.J., Lovelock, J.E., Andrea, M.O. and Warren, S.G., 1987. Oceanic phytoplankton, atmospheric sulfur, cloud albedo and climate. Nature. 326, 655-661.

Chebbi, A. and Carlier, P., 1996. Carboxylic acids in the troposphere, occurrence, sources, and sinks: A review. Atmos. Environ., 24, 4233-4249.

Cruz, C.N. and Pandis, S.N., 1997. A study of the ability of pure secondary organic aerosol to act as cloud condensation nuclei. Atmos. Environ., 31, 2205-2214.

Dawson, G. A., Farmer, J. C. and Moyers, J. L., 1980. Formic and acetic acids in the atmosphere of the southwest U.S.A. Geophys. Res. Lett., 7, 725-728.

Dawson, G.A. and Farmer, J.C., 1988. Soluble atmospheric trace gases in the southeastern United States, 2. Organic species HCHO, HCOOH, CH_3COOH. J. Geophys. Res., 93, 5200-5206.

DeFelice, T.P., Saxena, V.K., and Yu, Shaocai., 1997. On the measurement of cloud condensation nuclei at Palmer Station, Antarctica. Atmos. Environ., 31, 4039-4044.

Desalmand, F., Baudet, J and Serpolay, R., 1982. Influence of rainfall on the seasonal variations of cloud condensation nucleus concentrations in a sub-equatorial climate. J. Atmos. Sci., 39, 2076-2082.

Desalmand, F., Serpolay and Podzimek, J., 1985. Some specific features of the aerosol particle concentrations during the dry season and during a bushfire event in West Africa. Atmos. Environ., 19, 1535-1543.

Dinger, J.E., Howell, H.B. and Wojciechowski, T.A., 1970. On the source and composition of cloud nuclei in a subsident air mass over the North Atlantic. J. Atmos. Sci., 27, 791-797.

Dufour, L., and Defay, R., 1963. Thermodynamics of clouds. Academic Press, New York and London.

Farmer, J.C. and Dawson, G.A., 1982. Condensation sampling of soluble atmospheric

gases. J. Geophys. Res., 87, 8931-8942.

Fukuta, N. and Saxena, V.K., 1975. Field measurements of a cloud condensation nucleus spectrometer in marine fogs. Marine Fog Cruise, USNS Hayes pp. 398-409, Naval Research Lab, Naval Air Systems Command, Office of Naval Research Washington.

Garcia, J.A., Perez, P.J., Fernandez, F.F., Gaya, M., De Grado, J.R. and Serpolay, R., 1981. Analyse statistique des resultats d'une campagne de measures de noyaux de condensation nuageuse. J. Rech. Atmos., 15, 143-148.

Graedel, T.E., Hawkins, D.T. and Claxton, L.D., 1986. Atmospheric Chemical Compounds-Sources, Occurrence, and Bioassay. Academic Press, Orlando, FL.

Gras, J.L., 1990. Cloud condensation nuclei over the Southern Ocean. Geophys. Res. Lett., 17, 1565-1567.

Gregory, G.L., Harriss, R.C., Talbot, R.W., Rasmussen, R.A., Garstang, M., Andreae, M.O., Hinton, R.R., Browell, E.V., Beck, S.M., Khalil, M.A.K., Ferek, R.J. and Harris, S.V., 1986. Air chemistry over the tropical forest of Guyana. J. Geophys. Res., 91, 8063-8612.

Grosjean, D., 1977. Aerosols. In ozone and other photochemical oxidants. National Academy of Science- National Research Council, Committee on Medical and biological effects of environmental pollutants, Washington, D. C., pp 45-125.

Grosjean, D., 1984. Atmospheric reactions of orthol cresol: Gas phase and aerosol products. Atmos. Emviron., 18, 1641-1652.

Grosjean, D., 1989. Organic acids in southern California air: Ambient concentrations, mobile source emissions, and in situ formation and removal processes. Environ. Sci. Technol., 27, 830-840.

Hallett, J., Hudson, J.G. and Rogers, C.F., 1989. Characterization of combustion aerosols for haze and cloud formation. Aerosol Sci. Technol., 10, 70-83.

Hartmann, W.R., 1990. Carboxylic acids in the atmosphere. Ph. D. thesis, Johannes Gutenberg Universitat, Mainz (German).

Hartmann, W.R., Andreae, M.O. and Helas, G., 1989. Measurements of organic acids

over central Germany. Atmos. Environ., 23, 1531-1533.

Hegg, D.H., Radke, L.F. and Hobbs, P.V., 1990. Particle production associated with marine cloud. J. Geophys. Res., 95, 917-926.

Hegg, D.H., Radke, L.F. and Hobbs, P.V., 1991. Measurements of Aitken nuclei and cloud condensation nuclei in the marine atmosphere and their relation to the DMS-cloud-climate hypothesis. J. Geophys. Res., 96, 18727-18733.

Hegg, D.H. and Hobbs, P.V., 1992. Cloud concentration nuclei in the marine atmosphere: A review, In Nucleation and Atmospheric aerosols, edited by N. Fukuta and P. Wagner, 181-191.

Hegg, D.H., 1994. Cloud condensation nucleus-sulfate mass relationship and cloud albedo. J. Geophys. Res., 99, 25,903-25,907.

Hegg, D.H., Ferek, R.J. and Hobbs, P.V. 1995a. Cloud condensation nuclei over the Arctic ocean in early spring. J. Appl. Met., 34, 2076-2082.

Hegg, D.H., Hobbs, P.V., Ferek, R.J. and Waggoner, A.P., 1995b. Measurements of some aerosol properties relevant to radiative forcing on the East Coast of the United States. J. Appl. Met., 34, 2306-2315.

Helas, G., Bingemer, H. and Andreae M.O., 1992. Organic acids over Equatorial Africa: Results from DECAFE 88. J. Geophys. Res., 97, 6187-6193.

Heist, R.H., Colling, K.M. and DuPuis, C.S., 1976. Homogeneous nucleation in associated vapors. I. Acetic acid. J. Chem. Phys., 65(12), 5147-5154.

Hobbs, P.V. and Radke, L.F., 1969. Cloud condensation nuclei from a simulated forest fire. Science, 1163, 279-284

Hobbs, P.V., 1971. Simultaneous airborne measurements of cloud condensation nuclei and sodium-containing particles over the ocean. Quart. J. Roy. Meteor. Soc., 97, 263-271.

Hobbs, P.V., Harrison, H. and Robinson, E., 1974. Atmospheric effects of pollutants. Science, 183, 909-915.

Hogan, A.W., 1975. Antarctic aerosols. J. Appl. Meteorol., 14, 550-559.

Hoppel, W.A., Dinger, J.E. and Ruskin, R.E., 1973. Vertical profiles of CCN at various

geographical locations. J. Atmos. Sci., 30, 1410-1420.

Hoppel, W.A., Fitzgerld, J., Frick, G. M. and Larson, R. E., 1990. Aerosol size distribution and optical properties found in the marine boundary layer over the Atlantic Ocean. J. Geophys. Res., 95, 3659-3686

Hudson, J.G., 1980. Relationship between fog condensation nuclei and fog microstructure. J. Atmos. Sci., 37, 1854-1867.

Hudson, J.G., Hallett, J. and Rogers, C.F., 1991. Field and laboratory measurements of cloud-forming properties of combustion aerosols. J. Geophy. Res., 96, 10847-10859.

Jacob, D.J. and Wofsy, S.C., 1988. Photochemistry of biogenic emissions over the Amazon forest. J. Geophys. Res., 93, 1477-1486.

Jiusto, J.E., 1967. Aerosol and cloud microphysics measurements in Hawaii. Tellus. 19, 359-368.

Jiusto, J.E. and Kocmond, W.C., 1968. Note on cloud nucleus measurements in Lannemezan, France. J. Rech. Atmos., 3, 101-104.

Kawamura, K., Ng, L.L. and Kaplan, I.R., 1985. Determination of organic acids (C_1-C_{10}) in the atmosphere, motor exhausts, and engine oils. Environ. Sci. Technol., 19, 1082-1086.

Kawamura, K., Ng, L.L. and Kaplan, I.R., 1991. Organic compounds in rainwater. In Organic Chemistry of the Atmosphere (ed. by Hansen, L. D and Eatough, D. J). CRC Press. pp 233-284.

Kawamura, K., Semere, R., Imai, Y., Fuji, Y. and Hayashi, M., 1996. Water soluble dicarboxylic acids and related compounds in Antarctic aerosols. J. Geophys. Res., 101, 18721-18728.

Keene, W.C. and Galloway, J.N., 1988. The biogeochemical cycling of formic and acetic acids through the troposphere: An overview of current understanding. Tellus, 40B, 322-334.

Keene, W.C., et al., 1995. Carboxylic acids in clouds at a high-elevation forested site in central Virginia, J. Geophys. Res., 100, 9321-9334.

Kerminen, V., Wexler, A.S. and Potukuchi, S., 1997. Growth of freshly nucleated particles in the troposphere: Roles of NH_3, H_2SO_4, HNO_3, and HCl. J. Geophys. Res., 102, 3715-3724.

Khwaja, H.A., 1995. Atmospheric concentrations of carboxylic acids and related compounds at a semiurban site. Atmos. Environ., 29, 127-139.

Kiang, C.S., Stauffer, D., Mohnen, V.A., Bricard, J. and Vigla, D., 1973. Heteromolecular nucleation theory applied to gas-to-particle conversion. Atmos. Environ., 7, 1279-1283.

Kulmala, M., Laaksonen, A., Korhonen, P., Vesala, T. and Ahonen, T., 1993. The effect of atmospheric nitric vapor on cloud condensation nuclei activation. J. Geophys. Res., 98, 22949-22958.

Laaksonen, A., Korhonen, P., Kulmala, M., and Charlson, R.J., 1998. Modification of the Kohler equation to include soluble trace gases and slightly soluble substances. J. Atmos. Sci., 55, 853-862.

Lamb, B., Westberg, G.A. and Quarles, T., 1985. Biogenic hydrocarbon emissions from deciduous and coniferous trees in the United States. J. Geophys. Res., 90, 2380-2390.

Lammel, G. and Novakov, T., 1995. Water nucleation properties of carbon black and diesel soot particles. Atmos. Environ., 29, 813-823.

Lacaux, J.P., Delmas, R., Kouadio, G., Cros, B. and Andreae, M.O., 1992. Precipitation chemistry in the Mayombe Forest of Equatorial Africa. J. Geophys. Res., 97, 6195-6206.

Legrand, M. and Angelis. M.D., 1995. Origins and variations of light carboxylic acids in polar precipitation. J. Geophys. Res., 100, 1445-1462.

Li, S.-M. and Winchester, J.W., 1989. Geochemistry of organic and inorganic ions of late winter Arctic aerosols. Atmos. Environ., 23, 2401-2415.

Liu, P.S.K., Leaith, W.R., Banic, C.M., Li, S.–M., Ngo, D. and Megaw, W.J., 1996. Aerosol observations at Chebogue point during the 1993 North Atlantic Regional Experiment: Relationships among cloud condensation nuclei, size distribution, and

chemistry. J. Geophys. Res., 101, 28971-28990.

Marley, N.A., Gaffney, J.S. and Cunningham, M.M., 1993. Aqueous greenhouse species in clouds, fogs and aerosols. Environ. Sci. Technol., 27 (13), 2864-2869.

Madronich, S. and Calvert, J.G., 1990. Permutation reactions of organic peroxy radicals in the troposphere, J. Geophys. Res., 95, 5697-5715.

Marti, J.J., Weber, R.J., McMurry, P.H., Eisele, F., Tanner, D. and Jefferson A., 1997. New particle formation at a remote continental site: assessing the contributions of SO_2 and organic precursors. J. Geophys. Res., 102, 6331-6339.

Mason, B.J., 1971. The physics of clouds, Clarendon Press, Oxford.

Matsumoto, K., Tanaka, H., Nagao, I. and Ishizaka, Y., 1997. Contribution of particulate sulfate and organic carbon to cloud condensation nuclei in the marine atmosphere. Geophys. Res. Lett., 24, 655-658.

Meng, Z., Seinfeld, J.H. and Saxena, P., 1995. Gas/aerosol distribution of formic and acetic acids. Aerosol Sci. and Technol., 23,561-578.

Meszaros, E., 1988. CCN. In Atmospheric aerosols and Nucleation (ed. by P. Wagner and G. Vali), pp 551-562, Springer-Verlag, Berlin.

Norton, R.B., 1992. Measurements of gas phase formic and acetic acids at the Mauna Loa, observatory, Hawaii during the Mauna Loa observatory photochemistry experiment 1988. J. Geophys. Res., 97, 10389-10393.

Novakov, T. and Penner, J.E., 1993. Large contribution of organic aerosols to cloud-condensation-nuclei concentrations. Nature. 365, 823-826.

Novakov, T. and Corrigan, C.E., 1996. Cloud condensation nuclei activity of the organic component of biomass smoke particles. Geophy. Res. Lett., 23, 2141-2144.

Novakov, T., Corrigan, C.E., Penner, J.E., Chuang, C.C., Rosario, O. and Mayol Bracerio, O.L., 1997. Organic aerosols in the tropical trade winds: a natural source? J. Geophys. Res., 102, 21307-21313.

Penkett, S.A., 1994. Atmospheric photochemistry and its role in the generation of acidity in rain, in the Chemistry of the Atmosphere: Its Impact on Global Change, ed. J.G Calvert, Blackwell Scientific Publications, 1994, pp327-344.

Pruppacher, H.R. and Klett, J.D., 1978. Microphysics of cloud precipitation. 714, D. Reidel Publishing Company (Dorarecht)

Puxbaum, H., Rosemberg, C., Lanzersorfer C., Ober E. and Winwarter, W., 1988. Atmospheric concentrations of formic and acetic acids and related compounds in the eastern and northern Austria. Atmos. Environ., 22, 2841-2850.

Rogers, C.F., Hudson, J.G., Hallett J. and Penner, J.E., 1991. Cloud droplet nucleation by crude oil smoke and coagulated crude oil/wood smoke particles. Atmos. Environ., 25, 2571-2580.

Rogge, W.F., Mazurek, M.A., Hildemann, L.M., Cass, G.R. and Simoneit, B.R.T., 1993. Quantification of urban organic aerosols at a molecular level: Identification, abundance and seasonal variation. Atmos. Environ., 27,1309-1330.

Russell, Y.G. and Heist, R.H., 1978. Homogeneous nucleation in associated vapors. II. Formic and propanoic acids. J. Chem. Phys., 69, 3723-3728.

Sanhueza, E. and Andreae, M.O., 1991. Emission of formic and acetic acids from tropical savanna soils. Geophys. Res. Lett., 18, 1707-1710.

Sanhueza, E., Harias, M.C., Donoso, L., Graterol, N., Hermoso, M., Marti, I., Rondon, A. and Santana, M., 1992. Chemical composition of acid rains in Venezuelan savannah region. Tellus, 44B, 54-62.

Saxena, P., Hildmann, L.M., McMurry, P.H. and Seinfeld, J.H., 1995. Organics alter hygroscopic behavior of atmospheric particles. J. Geophys.Res., 100,18755-18770.

Saxena, P. and Hildmann, L. M., 1996. Water-soluble organics in atmospheric particles: A critical review of the literature and application of thermodynamics to identify candidate compounds. J. Atmos. Chem., 24, 57-109.

Saxena, V.K. and Rathore, R.S., 1984. Transport and formation of summertime cloud condensation nuclei over the Arctic Ocean, In: Preprint Volume I; Eleventh International Conference On Atmospheric Aerosols, Condensation and Ice Nuclei, Hung. Meteoro. Serv., Budapest, Hungary, pp 293-298.

Saxena, V.K. and Ruggiero, F.H., 1990. Antarctic coastal stratus clouds: Microstructure and acidity. In Bently et al. (editors), contributions to Antarctic Research I.

Antarctic Res. Ser., vol. 50, Aug, Washington, D.C., pp 7-18.

Seinfeld, J.H. and Bassett, M., 1982. Effect of the mechanism of gas-to-particle conversion on the evolution of aerosol size distributions. In Heterogeneous Atmospheric Chemistry, pp 6-12, editor D. R. Schryer, America Geophysical Union, Washington D. C.

Sempere, R. and Kawamura, K. 1994. Comparative distributions of dicarboxylic acids and related polar compounds in snow, rain and aerosols from urban atmosphere. Atmos. Environ., 28, 449-459.

Schnell, R.C., Kahl, J.D., Bridgeman, H.A. and Herbert, G. A., 1988. A "major" arctic haze even north of point Barrow, Alasks, April 1986. In: Preprint of the Second Conference on Polar Meteorology and Oceanography, American Meteorological Society, March 29-31, pp 112-115.

Shaw, G.E., 1989. Production of condensation nuclei in clear air by nucleation of H_2SO_4. Atmos. Environ., 23, 2841-2846.

Shulman, M.L., Jacobson, M.C., Charlson, R.J., Synovec, R.E., and Young, T.E., 1996. Dissolution behavior and surface tension effects of organic compounds in nucleating cloud droplets. Geophys. Res. Lett., 23, 277-280.

Squires, P. and Twomey, S., 1966. A comparison of cloud nucleus measurement over central North America and the Caribbean Sea. J. Atmos. Sci., 23, 401-405.

Studzinski, W., Spiegel G.H. and Zahoransky, R.A., 1986. Binary nucleation and condensation in associated vapors. J. Chem. Phys., 84, 4008-4014.

Talbot, R.W., Harris, R.C., Browell, E.V., Gregory, G.L., Sebacher, D.I. and Beck, S.M., 1986. Distribution and geochemistry of aerosols in the tropical North Atlantic troposphere: Relationship to Saharan dust. J. Geophys. Res., 91, 5173-5182.

Talbot, R.W., Beecher, K.M., Harris, R.C. and Cofer, W.R., 1988. Atmospheric geochemistry of formic and acetic acids at a mid-latitude temperate site. J. Geophys. Res., 93, 1638-1652.

Talbot, R.W., Andreae, M.O., Berresheim, H., Jacob, D.J. and Beecher, K.M., 1990. Sources and sinks of formic, acetic, and pyruvic acids over central Amazonia, 2.

Wet season. J. Geophys. Res., 95, 16799-16811.

Talbot, R.W., Vijgen, A.S. and Harriss, R.C., 1992. Soluble species in the Arctic summer troposphere: Acidic gases, aerosols and precipitation. J. Geophys. Res., 97, 16531-16543

Talbot, R.W., Mosher, B. W., Heikes, B. G., Jacob, D. J., Munger, J. W., Daube, B. C., Keene, W. C., Maben, J. R. and Artz, R. S., 1995. Carboxylic acids in the rural continental atmosphere over the eastern United States during the Shenandoah Cloud and Photochemistry Experiment. J. Geophys. Res., 100, 9335-9343.

Terliuc, B. and Gagin, A., 1971. Cloud condensation nuclei and their possible influence on precipitation. J. Appl. Meteor., 10, 474-481.

Twomey, S., 1959. The nuclei of natural cloud formation. Part I: the chemical diffusion method and its application to atmospheric nuclei. Geofis. Pura Appl., 43, 227-242.

Twomey, S., 1968. On the composition of cloud nuclei in northeastern United States. Atmos. Res., 4, 281-285.

Twomey, S. and Wojciechowski, T.A., 1969. Observations of the geographical variations of cloud nuclei. J. Atmos. Sci., 26, 684-690.

Twomey, S. and Davidson, K.A., 1971. Automated observations of cloud nuclei, September 1969-August 1970. J. Atmos. Sci., 28, 1295-1302.

Twomey, S., 1977. Atmospheric aerosols, Elsevier, Amsterdam, Oxford and New York.

Wang, Peng-Yun., 1988. Airborne observations of summertime CCN concentration in the middle-lower troposphere over Northern China. In Atmospheric aerosols and nucleation, edited by P. Wagner and G. Vali, 605-609.

Warner, J. and Twomey, S. 1967. The production of cloud nuclei by cane fires and the effect on cloud drop concentrations. J. Atmos. Sci., 24, 704-706.

Weathers, K.C., Likens, G.E., Eaton, J.S., Bormann, F.H., Bowden, W.B., Andersen, J.L., Cass, D.A., Galloway, J.N., Keene, W.C., Kimball, K.D., Huth, P. H. and Smiley, D., 1986. A regional acidic cloud/fog water event in the eastern United States. Nature. 319, 657-658.

Weast, R.C., (Ed). 1978. Handbook of Chemistry and Physics, 59th ed. Chemical Rubber

Company, Cleveland, Ohio

White, W.H., 1990. Contribution to light extinction, in Visibility: Existing and Historical Conditions: Causes and Effects, Acidic Deposition State Sci. Rep. 24, section 4, Natl. Acid Prec. Assess. Program, Washington, D. C., 1990.

Wieland, W., 1955. Eine neue Methode des Kondensationskernzahlung. Eid. Kom. Stud. Hagenbildung, Hagelabwehr. ETH Pub. No. 6, Zurich.

Williams, A.L., Caughey, M.E., McClure, K.E., Alofs, D.J., Hagen, D.E. and Trueblood, M.B., 1994. Determining the chemical composition of cloud condensation nuclei. Fourth Progress Report, SWS contract Report 568, February, Available from Illinois State Water Survey.

Winwarter, W., Puxbaum, H., Facchini, M.C., Orsi, G., Beltz, N., Enderle, K. and Jaeschke, W., 1988. Organic acid gas and liquid phase measurements in Po Valley fall-winter conditions in the presence of fog. Tellus, 40B, 348-357.

Wolff, G.T., Groblicki, P.J., Cadle, S.H. and Countess, R.J. 1982. Particulate carbon at various locations in the United States. In particulate carbon-Atmospheric Life Cycle (edited by Wolff G.T. and Klimisch, R.L.), Plenum Press., New York.

Yaws, C.L., 1994. Handbook of Vapor Pressure. Gulf Pub. Co., Houston.

Yu, Shaocai., Bi, mutian., and Lin, Xin., 1988. Primary investigation about natural sources of organic acids in the atmosphere and rain. Atmos. Environ., 4, 36-40 (in Chinese).

Yu, Shaocai., Bi, Mutian., and Lin, Xin., 1990. An investigation about the determination of formic and acetic acids in the atmosphere. Ch. J. Environ. Sci., 11(3), 43-48.

Yu, Shaocai., Bi, Mutian., Lin, Xin., Yao, Rongkui., and Tang, Xiaoyan., 1991a. Organic acids in precipitation from Baiyun Mountain, Guanzhou and in cloudwater from Miaoer Mountain, Guangxi, Acta Sci. Circumstantiae., 11(1), 25-30.

Yu, Shaocai., Bi, Mutian., and Lin, Xin., 1991b. Determination of organic acids By IC with p-toluene sulfonic acid as eluant. Anal. Chem., 19(1), 73-76.

Yu, Shaocai., Chen, Xiaojian., and Chen, Zemian., 1992. Organic acids in the oceanic acid rain of Xiamen Island. Shanghai Environ. Sci., 11(12), 30-32.

Yu, Shaocai., Gao, Chentie., Cheng , Zhemian., Cheng, Xiaojian., Cheng, Shuentian., Xiao, Jian. and Ye, Wenxian., 1998. An analysis of chemical composition of different rain types in "Minnan Golden Triangle" region in the southeastern coast of China. Atmos. Res., 47-48,245-269.

Table 8.1. Compilation of published gaseous and aerosol organic acid concentrations in the different parts of the world (nmol/m^3). * Fraction of organic ions in the fine particles (aerodynamic diameter<1.0 μm)

Locations and situation	Acid	Gas phase	Aerosol phase	%Aerosol	% fine fraction*	Authors
Amazon, Brazil, Mixed layer	Formic	66±25	1.0±0.5	1.5	58	Andreae et al. (1988a)
Amazon, Brazil, 2800-3500m	Formic		0.4±0.3		56	Andreae et al. (1988a)
Amazon, Brazil, 3600-3900m	Formic		0.3±0.2		56	Andreae et al. (1988a)
Amazon, Brazil, 4000-5300m	Formic		0.4±0.1		34	Andreae et al. (1988a)
Amazon, Brazil, Free troposphere	Formic		0.4±0.2		47	Andreae et al. (1988a)
Amazon, Brazil (burning plume)	Formic		2.8±1.4		77	Andreae et al. (1988a)
Tallahssee, FL,USA	Formic	75±44	0.8±0.7	1.1	75	Andreae et al. (1987)
Charlottesville, VA, USA	Formic		1.0±0.4		50	Andreae et al. (1987)
N. N Atlantic Ocean, all data	Formic		1.4±0.6		61	Andreae et al. (1987)
N. N Atlantic Ocean, continental	Formic		1.6±0.4		63	Andreae et al. (1987)
Amazon, Brazil, Dry	Formic	53-118				Andreae et al. (1988a)
Guyana	Formic		0.02			Gregory et al. (1986)
Tucson, AZ	Formic	58-141				Dawson et al. (1980)
Tucson, AZ	Formic	8-116				Farmer and Dawson (1982)
S.W. U.S., Rural	Formic	28.6				Dawson and Farmer (1988)
S.W. U.S. , Urban	Formic	122.4				Dawson and Farmer (1988)
Pacific Ocean	Formic	1.2-69.4				Arlander et al. (1990)
Indian Ocean	Formic	0.8-44.9				Arlander et al. (1990)
Boston, Urban	Formic	73-612				Lawrence and Koutrakis (1994)
Schenectady, N. Y., Semiurban	Formic	33-102				Khwaja (1995)
Los Angeles, Urban	Formic	53-531				Grosjean (1989)
Los Angeles, Urban	Formic	33±36	3.0±3	9.1		Kawamura et al (1985)
Hampton, VA, USA, Nongrowing	Formic	28				Talbot et al. (1988a)
Hampton, VA, USA, Growing	Formic	78	0.5±0.3	<1.0		Talbot et al. (1988a)
Barbados	Formic		1.0±1			Talbot et al. (1986)
Barrow, AK, USA	Formic		5.3±0.7		45	Li and Winchester (1989)
Beijing, China	Formic	10-43				Yu et al. (1991)
Baiyun Mt. China	Formic	4-22				Yu et al. (1991)
Guilin, China	Formic	8-9				Yu et al. (1991)
Hawaii, Rural	Formic	20				Norton (1992)
Shenandoah, Virginia, USA	Formic	228±139				Talbot et al. (1995)
Alaska, USA, Plume, 2.2km	Formic	14.3				Wofsy et al. (1992)
Alaska, USA, 4-5km	Formic	9.4				Wofsy et al. (1992)
Alaska, USA, Plume,3-4km	Formic	12				Wofsy et al. (1992)
Alaska, USA, 3-5km	Formic	7.3				Wofsy et al. (1992)
Guayana, Venezuela, Savanna	Formic	6.1				Sanhueza and Andreae (1991)
Congo, Surface	Formic	20±85				Helas et al. (1992)
Congo, Boundary layer	Formic	151±40				Helas et al. (1992)
Congo, Free troposphere	Formic	37±12				Helas et al. (1992)
Venezuela, Guri	Formic	61±30				Hartmann (1990)
Venezuela, A. Pipe, Dry season	Formic	69.4				Sanhueza et al. (1992)
Venezuela, A. Pipe, Wet season	Formic	32.2				Sanhueza et al. (1992)
Central Germany, Surface	Formic	36±57				Hartmann et al. (1989)
Central Germany, Continental air	Formic	28±37				Hartmann et al. (1989)

Table 8.1. (Continued)

Locations and situation	Acid	Gas phase	Aerosol phase	%Aerosol	% fine fraction*	Authors
Central Germany, Maritime air	Formic	8±4				Hartmann et al. (1989)
Austria, rural	Formic	65±24				Puxbaum et al. (1988)
High Arctic (>60N), Boundary layer	Formic	11±4				Talbot et al. (1992)
High Arctic (>60N), Free troposphere	Formic	7±4				Talbot et al. (1992)
Sub-Arctic(50-60N), Boundary layer	Formic	11±5				Talbot et al. (1992)
Sub-Arctic(50-60N), Free troposphere	Formic	8±3				Talbot et al. (1992)
Po Valley, Italy	Formic	11±5				Winiwarter et al. (1988)
Amazon, Brazil, Mixed layer	acetic	90±41	0.8±0.5	0.9	57	Andreae et al. (1988a)
Amazon, Brazil, 2800-3500m	acetic		0.4±0.2		21	Andreae et al. (1988a)
Amazon, Brazil, 3600-3900m	acetic		0.3±0.2		65	Andreae et al. (1988a)
Amazon, Brazil, 4000-5300m	acetic		0.3±0.2		56	Andreae et al. (1988a)
Amazon, Brazil, Free troposphere	acetic		0.3±0.2		50	Andreae et al. (1988a)
Amazon, Brazil, Burning plume	acetic		2.0±0.6		66	Andreae et al. (1987)
Guyana	acetic		0.03			Gregory et al. (1986)
Tucson, AZ	acetic	46-257				Dawson et al. (1980)
Tucson, AZ	acetic	10-133				Farmer and Dawson (1982)
Los Angeles, USA	acetic	50±45	2.0±3	6.9		Kawamura et al (1985)
Hampton, VA, USA	acetic	5-166	0.3±0.1	<1.0		Talbot et al. (1988a)
Barbados	acetic		0.7±1.0			Talbot et al. (1986)
Barrow, AK, USA	acetic		12.4±2.2		31	Li and Winchester (1989)
Beijing, China	acetic	10-145				Yu et al. (1991)
Baiyun Mt. China	acetic	<6-33				Yu et al. (1991)
Guilin, China	acetic	8-18				Yu et al. (1991)
Shenandoah, Virginia, USA	acetic	85.7±45				Talbot et al. (1995)
Alaska, USA, Plume, 2.2km	acetic	22				Wofsy et al. (1992)
Alaska, USA, 4-5km	acetic	10.4				Wofsy et al. (1992)
Alaska, USA, Plume,3-4km	acetic	14.3				Wofsy et al. (1992)
Alaska, USA, 3-5km	acetic	9.8				Wofsy et al. (1992)
Guayana, Venezuela, Savanna	acetic	2.9				Sanhueza and Andreae (1991)
Congo, Surface	acetic	24±216				Helas et al. (1992)
Congo, Boundary layer	acetic	110±37				Helas et al. (1992)
Congo, Free troposphere	acetic	28±4				Helas et al. (1992)
Venezuela, Guri	acetic	30±20				Hartmann (1990)
Venezuela, A. Pipe, Dry season	acetic	57.1				Sanhueza et al. (1992)
Venezuela, A. Pipe, Wet season	acetic	22				Sanhueza et al. (1992)
Central Germany, Surface	acetic	36±48				Hartmann et al. (1989)
Central Germany, Continental air	acetic	44±29				Hartmann et al. (1989)
Central Germany, Maritime air	acetic	28±4				Hartmann et al. (1989)
Austria	acetic	41±16				Puxbaum et al. (1988)
High Arctic (>60N), Boundary layer	acetic	11±2				Talbot et al. (1992)
High Arctic (>60N), Free troposphere	acetic	8±4				Talbot et al. (1992)
Sub-Arctic(50-60N), Boundary layer	acetic	9±4				Talbot et al. (1992)
Sub-Arctic(50-60N), Free troposphere	acetic	9±3				Talbot et al. (1992)
Po Valley, Italy	acetic	21±5				Winiwarter et al. (1988)

Table 8.1. (Continued)

Locations and situation	Acid	Gas phase	Aerosol phase	%Aerosol	% fine fraction*	Authors
S.W. U.S., Rural	acetic	24.4				Dawson and Farmer (1988)
S.W. U.S. , Urban	acetic	163				Dawson and Farmer (1988)
Pacific Ocean	acetic	2-78				Arlander et al. (1990)
Indian Ocean	acetic	4.1-48				Arlander et al. (1990)
Boston, Urban	acetic	33-220				Lawrence and Koutrakis (1994)
Schenectady, N. Y., Semiurban	acetic	24-139				Khwaja (1995)
Los Angeles, Urban	acetic	1.2-160				Grosjean (1989)
Los Angeles, Urban	acetic	78-653				Kawamura et al (1985)
Hampton, VA, USA, Nongrowing	acetic	28.5				Talbot et al. (1988a)
Hampton, VA, USA, Growing	acetic	53.1				Talbot et al. (1988a)
Tallahssee, FL, USA	Pyruvic	2.2±2.5	0.3±0.2	13.6	53	Andreae et al. (1987)
Charlottesville, VA, USA	Pyruvic	3.6±1.3	0.6±0.1	16.7	68	Andreae et al. (1987)
N. N Atlantic Ocean, all data	Pyruvic	1.6±0.5	0.1±0.06	6.5	60	Andreae et al. (1987)
N. N Atlantic Ocean, continental air	Pyruvic	1.6±0.5	0.1±0.04	6.5	63	Andreae et al. (1987)
Amazon, Brazil, Boundary layer	Pyruvic	7±4	0.2±0.05	2.8	63	Andreae et al. (1987)
Amazon, Brazil, Free troposphere	Pyruvic		0.03±0.03		69	Andreae et al. (1987)
Amazon, Brazil, Burning plume	Pyruvic		0.4±0.1		54	Andreae et al. (1987)
Barrow, AK	Pyruvic		0.1±0.04		58	Li and Winchester (1989)
Shenandoah, Virginia, USA	Pyruvic	3.1±2.0				Talbot et al. (1995)
Amazon, Brazil, Mixed layer	Oxalic		1.8±0.7		44	Talbot et al. (1988b)
Amazon, Brazil, Free troposphere	Oxalic		0.21±0.13		52	Talbot et al. (1988b)
Alaska, USA, Plume, 2.2km	Oxalic		0.82			Wofsy et al. (1992)
Alaska, USA, 4-5km	Oxalic		0.2			Wofsy et al. (1992)
Alaska, USA, Plume,3-4km	Oxalic		0.53			Wofsy et al. (1992)
Alaska, USA, 3-5km	Oxalic		0.24			Wofsy et al. (1992)
High Arctic (>60N), Boundary layer	Oxalic		0.22±0.14			Talbot et al. (1992)
High Arctic (>60N), Free troposphere	Oxalic		0.17±0.10			Talbot et al. (1992)
Sub-Arctic(50-60N), Boundary layer	Oxalic		0.33±0.29			Talbot et al. (1992)
Sub-Arctic(50-60N), Free troposphere	Oxalic		0.21±0.12			Talbot et al. (1992)
Los Angeles, USA	Propanoic	4±3	0..3±0.06	7.5		Kawamura et al. (1985)
Barrow, AK	Propanoic		0.3±0.1		32	Li and Winchester (1989)
Alaska, USA, Plume, 2.2km	MSA		0.45			Wofsy et al. (1992)
Alaska, USA, 4-5km	MSA		<0.04			Wofsy et al. (1992)
Alaska, USA, Plume,3-4km	MSA		<0.04			Wofsy et al. (1992)
Alaska, USA, 3-5km	MSA		<0.04			Wofsy et al. (1992)
Amazon, Brazil, Boundary layer	MSA		0.25±0.07		84	Andreae et al (1988b)
Amazon, Brazil, Free troposphere	MSA		0.08±0.03		75	Andreae et al (1988b)

Table 8.2. The physical-chemical properties of several organic and inorganic salts (Weast, 1978)

	Melting point (^{0}C)	Boiling point (^{0}C)	Solubility in grams per 100cc	
			cold water	hot water
		Ammonium		
Acetate	114	decompose	148	decompose
Formate	116	decompose, 180	102	531
Nitrate	169.6	210	118.3	871
Chloride	subl 340	520	29.7	75.8
Sulfate	decompose 235		70.6	103.8
Pyruvate	\	\	\	\
Oxalate	\	\	2.5	11.8
		Sodium		
Acetate	324		119	170.15
Formate	253	decompose	97.2	160
Nitrate	306.8	decompose, 380	92.1	180
Chloride	801	1413	35.7	39.12
Sulfate	884		s	42.5
Pyruvate	\	\	\	\
Oxalate			3.7	6.33
		Potassium		
Acetate	292	\	253	492
Formate	167.5	decompose	331	657
Nitrate	334	decompose, 400	13.3	247
Chloride	770	subl, 1500	34.4	56.7
Sulfate	558	1689	12	24.1
Pyruvate	\	\	\	\
Oxalate	\	\	28.7	83.2

* \ means that the data are not available

Table 8.3. Values of critical radius r_c and supersaturation S_c as a function of nucleus mass of different organic salts. Assuming organic salt spheres at a temperature of 293 k (20 C)

dissolved salts (g)	nmole	r_c(μm)	S_c (S*-1) (%)	dissolved salts (g)	nmole	r_c(μm)	S_c (S*-1) (%)
HCOONa				$CH_3(CO)COONa$			
4.00E-17	5.88E-10	0.12	0.65	4.00E-17	3.64E-10	0.09	0.82
1.00E-16	1.47E-09	0.18	0.41	1.00E-16	9.09E-10	0.14	0.52
4.00E-16	5.88E-09	0.37	0.20	4.00E-16	3.64E-09	0.29	0.26
1.00E-15	1.47E-08	0.58	0.13	1.00E-15	9.09E-09	0.46	0.16
4.00E-15	5.88E-08	1.16	0.06	4.00E-15	3.64E-08	0.91	0.08
1.00E-14	1.47E-07	1.84	0.04	1.00E-14	9.09E-08	1.44	0.05
$HCOONH_4$				$CH_3(CO)COONH_4$			
4.00E-17	6.35E-10	0.12	0.62	4.00E-17	4.00E-10	0.09	0.80
1.00E-16	1.59E-09	0.19	0.39	1.00E-16	1.00E-09	0.15	0.51
4.00E-16	6.35E-09	0.38	0.20	4.00E-16	4.00E-09	0.30	0.25
1.00E-15	1.59E-08	0.60	0.12	1.00E-15	1.00E-08	0.47	0.16
4.00E-15	6.35E-08	1.21	0.06	4.00E-15	4.00E-08	0.93	0.08
1.00E-14	1.59E-07	1.91	0.04	1.00E-14	1.00E-07	1.48	0.05
CH_3COONa				$(COO)_2Na_2$			
4.00E-17	4.88E-10	0.11	0.71	4.00E-17	2.99E-10	0.10	0.74
1.00E-16	1.22E-09	0.17	0.45	1.00E-16	7.46E-10	0.16	0.47
4.00E-16	4.88E-09	0.33	0.22	4.00E-16	2.99E-09	0.32	0.23
1.00E-15	1.22E-08	0.53	0.14	1.00E-15	7.46E-09	0.51	0.15
4.00E-15	4.88E-08	1.06	0.07	4.00E-15	2.99E-08	1.01	0.07
1.00E-14	1.22E-07	1.67	0.04	1.00E-14	7.46E-08	1.60	0.05
CH_3COONH_4				$(COO)_2(NH_4)_2$			
4.00E-17	5.19E-10	0.11	0.69	4.00E-17	3.23E-10	0.11	0.71
1.00E-16	1.30E-09	0.17	0.44	1.00E-16	8.06E-10	0.17	0.45
4.00E-16	5.19E-09	0.35	0.22	4.00E-16	3.23E-09	0.33	0.23
1.00E-15	1.30E-08	0.55	0.14	1.00E-15	8.06E-09	0.53	0.14
4.00E-15	5.19E-08	1.09	0.07	4.00E-15	3.23E-08	1.05	0.07
1.00E-14	1.30E-07	1.73	0.04	1.00E-14	8.06E-08	1.66	0.05

Table 8.4. The possible CCN concentration calculated on the basis of measured aerosol organic salts (nmol/m^3) (from Table 1) in the different parts of the world.
** Calculated by assuming that one of CCN only contained 10^{-16} g organic salt.

Locations and situation	Acid	Gas phase	Aerosol phase	CCN (/cm^3)**	Authors
Amazon, Brazil, Mixed layer	Formic	66±25	1.0±0.5	680±340	Andreae et al. (1988a)
Amazon, Brazil, 2800-3500m	Formic		0.4±0.3	272±204	Andreae et al. (1988a)
Amazon, Brazil, 3600-3900m	Formic		0.3±0.2	204±136	Andreae et al. (1988a)
Amazon, Brazil, 4000-5300m	Formic		0.4±0.1	272±68	Andreae et al. (1988a)
Amazon, Brazil, Free troposphere	Formic		0.4±0.2	272±136	Andreae et al. (1988a)
Amazon, Brazil (burning plume)	Formic		2.8±1.4	1905±952	Andreae et al. (1988a)
Tallahssee, FL,USA	Formic	75±44	0.8±0.7	544±476	Andreae et al. (1987)
Charlottesville, VA, USA	Formic		1.0±0.4	680±272	Andreae et al. (1987)
N. N Atlantic Ocean, continental air	Formic		1.6±0.4	1088±272	Andreae et al. (1987)
Guyana	Formic		0.02	14	Gregory et al. (1986)
Los Angeles, Urban	Formic	33±36	3.0±3	2041±2041	Kawamura et al (1985)
Hampton, VA, USA, Growing	Formic	78	0.5±0.3	340±204	Talbot et al. (1988a)
Barbados	Formic		1.0±1	680±680	Talbot et al. (1986)
Barrow, AK, USA	Formic		5.3±0.7	3605±476	Li and Winchester (1989)
Amazon, Brazil, Mixed layer	acetic	90±41	0.8±0.5	656±410	Andreae et al. (1988a)
Amazon, Brazil, 2800-3500m	acetic		0.4±0.2	328±164	Andreae et al. (1988a)
Amazon, Brazil, 3600-3900m	acetic		0.3±0.2	246±164	Andreae et al. (1988a)
Amazon, Brazil, 4000-5300m	acetic		0.3±0.2	246±164	Andreae et al. (1988a)
Amazon, Brazil, Free troposphere	acetic		0.3±0.2	246±164	Andreae et al. (1988a)
Amazon, Brazil, Burning plume	acetic		2.0±0.6	1639±492	Andreae et al. (1987)
Guyana	acetic		0.03	25	Gregory et al. (1986)
Los Angeles, USA	acetic	50±45	2.0±3	1639±2460	Kawamura et al (1985)
Hampton, VA, USA	acetic	5-166	0.3±0.1	246±82	Talbot et al. (1988a)
Barbados	acetic		0.7±1.0	574±820	Talbot et al. (1986)
Barrow, AK, USA	acetic		12.4±2.2	10164±1803	Li and Winchester (1989)
Tallahssee, FL, USA	Pyruvic	2.2±2.5	0.3±0.2	330±220	Andreae et al. (1987)
Charlottesville, VA, USA	Pyruvic	3.6±1.3	0.6±0.1	660±110	Andreae et al. (1987)
N. N Atlantic Ocean, all data	Pyruvic	1.6±0.5	0.1±0.06	110±66	Andreae et al. (1987)
N. N Atlantic Ocean, continental air	Pyruvic	1.6±0.5	0.1±0.04	110±44	Andreae et al. (1987)
Amazon, Brazil, Boundary layer	Pyruvic	7±4	0.2±0.05	220±55	Andreae et al. (1987)
Amazon, Brazil, Free troposphere	Pyruvic		0.03±0.03	33±33	Andreae et al. (1987)
Amazon, Brazil, Burning plume	Pyruvic		0.4±0.1	440±110	Andreae et al. (1987)
Barrow, AK	Pyruvic		0.1±0.04	110±44	Li and Winchester (1989)
Amazon, Brazil, Mixed layer	Oxalic		1.8±0.7	2413±938	Talbot et al. (1988b)
Amazon, Brazil, Free troposphere	Oxalic		0.21±0.13	282±174	Talbot et al. (1988b)
Alaska, USA, Plume, 2.2km	Oxalic		0.82	1099	Wofsy et al. (1992)
Alaska, USA, 4-5km	Oxalic		0.2	268	Wofsy et al. (1992)
Alaska, USA, Plume,3-4km	Oxalic		0.53	710	Wofsy et al. (1992)
Alaska, USA, 3-5km	Oxalic		0.24	322	Wofsy et al. (1992)
High Arctic (>60N), Boundary layer	Oxalic		0.22±0.14	295±188	Talbot et al. (1992)
High Arctic (>60N), Free troposphere	Oxalic		0.17±0.10	228±134	Talbot et al. (1992)
Sub-Arctic(50-60N), Boundary layer	Oxalic		0.33±0.29	442±389	Talbot et al. (1992)
Sub-Arctic(50-60N), Free troposphere	Oxalic		0.21±0.12	282±161	Talbot et al. (1992)

Table 8.5. The concentrations of CCN at two different supersaturations as observed at the ground level under the different conditions.

Location/Conditions	0.10%	0.50%	Author (s)
Marine air			
Sydney, maritime air	80	150	Twomey (1959)
Hawaii, oceanic air	25	65	Jiusto (1967)
N. S. Atlantic Ocean, oceanic air	32	71	Twomey and Wojciechowski (1969)
N. S. Pacific Ocean, oceanic air	30	109	Dinger et al. (1970)
N. S. Pacific Ocean, oceani air	13	102	Hoppel et al. (1973)
N. Atlantic Ocean, oceanic air	40	123	Saxena and Fukuta (1976)
Cape Grim, Astralia, maritime air	56	106	Gras (1990)
N. Atlantic Ocean, oceanic air	79	177	Hoppel et al. (1990)
Equatorial Pacific Ocean, oceanic air	40	76	Covert (1992)
N. Pacific Ocean, oceanic air	7	34	Hegg et al. (1991)
Arctic Ocean, oceanic air	9	29	Hegg et al (1995)
Palmer Station, Antarctica, January	95	131	DeFelice et al. (1997)
Palmer Station, Antarctica, January	2	5	DeFelice et al. (1997)
North China, over sea		100	Wang (1988)
ContinentaL air			
Sydney, continental air	300	630	Twomey (1959)
California, unpolluted continental air	120	700	Hudson (1980)
Lannemezan, France, country air	300	670	Jiusto and Kocmond (1968)
Valladolid, Spain, country air, W wind	370	730	Garcia et al. (1981)
Valladolid, Spain, country air, E wind	520	1200	Garcia et al. (1981)
Rolla, Missouri, nonindustrial town	700	2300	Alofs and Lin (1981)
Ivory Coast, dry season	/	1960	Desalmand et al. (1982)
Ivory Coast, subequatorial monsoon	/	1660	Desalmand et al. (1982)
Switzerland, mixed continental air	600	3800	Wieland (1955)
North China, rural area		1000	Wang (1988)
Lamto, West africa, Savannah continental	1128	2700	Desalmand et al. (1985)
Polluted air			
San Diego. California, urban air	400	2000	Hudson (1980)
Buffalo, N.Y. polluted air	550	1800	Jiusto and Kocmond (1968)
Near Jerusalem,	180	930	Terliuc and Gagin (1971)
North China, polluted air in city		10000	Wang (1988)
EL Yunque, Puerto Rico, polluted marine air		558	Novakov and Penner (1993)
Burning plume			
Abidjan, West Africa, bushfire event	5117	8030	Desalmand et al. (1985)
Petterlong, Canada, fire plume	1164	14468	Hudson et al. (1991)

Table 8.6. Comparison of N(CCN)/N(CN) activated fraction of aerosol particles which contain formate, acetate and other soluble inorganic ions (Na^+, NH_4^+, K^+, Cl^-, NO_3^-, SO_4^{2-}) (CCN at 1% supersaturation).

Location or fuel types for combustion	CN (cm^{-3})	CCN (cm^{-3})	N(CCN)/ N(CN)	Soluble ions (meq/g)	Cited refs
Washington, D. C	78000	2000	0.026	/	Pruppacher and Klett, 1978
	68000	2000	0.029	/	Pruppacher and Klett, 1978
	57000	5000	0.088	/	Pruppacher and Klett, 1978
	50000	7000	0.14	/	Pruppacher and Klett, 1978
Long Island (N. Y)	51000	220	0.0043	/	Pruppacher and Klett, 1978
	18000	110	0.0061	/	Pruppacher and Klett, 1978
	6500	150	0.023	/	Pruppacher and Klett, 1978
	5700	30	0.0052	/	Pruppacher and Klett, 1978
Yellowstone National Park, Wyoming	1000	15	0.015	/	Pruppacher and Klett, 1978
Pine wood, smoldering	500000	120000	0.24	1.3-3.8	Hudson et al., 1991; Hallett et al., 1989
Pine wood, flaming	60000	43000	0.72	1.3-3.8	Hudson et al., 1991; Hallett et al., 1989
Chaparral, brush mixture	136000	115000	0.85	1.3-3.8	Hudson et al., 1991; Hallett et al., 1989
JP-4 aviation fuel	543000	4343	0.008	/	Hudson et al., 1991; Hallett et al., 1989
JP-4 aviation fuel	433000	4332	0.01	/	Hudson et al., 1991; Hallett et al., 1989
Sweet crude oil, low sulfur	129000	8000	0.06	1.25	Rogers et al., 1991
Light crude oil, high-sulfur	155000	11500	0.07	1.22	Rogers et al., 1991
Acetylene gas, welding torch	/	/	0.49-0.53	3.13	Hallett et al., 1989
Diesel, diffuse flaming	/	/	0.42	0.094	Lammel and Novakov, 1995
Arctic Ocean	648±1185	47±19	0.15±0.08	/	Hegg et al., 1995

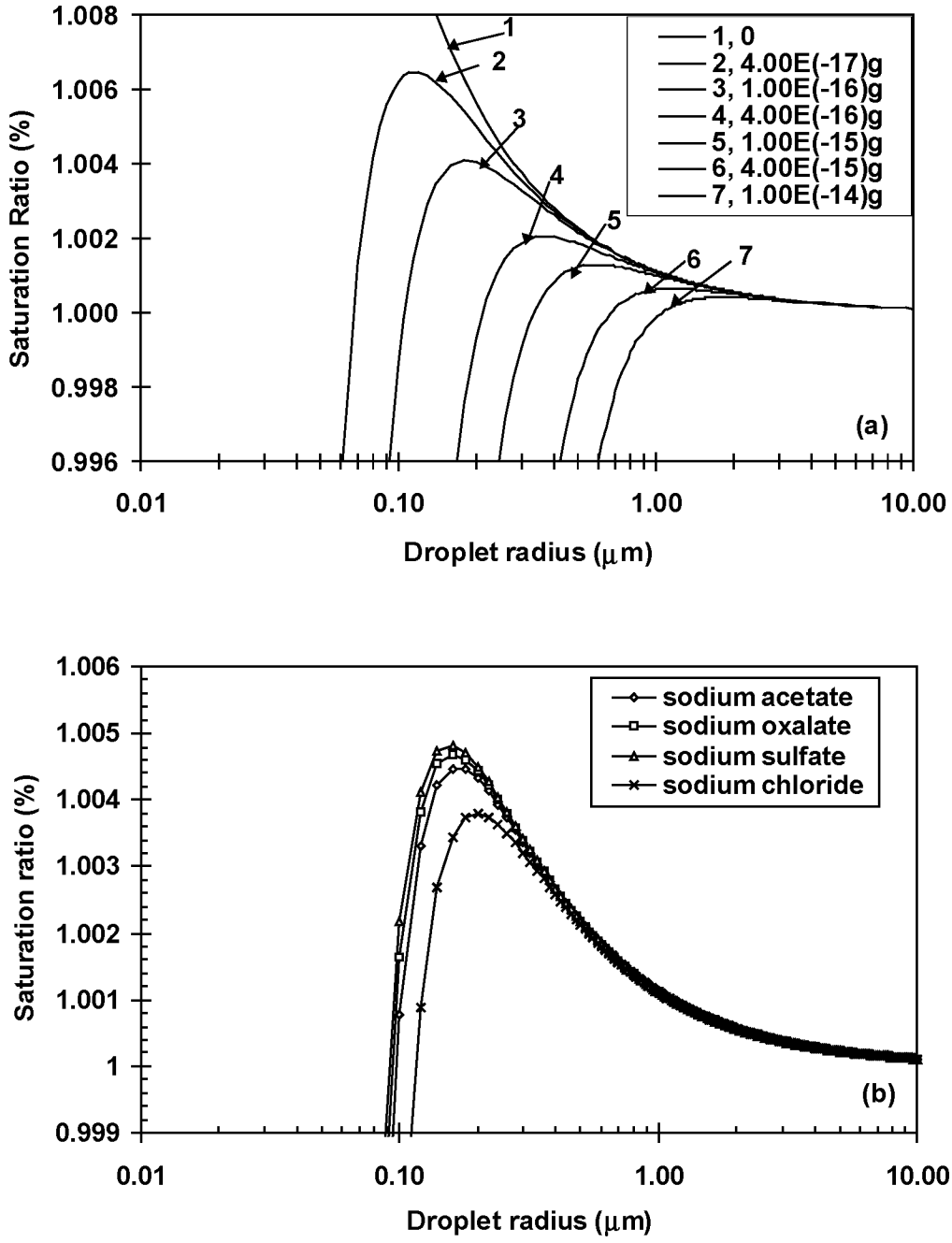

Figure 8.1. (a) Saturation ratio versus droplet size for droplets containing different mass of sodium formate at 20 C (b) Comparison of relationships between saturation ratio and droplet size for droplets containing different organic and inorganic salts with the same nuclear masses (10^{-16}g) for different sodium salts

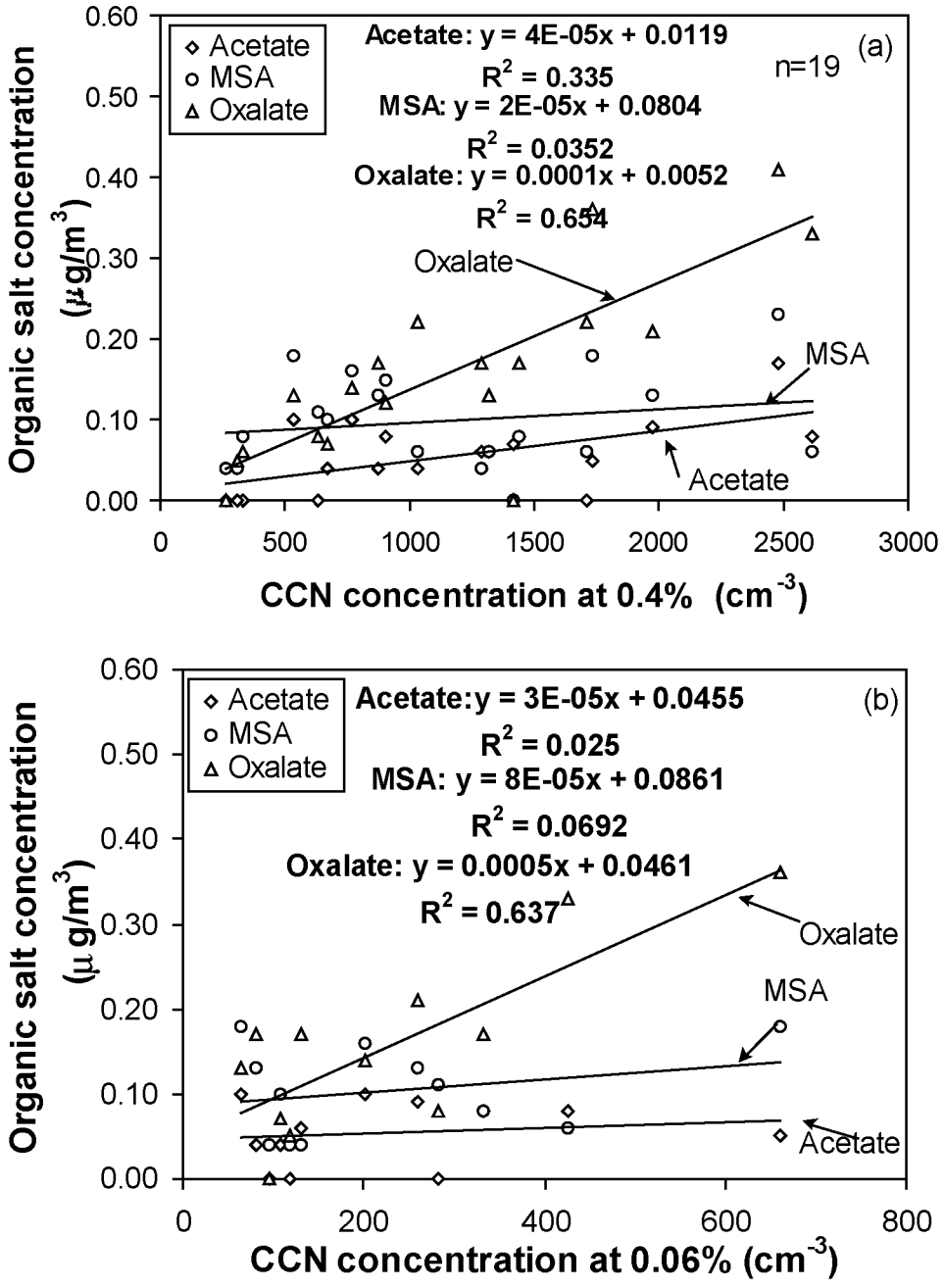

Figure 8.2. (a) The correlation coefficients between CCN concentration at 0.4% supersaturation and acetate, MSA, Oxalate (b)The correlation coefficients between CCN concentration at 0.06% supersaturation and acetate, MSA, Oxalate (from the Table 1 of Liu et al. (1996))

9. OBSERVATIONS OF BLACK CARBON (BC) AND CLOUD CONDENSATION NUCLEI (CCN): CLIMATIC IMPLICATIONS IN THE SOUTHEASTERN US

V.K. Saxena and Shaocai Yu

Department of Marine, Earth and Atmospheric Sciences
North Carolina State University
Raleigh, NC 27695-8208, USA

In preparation for submission to Atmospheric Research, 1999

9.1. Abstract

New evidence for substantial and definitive CCN (cloud condensation nuclei) enhancement near and within cloud has been observed at a regionally representative site in the southeastern US. The measurements used in this study were obtained during 1996 and 1997 at Mt. Mitchell ($35^0$44'05'' N, $82^0$17'15'' W, 2038 m MSL, highest peak in eastern US), North Carolina. The results show that the average monthly CCN concentrations ranged from 152 to 937 cm^{-3} (average: 460±217 cm^{-3}), 107 to 1006 cm^{-3} (average: 386±286 cm^{-3}), 124 to 548 cm^{-3} (average: 429±228 cm^{-3}) and 66 to 326 cm^{-3} (average: 238±134 cm^{-3}) for incloud, overcast, clear and rainy conditions, respectively. The average monthly CCN concentrations ranged from 261 to 1367 cm^{-3}, 63 to 377 cm^{-3} and 66 to 326 cm^{-3} for polluted, continental and marine air masses, respectively. The typical CCN spectra show that there were a lot of small CCN produced and the ion concentrations (especially H^+ and SO_4^{2-}) were very high during the CCN enhancement period. It also indicates that the meteorological conditions (relative humidity and temperature) were favorable for H_2SO_4 nucleation during the CCN enhancement period on the basis of the classic nucleation theory. The significantly positive correlation between black carbon (BC) and CCN at 1% supersaturation indicates that a percentage of the BC measured at the site may be in the form of an internal mixture and participated in the formation of CCN.

Key word index: Cloud condensation nuclei, black carbon, marine and continental air masses.

9.2. Introduction

Global climate effects of aerosols are manifested either through direct or indirect interactions with the solar radiation and/or water substance (Shaw, 1987). It has been suggested that CCN potentially play an effective role in climate-regulation (i.e. counteracting the greenhouse warming due to CO_2 etc.), and an increase in CCN number concentration, by as much as a factor of four, would cause an global albedo increase of ~1.7% (Ghan et al., 1990). A large number of studies have demonstrated the relationship between CCN concentration and cloud microphysics (Twomey and Wojciechowski, 1969; Hegg et al., 1990; Saxena, 1996; DeFelice et al., 1997). Twomey and Wojciechowski (1969) showed that the observed difference in cloud droplet concentrations between maritime and continental air masses was determined to be caused by systematic differences in the concentrations of CCN between maritime and continental air masses. Hegg et al. (1990) thought that clouds might be a necessary precursor to the development of significant concentrations of CCN in the marine atmosphere. A number of laboratory and field studies (Twomey and McMaster, 1955; Hegg et al., 1990; Hegg and Hobbs, 1992; Perry and Hobbs, 1994; Saxena, 1996) have reported an enhancement (relative to the one upon which the droplets were formed) in the number of CCN found in the vicinity of cloud droplets in the subsaturated environs.

The purpose of this study is to present the extensive measurement of CCN and BC concentrations and analyze episodes of enhanced CCN concentrations near cloud boundaries at a regionally representative site in the southeastern US, namely, Mt. Mitchell.

9.3. Experimental site and Instrumentation

The research site is a mountain top station located on the peak of Mt. Gibbes (35.78 ^{0}N, 82.29 ^{0}W, 2006 m MSL), in the Blue Ridge Mountains of western North Carolina (for details see Saxena et al. (1989)). The experimental site lies approximately 4 km

southwest of Mt. Mitchell, NC (elevation 2038 m), the highest peak in the eastern United States. The measurements used in this study were obtained from May to August 1996, May to August 1997 and November 1997. The site has many interesting characteristics that make it a convenient location for cloud-aerosol interaction study. The elevation (2006 m) of the site and its remote location allow it to be virtually immune to local sources. Saxena et al. (1989) have reported that during the summer months nearly 71% of the days have a cloud event in which the site is immersed. The instruments include an ASRC passive cloud water collector, a Cal-Tech active cloud water collector and a PMS Forward Scattering Spectrometer Probe. The ion concentrations (Na^+, K^+, Ca^{2+}, Mg^{2+}, NH_4^+, Cu^{2+}, Zn^{2+}, Fe^{3+}, Al^{3+}, NO_3^-, Cl^-, SO_4^{2+}) in the cloud water were measured by Ion Chromatography (IC).

All measurements of CCN activation spectrum reported in this paper were obtained with the CCN Spectrometer (Fukuta and Saxena, 1979), that yields a continuous measure of the number of aerosols activated over the entire range of atmospheric supersaturations (0.1% to 2%) in any instant. The concentrations of CCN (N, in cm^{-3}) active at a supersaturation S (in percent) can often be fitted to an expression of the form:

$$N=cS^k$$

where, N is the cumulative concentration of CCN active at or below a supersaturation S and c is the concentration of CCN active at 1% supersaturation, and k is dimensionless slope parameter. Since those particles with critical supersaturation greater than the supersaturation in the cloud (S_{eff}) will be incorporated into the cloud droplets and other with critical supersaturation less than S_{eff} will remain as particles, our in-cloud measurements represent interstitial CCN due to the fact that no cloud droplets were sampled during the CCN measurements. Real-time, continuous measurements of BC mass concentration were made by a commercial instrument named the Aethalometer (Hansen et al., 1996), manufactured by Magee Scientific. A detailed description of the instrumentation, methodology, data quality assurance and quality control with respect to BC measurement at the site has been given by Bahrmann and Saxena (1998). The air masses, approaching the research site, are classified (Ulman and Saxena, 1997) by the

Hybrid Single-Particle Lagrangian Integrated Trajectory (HY-SPLIT) (Draxler, 1992) model as highly polluted (HP), continental (C), and marine (M) based on the SO_2 and NOx emission inventory of the U.S. Environmental Protection Agency.

9.4. Results and discussion

9.4.1. General trend of CCN on Mt. Mitchell

Table 9.1 lists the concurrent measurement results of average monthly BC concentrations, CCN parameters for four different weather types (e. g. in-cloud, overcast, clear and rain) during the summer time of 1996 and 1997. The average monthly CCN concentrations ranged from 152 to 937 cm^{-3}, 107 to 1006 cm^{-3}, 124 to 548 cm^{-3} and 66 to 326 cm^{-3} for incloud, overcast, clear and rain weather conditions respectively. The average monthly k values ranged from 0.60 to 0.89, 0.60 to 0.94, 0.53 to 1.09 and 0.38 to 0.76 for incloud, overcast, clear and rain weather conditions respectively. As can be seen, the CCN concentrations during rain period were lower than those during other weather conditions. Hobbs et al. (1985) found that precipitation could reduce the concentration of larger (lower S_c) CCN. The average CCN concentrations during the cloud period had larger standard deviation and were often higher than those of other weather conditions, but not exclusively during these two summer field seasons. For the winter season (November of 1997), it is interesting to note that the CCN concentrations during the snowing period were higher than those during the other weather conditions although the concurrent BC concentrations were lower during the snowing period. This may be due to the fact that the snowing process can produce a large number of particles.

The dependence of CCN concentration on air mass history was investigated with the classification of air masses influencing the site as polluted, marine and continental as previously stated. Table 9.2 gives the list of concurrent measurements of average monthly BC mass concentrations and CCN parameters for these three air mass types. The average monthly BC concentrations ranged from 169 to 305 (245±61) ng m^{-3}, 86 to 225

(155±61) ng m^{-3} and 56 to 104 (79±14) ng m^{-3} for polluted, continental and marine air masses, respectively. The average monthly CCN concentrations ranged from 261 to 1367 cm^{-3}, 63 to 377 cm^{-3} and 66 to 326 cm^{-3} for polluted, continental and marine air masses, respectively. The average monthly k values ranged from 0.57 to 1.09, 0.56 to 1.01 and 0.48 to 1.07 for polluted, continental and marine air masses, respectively. It is apparently that CCN and BC concentrations of polluted air mass were much higher than those of other air masses. Twomey and Wojciechowski (1969) showed that CCN concentrations of maritime, unpolluted continental and polluted air masses were typically less than 200 cm^{-3}, between 200 and ~2000 cm^{-3} and above 2000 cm^{-3}, respectively. Obviously, the continental and marine classifications for our research site do not imply pure continental and marine air masses, but rather modified continental and marine air masses caused by additional influences from pollution sources over land.

9.4..2. Case studies of episodes of enhanced CCN concentrations near cloud boundaries

Figures 9.1-9.2 show the temporal variations of the concurrent CCN and BC concentrations for three cloud episodes of June 15-16 1997, June 20-22 1997, and June 22-23 1997. Tables 9.3 and 9.4 lists the cloud water ion concentrations, liquid water content (LWC), BC concentration and pH for these three cloud episodes in which enhanced CCN concentrations were frequently observed. Figure 9.3 displays the relationship between wind speed, wind direction, temperature, relative humidity, BC and CCN at 1% supersaturation for the concurrent data of July 1997. A close inspection of the temporal CCN, BC and total ion concentration data in Figures 9.1-9.3 and Tables 9.1-9.4 indicates several noteworthy features. The CCN concentration increased dramatically during the cloud period in these three cloud episodes, and high CCN concentrations were always accompanied by high BC concentration. The high CCN and BC concentrations were also accompanied by high total ion concentration in the cloud water. There is an apparent positive correlation between the CCN concentration and BC concentration for

both cloud and non-cloud periods.

Freshly emitted BC is hydrophobic and chemical inert in all atmospheric conditions. BC can not act as CCN by itself. However, aerosol mechanism and in-cloud processes can render a BC particle hygroscopic in the atmosphere. For example, aqueous phase reactions in the cloud such as the oxidation of SO_2 to sulfate can leave the BC aerosol with a coating of this hygroscopic material (Pininick et al., 1993). Pininick et al. (1993) showed a significant correlation between sulfate and BC and suggested that they might be internally mixed. In addition, Novakov et al. (1974) indicated that BC could increase sulfate production by acting as a catalyst in the oxidation of SO_2. Therefore, the change trend of BC may be used as a tracer of the change trend of anthropogenic aerosols in the atmosphere at our research site. The regression equations between the concurrent measurement data of BC and CCN active at 1% and 0.3% supersaturations for the data from June to August 1996 are as follows:

$$CCN(1\%)\ (cm^{-3}) = 180.3 + 2.13 \times BC\ (ng\ m^{-3}) \quad R=0.69 \quad n=272$$

$$CCN(0.3\%)\ (cm^{-3}) = 136.9 + 0.40 \times BC\ (ng\ m^{-3}) \quad R=0.52 \quad n=272$$

where R is correlation coefficient and n is sample number. It is clear that correlation between BC and CCN at 1% supersaturation (small CCN) is more significant than that between BC and CCN at 0.3% supersaturation (large CCN). This seems reasonable because most of BC was present in the accumulation mode (0.1-1.0 μm) as shown by the studies of Pininick et al. (1993), and can only be activated to be CCN at high supersaturation. Figure 9.3 indicates that local meteorological parameters (wind speed, direction, temperature and relative humidity) have not significant effects on the CCN number concentration at our research site. Note that the slopes between BC and CCN at 1% supersaturation were very different for the data of June to August 1996 and July 1997. This implies that the different BC contained particles for different period may have different activation fraction. The positive correlation between BC and CCN as shown in Figures 9.3e indicates that a percentage of BC measured at the site might be in the form

of an internal mixture and participate in the formation of CCN. This is consistent with the result of Bahrman and Saxena (1998), who showed that BC could incorporated into cloud droplets with the concentration ranges from 20 to 196 μg of BC per kilogram of cloud water at the research site.

Since the CCN concentrations during the cloud episodes of June 15-16 1997 (Figure 9.1a), June 20-22 1997 (Figure 9.1b) and June 22-23 1997 (Figure 9.2a) exceeded 1500 cm^{-3}, much higher than those during other cloud episodes, the cloud-mediated production mechanism of CCN should occur during these three cloud episodes. Here, we refer to the process that the CCN concentration increase unusually during the cloud period as the CCN burst or nucleation burst. Note that the BC concentrations during the cloud episodes of June 15-16 and June 20-22 1997 were in the ranges of 13 to 287 ng m^{-3} and 32 to 282 ng m^{-3} respectively, which were not higher than those of other cloud episodes. The CCN burst lasted for about 23 hours (from 8:30 AM June 15 and 7:30 June 16 1997) (Figure 9.1a), 25 hours (from 23:00 AM 20 June to 4:00 AM of 22 June 1997) (Figure 9.1b) and 7 hours (from 7:00 AM 23 June to 15:00 PM 23 June 1997) (Figure 9.2a) for these three episodes, respectively. Figures 1a, 1b, and 2 show that the different air masses during the cloud periods approach to our research site. Table 9.3 lists the ranges of wind speed, temperature, relative humidity, BC concentration, total ion (H^+, Na^+, K^+,Ca^{2+}, Mg^{2+}, NH_4^+, Fe^{3+}, Al^{3+}, NO_3^-, Cl^-, SO_4^{2+}) concentration in the cloud water and the main air mass types during the three CCN burst periods. As can be seen, the wind speed, temperature and relative humidity were in the ranges of 1-10 m/s, 9.3-16.6 ^0C and 57-99% during the CCN burst period respectively. The C and k of CCN parameters were in the range of 406 to 2956 cm^{-3} and 0.37 to 1.18 respectively. Table 9.4 lists the *in situ* measurement results of CCN parameters, cloud water ion concentrations (pH, NH_4^+, Fe^{3+}, Al^{3+}, NO_3^-, SO_4^{2+}), liquid water content, BC concentration and air mass types during these three nucleation burst periods. As can be seen, the NH_4^+, NO_3^- and SO_4^{2+} concentrations in the cloud droplets were very high. The very low pH (range from 2.66 to 3.56) of cloud water during the CCN burst periods also indicates that the pollution was very high within the clouds in these three cases.

Figures 9.4a, 9.4b and 9.4c show the typical CCN spectra for air masses before cloud, within cloud and after cloud during the CCN burst for the cloud episode of June 15-17 and June 20-22 1997, respectively. The curves labeled as 0.3 and 0.5 μm represent those activated CCN that grow as water droplets larger than 0.3 (small CCN will be counted) and 0.5 μm (only large CCN will be counted) in diameter, respectively. As can be seen, the C and k values of CCN spectra during CCN burst period were higher than those before and after cloud. The C and k for 0.3 μm threshold were much high than those for 0.5 μm threshold as shown in Figures 9.4b and 9.4c. For example, the total CCN concentration is 2202 cm^{-3} for 0.3 μm threshold and is 508 cm^{-3} for 0.5 μm threshold at 3:00 AM of 21 June 1997. This indicates that there were a lot of small CCN instead of large CCN produced during the CCN burst because small CCN require high supersaturation and an increase in small CCN population will result in higher k values. Since the air masses within the clouds had been involved in widespread cloud processes before reached at the mountain site, the CCN spectra measured at our site represented those of the aged continental or marine air masses within the clouds. Therefore, the CCN burst processes might occur during the long-range transportation before reached at our site or occurred at our mountain site. This may be one of reasons that lead CCN parameters (C and k) to be very variable for the CCN burst episodes at our site.

9.4.3. The evidence for enhanced CN (or CCN) near cloud boundary from the earlier experiments and possible particle enhancement mechanism analysis

Since, by definition, CCN serve as the nuclei for the formation of cloud droplets, it is to be anticipated that air that has been involved in cloud information will have reduced CCN concentrations, e.g., the nuclei with the critical supersaturation S_c less than the supersaturation (S_{eff}) within the cloud will be found preferentially within the cloud droplets which are removed from the sample. This removal mechanism is referred to as nucleation scavenging. Since the precipitation process can remove the dissolve CCN from

the atmosphere, it seems reasonable that the CCN concentrations during the rain period were lower than those of other weather conditions in Table 9.1. Other cloud scavenging processes causing the low CCN concentration in the cloud include coalescence scavenging by nonfreezing clouds, Brownian or diffusional scavenging (coagulation) and drizzle (Hobbs et al., 1985; Hudson an Frisbie, 1991).

However, the early work (Twomey and McMaster, 1955; Radke and Hobbs, 1969; Dinger et al., 1970; Saxena et al., 1970; Saxena and Rathore, 1984; Hegg et al., 1990; Hudson an Frisbie, 1991; Perry and Hobbs, 1994; Saxena, 1996; Clarke et al., 1998a; Allen et al., 1999) and our analysis in this study have demonstrated that enhanced CCN concentrations over the ambient levels are also found in the vicinity of clouds. Table 9.5 lists the locations, CN (or CCN) concentration, k values and possible explanations of up to date observations with respects to the episodes of enhanced CCN (or CN) concentrations near and within clouds. Some model calculation and laboratory experiment about the CN enhancement are also listed in Table 9.5. The study areas encompass a variety of different degrees of anthropogenic influence, ranging from the pristine Antarctic to the polluted California coast. Therefore, there is some basis for an assertion that the database used here are globally representative.

Theoretical explanation and laboratory simulations about these CN (or CCN) enhancement mechanism near and within the clouds so far have been few. As previously analyzed and summarized in Table 9.5, the possible explanations for the observed particle enhancement near clouds can be classifies into four categories, e.g., (1) advection of CCN rich air to the measurement site; (2) sulfate production followed by the cycles of evaporation and condensation; (3) homogeneous, heteromolecular nucleation of new aerosol particles (CN) followed by their growth through the cloud evaporation-condensation cycles and/ coagulation of CN to produce enhanced CCN concentrations; (4) sampling artifacts (such as fragmentation of water drops) encountered during airborne observation. As a summary, common features of cloudy /moist layers within which enhanced CN concentrations may be observed are high relative humidity, relative abundance of gaseous precursors such as SO_2 and oxidants such as OH resulting from

photochemical reactions and long life span of clouds. Note that BC concentration was also high during the CCN enhancement period in this study.

It is assumed that in the non-precipitation clouds (stratus clouds), the photochemical reactions result in enhanced production of sulfuric acid gas (or maybe organic acids) that can lead to rapid homogeneous nucleation of new particles if the cloud event coincides with a relative maximum of OH. If the sulfuric acid gas was added to the existing CCN, no more CCN were produced. As shown in the experiment of Clarke et al. (1998a), the vapor pressure of sulfuric acid and the presence of preexisting aerosol surface area are the two key parameters that determine whether nucleation of new particle will occur as opposed to condensation upon existing aerosols. To find out whether the conditions were favorable for nucleation during our CCN enhancement periods, the following empirical equation was used to calculate the critical concentration C_{crit} ($\mu g\ m^{-3}$) of H_2SO_4 (g), required to achieve a nucleation rate of J=1 $cm^{-3}\ s^{-1}$ (Clarke et al., 1998b) under the steady-state condition:

$$C_{crit}=0.16 \exp(0.1T-3.5RH-27.7) \qquad (9.1)$$

where the temperature, T, is in Kelvin, and the relative humidity (RH) scale 0-1 is used. If an ambient H_2SO_4(g) concentration exceeds C_{crit}, excess H_2SO_4 mass becomes available to form new particles by the homogeneous nucleation. Figures 9.1a, 9.1b, and 9.2a show the change of $C_{crit}(H_2SO_4)$ during the three nucleation burst periods on the basis of the measured temperature and RH (See Figures 9.2b) in the air parcel within the clouds. It is of interest to note that the $C_{crit}(H_2SO_4)$ during the CCN enhancement period was lower than other times. The low $C_{crit}(H_2SO_4)$ represents the favored regions for nucleation. It is apparently that the atmospheric conditions in the air parcel within the clouds are favorable for nucleation during the CCN enhancement periods.

Since liquid water content (LWC) and cloud water ion concentrations were measured during the cloud period, the sulfate mass concentration per unit volume air can be derived using the equation from Lin and Saxena (1991) as:

$$(SO_4^{2-})_{airmass}=(SO_4^{2-})_{cloudwater}*LWC/\rho_w \qquad (9.2)$$

where ρ_w is the density of liquid water. Note that the equation (9.2) assumes that the cloud water sulfate concentration is the same as that in the air masses. In the observation on scavenging of aerosol sulfate in cloud water for moderate convective clouds, Hegg and Hobbs (1983) found an average of ~63% of aerosol sulfate that got incorporated in cloud water on the basis of 12 cases. Bahrman and Saxena (1998) showed that BC could incorporated into cloud droplets with the concentration ranges from 20 to 196 μg of BC per kilogram of cloud water at the research site. Deininger (1995) found that the sulfate concentrations in fine ambient aerosol phase at Mt. Mitchell were 2.94 ±1.58 and 5.99± 0.04 g/m^3 for continental and polluted air masses respectively. By subtraction of these aerosol sulfate concentration from the total sulfate concentration in the air masses, the net sulfuric acid concentration in the air masses can be estimated. Table 9.4 lists the CCN concentration, liquid water content, cloud water ion concentrations, $C_{crit}(H_2SO_4)$ and the estimates of sulfuric acid concentration (C_s) for the three nucleation burst events. The C_s/ C_{crit} ratios are also listed in Table 9.4. As can be seen, H_2SO_4 concentration (C_s) were in the range of 0.60 (0.15 ppbv) to 30.8 (7.6 ppbv) μg m^{-3}. C_s/ C_{crit} ratios range from 40 to 3226. Obviously, the sulfuric acid vapor concentrations were sufficient to achieve nucleation and nucleation burst during the three nucleation burst period at the research site.

Our observational results in Table 9.4 show that the ion (NH_4^+, NO_3^- and SO_4^{2+}) concentrations in the cloud water were also extremely high and pH was also very low (pH ranges from 2.67 to 3.37). This indirectly indicates that very active chemical reactions, which produce a lot of sulfuric acid, occurred within the clouds during the three nucleation burst periods. The very high concentrations of NO_3^- and NH_4^+ suggest that other gases such as HNO_3 and NH_3 may have potential to induce rapid nuclei growth in many continental aerosol system. The model calculation of Hegg (1990) also showed the

importance of the co-condensation of other acids or species than H_2SO_4 in the nucleus growth. Since a lot of parameters, such as H_2SO_4 vapor, OH, SO_2, HNO_3, O_3, organic compounds, actinic flux, aerosol size and number distribution, aerosol chemical composition, and total aerosol surface area, have not been measured simultaneously at the research site, the above results obviously need more careful study. However, on the basis of our observation and analysis, it is believed that homogeneous nucleation burst is one of natural phenomenons and may play an important role in the production of aerosol particles, especially for some specific surroundings such as near and within the clouds..

9.5. Concluding remarks

In this paper we have presented the extensive measurements of CCN and BC, and analyzed the episodes of CCN enhancement at Mt. Mitchell to look for evidence of enhanced CCN concentrations near cloud boundaries during the summer periods of 1996 and 1997. Our results provide additional support for the idea that clouds are not only a sink of CCN but also a source of CCN under special circumstances (Hegg et al., 1990; Hegg and Hobbs, 1992; Saxena and Grovenstein, 1994; Perry and Hobbs, 1994; Saxena 1996; Clarke et al., 1998a). The high sulfate concentration in cloud water and the favorable meteorological conditions for the nucleation on the basis of classic nucleation theory support the hypothesis that the very active photochemical reaction in both inside cloud water droplets and the space surrounding cloud droplets, and the following nucleation burst might be mainly responsible for the CCN enhancement near and within clouds. As suggested by the recent observations of Clarke et al. (1998b), nucleation can take place for H_2SO_4(g) levels in the boundary layer that are nearly an order of magnitude less than required by classic nucleation theory. This points to a deficiency in the classic theory as applied to the current setting or possibly to the existence of alternative mechanisms for nucleation. Our observations also indicate that many processes interact to determine the CCN concentrations on Mt. Mitchell.

Acknowledgments. This research was supported in part through the Southeast Regional Center (University of Alabama) for the National Institute for Global Environmental Change, in Tuscaloosa, Alabama, by the United States Department of Energy under cooperative agreement number DE-FCO3-90ER61010. We also thank Dr. Robert Griffin, Mr. William Herz and Mr. William Stelz for their encouragement.

9.6. REFERENCES

Allen, A.G. Grenfell, J.L., Harrison, R.M. James, J., and Evans, M.J., (1999) Nanoparticle formation in marine airmasses: contrasting behaviour of the open ocean and coastal environments. *Atmospheric Research,* **51**, 1-14.

Bahrmann, C.P., and Saxean, V.K., (1998) The influence of air mass history on black carbon concentrations in the southeastern US. *Journal of Geophysical Research*, 103, 23153-23161.

Clarke, A.D., J.L. Varner, F. Eisele, R.L. Mauldin, D. Tanner, and Litchy, M., (1998a) Particle production in the remote marine atmosphere: cloud outflow and subsidence during ACE 1, *Journal of Geophysical Research.*, **103**, 16397-16409.

Clarke, A.D., D. Davis, V.N. Kapustin, F. Eisele, G. Chen, I. Paluch, D. Lenschow, A.R. Bandy, D. Thornton, K. Moore, R.L. Mauldin, D. Tanner, M. Litchy, M.A. Carroll, J.Collins, and Albercook, G., (1998b) Particle nucleation in the tropical boundary layer and its coupling to marine sufur sources,. *Science,* **282**, 89-92.

DeFelice, T.P., Saxena, V.K., and Yu, Shaocai, (1991) On the measurement of cloud condensation nuclei at Palmer Station, Antarctica. *Atmospheric Environment,* **31,** 4039-4044.

Deininger, C.K., (1995) Aerosol sources and origins of air masses as determined by electron microscopy and ion chromatography. MS thesis, North Carolina State University, Raleigh.

Dinger, J.E., Howell, H.B. and Wojciechowski, T.A., (1970) On the source and composition of cloud nuclei in the subsident air mass over the North Atlantic. *Journal*

of Atmospheric Sciences, **27**, 791-797.

Fukuta, N. and Saxena, V.K., (1979)A horizontal thermal gradient cloud condensation nucleus spectrometer. *Journal of Applied Meteorology,* **18**, 1352-1362.

Fukuta, N. and Saxena, V.K., (1975) Field measurements of a cloud condensation nucleus spectrometer in marine fogs. Marine Fog Cruise, USNS Hayes pp. 398-409, Naval Research Lab, Naval Air Systems Command, Office of Naval Research Washington.

Ghan, S.J., K.E. Taylor, and Penner, J.E., (1990) Model test of the CCN-cloud albedo climate forcing. *Geophysical Research Letters*., **17**, 607-610.

Hansen, A.D.A., (1996) Magee Scientific Aethalometer user's guide, Magee Scientific Company, Berkeley, CA, 56 pp.

Hegg, D.H., and Hobbs, P.V., (1983) Preliminary measurements of the scavenging of sulphate and nitrate by clouds. In: Pruppacher, H.R., Semonin, R.G., Slinn, W.G.N. (Eds), Precipitation Scavenging, Dry Deposition and Resuspension, Vol. 1, pp. 79-89, Elservier, New York.

Hegg, D.H., Radke, L.F. and Hobbs, P.V., (1990) Particle production associated with marine cloud. *Journal of Geophysical Research.*, **95**, 917-926.

Hegg, D.H. and Hobbs, P.V., (1992) Cloud condensation nuclei in the marine atmosphere: A review, In Nucleation and Atmospheric aerosols, edited by N. Fukuta and P. Wagner, 181-191.

Hobbs, P.V., Bowdle, D.A. and Radke, L.F., (1985) Particles in the lower troposphere over the High Plains of the United States. Part II: cloud condensation nuclei. *J. Clim. Appl. Meteorol.*, **24**, 1344-1356.

Hudson, J.G. and Frisbie, P.R., (1991) Cloud condensation nuclei near marine stratus. *Journal of Geophysical Research,* **96**, 20795-20808.

Lin, N.H. and Saxena, V.K., (1991) In-cloud scavenging and deposition of sulfates and nitrates: case studies and parameterization. *Atmospheric Environment*, **25**, 2301-2320.

Novakov, T., Change, S.G., and Harker, A.B., (1974) Sulfates as pollution particulates: Catalytic formation on carbon (soot) particles. *Science*, **186**, 259-261.

Perry, K.D. and Hobbs, P.V., (1994) Further evidence for particle nucleation in clear air

adjacent to marine cumulus clouds. *Journal of Geophysical Research*. **99**, 22803-22818.

Pininick, R.G., Fernandez, G., Martinez-Andazola, E., Hinds, B.D., Hansen, A.D.A and Fuller, K., (1993) Aerosol in the arid southwestern United States: Measurements of mass loading, volatility, size distribution, absorption characteristics, black carbon content, and vertical structure to 7 km above sea level. *Journal of Geophysical Research.*, **98**, 2651-2666.

Radke, L.F., and Hobbs, P.V., (1969) Measurement of cloud condensation nuclei, cloud scattering coefficient, sodium containing particles, and Aitken nuclei in the Olympic Mountains of Washington. *Journal of Atmospheric Sciences*, **26**, 281-288.

Saxena, V. K. (1996) Bursts of cloud condensation nuclei (CCN) by dissipating clouds at Palmer Station, Antarctica. *Geophysical Research Letters.*, **23**, 69-72.

Saxena, V.K. and Rathore, R.S., (1984) Transport and formation of summertime cloud condensation nuclei over the Arctic Ocean, In: Preprint Volume I; Eleventh International Conference On Atmospheric Aerosols, Condensation and Ice Nuclei, Hung. Meteoro. Serv., Budapest, Hungary, pp 293-298.

Saxena, V.K. and Grovenstein, J.D., (1994) The role of cloud in the enhancement of cloud condensation nuclei concentrations. *Atmospheric Research*, **31**, 71-89.

Saxena, V.K., Burford, J.N., and Kassner, J.M., (1970) Operation of a thermal diffusion chamber for measurements on cloud condensation nuclei. *Journal of Atmospheric Sciences*, **27**, 73-80.

Saxena, V.K., R.E. Stogner, A.H. Hendler, T.P. DeFelice, and Yeh, R.J., (1989) Monitoring the chemical climate of the Mt. Mitchell State Park for evaluation of its impact on forest decline. *Tellus,* **41B**, 92-109.

Shaw, G.S., (1987) Aerosols as climate regulators: A climate-biosphere linkage? *Atmospheric Environment*, **21**, 985-986.

Twomey, S., and McMaster, K.N., (1955) The production of condensation nuclei by crystallizing salt particles. *Tellus*, **7**, 458-461.

Twomey, S. and Wojciechowski, T.A., (1969) Observations of the geographical

variations of cloud nuclei. *Journal of Atmospheric Sciences*, **26**, 684-690.

Ulman, J.C. and Saxena, V.K., (1997) Impact of air mass histories on the chemical climate of Mount Mitchell, North Carolina, *Journal of Geophysical Research.*, **102**, 25451-25465.

Table 9.1. Average monthly BC mass concentrations (ng m^{-3}), CCN parameters (C and k) and sample number (n) for four type of different weather conditions. Average values and standard deviation

	incloud				overcast				clear				rain			
Month	BC	k	C(cm^{-3})	n	BC	k	C(cm^{-3})	n	BC	k	C(cm^{-3})	n	BC	k	C(cm^{-3})	n
Jun-96	179±167	0.89±0.33	440±325	54	208±82	0.94±0.36	397±148	20	262±101	1.09±0.30	773±313	28				
Jul-96	131±89	0.60±0.38	531±330	42	95±98	0.60±0.21	270±81	10	89±52	0.53±0.23	335±178	53	98±30	0.51±0.11	286±53	7
Aug-96	136±70	0.69±0.22	585±324	24	265±114	0.72±0.16	1006±102	8	118±45	0.75±0.23	427±225	31	53	0.38	244	1
Aver.-96	149±26	0.72±0.14	519±73	120	189±86	0.75±0.17	558±393	38	156±92	0.79±0.28	511±231	112	75±32	0.44±0.09	265±30	8
May-97	84±80	0.73±0.40	263±337	105	260±175	0.73±0.14	107±82	2	281±125	0.83±0.30	536±455	60	/	/	/	/
Jun-97	146±80	0.79±0.25	937±774	146	199±116	0.63±0.21	480±473	77	157±65	0.64±0.20	548±471	86	132±82	0.76±0.34	378±578	14
Jul-97	168±100	0.80±0.28	152±126	91	273±140	0.77±0.36	123±100	34	306±105	0.74±0.21	180±120	79	198±151	0.69±0.20	41±16	4
Aug-97	249±142	0.81±0.18	247±131	80	189±83	0.76±0.15	145±56	30	120±89	0.79±0.21	124±70	37	/	/	/	/
Aver.-97	162±68	0.78±0.04	400±361	422	230±42	0.72±0.06	213±178	143	216±91	0.75±0.08	347±225	262	165±46	0.72±0.05	210±238	18
Total average	155±47	0.75±0.09	460±217	542	210±64	0.74±0.12	386±286	221	186±91	0.77±0.18	429±228	374	120±39	0.58±0.07	238±134	36
	incloud				snowing				clear,snow				rain			
Month	BC	k	C(cm^{-3})	n	BC	k	C(cm^{-3})	n	BC	k	C(cm^{-3})	n	BC	k	C(cm^{-3})	n
Nov-97	92±58	0.63±0.30	152±38	54	80±110	0.52±0.27	191±75	24	90±74	0.88±0.38	164±120	138	13±10	0.66±0.13	170±52	6

Table 9.2. Average monthly BC mass concentrations (in ng m^{-3}), CCN parameters (C and k) and sample number (n) for three types of air masses.

	Polluted				Marine				Continental			
Month	BC	k	C(cm^{-3})	n	BC	k	C(cm^{-3})	n	BC	k	C(cm^{-3})	n
Jun-96	305±89	1.09±0.28	942±253	32	75±42	0.74±0.32	326±147	32	225±142	1.01±0.31	338±79	38
Jul-96	169±82	0.57±0.17	660±306	30	70±31	0.48±0.18	258±124	16	86±58	0.57±0.35	314±159	67
Aug-96	197±84	0.72±0.19	895±232	25	78±31	0.63±0.21	315±81	27	162±54	0.89±0.24	377±75	13
Aver.-96	224±71	0.79±0.26	832±151	87	74±4	0.61±0.13	299±36	75	157±69	0.82±0.22	343±32	118
May-97	263±137	0.82±0.31	647±494	78	56±28	1.07±0.31	215±92	28	141±22	0.56±0.31	106±51	61
Jun-97	195±60	0.77±0.22	1367±642	121	94±62	0.64±0.21	263±183	61	157±105	0.68±0.25	313±168	140
Jul-97	304±94	0.76±0.17	261±91	97	104±56	0.89±0.37	66±56	35	218±130	0.73±0.30	63±42	76
Aug-97	304±91	0.78±0.09	275±98	82	/	/	/	/	90±47	0.81±0.24	97±46	66
Aver.-97	267±51	0.78±0.03	638±518	378	84±25	0.86±0.21	182±102	124	152±52	0.69±0.10	145±113	343
Total average	245±61	0.78±0.14	735±334	465	79±14	0.73±0.17	240±69	199	155±61	0.75±0.16	244±73	451

Table 9.3. CCN parameters, meteorological conditions, black carbon concentration and total ion concentration in cloud water and main air mass types during the cloud dissipation period in 1997 on Mt. Mitchell, NC

CCN burst time	CCN parameters		Meteorological condition					
(1997)	C(1%,cm^{-3})	k	wind speed (m/s)	Temperature (C)	RH (%)	BC (ng/m^{-3})	Total ion ($\mu eq/l$)	main air mass
6/15, 8:30-6/16, 7:30	773-2817	0.51-1.18	1-8	9.3-12.8	70-98	103-286	1058-6798	Continental
6/20, 3:00-6/22, 3:00	598-2956	0.42-1.16	1-9	12.2-16.6	57-96	104-298	1169-4284	Continental
6/22,19:00-6/23, 15:00	406-2945	0.37-0.94	5-10	11.4-15.6	66-99	31-234	1800-4843	Marine

Note: Total ion=$Na^{+}+K^{+}+Ca^{2+}+Mg^{2+}+NH_4^{+}+Cu^{2+}+Zn^{2+}+Fe^{3+}+Al^{3+}+NO_3^{-}+Cl^{-}+SO_4^{2+}$

Table 9.4. In-situ measurements of CCN parameters (C, k), air mass type, black carbon (BC), liquid water content (LWC), cloud water ion concentrations (μeq/l), and the estimation of sulfuric acid concentration (C_s), critical concentrations of sulfuric acid (C_{crit}) and the ratios of C_s to C_{crit} during the three CCN enhancement period within the cloud at Mt. Mitchell.

Local time	k	CCN(1%)	Air	BC	LWC (g m^{-3})	*pH*	Fe^{+3}	Al^{+3}	NH^{4+}	NO_3^-	SO_4^{2-}	C_s(μg/m-3)	C_{crit}(μg/m^{-3})	C_s/C_{crit}
Nucleation burst case 1:														
6/15/97 17:30	0.79	1374	HP	267	0.123	*2.76*	14.8	40.9	1233.9	758.0	3050.4	1.23E+01	4.23E-02	291
6/15/97 18:30	0.69	1370	HP	248	0.428	*3.30*	2.9	17.3	546.2	262.6	1099.8	1.71E+01	1.84E-02	931
6/15/97 21:30	0.59	1028	HP	167	0.251	*3.31*	2.2	26.5	425.2	210.9	984.8	6.11E+00	1.19E-02	511
6/15/97 22:30	0.69	1433	HP	143	0.209	*3.12*	2.7	23.8	432.2	277.1	1182.1	6.13E+00	1.24E-02	493
6/15/97 23:30	0.56	1507	HP	104	0.366	*3.16*	2.5	35.1	339.8	251.8	1067.8	1.32E+01	1.19E-02	1109
6/16/97 1:30	0.77	1303	HP	195	0.466	*3.07*	2.9	23.3	285.2	193.8	784.2	1.19E+01	1.00E-02	1189
6/16/97 2:30	0.90	1236	HP	154	0.677	*2.98*	4.3	31.2	351.0	252.5	1107.6	3.08E+01	9.54E-03	3227
6/16/97 3:30	1.18	1455	HP	224	0.300	*2.96*	7.8	49.0	295.4	252.9	869.8	6.79E+00	1.01E-02	671
6/16/97 4:30	1.07	1608	HP	204	0.304	*3.02*	3.4	33.8	248.6	203.4	709.7	4.61E+00	1.10E-02	420
6/16/97 5:30	0.77	1787	C	175	0.195	*3.31*	2.3	26.0	161.3	154.1	415.2	9.80E-01	9.98E-03	98
6/16/97 6:30	0.91	1413	C	180	0.240	*3.41*	2.0	17.4	120.9	120.3	311.9	6.81E-01	9.98E-03	68
Nucleation burst case 2:														
6/21/97 0:00	0.81	2078	C	194	0.283	*3.27*	1.7	9.8	226.1	125.5	518.7	4.20E+00	1.96E-02	214
6/21/97 1:00	0.81	1603	C	174	0.282	*3.29*	3.2	11.4	453.1	212.0	548.7	4.60E+00	1.70E-02	270
6/21/97 2:00	0.64	1292	C	163	0.211	*3.37*	2.0	5.8	267.1	145.8	348.1	6.04E-01	1.49E-02	41
6/21/97 3:00	0.81	2202	C	212	0.220	*3.15*	5.1	12.3	405.6	227.0	654.6	4.06E+00	1.49E-02	273
6/21/97 3:45	0.91	2751	C	204	0.220	*3.02*	3.4	14.8	287.5	263.9	895.3	6.66E+00	1.42E-02	470
6/21/97 4:00	0.97	2609	C	194	0.121	*2.88*	5.4	22.2	522.5	377.9	1226.4	4.30E+00	1.38E-02	312
Nucleation burst case 3:														
6/23/97 0:00	0.89	1075	M	63	0.088	*2.90*	7.1	43.2	270.0	302.9	1116.8	1.83E+00	1.26E-02	146
6/23/97 1:00	0.84	760	M	90	0.092	*2.67*	10.2	32.0	361.0	995.9	1085.1	1.92E+00	1.23E-02	156
6/23/97 2:00	0.83	1003	M	78	0.098	*2.79*	6.9	31.6	269.0	599.4	903.1	1.33E+00	1.28E-02	104
6/23/97 12:00	0.97	2945	HP	177	0.108	*2.78*	10.8	40.3	463.9	394.8	1693.0	5.95E+00	1.37E-02	433

Table 9.5. Observation of the CCN (or CN) enhancement near and within the cloud boundaries around the world. The ranges of CCN parameters (c and k) are listed.

Location	c (cm^{-3})	k	Location and condition	Explanation	Reference
Laboratory study*				particle fragmentation	Twomey and McMaster [1955]
Olympic Mt, Washington			near the cloud boundary	dissipating cloud	Radke and Hobbs [1969]
North Atlantic			near the cloud boundary	nucleation	Dinger et al. [1970]
Rolla, Missouri	57-224		near the cloud boundary	dissipating cloud	Saxena et al. [1970]
Nova Scotia and Newfoundland	145-2300	0.34-1.36	near the fog forming boundary	fog dissipating	Fukuta and Saxena [1975]
California coast	1350	0.95	near the cloud top	cloud evaporation	Fukuta and Saxena [1978]
Lake Michigan	~3245	1.70	in the subcloud layer	aged aerosol	Saxena [1980]
Barrow, Alaska	100-4800		in the subcloud layer	in-cloud sulfate production	Saxena and Rather [1984]
Southern California coast**	~1500-~5000		near the top of marine stratiform clouds	homogeneous heteromolecular nucleation of sulfates particles	Hegg et al., [1990]
Pacific Northwest coast	1100-1800	~0.9-~1.5		photochemical reaction	Hegg and Hobbs [1992]
Southern California coast	500~2500		in & out of the cloud	artifact of the measurement or residual polluted aerosol	Hudson and Frisbie [1991]
Pacific Ocean**	7350~7620		adjacent to an isolated, marine, cumulus cloud	homogeneous-bimolecular nucleation of H_2SO_4 and H_2O	Perry and Hobbs [1994]
Palmer Station, Antarctica	1372-10050	0.73-0.97	near cloud base	cloud dissipation	Saxena [1996]
First Aerosol Characteristic Experiment (ACE1)**	~4000		in cloud outflow, free troposphere	photochemical reaction	Clarke et al. [1998a]
Atlantic Stratocumulus Transition Experiment**	~3000		within cloud, continental air	particle shatter	Clarke et al. [1997]
South Australia**	~2600		in the vicinity of cloud	fragmentation of cloud drops impacting the aerosol inlet	Web et al. [1998]
Mt. Mitchell	406-2956	0.37-1.18	near or within the cloud, continental air	photochemical reaction of OH, nucleation burst and homogeneous nucleation	This work
Model calculation***	~5000		in the case of cloud	a burst of nucleation and OH photochemical reaction	Russell et al. [1994]

*Particle fragmentation occur during the crystallization of evaporating cloud droplets.
** Only local maxima in CN concentrations near or within the cloud were observed.
*** Model study for DMS-CCN system.

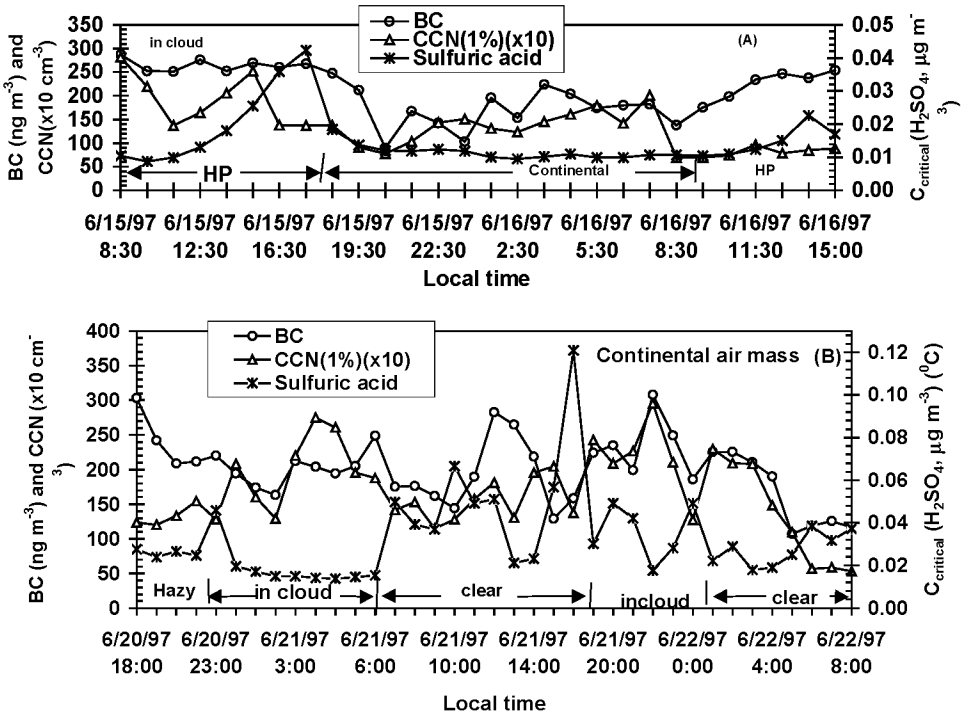

Figure 9.1. The temporal change of CCN, critical concentration of H_2SO_4, BC concentration, air mass types and weather conditions for CCN burst periods from 8:30 AM June 15 to 15:00 June 16 1997 (A), and from 18:00 June 20 8:00 June 22 1997 (B)

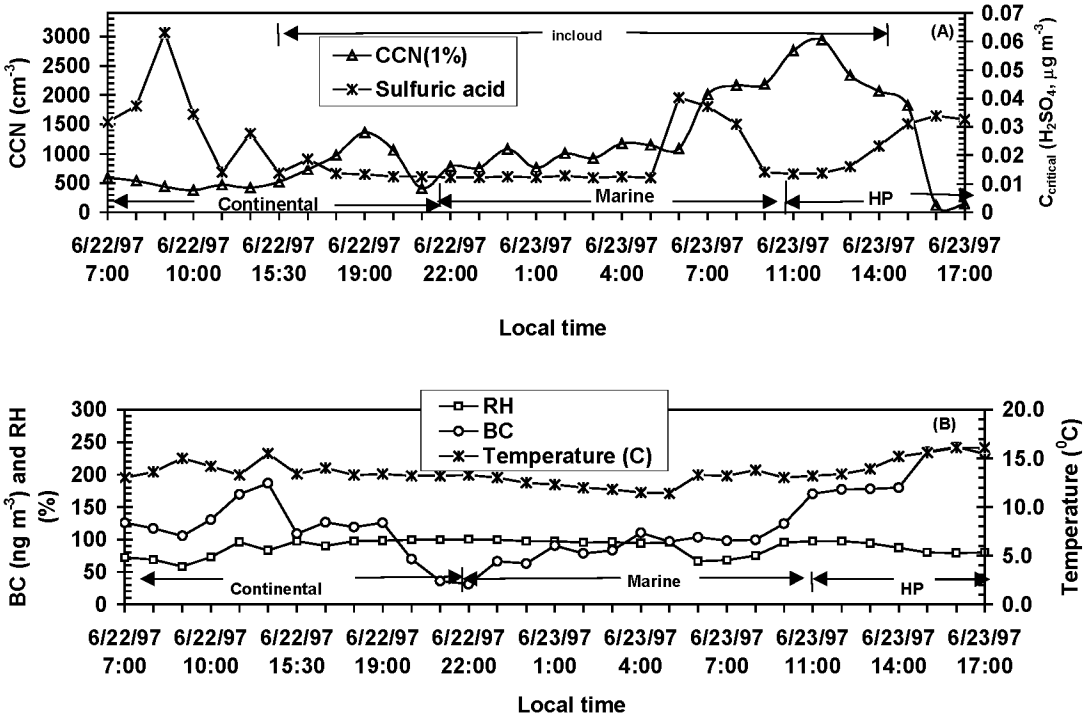

Figure 9.2. The temporal change of CCN, critical concentration of H_2SO_4 (A), BC, air mass types, temperature and relative humidity (B) for CCN burst period from 7:00 23 June to 15:00 23 June 1997

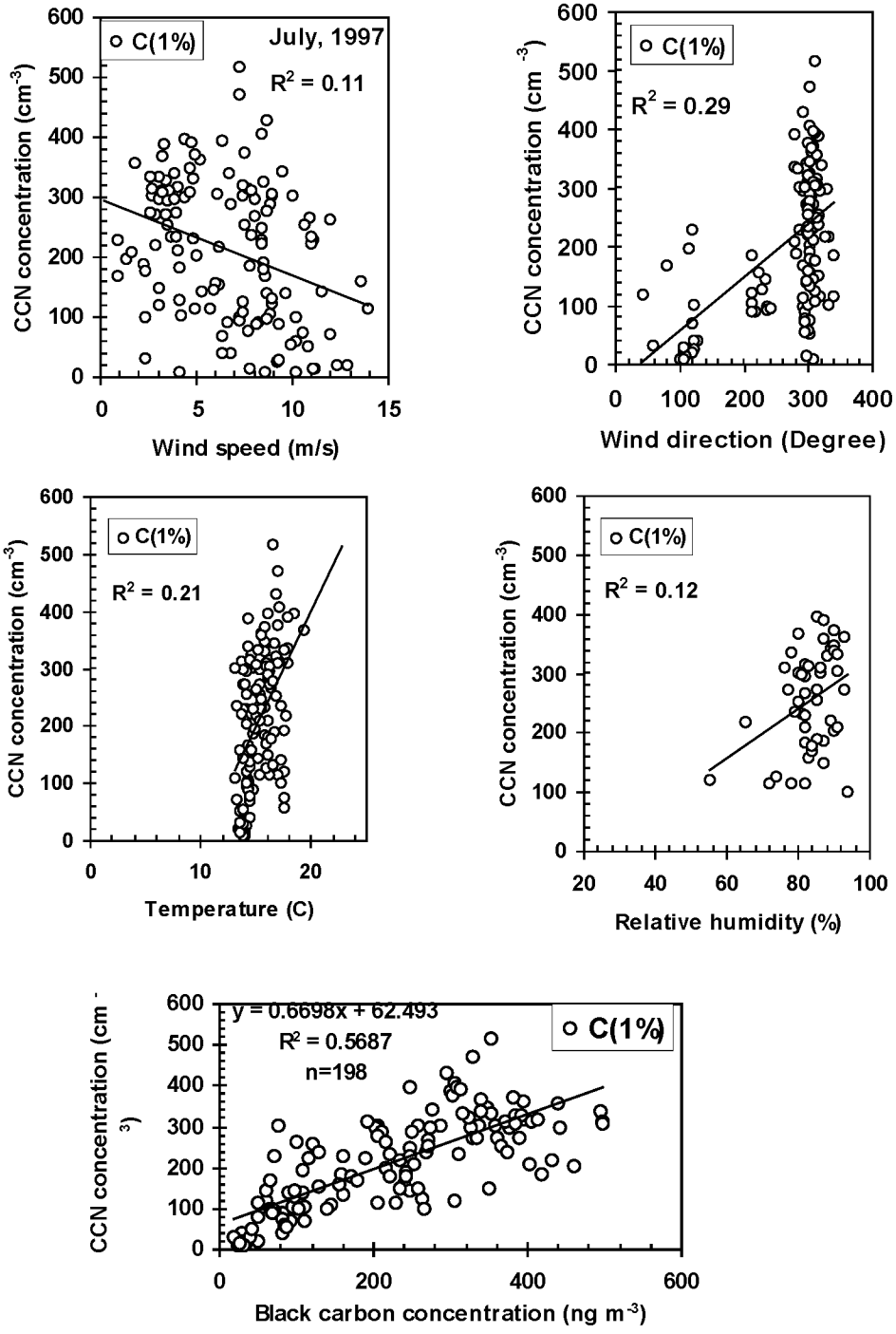

Figure 9.3. The correlation coefficients between CCN at 1% supersaturation and BC concentration and meteorological parameters for the measurement of July 1997.

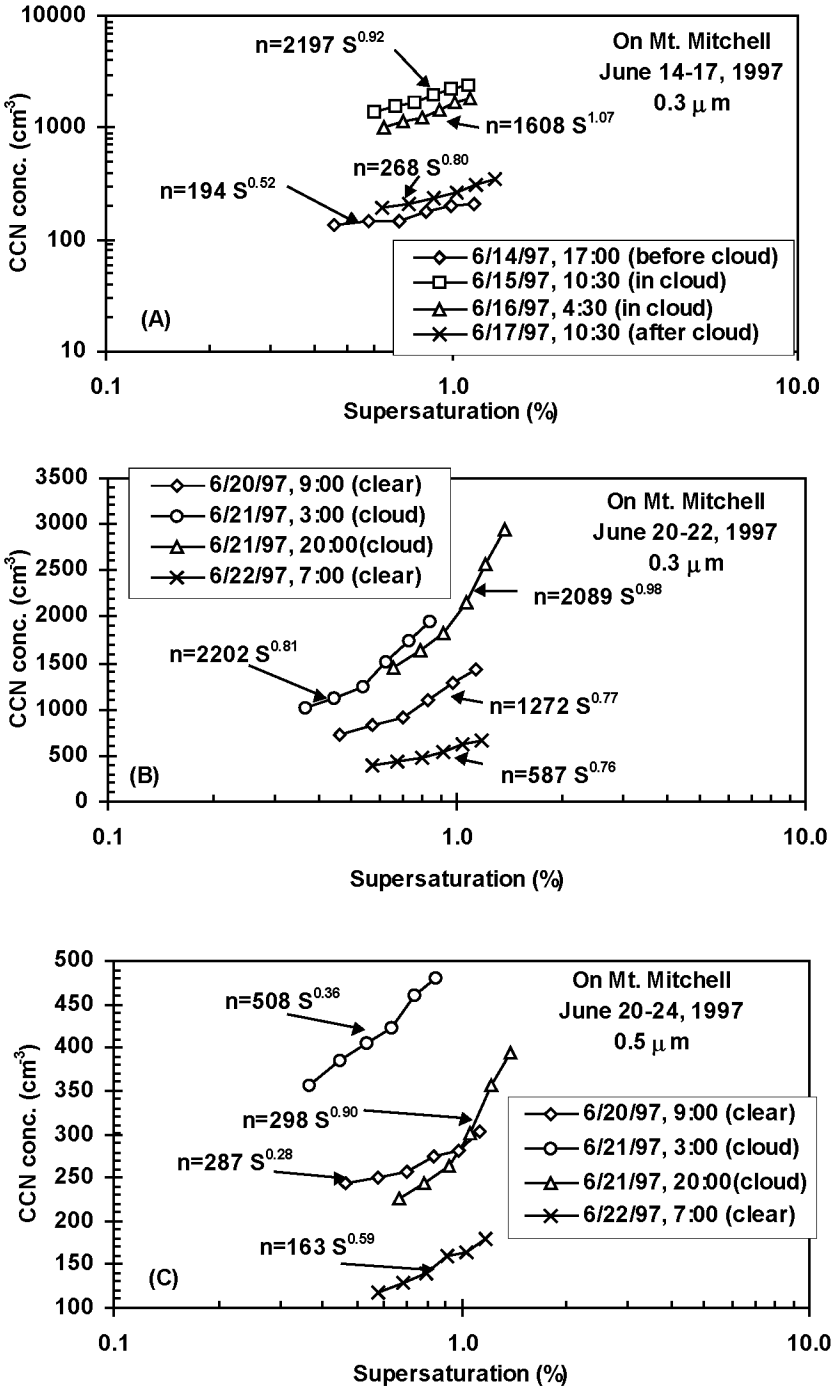

Figure 9.4. CCN activation spectra obtained before, during and after the cloud for CCN burst episode of (A) 15-16 June, 1997; (B) (for 0.3 μm) and (C) (for 0.5 μm) 20-23 June 1997

10. DIRECTION FOR FUTURE RESEARCH

10.1. Recommendations

Aerosol-cloud-climate interactions are obviously nonlinear. Such nonlinear interactions make a description of the influences of aerosols and clouds on climate much more complex than a treatment of the radiative influence of greenhouse gases (Charlson et al., 1992; COSEPUP, 1992; Hobbs, 1993; NRC, 1996; Pener et al., 1994; Schwartz and Andreae, 1996; Stowe et al., 1995; Charlson and Heintzenberg, 1995; Kiehl, 1999). The complexity of this aerosol puzzle seems to grow with each new study (Kiehl, 1999). The general circulation model (GCM) studies predict a climate sensitivity (i.e. the amount of warming caused by a doubling of CO_2) of 1.5-4.5 K with a consensus "best estimate" of 2.5 K when a negative climate forcing due to increasing aerosols is included (IPCC, 1995; Andreae, 1995). However, the internal natural noise of the climate system makes the real-time observation of externally induced changes quite difficult. If anthropogenic sulfate aerosols have a significant cooling effect on regional climate, as argued in this study, the actions taken in some regions such as southeastern US and eastern China to control acidic rain, by decreasing the aerosol forcing, might ironically enhance warming over these regions. Based on this study, the following future research is recommended:

(1) Since aerosol and cloud fields are inhomogeneous in time and space, it still remains a challenge to extrapolate information obtained at our representative research site during an intensive campaign to the seasonal and regional scales for the whole southeastern US. A more complex regional chemical transport/radiation model is needed.
(2) Continuity in the long-term monitoring of aerosol properties and climatological variables such as maximum and minimum temperatures in different seasons is crucial in understanding the role of aerosols in climate change in both eastern China and eastern US.

(3) As a policy, it is also recommended to decrease the absorptive characteristics of the aerosol in the winter season in eastern China by reducing the soot content associated with fossil-fuel burning in order to have cooling effect of aerosol forcing.

(4) There is a need for the comparison of our observations at the mountain site with remotely sensed satellite data to enable transferability of results to other regions and validate climate models for climate change predictions.

(5) Calculate refractive index, σ_e, ω and g using aerosol chemical composition for particle size-segregated aerosol samples (0.093-18 μm), and aerosol number size distribution collected in situ, and compare these with those obtained by the aerosol optical depth and diffuse-direct ratio.

(6) There is a need for accurate laboratory and field experiments to prove whether pure organic acids and their salts can be intrinsically CCN active in atmospheric conditions. A homogeneous and heterogeneous nucleation/condensation model study is needed for multiple gas systems such as an $HCOOH$-CH_3COOH-NH_3-H_2SO_4-HNO_3-HCl-H_2O system. The important role of organic acids in the formation of CCN from special sources in the atmosphere needs to be better confirmed. If organic acids can make a major contribution to the formation of CCN in a biomass-burning plume, organic acids can significantly affect the indirect forcing by biomass-burning aerosols.

(7) There is a need for further observational, theoretical and modeling studies of aerosol production (CCN enhancement) near and within the cloud boundaries in various parts of the world to determine the significance of this source in the global budget of CCN.

(8) Determination of relative contributions of sulfates, organic acids and other non-sulfate aerosols to the formation of CCN at the representative locations such as the marine and remote continental sites is needed. At a minimum, the relations between the mass of each specie and number size distribution, especially in CCN size range (diameter<0.1 μm), must be established. The relationship between CCN and cloud albedo is needed to estimate the contribution of CCN from organic acids and cloud to the indirect aerosol forcing in the southeastern US.

(9) A global inventory of the principal sources and nature of CCN is required for indirect aerosol forcing. More information on CCN spectra is needed, particularly long time-series measurements at a variety of locations around the world. The role of clouds and organic acids as sources of aerosol and CCN is potentially of global importance, however, more data are needed to determine the magnitude of this source and the mechanisms involved in the production of CCN.

(10) Reduced uncertainties in both direct and indirect aerosol forcing will only be achieved through coordinated integration of the field observation and numerical modeling techniques. There is a need for this kind of coordination

Lack of availability of long term measurements (such as aerosol optical depth and cloud reflectivity) precludes a rigorous cause-and-effect analysis for climate change in both eastern China and southeastern US. We highly recommend that a network of such measurements be established for a global coverage. Within the continental US and China, the need for establishing such a network in the southeastern US and eastern China regions is rather urgent.

10.2. References

Andreae, M.O., Climatic effects of changing atmospheric aerosol levels, in *World Survey of Climatology*, 16, Future climates of the world, edited by A. Henderson-Sellers, Elsevier, Amsterdam, 1995

Charlson R. J., , S.E. Schwartz, J. M. Hales, R. D. Cess, J. A. Coakley, J. E. Hansen, and D. J. Hofmann, Climate forcing by anthropogenic aerosols. *Science*. 225, 423-430,1992.

Charlson, R.J., and Heintzenberg, J. (ed.) Aerosol forcing of climate. John Wiley & Sons. 1995.

COSEPUP (Committee on Science, Engineers, and Public Policy), Policy implications of greenhouse warming, mitigation, adaptation, and the science base. Panel on Policy

Implications of Greenhouse Warming, National Academy of Sciences, National Academy Press, pp 918, 1992.

Hobbs, P.V. (ed.) Aerosol-Cloud-Climate Interactions, Academic Press, Inc., 1993

IPCC, Climatic change 1995: Radiative forcing of climate and an evaluation of the IPCC 1992 emission scenarios. J.T. Houghton et al. (Eds). Cambridge University Press, Cambridge, UK, 1995.

Kiehl, J.T., Solving the aerosol puzzle, *Science*, 283, 1273-1275, 1999.

National Research Council (NRC), Aerosol radiative forcing and climate change, National Academy Press, Washington, D.C., 1996.

Penner J.E., R. J. Charlson, J. M. Hales, N. S. Laulainen, R. Leifer, T. Novakov, J. Ogren, L. F. Radke, S. E. Schwartz, and L. Travis, Quantifying and minimizing uncertainty of climate forcing by anthropogenic aerosols. *Bull. Amer. Meteorol. Soc.* 75, 375-400, 1994.

Schwartz S.E. and M. O. Andreae, Uncertainty in climate change caused by aerosols. *Science*. 272, 1121-1122, 1996

Stowe, L.L., Hobbs, P.V., and P. Russell, Plans for the implementation of the tropospheric aerosol radiative forcing observational experiment. Paper MB52A-12, p. 308 Abstracts for Week B, XXI Assembly IUGG, Boulder, Colorado., 1995

APPENDICES

APPENDIX A

LIST OF PUBLICATIONS AND PRESENTATIONS

Papers published or to appear in referred journals:

1. Yu, Shaocai, et al., 1999. Comparison of regional aerosol radiative forcing and its effect on climate changes in eastern China and southeastern US. Geophys. Res. Lett. (in preparation)

2. Yu, Shaocai, C.S. Zender and V.K. Saxena, 1999. Aerosol direct radiative forcing in the southeastern US: estimates from the measurement and model results. Geophys. Res. Lett. (to be submitted)

3. Yu, Shaocai, Saxena, V.K., and B.N. Wenny, 1999. An evaluation of chemical and size effects on radiative properties of multi-component aerosols. Atmospheric Research. (to be submitted)

4. Yu, Shaocai, Saxena, V.K., and Zhao, Zongci, 1999. On detecting the signature of aerosol radiative forcing in the eastern China. Atmos. Environ., (in review).

5. Saxena, V.K. and Yu, Shaocai, 1999. Observations of black carbon (BC) cloud condensation nuclei (CCN): climatic implications in the southeastern US. Atmospheric Research (in preparation)

6. Yu, Shaocai, 1999. The role of organic acids (formic, acetic, pyruvic and oxalic) in the formation of CCN. Atmos. Res. (in revision)

7. Yu, Shaocai, V. K. Saxena, B. N. Wenny, J. J. DeLuisi, G. K. Yue and I. V. Petropavlovskikh, 1999. A study of the aerosol radiative properties needed to compute direct aerosol forcing in the southeastern US. J. Geophys. Res., (in revision)

8. Saxena V.K., and Yu, Shaocai, 1998. Searching for a regional fingerprint of aerosol forcing in the southeastern US. Geophys. Res. Lett. 25: 2833-2836.

9. Yu, Shaocai, Gao, Chentie, Chen, Zemian., Chen, Xiaojian, Chen, Shuentian, Xiao Jian, and Ye Wenxian, 1998. An analysis of chemical composition of different rain types in "Minnan Golden Triangle" region in the southeastern coast of China. Atmos. Res. 47-48: 245-269.

10. DeFelice, T. P., Saxena, V. K., and Yu, Shaocai, 1997.On the measurements of cloud condensation nuclei (CCN) at Palmer Station, Antarctica., Atmos. Environ. 31:4039-4044.

11. Saxena, V.K., Yu, Shaocai, and J. Anderson, 1997. Impact of stratospheric volcanic aerosols on climate: Evidence of aerosol radiative forcing in the southeastern US. Atmos. Environ. 31:4211-4221.

12. Yu, Shaocai, Chen, Zemian, Cai, Xiaopin, Chen Xiaojian, and Shong, Weijian, 1994. A study of acid precipitation in the oceanic environment of Xiamen Island. Atmos. Res. 32: 297-311.

13. Yu, Shaocai, 1994. Relationship between meteorological elements and acid rain and its sources at Xiamen Island. Meteorology. 20(5): 20-23.

14. Yu, Shaocai, 1994. Physical-chemical model study of oceanic acid rain in Xiamen Island. Shanghai Environ. Monitoring. 1: 1-11.

15. Yu, Shaocai, 1993. Investigation about the calculation method of average pH. Environ. Monitoring In China. 9(1): 28-29.

16. Yu, Shaocai, 1993. Determination of optional variance set on Xiamen acid precipitation by major component analysis. Shanghai Environ. Monitoring. 3: 6-11.

17. Yu, Shaocai, Chen, Xiaojian, and Chen, Zemian, 1992. Organic acids in the oceanic acid rain of Xiamen Island. Shanghai Environ. Sci. 11(12): 30-32.

18. Yu, Shaocai, Chen, Zemian, Cai, Xiaopin, Chen Xiaojian, 1992. An investigation about chemical compositions of acid rain and their relationship with the meteorological conditions in Xiamen Island. Environ. Prot. Sci. 3: 68-73.

19. Yu, Shaocai, 1992. A review about the measurement methods of H2O2 in the atmosphere and precipitation. Environ. Monitoring In China. 8(4): 49-52 .

20. Yu, Shaocai, 1992. A study about the sources of acid rain in Xiamen Island. In Acid Rain in China and Its Control Policy (ed. By Z. Zhong). PP54-56. published by Chinese Scientific and Technological Publication House.

21. Yu, Shaocai, Bi, Mutian, Lin, Xin, Yao, Rongkui, and Tang, Xiaoyan, 1991. Organic acids in precipitation from Baiyun Mountain, Guanzhou and in cloudwater from Miaoer Mountain, Guangxi. Acta Sci. Circumstantiae. 11(1): 25-30.

22. Yu, Shaocai, Bi, Mutian, and Lin, Xin, 1991. Determination of organic acids By IC with p-toluene sulfonic acid as eluant. Analytical. Chem. 19(1):73-76.

23. Yu, Shaocai, 1991. A review about the natural sources of precursors of acid rain. Shanghai Environ. Monitoring. 1:26-32.

24. Yu, Shaocai, Bi, Mutian, and Lin Xin, 1990. An investigation about the determination of formic and acetic acids in the atmosphere. Ch. J. Environ. Sci. 11(3): 43-48.

25. Yu, Shaocai, 1990. Primary study about the sources and causes of acid rain in Xiamen Island. Atmos. Environ. 5: 43-44. (in Chinese)

26. Yu, Shaocai, Bi, Mutian, and Lin, Xin, 1988. Primary investigation about natural sources of organic acids in the atmosphere and rain. Atmos. Environ. 4: 36-40 (in Chinese)

27. Yu, Shaocai, The energy at the deep ocean. New Energy, 8(9): 34, 1986 (in Chinese).

28. Yu, Shaocai, 1987. The global natural sources of precursor NOx of acid rain: a review. Environ. Prot. Sci. 2: 8-13 (in Chinese).

Papers published in conference proceedings:

29. Yu, Shaocai, Saxena, V.K., and Zhao Zongci, 2000. Remotely sensed aerosol optical depth over eastern China by SAGE II satellite: A confirmation of the surface cooling effect following the Mount Pinatubo eruption. 28th International Symposium on Remote Sensing of Environment, 27-31 March 2000, Cape Town, South Africa.

30. Yu, Shaocai, Saxena, V.K., and Zhao Zongci, 2000. On detecting the signature of aerosol radiative forcing in the eastern China. Proceedings of 11th Symposium on Global Change Studies, AMS, 9--14 January 1999, Long Beach, CA

31. Yu, Shaocai, Saxena, V.K., and Zhao Zongci, 1999. Comparison of aerosol radiative forcing and its effect on the climate change in eastern China and southeastern US. Symposium on 21st Century China and the Challenge of sustainable Development, Washington, D.C., USA, September 3-5, 1999.

32. Saxena, V.K. and Yu, Shaocai, 1999. Climate variations in the southeastern US during 1949-94: Did a volcano affect it during 1992-94? Eighth conference on climate variations, 13-17 September 1999, Denver, Colorado.

33. Saxena, V.K. and Yu, Shaocai, 1999. Regional climate change in the southeastern US: aerosol cooling VS. greenhouse warming, Proceedings of 10th Symposium on Global Change Studies, 10-15 January 1999, Dallas, TX.

34. Saxena, V.K., and Yu, Shaocai, 1998, Sustainable coal consumption in the Southeast: Impact analysis of Kyoto Treaty. Proceedings of the SAMAB 9th Annual Fall Conference, 4-6 November, 1998, Gatlinburg, TN

35. Saxena, V.K. and Yu, Shaocai, 1998. A comprehensive global analysis of episodes of enhanced CCN concentrations near cloud boundaries. Proceedings of Ninth Symposium of the IAMAS Commission on Atmospheric Chemistry & Global Pollution and Fifth Scientific Conference on the International Global Atmospheric Chemistry Project. 19-25 August 1998, Seattle, Washington.

36. Yu, Shaocai, and Saxena, V. K., Organic acids (formic, acetic, pyruvic and oxalic) in the formation of CCN: a hypothesis. Proceedings of Conference on Cloud Physics, 17-21 August, 1998, Everett, Washington, pp230-234.

37. Yu, Shaocai, V. K. Saxena, B. N. Wenny, J. J. DeLuisi, G. K. Yue and I. V. Petropavlovskikh, 1997. A study of the diffuse to direct solar irradiance ratio and aerosol optical depth in the southeastern US. Proceedings of A&WMA/AGU Specialty Conference on Visual Air Quality, Aerosol, and Global Radiation Balance, September 9-12, Bartlett, NH, 1997.

38. Yu, Shaocai, V.K. Saxena, and B.N. Wenny, 1997. A theoretical evaluation of chemical and size effects on radiative properties of multicomponent aerosols. Proceedings of AGU 1997 Spring Meeting, May 25-27, Baltimore, MD, S70.

39. Saxena, V. K., Yu, Shaocai, and Anderson, J.1997. On the spatial, temporal, and seasonal variations of climatological variables, and the impact of stratospheric volcanic aerosols on radiative forcing in the Southeastern US. Proceedings of Eight Symposium on Global Change Studies, AMS, Long Beach, CA,1997, pp17-25.

40. Yu, Shaocai, Chen, Zemian, Cai, Xiaopin, 1996. A simultaneous study of acid precipitation in the rapidly developing areas of Xiamen, Quanzhou, Zhangzhou and Tongan in the southeast coast of China. Proceedings of 12th international conference on clouds and precipitation. 19-23 August 1996, Zurich, Switzerland, PP 1080-1083, published by Elsevier Science Publishers.

41. Yu, Shaocai, 1996. CCN-Cloud-Climate hypothesis: Chemical Role. Proceedings of 14th International Conference on Nucleation and Atmospheric Aerosols. 26-30 August, 1996, Helsinki, Finland, P 915-918, published by Elsevier Science Publishers.

42. Saxena, V. K., Aneja, V.P., Yu, Shaocai, Lin, N.H., Li, Xin. 1995. A comparative study of acid deposition on montane forest ecosystem in the eastern US and eastern Asia. Proceeding of WMO-IGAC Conference on the Measurement and Assessment of Atmospheric Composition Change. Beijing, China, October 9-13, 1995.

43. Yu, Shaocai, Chen, Xiaojian., and Chen, Zemian., 1992. A study of spring rain, mold rain and typhoon rain in the oceanic environment of Xiamen Island. Proceedings of the 11th International Conference on Cloud and Precipitation. Montreal, Canada, Aug. 17-21, 1992: 723-726, published by Elsevier Science Publishers.

44. Yu, Shaocai, Bi, Mutian., Lin, Xin., 1989. Sampling methods for formic acetic acids in the atmosphere. Proceedings of the International Meeting on Global and Regional Atmospheric Chemistry, Beijing, China, May 3-8, 1989; P 751-752, published by Energy Department of U.S.A.

45. Lin, Xin, Chen, Bozeng and Yu, Shaocai, The comparative study about the analysis of ion concentration by IC in the acid rain. Proceedings of the Second National Ion Chromatography Conference, Beijing, China, October 2-6, 1989; P 125-136.

Reports:

46. V.K. Saxena, J. Anderson, Yu, Shaocai, 1999. Stratospheric Aerosol and Gas Experiment: SAGE II (NASA Constract No. NAS1-18944) covering the period: Feb 1998-Jan 1999. Annual progress report. NASA Langley Research Center, MS 475, Hampton, VA.

47. V.K. Saxena, S. Menon, Shaocai Yu and C. Petrusak, 1998. Direct and cloud-mediated effects of aerosols in counteracting greenhouse warming in the southeastern US. In: *Annual Report Fiscal Year 1997*, National Institute of Global Environmental Change (NIGEC), Univ. of CA, Davis.

48. V.K. Saxena, S. Menon, C. Bahrmann, Shaocai Yu, B. Wenny and J. Anderson, 1997. Direct and cloud-mediated effects of aerosols in counteracting greenhouse warming in the southeastern US. In: *Annual Report Fiscal Year 1996*, National Institute of Global Environmental Change (NIGEC), Univ. of CA, Davis, 56-60.

49. V.K. Saxena, S. Menon, P.A. Durkee, W.P. Robarge, J. Anderson, B.N. Wenny, C.K. Deninger, B.D. Logie, J.S. Schafer, J.C. Ulman, Shaocai Yu and C. Bahrmann. 1997. Cloud-Climate Feedback Mechanisms: Impact of Reduction in Fossil-Fuel Emissions. Submitted in Partial Fulfillment of U.A. Project No. 91NCS48-05 from the Southeast Regional Center of the National Institute for Global Environmental Change.

50. V. K. Saxena, S. Menon, C. Bahrmann, Shaocai Yu, B. Wenny and J. Anderson, 1996. Direct and cloud-mediated effects of aerosols in counteracting greenhouse warming in the Southeastern US. NIGEC annual report, pp4.

51. V. K. Saxena, Shaocai Yu, S. Menon, J. Anderson, B. N. Wenny, and C. Bahrmann, 1995. Consequences of anticipated greenhouse warming in the southeast US. NIGEC annual report, pp4.

52. Yu, Shaocai, 1992. Investigation about situation sources and causes of acid precipitation in the oceanic environment of Xiamen Island. P199. Xiamen Environmental Protection Agency report (in Chinese).

53. Yu, Shaocai, 1991. Assessment of environmental effects of DongDu oil factory in Xiamen city. pp110, Xiamen Environmental Protection Agency report (in Chinese).

Theses finished:

54. Yu, Shaocai, 1985. A study of artificial nitrate and sulfate on several types of filters in the process of sampling aerosols. B.S. thesis. pp50, Dept. of Technical Physics, Peking University.

55. Yu, Shaocai, 1988. An investigation of organic acids in the acid rain and the atmosphere, and their natural sources. M.S. thesis. pp60, Center for Environmental Sciences, Peking University.

56. Yu, Shaocai, 1996. On the spatial, temporal, and seasonal variations of climatological variables, and the impact of stratospheric volcanic aerosols on radiative forcing in the Southeastern US. M.S. thesis. pp 108, Dept. of Marine, Earth and Atmospheric Sciences, North Carolina State University.

57. Yu, Shaocai, 1999. A study of direct and cloud-mediated radiative forcing of climate by aerosols in the southeastern US. pp 244, Dept. of Marine, Earth and Atmospheric Sciences, North Carolina State University.

APPENDIX B

ABSTRACTS OF SELECTED PUBLICATIONS

Abstracts of selected publications are as follows.

Impact of stratospheric volcanic aerosols on climate: evidence for aerosol shortwave and longwave forcing in the southeastern US

V.K. Saxena, Shaocai Yu and J. Anderson

Atmospheric Environment 31, 4211-4221, 1997

Abstract Major volcanic eruptions inject massive amounts of dust and gases into the lower stratosphere and upper troposphere. Stratospheric volcanic aerosols can scatter incoming solar radiation to space, increasing planetary albedo, reducing the total amount of solar energy reaching the troposphere and the earth's surface, and decreasing the daytime maximum temperature (aerosol shortwave forcing). They can also absorb and scatter outgoing terrestrial longwave radiation, increasing the nighttime minimum surface temperature (longwave forcing). However, persuasive evidence of climate response to this forcing has thus far been lacking. Here we examine patterns of annual and seasonal variations in mean maximum and minimum temperature trend during the periods 1992-94 and 1985-87 relative to that during the period 1988-90 at 47 stations in the southeastern US for evidence of such climate responses. The stratospheric volcanic aerosol optical depths over the southeastern US during the period 1985-1994 were inferred from the Stratospheric Aerosol and Gases Experiment (SAGE) II satellite extinction measurement. After the long-term trend signals are removed, it is shown that the dominant decreasing trend of mean maximum temperature and the dominant increasing trend of mean minimum temperature over periods 1992-94 and 1985-87 relative to that over the period 1988-90 are consistent with the distribution of stratospheric volcanic aerosols and predictions from aerosol radiative forcing in the southeastern US.

Keyword index: Aerosol; radiative forcing; minimum and maximum temperature; volcano; stratosphere.

An analysis of chemical composition of different rain types in "Minnan Golden Triangle" region in the southeastern coast of China

Shaocai Yu, Chentie Gao, Zhemian Cheng, Xiaojian Cheng, Shuentian Cheng, Jian Xiao and Wenxian Ye

Atmospheric Research 47-48, 245-269, 1998

ABSTRACT The pollutants from anthropogenic activities can affect precipitation composition and subsequently affect aquatic and terrestrial ecosystems. Here we reported the results from the simultaneous collection and chemical analysis (including F^-, Cl^-, NO_3^-, SO_4^{2-}, $HCOO^-$, CH_3COO^-, Na^+, NH_4^+, K^+, Ca^{2+}, Mg^{2+}, pH) of spring rain, mold rain and typhoon rain during 1990 and 1991 in the region of Xiamen, Quanzhou, Zhangzhou and Tongan, which is called "Minnan Golden Triangle" and is a rapidly growing urban area in the southeastern Coast of China. It is found that the average pHs of spring rain, mold rain and typhoon rain in 1990 in this region were 4.51, 4.93 and 5.14, respectively. Obviously, the spring rain was the most acidic in the three types of rains in this region. The average concentrations of formic and acetic acids in Xiamen mold rain were 5.67 and 2.91 μeq/l, respectively, and the average maximum contribution of organic acids to free acidity was in the range of 2.8% to 100% (average 66.3%). The regression equations between acidity and ions showed that SO_4^{2-}, NO_3^-, NH_4^+ and organic acids (formic and acetic) made a major contribution to the precipitation acidity in this region. The chemical characteristics of different precipitation types in this region indicated that spring rain had the character of continental origin, but the mold rain and typhoon rain had more effects from the ocean. Since spring rain, mold rain, and typhoon rain were caused by precipitation cloud approaching to this region from different directions and had different acidity, and that the average pH of cloud rainwater on the mountain site was 4.90, it was suggested that acid rain in this region might be mainly caused by long-range transport of pollutants from the southern Chinese mainland, and the local pollution sources were less as significant.

Keywords: Acid precipitation; inorganic and organic ions; growing urban; rain type